

**Investigation of the effects of MFN2
mutations in cellular and *Drosophila*
models**

Qurat-ul-ain Afzal Mahmood

Thesis Submitted for the Degree of PhD

**Department of Biomedical Sciences
University of Sheffield**

July 2015

Table of Content

Abstract	vi
Acknowledgements	vii
Abbreviations	viii

Chapter 1: Introduction

1.1	Mitochondrial dynamics	2
1.2	Mitochondrial Fusion	5
1.2.1	Mfn1 and Mfn2	5
1.2.2	OPA1	7
1.2.3	Other proteins involved in mitochondrial fusion	9
1.3	Regulation of mitochondrial fusion	9
1.3.1	Ubiquitination of Mfns	9
1.3.2	Bcl-2 family members	10
1.3.3	Mitofusin binding protein	12
1.3.4	OPA1 proteases	12
1.3.5	Lipids	12
1.4	Mitochondrial Fission	13
1.4.1	Dynamamin-related protein1 (Drp1)	14
1.4.2	Drp1 anchoring proteins: Fis1 and Mff	15
1.5	Regulation of mitochondrial fission	16
1.5.1	Post translational modifications of Drp1	16
1.5.2	Other proteins involved in fission regulation	17
1.6	Biological significance of mitochondrial dynamics	17
1.6.1	Mitochondrial dynamics and maintenance of mtDNA	17
1.6.2	Mitochondrial dynamics and development	19
1.6.3	Neurons and Mitochondrial dynamics	19
1.6.3.1	Mitochondrial fusion, fission and transport in neurons	21
1.6.3.2	Mitochondrial dynamics and neurodegenerative diseases	23
1.7	Charcot-Marie Tooth (CMT) Disease	25
1.7.1	Charcot-Marie Tooth type 2A2 and Hereditary motor and sensory neuropathy type VI	30
1.7.2	Mitochondrial morphology in patient derived fibroblasts	36
1.7.3	In-vitro analysis of CMT2A associated <i>Mfn2</i> mutations	37
1.7.4	Transgenic models for CMT2A	37
1.8.	<i>Drosophila melanogaster</i> as a model system	38
1.9	Aims and Objectives of the PhD Project	40

Chapter 2: Materials and Methods

2.1	Maintenance of tissue culture cell lines	43
2.2.	Quantification of mitochondrial morphology for human fibroblasts	46
2.3	Screen for mitochondrial fusion inducing compounds	52
2.4	Cell Viability Assay	53
2.5	Quantification of mitochondrial fusion	54
2.6.	Fis1 overexpression in CV14A cells	55
2.7.	Fly Stocks	60
2.8	Fly Husbandry	60
2.9	Behavioural Assays	60

2.10	Neuromuscular Junction study	62
2.11	Culture S2R plus cells and incubation with EA	64
2.12	EMS mutagenesis screen for <i>Marf</i> mutant	65

Chapter 3: Mitochondrial morphology in axonal neuropathies associated with *Mfn2* mutations

3.1	Introduction	74
3.2	Fibroblasts used in the study	74
3.3	Mitochondrial morphology in CMT2A and HMSNVI derived patient fibroblasts	75
3.3.1	Subjective Analysis for mitochondrial morphology	79
3.3.2	Mitochondrial morphology analysis using ImageJ Software	81
3.4.	Discussion	83

Chapter 4: Effect and role of Ethacrynic Acid on mitochondrial fusion

4.1	Introduction	87
4.2	Background and initial compound screen	89
4.2.1	Effect of candidate compounds on mitochondrial morphology in CV14A cells	89
4.2.2	Analysis of compound toxicity for EA, NEM and Cycloheximide	96
4.3	PEG fusion assay for EA and Cycloheximide	98
4.4.1	Fis1 overexpression assay to observe the effect of EA on mitochondrial morphology	100
4.4.2	Fis1 overexpression assay to observe the effect of EA on peroxisome morphology	110
4.5	Effect of EA on the mitochondrial morphology in fibroblasts derived from Patient 3 carrying <i>Mfn2</i> ^{R364W} mutation	113
4.6	Discussion	120

Chapter 5a: Characterisation of *Drosophila melanogaster* Marf

5.1.	Introduction	129
5.2.	Characterisation of Marf and its role in <i>Drosophila melanogaster</i> development, locomotion and mitochondrial morphology	130
5.2.1	<i>Marf</i> RNAi lines used	130
5.2.2	Characterisation of lethal phase of <i>Marf</i> knockdown in basic tissues	130
5.2.3	Western blot analysis for <i>Marf</i> RNAi effectiveness	134
5.2.4	Locomotion defects in <i>Marf</i> ubiquitous knockdown larvae	137
5.2.5	Survival rate for <i>Marf</i> nervous system and motor neuron knockdown flies	137
5.2.6	Locomotion defects in <i>Marf</i> nervous system and motor neuron knockdown flies	140
5.2.7	Mitochondrial morphology and neuromuscular junction structure analysis in <i>Marf</i> motor neuron knockdown and <i>Marf</i> motor neuron overexpression larvae	144
5.2.8	Effects of Ethacrynic acid on <i>Marf</i> knockdown flies	152
5.3	Discussion	156

Chapter 5b: EMS genetic screen for *Drosophila melanogaster*

Marf

5.4	Introduction	162
5.4.1	Forward Genetic screen for <i>Marf</i> using EMS mutagenesis	163
5.4.1.1	Complementation test for <i>Df(1)Exel6239</i> used in EMS screen	163
5.4.1.2	Isolation of EMS mutants	167
5.4.1.3	Characterisation of EMS screen hits	169
5.5	Complementation assay for EMS mutants	172
5.6	Sequencing of <i>Marf</i> in isolated mutants	174
5.7	Protein analysis of Marf in isolated mutants	174
5.8	Discussion	178

Chapter 6: General Discussion 181

Appendix A 190

Bibliography 191

List of Figures

Figure 1.1:	Mitochondrial Dynamics.	3
Figure 1.2:	Schematic of Mfn1 and Mfn2 domain structures.	6
Figure 1.3:	Schematic of OPA1 domain structure.	8
Figure 1.4:	Schematic for the localization of fusion and fission machinery and various regulatory components.	11
Figure 1.5:	Schematic of Drp1 domain structures.	14
Figure 1.6:	Schematic of Fis1 and Mff domain structures.	16
Figure 3.1:	Location of <i>Mfn2</i> ^{R364W} and <i>Mfn2</i> ^{Q674P} in the gene.	75
Figure 3.2:	Mitochondrial morphology in Control fibroblasts.	76
Figure 3.3:	Mitochondrial morphology in CMT2A patient fibroblasts.	77
Figure 3.4:	Mitochondrial morphology in HMSNVI patient fibroblasts.	78
Figure 3.5:	Subjective analysis for mitochondrial morphology.	80
Figure 3.6:	ImageJ analysis of the mitochondrial morphology.	82
Figure 4.1:	Schematic of EA working hypothesis.	88
Figure 4.2:	Screen for mitochondrial fusion inducing compounds in CV14A cells.	92
Figure 4.3:	MTT assay.	97
Figure 4.4:	Mitochondrial fusion assay.	99
Figure 4.5:	Fis1 overexpression assay for mitochondrial morphology.	101
Figure 4.6:	Classification of mitochondrial morphology for Fis1 overexpression assay.	105
Figure 4.7:	Mitochondrial morphology in CV14A cells overexpressing hFis1 and incubated with EA.	108
Figure 4.8:	Nuclear morphology in in CV14A cells overexpressing hFis1 and incubated with EA.	109
Figure 4.9:	Fis1 overexpression assay for peroxisome number.	111
Figure 4.10:	Peroxisome number analysis in Fis1 overexpression assay.	112
Figure 4.11:	Mitochondrial morphology in Patient 3 <i>Mfn2</i> ^{R364W} fibroblasts incubated with EA.	114
Figure 4.12:	Subjective analysis of mitochondrial morphology in Patient 3 <i>Mfn2</i> ^{R364W} fibroblasts incubated with EA.	118

Figure 4.13: ImageJ analysis of mitochondrial morphology in Patient 3 <i>Mfn2</i> ^{R364W} fibroblasts incubated with EA.	119
Figure 5.1: RNAi lines.	131
Figure 5.2: Lethal phase of <i>Marf</i> knockdowns.	132
Figure 5.3: Western blot analysis for <i>Marf</i> RNAi effectiveness.	135
Figure 5.4: Larval locomotion assay for <i>Marf</i> ubiquitous knockdowns.	138
Figure 5.5: Survival curves for <i>Marf</i> nervous system and motor neuron knockdown flies.	139
Figure 5.6: Climbing assay for <i>Marf</i> knockdown flies.	142
Figure 5.7: Flight assay for <i>Marf</i> knockdown flies.	143
Figure 5.8: Mitochondrial morphology in cell bodies of <i>Drosophila</i> larvae motor neurons.	145
Figure 5.9: Mitochondrial morphology in axons of <i>Drosophila</i> larvae motor neurons.	147
Figure 5.10: <i>Drosophila melanogaster</i> neuromuscular junctions.	148
Figure 5.11: Mitochondrial morphology in neuromuscular junctions of <i>Drosophila</i> larvae motor neurons.	149
Figure 5.12: Structure analysis of neuromuscular junctions in <i>Drosophila</i> larvae.	151
Figure 5.13: Mitochondrial morphology in S2R ⁺ cells incubated with EA.	153
Figure 5.14: Locomotion assays for 2 days old and 15 days old <i>Marf</i> ^{RNAi} flies fed on EA.	155
Figure 5.15: Genomic map for the <i>Df(1)Exel6239</i> deficiency chromosome.	164
Figure 5.16: Crossing scheme for deficiency chromosomes complementation assay.	166
Figure 5.17: Crossing scheme for EMS mutagenesis.	168
Figure 5.18: Characterisation of EMS screen hits.	171
Figure 5.19: Crossing scheme for mutant lines complementation assay.	172
Figure 5.20: <i>Marf</i> overlapping amplicons PCRs strategy.	175
Figure 5.21: Sequencher® generated contig.	176
Figure 5.22: Western blot for EMS mutants.	177

List of Tables

Table 1.1: Genetics of CMT	27
Table 1.2: <i>Mfn2</i> mutations associated with CMT2A and HMSNVI	31
Table 2.1: Amplification and sequencing primers	69
Table 4.1: Compounds tested in secondary drug screen	91
Table 5.1: Phenotypes for <i>Drosophila melanogaster</i> <i>Marf</i> knockdowns	132
Table 5.3: Genes deleted in <i>Df(1)Exel6239</i> deficiency chromosome	165
Table 5.4: EMS mutagenesis screens results	170
Table 5.5: Complementation Table for EMS mutant lines	173

ABSTRACT

Mitochondria continuously undergo changes in their morphology by two dynamic processes called mitochondrial fusion and mitochondrial fission. Mitochondrial fusion results in longer mitochondria and is important for the complementation of mtDNA and intermixing of essential mitochondrial proteins and nutrients to maintain healthy mitochondrial population. Mfn1 and Mfn2 are involved in outer mitochondrial membrane fusion while OPA1 mediates inner mitochondrial membrane fusion. On the other hand, mitochondria are broken into smaller units for easy transport and removal of damaged mitochondria by Drp1. Defective mitochondrial dynamics has been linked with various common neuropathies and neurodegenerative diseases. Charcot Marie Tooth Type 2A (CMT2A) and its subtype Hereditary motor and sensory neuropathy type VI (HMSNVI) are caused by mutations in *Mfn2* and result in progressive loss of distal motor and sensory neurons of peripheral nervous system. However, the pathomechanism of *Mfn2* mutations and specific degeneration of peripheral motor and sensory neurons is still unclear. In the PhD, I studied the mitochondrial morphology in the skin fibroblasts obtained from CMT2A and HMSNVI patients. HMSNVI patient carrying *Mfn2*^{R364W} mutation showed fragmented mitochondria with reduced mitochondrial aspect ratio, length, branching and networks. However, CMT2A patients carrying *Mfn2*^{Q674P} mutation showed normal mitochondrial morphology. The second part of project involved characterising the effect of mitochondrial fusion inducing compound Ethacrynic acid (EA) in various cellular assays. Our results showed that EA increases mitochondrial fusion in PEG fusion assay and in CV14A cells overexpressing Fis1. EA also showed reduced number of fragmented mitochondrial morphology in *Mfn2*^{R364W} patient fibroblasts. Third part of project involved the characterisation of *Drosophila melanogaster* mitochondrial assembly regulatory factor (Marf) and its role in fly development, locomotion and mitochondrial morphology in motor neurons. Our results suggest that Marf is essential for fly development and locomotion.

ACKNOWLEDGEMENT

To start with I would like to thank my mother Dr Farhat Jabeen for all her continued love, support and confidence in me and for never letting me go of my dreams in the times when I myself was unable to continue. Mother I will always remember you saying to me ‘perseverance and patience always bring successes so never give up’.

I would say huge thank you to my supervisors Dr. Alex Whitworth and Dr. Andy Grierson for giving me the opportunity to do PhD and for their continued guidance, advice, endurance, criticism and encouragement through out the project. Their support and help at every step of the project is invaluable for me.

I would also extend my thankfulness to my PhD advisor Dr. Liz Seward for her suggestions and encouragement during the PhD. I would also extend my big gratitude to my various lab colleagues including Nala Tao, Venus Ho, Joe Pogson, Luke Tain, Matt Oswald, Roy Milner, Sandy Rajan, Anna Chapman and Lynn Duffy for helping me out in various techniques and procedures and providing valuable suggestions throughout the time of my PhD.

My special recognition goes to some very respected and loving people in my life including Dr Saqib Mahmood, Dr Fareed Aslam and my aunty Tanveer who always believed in me and encouraged me.

ABBREVIATIONS

ADOA	Autosomal Dominant Optic Atrophy
AR	Aspect Ratio
ATP	Adenosine-5'-triphosphate
CMT	Charcot-Marie-Tooth
CMT1	Charcot-Marie-Tooth type 1
CMT2	Charcot-Marie-Tooth type 2
Complex V	F1F0 ATP synthase
Cyto	Cytoplasmic
CV1	Normal african green monkey kidney fibroblast cells
<i>Da</i>	<i>daughterless</i> gene
Df	Deficiency chromosome
DMEM	Dulbecco's modified Eagle's medium
DMSO	Dimethylsulfoxide
Dp	Duplication chromosome
Drp1	Dynein Related Protein 1
DsRed	Discosoma red fluorescent protein
EA	Ethacrynic acid
EDTA	Ethylene diamine tetra acetate
EMS	Ethyl methanesulfonate
<i>Elav</i>	<i>embryonic lethal abnormal vision</i> gene
ER	Endoplasmic reticulum
F	Filial
FCS	Fetal calf serum
Fis1	Mitochondria fission 1
Fzo	Fuzzy onions protein
GFP	Green fluorescent protein
GTP	Guanosine-5'-triphosphate
GTPase	Guanosine triphosphatases
HMSNVI	Hereditary motor and sensory neuropathy type VI
HR	Heptad repeat
IR	Inverted repeat sequences
Marf	Mitochondrial assembly regulatory factor
MEF	Mouse embryonic fibroblasts
MEM	Minimum essential medium
Mff	Mitochondrial fission factor
Mfn1	Mitofusin 1

Mfn2	Mitofusin 2
Mgm1	Mitochondrial genome maintenance protein 1
MIB	Mitofusin binding protein
MIS	Mitochondrial import sequence
Mito	Mitochondrial
MPP	Matrix processing peptidase
MTT	3-(4,5-dimethylthiazol-2-yl)-2,5-diphenyl tetrazolium bromide
N	Number of cells
N	Number of experiments
NEM	N-ethylmaleimide
NMJ	Neuromuscular Junction
OPA1	Optic Atrophy 1
PARL	Presenilin-associated rhomboid-like
PBS	Phosphate buffered saline
Pcp1	Processing of cytochrome c peroxidase protein 1
PCR	Polymerase chain reaction
PEG	Poly-ethylene glycol
PINK1	PTEN-induced putative kinase 1
<i>Rh4</i>	<i>Rhodopsin 4 gene</i>
RPM	Revolutions per minute
RNAi	RNA interference
SDS-PAGE	Sodium dodecyl sulfate polyacrylamide gel electrophoresis
SLP-2	Stomatin like protein-2
SNARE	Soluble N-ethylmaleimide-sensitive fusion protein attachment protein receptor
S2R ⁺	S2 receptor plus cells
TIFF	Tagged Image File Format
UAS	Upstream activation sequence
VDRC	Vienna <i>Drosophila</i> RNAi Centre
<i>W</i>	<i>Drosophila white gene</i>
<i>Y</i>	<i>Drosophila yellow gene</i>

Chapter 1: Introduction

Mitochondria are crucial for numerous cellular processes including energy metabolism, programmed cell death, cell signalling and metabolic pathways involving iron, lipids and amino acids. Over 1.5 billion years ago mitochondria evolved from a symbiotic relationship between free living aerobic α -proteobacteria and primitive eukaryotic cell (Bereiter-Hahn, 1990; de Duve, 2007). Majority of bacterial chromosome got incorporated in the genome of host eukaryotic cell but each mitochondrion also contains a few copies of the remnant chromosomes known as mtDNA (de Duve, 2007). Mitochondria are double membranous organelles consisting of the outer membrane and the inner membrane (Bereiter-Hahn and Voth, 1994). Mitochondrial inner membrane forms folding structures known as cristae that hold two aqueous compartments, the intermembrane space and the matrix. Mitochondria being the power house of the cell generate ATP through the Krebs's cycle in the matrix and oxidative phosphorylation across the inner mitochondrial membrane (Bereiter-Hahn, 1990; Bereiter-Hahn and Voth, 1994).

1.1 Mitochondrial dynamics

Initially, mitochondria were described as isolated membranous granular cytoplasmic compartments, however later it was found that mitochondria have a dynamic nature and show distinct morphologies (Lewis and Lewis 1914). However, the visualization of mitochondrial dynamics in live cells became possible by late 20th century, with the development of live imaging and mitochondrially targeted fluorescent proteins and dyes (Bereiter-Hahn et al., 1994; Nunnari et al., 1997). The dynamic behaviour of mitochondria involves mitochondrial shape changes and distribution of mitochondria in the cells. In mitochondrial fusion, an individual mitochondrion moving along the cytoskeleton meets another mitochondrion and undergoes merging of lipid bilayers and mixing of mitochondrial contents (Parone et al., 2008). Fusion allows mixing of heterogeneous mitochondrial components which contribute towards the maintenance and/or inter-complementation of mtDNA and distribution of proteins, nutrients and reorganization of membranes (Chen et al., 2005; Detmer and Chen, 2007b; Parone et al., 2008) (**Figure 1.1**). In contrast, an individual mitochondrion divides by fission producing smaller mitochondrial units separating out the damaged mitochondria which are removed from cell by mitophagy (Twig et al., 2008) (**Figure 1.1**). A balance of fusion and fission is important for varying physiological conditions of any cell (Olichon et al., 2003).

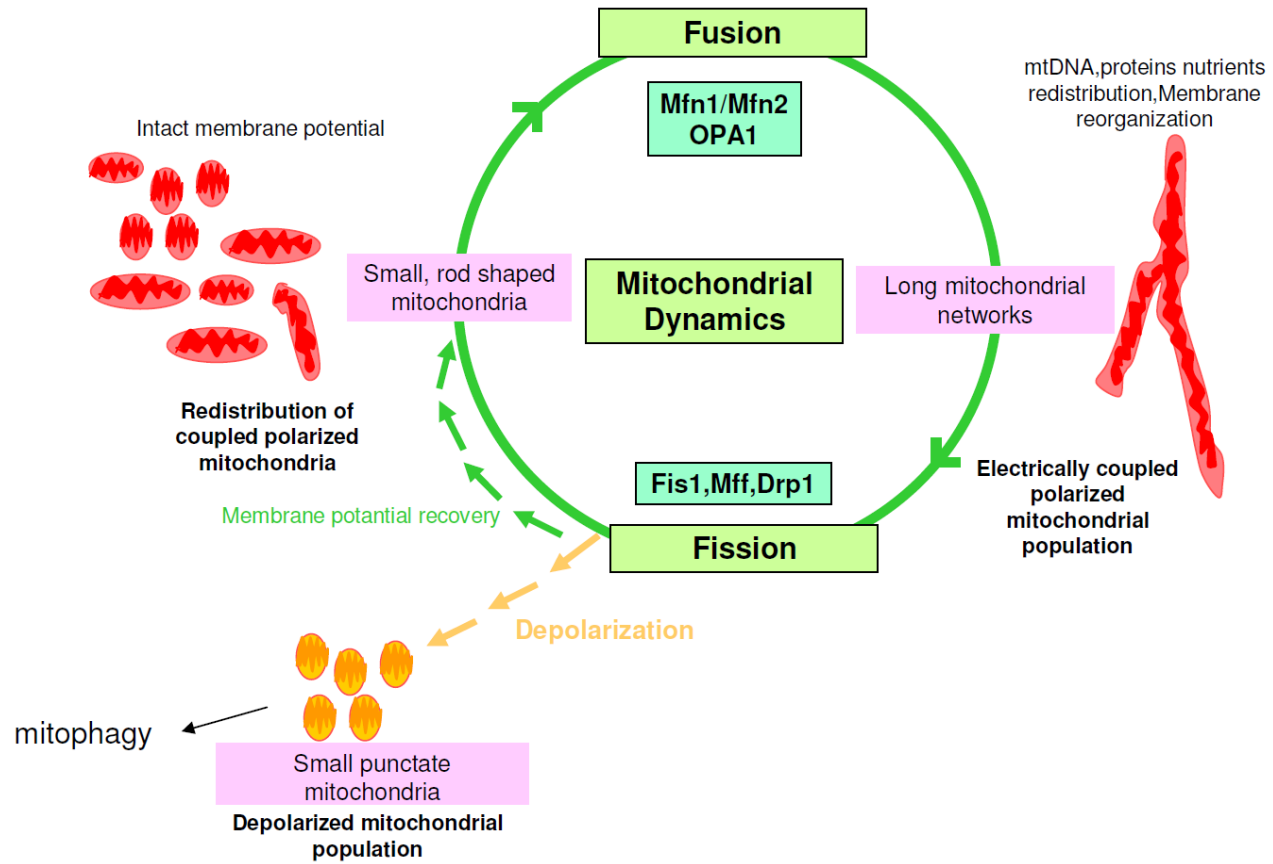


Figure 1.1: Mitochondrial Dynamics. Schematic of mitochondrial fusion and fission (adapted from Twig et al., 2008). Under normal conditions mitochondrial fusion and fission events depend on mitochondrial membrane potential. Mitochondrial fusion results in long mitochondria and mitochondrial networks with electrically coupled polarised mitochondria. Mitochondrial fusion is mediated by Mfn1, Mfn2 and OPA1. Mitochondrial fusion results in complementation of mtDNA, intermixing of mitochondrial proteins and nutrients and membrane reorganisation. Upon loss of mitochondrial membrane potential mitochondrial networks are broken down into smaller mitochondria. Mitochondrial fission is mediated by Drp1, Fis1 and Mff. The depolarised and damaged mitochondrial population is eliminated from the healthy mitochondrial population by mitophagy. Smaller mitochondria with intact membrane potential are kept and transported to the regions of energy requirement.

1.2 Mitochondrial Fusion

Mitochondrial fusion occurs in multiple steps. It involves tethering of mitochondrial membranes of adjacent mitochondria resulting in outer membrane fusion following the tethering of inner membranes and mixing of the matrix contents. Mitochondrial fusion provides a mechanism to maintain homogeneity within the organelle (Detmer and Chen, 2007b). The main fusion proteins are Mitofusins (Mfn1 and Mfn2) and Optic atrophy 1 (OPA1). Mfn1 and Mfn2 are outer mitochondrial membrane GTPases and share 63% amino acid identity (Koshiba et al., 2004). Both mediate fusion forming homodimers and heterodimers on adjoining mitochondria (Koshiba et al., 2004). Inner membrane fusion is primarily mediated by another GTPase, Opa1 (Cipolat et al., 2004).

1.2.1 Mfn1 and Mfn2

Drosophila melanogaster fuzzy onions (*Fzo*), was identified as the first fusion gene (Hales and Fuller, 1997). *Fzo* belongs to the family of dynamin-like GTPases that have homologues in eukaryotes from yeast to humans. During *Drosophila* spermatogenesis, *Fzo* initiates mitochondrial fusion forming giant mitochondrial structure known as Nebenkern, essential for sperm motility (Hales and Fuller, 1997). *Fzo* expression is restricted to the testes, however, a ubiquitously expressed *Drosophila* fusion mediator known as mitochondrial assembly regulatory factor (*Marf*), was later identified as *Fzo* homologue in *Drosophila* (Hwa et al., 2002). *Marf* has more general role in controlling mitochondrial outer membrane fusion in flies (Hwa et al., 2002). The expression and functional restrictions of fusion proteins as seen in flies has not been reported in yeast or higher eukaryotes. *Fzo1p* is the only factor for outer mitochondrial membrane fusion in yeast. Vertebrate orthologue for *Fzo* and *Marf* are two homologues Mitofusin 1 and Mitofusin 2 (*Mfn1* and *Mfn2*) (Santel and Fuller, 2001). Human *Mfn1* and *Mfn2* share 46% amino acid identity with *Drosophila* *Marf* and 31% amino acid identity with *Fzo*. A cladogram depicting the most parsimonious evolutionary relationship between mitofusin genes in species from *Drosophila* to man is available¹. The evolutionary distance between fly and man is too great to infer any meaningful evolutionary relationships between *Mfn* homologues and orthologues. *Drosophila Fzo*

¹ Ensembl gene tree for *Mfn* genes across species:
http://www.ensembl.org/Homo_sapiens/Gene/Compara_Tree?collapse=none;db=core;g=ENSG00000116688;r=1:12040238-12073571

and *Marf* are the result of a gene duplication event, but *Ciona* species apparently only have a single *Mfn* gene. All higher vertebrates including fish have at least two homologues. Thus based on this phylogenetic data we are able to deduce that *Mfn1* and *Mfn2* arose by a gene duplication event in the vertebrate lineage prior to the evolutionary branch leading to the fishes.

Mitofusins are present on the outer mitochondrial membrane and contain amino terminal GTPase domain, a coiled coil or heptad repeat domain 1 (HR1), a bi-partite transmembrane domain and a second coiled coil or heptad repeat domain 2 (HR2) in carboxy terminal (**Figure 1.2**). Bi-partite transmembrane domain of Mfn2 helps in anchoring the protein to the outer mitochondrial membrane with a small loop hanging in the middle in intermembrane space. The bi-partite transmembrane domain gives U-shape to the protein resulting in most of the protein facing cytosol. The topology of mitofusins is identical from yeast to higher eukaryotic cells indicating that the mitochondrial fusion remained conserved throughout evolution (Rojo et al., 2002). Fusion is mediated by tethering two opposing outer mitochondrial membranes of adjacent mitochondria through the formation of hairpin like structure by the HR2 domains of neighbouring mitochondria (Koshiba et al., 2004). These interactions are both homo dimeric (Mfn1-Mfn1 or Mfn2-Mfn2) and hetero-dimeric (Mfn1-Mfn2) in *trans* between two mitochondria (Detmer and Chen, 2007a). It is believed that mitofusins (Mfns) work similar to that of SNAREs proteins (soluble N-ethylmaleimide-sensitive fusion protein attachment protein receptors) and form inter or intra molecular interactions to tether the adjacent membranes followed by lipid bilayer destabilization by their hydrophobic domains and biochemical energy provided by GTP hydrolysis from GTPase domain (Chen and Scheller, 2001; Ishihara et al., 2004).

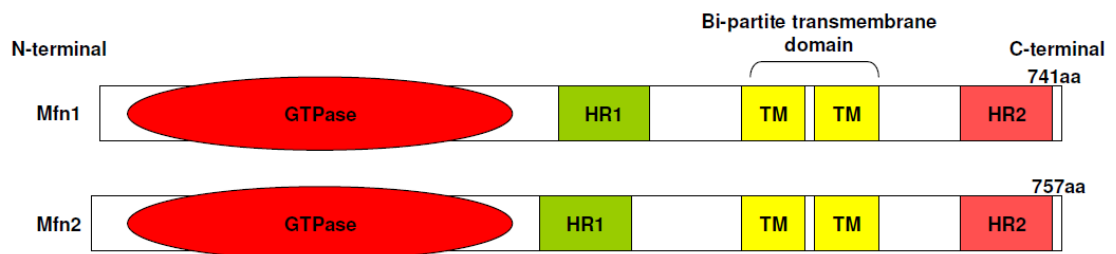


Figure 1.2: Schematic of Mfn1 and Mfn2 domain structures. GTPase: GTPase domain, HR1: Heptad repeat domain 1, TM: Bi-partite transmembrane domain, HR2: Heptad repeat domain 2. aa: amino acid residues.

The GTPase domain has catalytic regions and GTP binding regions (Santel et al., 2003). Mfn1 exhibits approximately 8 folds higher GTPase activity than Mfn2 (Ishihara et al., 2004). It is suggested that Mfn1 might be principally involved in mitochondrial tethering while Mfn2 participates only in the subsequent steps of outer membrane fusion (Ishihara et al., 2004). Cells lacking Mfn1 show smaller fragmented mitochondria that are unable to fuse, however Mfn2 deficient cells have larger and thicker mitochondrial fragments (Chen et al., 2003). Mfn1 overexpression showed enhanced mitochondrial networks while GTPase truncated Mfn1 or GTPase inactive Mfn1 expression showed mitochondria as trapped in a tethered state lacking mitochondrial fusion (Santel et al., 2003; Koshiba et al., 2004). GTPase dead mutant of Mfn2 displayed accumulation of docked mitochondrial intermediates (Eura et al., 2003). In contrast, mutations in HR2 domain of Mfn1 showed fragmented mitochondria (Koshiba et al., 2004). This suggests that GTPase domain and HR2 domains plays sequential steps during the fusion process. Additionally, Mfn2 is also present on endoplasmic reticulum (ER) and is involved in maintaining mitochondria-ER contact sites (de Brito and Scorrano, 2008). Silencing *Mfn2* affects both mitochondrial and ER morphologies (de Brito and Scorrano, 2008). Interestingly, besides their functional redundancy, the tissue expression patterns for Mfn1 and Mfn2 are different. Mfn1 is ubiquitously expressed and Mfn2 is a also ubiquitous protein but expressed at higher rates in brain, heart and skeletal muscles (Santel et al., 2003). Furthermore, Mfn2 reduced expression levels were found in obese and type 2 diabetic individuals and Mfn2 mutations are associated with Charcot-Marie-Tooth 2A and Hereditary motor and sensory neuropathy type VI (Zuchner et al., 2004; Bach et al., 2005).

1.2.2 OPA1

Optical Atrophy 1 (OPA1), a large GTPase, allows mitochondrial inner membrane fusion and involved in mitochondrial cristae remodelling (Cipolat et al., 2004; Ishihara et al., 2006). Mutations in OPA1 are associated with autosomal dominant optic atrophy (ADOA), a neuropathy of optic nerve (Alexander et al., 2000; Delettre et al., 2000). Additionally, in mammalian cells, knockdown of OPA1 showed fragmented mitochondria and aberrant inner membrane structures and were sensitive to apoptosis (Olichon et al., 2003; Griparic et al., 2004). OPA1 has a mitochondrial import sequence (MIS), protein anchoring transmembrane, first heptad repeat domain 1 (HR1), a GTPase domain, a middle domain and second heptad repeat domain 2 (HR2) (**Figure 1.3**).

In mammalian cells, alternative splicing results in eight OPA1 isoforms (Sato et al., 2003).

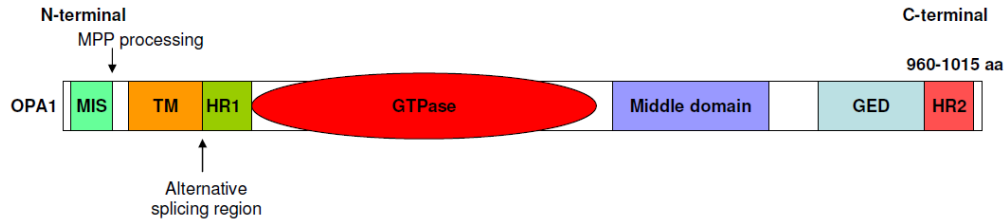


Figure 1.3: Schematic of OPA1 domain structure. MIS: Mitochondrial import sequence, MPP: Matrix-processing peptidase, TM: Transmembrane domain, HR1: Heptad repeat domain 1, GTPase: GTPase domain, Middle domain, GED: GTPase effector domain, HR2: Heptad repeat domain 2. aa: amino acid residues.

Matrix-processing peptidases (MPP) cleave MIS and imports OPA1 into the matrix. This cleavage results in mature or long-OPA1 isoform (L-OPA1). L-OPA1 is attached to the inner membrane by the transmembrane domain, hence, most of the protein protrudes in the intermembrane space. L-OPA1 is further processed into soluble-OPA1 (S-OPA1) by m-AAA protease, i-AAA protease and presenilin-associated rhomboid-like protease (PARL) (Cipolat et al., 2006; Song et al., 2007). Under normal conditions both isoforms are present (Griparic et al., 2007). In Mgm1p, yeast orthologue of OPA1, L-Mgm1p isoform forms homodimeric complexes *in trans* by the heptad repeats and tether opposing inner membranes and the mechanical energy to initiate lipid bilayer mixing is provided only by S-Mgm1p which is GTPase active (DeVay et al., 2009). Furthermore, apoptosis and mitochondrial depolarization results in enhanced proteolysis of L-OPA1 into S-OPA1 which leads to cytochrome c release and mitochondrial fragmentation (Ishihara et al., 2006).

1.2.3 Other proteins involved in mitochondrial fusion

In yeast, an outer mitochondrial membrane protein Ugo1p, is also required for the mitochondrial fusion (Sesaki and Jensen, 2001). Ugo1p links Fzo1p and Mgm1p through its carboxy-terminal exposed to the intermembrane space (Sesaki and Jensen, 2004). However, based on amino acid sequences no mammalian homolog of Ugo1p has been found yet. In mammalian cells Mfn1 interacts with OPA1 to facilitate the progress of outer membrane to inner membrane fusion therefore, it is still speculated that a functional homologue of Ugo1p may be involved (Cipolat et al., 2004).

Furthermore, a mitochondrial inner membrane protein; Prohibitin 2 is important for the maintenance of L-OPA1 (Merkwirth et al., 2008). Prohibitin 2 deficient cells showed fragmented mitochondria with disorganised cristae and introduction of L-OPA1 rescues the defect (Merkwirth et al., 2008). Another inner membrane scaffolding protein stomatin like protein-2 (SLP-2) regulates L-OPA1 stabilization and involved in stress induced cellular protective phenomenon of mitochondrial hyperfused morphology (Tondera et al., 2009). Additionally, SLP-2 also interacts with Mfn1 and Mfn2 and prohibitins to regulate outer and inner mitochondrial fusion during stress (Da Cruz et al., 2008; Tondera et al., 2009).

1.3 Regulation of mitochondrial fusion

Mitochondrial fusion is a well coordinated process initiating with outer membrane fusion and subsequently inner membrane fusion takes place. Mutations in the intermembrane loop present between two transmembrane domains of yeast Fzo1p showed loss of interaction of protein with the inner membrane leading to complete mitochondrial fusion failure (Fritz et al., 2001). In contrast, mutations in mitochondrial inner membrane proteins such as Opa1 and Mgm1p result into loss of mitochondrial inner membrane fusion only (Meeusen et al., 2006). Mitochondrial fusion is a synchronised process regulated by various factors and cellular signalling pathways or events as discussed below. **Figure 1.4** summaries various fusion regulating components.

1.3.1 Ubiquitination of Mfns

Regulating expression levels of fusion machinery is critical to maintain equilibrium between dynamic mitochondria. It has been shown in yeast, that an F-box

motif protein Mdm30 regulates the levels of Fzo1p by promoting its ubiquitylation (Escobar-Henriques et al., 2006). The modified ubiquitinated Fzo1p is then targeted by 26S proteasome for degradation (Cohen et al., 2008). Mdm30p mutants displayed fragmented mitochondria and suggest that it is essential for the normal mitochondrial morphology in yeast (Fritz et al., 2003). Various studies have shown that Mfn1 and Mfn2 levels are regulated by E3 ubiquitin ligase known as Parkin (Poole et al., 2010; Ziviani et al., 2010). It has been shown in *Drosophila* cells and mammalian cells that upon dissipation of membrane potential, Mfn1 and Mfn2 are polyubiquitinated and degraded in response to Parkin activation prior to mitophagy (Poole et al., 2010; Tanaka et al., 2010; Ziviani et al., 2010). Cells deficient with Parkin or PINK1; a mitochondrial kinase, resulted in elongated mitochondria. Furthermore, in *PINK1* and *parkin* mutant flies the steady-state levels of Marf is increased in contrast to decreased levels in *PINK1* and Parkin-overexpressing flies (Poole et al., 2010; Ziviani et al., 2010). It suggests that *PINK1*/Parkin pathway prevents or delays fusion as *PINK1* acts via its kinase activity to activate either Parkin and its recruitment to the depolarised mitochondria to process Mfns ubiquitylation or *PINK1* may directly act on Mfn to signal its removal via Parkin mediated ubiquitination and proteosomal degradation.

1.3.2 Bcl-2 family members

Bax and Bak, the two Bcl-2 family members, regulate mitochondrial fusion in both positive and negative manner. In healthy cells, cytosolic Bax and its homologue Bak interacts with Mfn1/Mfn2 and regulates the assembly of large complexes at the sites of mitochondrial fusion, thus positively progressing mitochondrial fusion (Karbowski et al., 2002; Karbowski et al., 2006; Hoppins et al., 2011). Bax interacts physically with Mfn2 (392-602 region of Mfn2) in yeast two-hybrid analysis. However, during apoptosis Bax dissociates from Mfn2, undergoes conformational changes to form apoptotic active form and translocates to the mitochondrial outer membrane (Karbowski et al., 2002). Bax/Bak double knockout cells showed short mitochondrial rods suggesting incompetency for efficient fusion (Karbowski et al., 2006). Additionally, Bcl-xL and Ced-9 also interact physically with mitochondrial fusion machinery by promoting mitochondrial fusion (Delivani et al., 2006; Hoppins et al., 2011). Together these findings propose a defined role for Bcl-2 family members as negative and positive regulators of mitochondrial fusion.

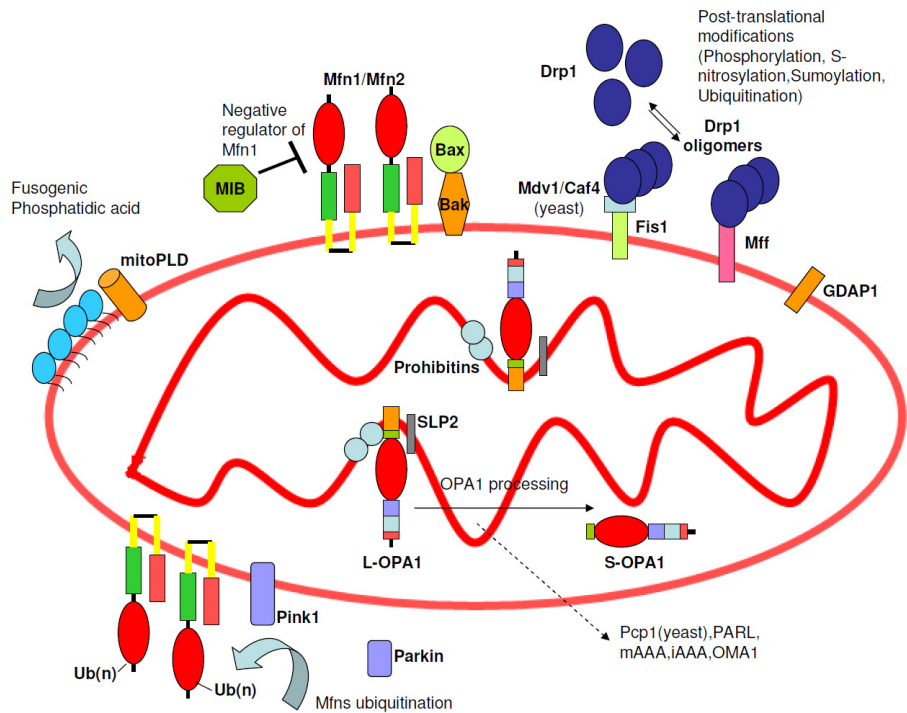


Figure 1.4: Schematic for the localization of fusion and fission machinery and various regulatory components. Mfn1 and Mfn2 are present on the outer mitochondrial membrane and mediate the outer membrane fusion by forming homo and heterodimers assembled in trans. PINK1/Parkin pathway influences mitochondrial fusion by Mfn ubiquitination and proteasomal degradation. Mitofusin binding protein (MIB) is a negative regulator of mitochondrial fusion by interacting with Mfn1. Bcl-2 family members Bax and Bak regulates Mfn1/Mfn2 both positively and negatively in response to cellular signals. Mitochondrial phospholipase D (mitoPLD) hydrolyses cardiolipin to produce fusogenic phosphatidic acid. Inner membrane fusion is mediated by long-OPA1 isoform (L-OPA1). L-OPA1 is anchored in inner membrane and forms homotypic complexes in *trans* to mediate fusion. L-OPA1 is cleaved to short-OPA1 isoform (S-OPA1) by pcp1 (in yeast) and proteases mAAA, iAAA, presenilin-associated rhomboid-like protease (PARL) and OMA1. Prohibitin-2 and SLP-2 are the inner membrane scaffolding proteins stabilising OPA1. Mitochondrial fission is facilitated by Drp1, a soluble cytosolic protein which is recruited by mitochondrial outer membrane anchored proteins Fis1 and Mff to oligomerise at the fission sites. Mdv1 and Caf4 are the adaptor proteins that enable Fis1 mediated Drp1 assembly on mitochondria in yeast. Drp1 undergoes various post-translational modifications such as phosphorylation, ubiquitination, sumoylation and S-nitrosylation for activation and recruited to mitochondria to induce fission. GDAP1 acts as a positive fission regulator.

1.3.3 Mitofusin binding protein

Mitofusin binding protein (MIB) acts as the negative regulator of Mfn1 activity. It belongs to a family of medium-chain dehydrogenase/reductase proteins carrying conserved coenzyme-binding domain. MIB functionally interacts with Mfns as Mfn1 expression rescues increased mitochondrial fission due to MIB overexpression in the cells (Eura et al., 2006). On the other hand, MIB knockdown leads to the formation of elongated mitochondria (Eura et al., 2006).

1.3.4 OPA1 proteases

Proteolytic processing of OPA1 by various proteases are also major regulatory mechanisms that control mitochondrial fusion and cristae morphology. As discussed in section 1.2.2 various mitochondrial proteases are responsible for maintaining the balance of OPA1 isoforms (**Figure 1.4**). In response to various cellular cues as mtDNA loss, low membrane potential, reduced ATP synthesis or apoptosis, L-OPA1 is processed to S-OPA1 by specific proteases (Ishihara et al; 2006; Griparic et al., 2007). L-OPA1 is processed by presenilin-associated rhomboid-like protein (PARL) to generate S-OPA1 in the intermembrane space which is important for maintaining close uniform cristae junctions (Cipolat et al., 2006). PARL indirectly regulates mitochondrial morphology as loss of PARL results in reduced levels of S-OPA1, cristae deformation and cytochrome c release. In addition three AAA-proteases; AFG3L2, Paraplegin and YmeL1 constitutively process OPA1 in the matrix and the inner membrane under various cellular responses and shift the balance towards S-OPA1 and resulting in enhanced mitochondrial fission (Duvezin-Caubet et al., 2007; Song et al., 2007). Also, in impaired mitochondria with low membrane potential Oma1 (overlapping activity with m-AAA protease), processes L-OPA1 to S-OPA1 and shuts down the fusion machinery of dysfunctional mitochondria (Ehse et al., 2009; Head et al., 2009). It suggests that such processing of OPA1 by Oma1 is a part of mitophagy process and works in concordance with Mfn ubiquitination and degradation, thus acting as quality control regulation of healthy mitochondrial population.

1.3.5 Lipids

Mitochondrial fusion involves tethering of adjacent mitochondria by Mfn1/Mfn2 followed by lipid bilayer destabilization and content mixing. Mitochondrial

phospholipase D (MitoPLD) is lipid modifying enzyme and a member of phospholipase D super family. It promotes mitochondrial fusion by the generation of phosphatidic acid at the outer mitochondrial membrane by hydrolysing mitochondria-enriched lipid known as cardiolipin (Choi et al., 2006). Phosphatidic acid is a fusogenic lipid which facilitates outer membrane proteins anchorage and membrane bending for fusion (Choi et al., 2006). These changes thermodynamically favour deformation and bilayer mixing. Additionally, cardiolipin is located in the inner membrane therefore it is suggested that phosphatidic acid promotes fusion where outer mitochondrial membrane is in close opposition to inner membrane. However, increased levels of phosphatidic acid acts as negative regulator of mitochondrial fusion and promotes mitochondrial fission (Huang et al., 2011). Increased levels of phosphatidic acid recruit phosphatase Lipin 1b to mitochondrial outer membrane. Phosphatase Lipin 1b then converts fusogenic phosphatidic acid into diacylglycerol which is not fusion efficient (Huang et al., 2011).

1.4 Mitochondrial Fission

To keep the balance between the dynamic behaviour of mitochondrial population, loner mitochondria and mitochondrial networks are broken into smaller units, by process know as mitochondrial fission. Firstly, mitochondrial fission is important for growth and proliferation of mitochondria as mitochondria can not be generated de-novo. Secondly, during mitosis fission allows segregation of pre-existing mitochondria to the daughter cells. Thirdly, fission generates small mitochondria that are easily transported to the distant regions of the cell. Last but not least fission is a quality control mechanism by which cell can get rid of old or damaged mitochondria (Twig et al., 2008). However, uncontrolled mitochondrial fission can result in mtDNA loss, impaired oxidative phosphorylation and increased susceptibility of cells to undergo apoptosis. Mitochondrial fission is mediated by Dynamin-related protein1 (Drp1) (Otsuga et al., 1998; Smirnova et al., 2001). Drp1 is a soluble cytosolic protein, however during fission Drp1 is recruited from cytosol by mitochondrial outer membrane anchored proteins Fis1/Mff to the fission sites (Otera et al., 2010). At the fission sites Drp1 assembles as oligomeric complexes enfolding around the fission spots to form a collar like structure (Smirnova et al., 2001). Such structure is maintained to constrict the lipid bilayer thus facilitating Drp1 to sever the membranes. Assembly of Drp1 from cytoplasm to the mitochondria is regulated by various post-translation modifications of Drp1 (**Figure 1.4**). Drp1 acts as a mechanochemical enzyme to break

the membranes by GTP hydrolysis (Smirnova et al., 2001). After the completion of fission Drp1 complexes are dissolved.

1.4.1 Dynamin-related protein1 (Drp1)

Drp1 is a member of the conserved dynamin superfamily and contains a GTPase domain, a middle domain (MID), variable domain (VD) and a GTPase effector domain (Otsuga et al., 1998; Mozdy et al., 2000; Smirnova et al., 2001) (**Figure 1.5**). MID is region for Drp1 oligomerization. Post translation modification sites are present in VD region of the protein. GED domain acts as GTPase activity regulator and is necessary for various protein interactions. Interestingly, GED folds back to interact in *cis* as well as in *trans* with the MID (Zhu et al., 2004). Cells lacking Drp1 lack mitochondrial fission and contain highly interconnected mitochondrial networks. *Drp1*^{K38A} GTPase mutant (inhibiting GTP binding) acts as dominant negative mutants by sequestering endogenous cytosolic Drp1 into uncharacterized cytosolic aggregates and inhibits fission (Smirnova et al., 2001). Drp1 activation as fission factor is regulated by various post-translational modifications such as phosphorylation, S-nitrosylation, ubiquitylation and sumoylation.

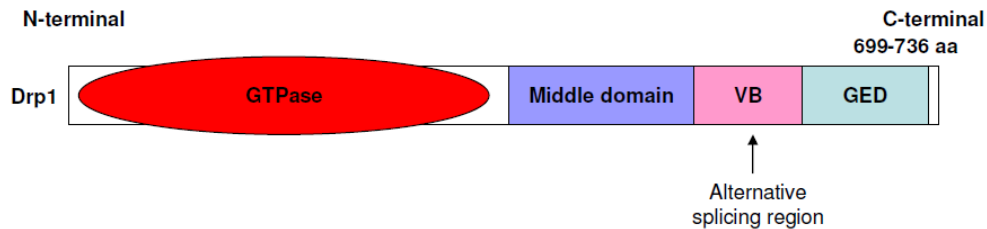


Figure 1.5: Schematic of Drp1 domain structures. GTPase: GTPase domain, Middle domain, VB: Variable domain, GED: GTPase effector domain. aa: amino acid residues.

Furthermore, various cellular stresses including treatment with the phorbol ester, increase of subcellular calcium and/or induction of apoptosis also results in enhanced Drp1 mitochondrial translocation and progression of mitochondrial fission (Labrousse et al., 1999; Frank et al., 2001; Breckenridge et al., 2003). A new born female with *Drp1*^{A395D} mutation presented several neurological disorder including abnormal brain

development, microcephaly and optic atrophy and died post 37 days of birth (Waterham et al., 2007).

1.4.2 Drp1 anchoring proteins: Fis1 and Mff

Fis1 (Fis1p in yeast) is a small protein present on the outer mitochondrial membrane with a short C-terminal tail protruding into the intermembrane space and N-terminal region containing multiple tetratricopeptide repeat (TPR) region facing the cytosol (Mozdy et al., 2000; Yoon et al., 2003) (**Figure 1.6**). In yeast, Dnm1p is recruited to the fission sites by Fis1p through WD-40 domain containing proteins: Mdv1p or Caf4p (Tieu et al., 2002; Griffin et al., 2005). Mdv1p and/or Caf4p are molecular adaptors. It has been suggested that in yeast Fis1p recruits Mdv1p from cytosol, where Mdv1p interacts with Dnm1p effector domains and stabilises Dnm1p oligomerization on the fission sites (Lackner et al., 2009). Caf4 also acts in similar manner, however in the presence of Mdv1p it has a dispensable role as it maintains residual levels of fission in yeast cells lacking Mdv1p (Griffin et al., 2005). In mammalian cells, Fis1 overexpression results in enhanced mitochondrial fragmentation (James et al., 2003; Yoon et al., 2003). Expression of Fis1 does not rescue Fis1p mutant phenotype in yeast (Stojanovski et al., 2004). Furthermore, in Fis1 knockdown cells Drp1 is still recruited to the fission sites suggesting another anchoring factor present in mitochondrial outer membrane (Lee et al., 2004). RNAi screen done in *Drosophila* cells to isolate novel proteins affecting mitochondrial morphology identified mitochondrial fission factor (Mff) (Gandre-Babbe and van der Blik, 2008). Mff have N-terminus heptad repeats exposed into the cytoplasm and a C-terminal transmembrane domain projecting into the intermembrane space of mitochondria and interacts transiently to Drp1 via cytoplasmic domain (Gandre-Babbe and van der Blik, 2008; Otera et al., 2010) (**Figure 1.6**). Mff is unable to initiate fission in Drp1 deficient mouse embryonic cells (MEFs) (Otera et al., 2010). Otera and colleagues have also shown Mff-dependent Drp1 recruitment in *Fis1* knockdown HeLa cells (Otera et al., 2010). Furthermore, overexpression of Mff produced stronger mitochondrial fragmentation as compared to Fis1-induced fragmentation (Otera et al., 2010). These findings indicate that, Mff has a major role in Drp1 recruitment and fission initiation and Fis1 is functionally dispensable for mitochondrial fission.

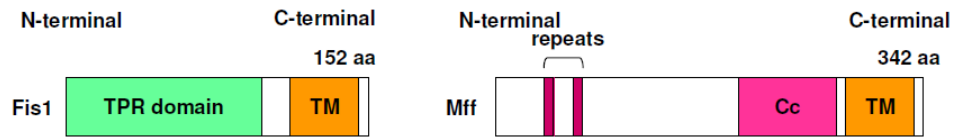


Figure 1.6: Schematic of Fis1 and Mff domain structures. TPR: Tetratricopeptide repeats, TM: Transmembrane domain, Cc: Coiled coil domain. aa: amino acid residues.

1.5 Regulation of mitochondrial fission

1.5.1 Post translational modifications of Drp1

Drp1-phosphorylation at two different conserved sites, serine 616 and 637 regulates the mitochondrial fission in an opposing manner. During cell cycle mitochondrial fission occurs at the early mitotic phase. Drp1 undergoes phosphorylation at serine 616 in the GED domain by CDK1/cyclin B at the initiation of S phase during mitosis (Taguchi et al., 2007). This enhances Drp1 activity and facilitates the segregation of mitochondria in new daughter cells as a result of mitochondrial division. Additionally, phosphorylation at Ser637 by Ca^{2+} /calmodulin-dependent protein kinase 1 α (PK1 α) increases transfer of Drp1 from cytosol to the mitochondria (Han et al., 2008). Ca^{2+} /calmodulin PK1 α is activated by intracellular calcium (Ca^{2+}) (Han et al., 2008). In contrast, Ser637 phosphorylation by cyclic adenosine monophosphate dependent protein kinase (PKA) inhibits the GTPase activity of Drp1 and restrains mitochondrial fission (Chang and Blackstone, 2007). Interestingly, increase in intracellular calcium levels activates the cytosolic phosphatase called calcineurin. Activated calcineurin dephosphorylates Drp1 at the Ser637, stimulates its translocation to the mitochondria and promotes mitochondrial fission (Cribbs and Strack, 2007).

In addition, Drp1-nitrosylation at Cys644 residue in GED domain has been shown to enhance mitochondrial fission in response to nitric oxide in neurons expressing β -amyloid protein (Cho et al., 2009). This modification results in enhanced GTPase activity and oligomer formation. It has been shown that Drp1 is also a target for Parkin mediated ubiquitination and degradation (Wang et al., 2011). In contrast, Drp1 sumoylation by small ubiquitin-like modifier (SUMO) protein promotes Drp1 assembly on mitochondria and protects Drp1 from ubiquitination and degradation (Harder et al., 2004). Also, a mitochondrially anchored SUMO E3 ligase known as mitochondrial

anchored protein ligase (MAPL) promotes mitochondrial fission (Braschi et al., 2009). However, sentrin/SUMO-specific protease 5 (SEN5) desumoylation of Drp1 is a negative regulator of mitochondrial fission (Zunino et al., 2007).

1.5.2 Other proteins involved in fission regulation

Endophilin B, a fatty acyl transferase belongs to endophilin protein family, containing amino-terminal BAR domain (Cuddeback et al., 2001). The BAR domain participates in the regulation of mitochondrial membrane curvature. Endophilin B knockdown displayed outer mitochondrial membrane abnormalities (Karbowski et al., 2004). Also, endophilin B1 has also been shown to interact with Bax and co-localizes with Bax during apoptosis (Cuddeback et al., 2001; Karbowski et al., 2002)

Ganglioside-induced differentiation activated protein 1 (GDAP1) is present on mitochondrial outer membrane and acts as a pro-fission factor (Niemann et al., 2005). *GDAP1* RNAi showed reduced mitochondrial fission (Wagner et al., 2009). Mutations in GDAP1 are also associated with a subtype of Charcot-Marie-Tooth disease. It involves the degeneration of Schwann cells and neurons of the peripheral nervous system (Niemann et al., 2005).

1.6 Biological significance of mitochondrial dynamics

1.6.1 Mitochondrial dynamics and maintenance of mtDNA

Mitochondrial fusion allows mitochondria to exchange lipid membranes and intra-mitochondrial content including mtDNA to maintain a healthy and relatively homogeneous mitochondrial population. The mtDNA genome encodes essential subunits of the respiratory complexes I, III and IV. In yeast, loss of the Fzo1p results in reduced mtDNA molecules and respiratory defects (Hermann et al., 1998). Likewise, Mgm1 mutant yeast also showed fewer mtDNA molecules (Jones and Fangman, 1992). Also, treating HeLa cells with carbonyl cyanide m-chlorophenylhydrazone (CCCP) showed mtDNA loss in 25% of cell population with fragmented mitochondria (Legros et al., 2004). MEFs deficient in either Mfn1 or Mfn2 exhibit reduced ATP levels and cell growth retardation (Chen et al., 2005; Chen et al., 2007). Also significantly large population of fragmented mitochondria contain fewer mtDNA nucleoids (Chen et al., 2007). In fusion-deficient *Mfn* double null (*Mfn1*^{-/-}, *Mfn2*^{-/-}) and *OPA1* null cells

majority of mitochondria lack mtDNA nucleoids (Chen et al., 2007). *Mfn* double mutant mice (MLC-Cre/dm, *Mfn1*^{-/-} and *Mfn2*^{-/-} knockout in skeleton muscles) showed severe developmental and metabolic defects and died early at the age of 6-8 weeks (Chen et al., 2010). These mice had 50%-70% low body weight as compared to control pups and increased serum lactate suggesting impaired oxidative phosphorylation. The skeletal muscles from these mice presented swollen fragmented mitochondria aggregated into clumps disrupting the alignment of myofibril arrays (Chen et al., 2010). These mice show a low copy number of mtDNA nucleoids (~250) as compared to age-matched controls (~3500) at 7-8 weeks age. They showed that mtDNA copy number decreases significantly with age in these mice. Mice with single allele of either *Mfn1* or *Mfn2* showed normal body weight and normal mtDNA nucleoids per cell at the age of 7-8 weeks (Chen et al., 2010). Additionally, MEFs lacking both *Mfn1* and *Mfn2* show lower mtDNA and this defect is restored by overexpression of either *Mfn1* or *Mfn2* (Chen et al., 2010). These findings emphasized that the defective mitochondrial fusion is responsible for the lower mtDNA copy number and respiratory defects probably due to loss of efficient oxidative phosphorylation.

Reactive oxygen species (ROS) generated as a by-product in oxidative phosphorylation can cause various kinds of mtDNA mutations and lesions (Rossignol et al., 2003). Mitochondrial fusion is a defence mechanism which allows mutations in different mtDNA genomes to complement each other and prevents respiratory dysfunction. As most of mtDNA mutations are recessive a cell can hold up to 60-90% of mtDNA mutations before being functionally compromised (Rossignol et al., 2003). A threshold level of pathogenic mtDNA is also a trait for mtDNA point mutations and deletions associated mitochondrial encephalomyopathies. It is suggested that a patient only shows the clinical signs of disease after the mutation threshold is crossed (Ono et al., 2001; Rossignol et al., 2003). *Mfn1*^{-/-} mice carrying *PolgA*^{D257A/D257A} mutation in mitochondrial DNA polymerase resulted in neonatal death (Chen et al., 2010). Furthermore, MEFs expressing *Mfn1*^{-/-}*PolgA*^{D257A/D257A} showed reduced respiratory capacity and ATP production due to reduced complex 1 activity (Chen et al., 2010). Complex 1 is more prone to mtDNA mutations as compared to other complexes because it has seven mtDNA encoded subunits (Chen et al., 2010).

1.6.2 Mitochondrial dynamics and development

Various studies carried out in-vivo from simple to complex organisms, has established that mitochondrial dynamics is important for normal development. *Caenorhabditis elegans* lacking either *Fzo1(Mfn)* or *Eat-3(OPAI)* present slow growth, reduced body size and high percentages of embryonic lethality (Breckenridge et al., 2008). *Marf* ubiquitous knockdown in flies result in larval lethality (Dorn et al., 2011). *Mfn1* and *Mfn2* knockout mice die in midgestation due to placental defects. *Mfn2*^{-/-} showed reduced number of trophoblast giant cells of placenta (Chen et al., 2003). To bypass embryonic lethality conditional knock out mice for *Mfn1* and *Mfn2* (*Meox-Cre/Mfn1^{loxP}* and *Meox-Cre/Mfn2^{loxP}*) were generated which express normal levels of Mfns in placenta. These mice were born viable. *Meox-Cre/Mfn1^{loxP}* mice displayed no physiological defects and were fertile. However, *Meox-Cre/Mfn2^{loxP}* showed severe movement defects and impaired cerebellar development (Chen et al., 2007). Similarly, *OPAI* deficient mice (*OPAI*^{-/-}) show embryonic lethality however heterozygous *OPAI* (*OPAI*^{-/+}) mice were viable but showed age-dependent degeneration of retinal ganglion cells that develop into visual impairment (Davies et al., 2007). Perturbations in mitochondrial fission also results in developmental defects as *Drp1* knocked down by RNAi in *Caenorhabditis elegans* showed embryos dying before reaching 100 cells stage (Labrousse et al., 1999). Homozygous *Drp1* mutant flies were semi lethal. Escaper flies were uncoordinated and showed numerous neurological defects (Verstreken et al., 2005). *Drp1* knockout model mice showed brain hypoplasia due to enhanced apoptosis in neural cortex (Ishihara et al., 2009).

1.6.3 Neurons and mitochondrial dynamics

Mitochondria are required in neurons to generate ATP for various specialized functions such as active pumping of Ca²⁺ across the plasma membrane and Ca²⁺ buffering in presynaptic and postsynaptic terminals (Hollenbeck and Saxton, 2005). Mitochondria usually concentrate in pre and post synaptic areas but are also evenly spaced in the remaining portions of axons and dendrites (Hollenbeck and Saxton, 2005; Saxton and Hollenbeck, 2012). Synaptic transmission requires active population of mitochondria to provide ample ATP for the maintenance of plasma membrane potential and recycling of neurotransmitters and vesicles (Saxton and Hollenbeck, 2012). Furthermore, sufficient mitochondrial content and mobility in dendrites is vital for various aspects of synaptogenesis including spine formation, synaptic plasticity and

protein translation, which are all high energy demanding processes. To meet the energy demand of various processes, mitochondria need to be placed near the sites of activity and it requires an active system for transport within the polarised neurons (Saxton and Hollenbeck, 2012). In neurons, mitochondria are distributed to various regions by active transport mediated by microtubules, actin filaments and motor proteins. Mitochondria travel by fast axonal transport at an average speed of 0.3–2.0 $\mu\text{m}/\text{sec}$ (~20–70 mm/day) (Sheng and Cai, 2012). Mitochondria move bidirectionally with frequent pauses. One-third of axonal mitochondria are found mobile in mature cultured neurons (Kang et al., 2008). Mitochondria containing high membrane potential move from the cell body in anterograde direction to synaptic regions with high metabolic demand (anterograde movement) and low membrane potential carrying mitochondria are transported to the cell body for repair by fusion or destruction by mitophagy (retrograde movement) (Martin et al., 1999; Hollenbeck and Saxton, 2005). Both kinds of transport require molecular motor proteins which attach to mitochondrion and pull it along microtubules. Motor proteins such as kinesin superfamily proteins (KIFs) and cytoplasmic dynein are involved in directed anterograde and retrograde transport of mitochondria respectively in axons (Pilling et al., 2006). Members of the kinesin-1 family (KIF5) are the primary anterograde motor and kinesin-3 family members; KIF16 and KLP6 have also been identified as mitochondrial motors (Tanaka et al., 2011). KIF5 moves along microtubules by hydrolysing ATP taking steps of ~17nm (Yildiz et al., 2004). Short range transport of mitochondria primarily in dendritic spines, growth cones and synapse boutons is mediated by actin filaments and myosin motor proteins (Bridgman, 2004). Number of adaptor and linker proteins that bind the mitochondria to the motor proteins has been identified. Milton is an adaptor protein that binds to the KIF5 heavy chain to anchor mitochondria to the motor protein in *Drosophila* (Stowers et al., 2002). TRAK1 and TRAK2 are mammalian orthologues of Milton. In addition Miro, a mitochondrial outer membrane protein, links mitochondria to Milton (Guo et al., 2005). Miro has two EF-hands which are the Ca^{2+} -binding regions. These hands mediate the protein to regulate mitochondrial transport in the cell. Two mammalian orthologues for Miro are Miro1 and Miro2. Currently, there are two proposed models by which Miro exerts its effects on mitochondrial mobility. According to one model, in the absence of Ca^{2+} Miro-Milton-KIF5 complex is involved in mitochondrial anterograde transport. However, in the presence of Ca^{2+} influx following synaptic activity, EF hands of Miro sequesters and binds Ca^{2+} . This results in change in conformation of Miro and blocks KIF5 binding to microtubules by directly binding to the KIF5 motor domain. This halts

mitochondrial movement and facilitates mitochondria to buffer local elevated levels of Ca^{2+} (Wang and Schwarz, 2009). The second model known as motor releasing model accounts that in presence of Ca^{2+} influx, Miro-Milton complex is released from KIF5 binding and mitochondrial movement is halted (Macaskill et al., 2009). Furthermore, syntabulin, RAN-binding protein 2 (RANBP2) and fasciculation and elongation protein zeta-1 (FEZ1) are among other adaptor proteins identified as important for mitochondrial anterograde transport and synapse docking (Cai et al., 2005; Ikuta et al., 2007; Cho et al., 2007). In contrast, retrograde transport machinery is less well characterised. Dynein binds to microtubules by its heavy chain and by its light chain protein TCTEX1, it binds to voltage-dependent anion-selective channel 1 (VDAC1) present at the outer mitochondrial membrane (Schwarzer et al., 2002). Dynactin, is another large complex that binds to both dynein and microtubules and facilitates retrograde transport of organelles including mitochondria (King and Schroer, 2000). Genetic interactions showed that anterograde motors and retrograde motors are also dependent on each other for effective bi-directional mitochondrial transport. Dynein has been found to be present on mitochondria moving in anterograde direction as well. Miro is also required along with dynein in *Drosophila* neurons for mitochondrial retrograde movement (Hirokawa et al., 1990; Russo et al., 2009). However, dynein-Miro association has not been demonstrated yet.

1.6.3.1 Mitochondrial fusion, fission and transport in neurons

The connections between mitochondrial dynamics and mitochondrial transport are becoming clear with recent research. It has been established that mitochondrial fusion and fission takes place in all parts of the neuron. Mitochondrial morphology is distinct in various regions of the neuron. Mitochondria mostly form loose networks in neuronal cell bodies, small rod shaped and spherical mitochondria are present in axons and neuromuscular junction (Li et al., 2004). These smaller discrete morphologies are important because transport machinery can easily carry smaller mitochondria as compared to large mitochondria. Perturbing mitochondrial dynamics in chick peripheral axons, either by overexpressing *Mfn1* or inhibiting *Drp1* by RNAi resulted in long immotile mitochondria (Amiri and Hollenbeck, 2008). In addition, *Drosophila Drp1* mutants result in neuromuscular junctions devoid of mitochondria (Verstreken et al., 2005). Also, *Drp1* mutant flies are unable to mobilize reserve pools of synaptic vesicles due to inadequate ATP supply from the few synaptic mitochondria present in boutons (Verstreken et al., 2005). Likewise, neuronal cell specific *Drp1* deficient mice die

within a day of birth and showed brain hypoplasia due to enhanced apoptosis in the deep cortical neuronal cell layer (Ishihara et al., 2009). These neurons are the early-born cells but die due to apoptosis before maturing into neurites and synapses and showed aggregated mitochondria within cell body and neurite processes in cultures (Ishihara et al., 2009). Similarly, *Miro* and *Milton* deficient flies have shown fewer mitochondria in axons and synapses, inefficient Ca^{2+} buffering and diminished synaptic activity (Stowers et al., 2002; Guo et al., 2005). Thus, such inadequacies result in insufficient energy distribution, impaired local Ca^{2+} buffering and inefficient synaptic vesicle mobilization from reserve pool resulting in impaired synaptic activity. However, overexpression of *Miro* showed enhanced mitochondrial fusion and increased mitochondrial density in dendrites (Koutsopoulos et al., 2010). Dynein has been shown to interact with Drp1 as dynein disruption also resulted in enhanced mitochondrial fusion (Varadi et al., 2004). Additionally, actin is also involved in the employment of Drp1 to mitochondria for fission (De Vos et al., 2005). In comparison, mutations in *Mfn2* have been linked to inherited peripheral neuropathy suggesting an important role of this pro-fusion protein in neurons (Verhoeven et al., 2006). Disease associated *Mfn2* mutations presented improper mitochondrial distribution in axons of motor neurons from transgenic mice (Detmer et al., 2008). Sensory neurons expressing CMT2A associated *Mfn2* mutations and/or loss of *Mfn2* (*Mfn2*^{-/-}) showed mitochondrial clustering in proximal axonal segments, reduced density of mitochondria in distal regions, slower anterograde and retrograde mitochondrial mobility with prolonged pauses in axons (Baloh et al., 2007; Misko et al., 2010). On the other hand, a unique role of *Mfn2* as mitochondrial transport mediator has also been reported by Misko and colleagues. *Mfn2* interacts with *Miro* 2 and *Milton* 1 (*Milton* homolog 1) and mediates mitochondrial transport in axons (Misko et al., 2010). It is suggested that *Mfn2*:*Miro*2:*Milton*1 complex regulates mitochondrial motor transport activity as *Mfn2*^{-/-} or *Miro*^{-/-} neurons showed mitochondria spend increased time paused in the axons (Misko et al., 2010). However, this study has claimed that disruption in transport does not appear to be a consequence of attenuated fusion thus suggesting a fusion independent role for *Mfn2* in the regulation of mitochondrial motility (Misko et al., 2010). A recent paper by same group has shown axonal degeneration in neurons expressing disease associated *Mfn2* mutations. They showed the improper distribution of mitochondria along the axons resulting in hypoxia leading to axonal degeneration and this defect was rescued by either expressing *Mfn1* or treatment with tetrodotoxin (sodium channel blocker) (Misko et al., 2012). PINK1/Parkin pathway that mediates

selective degradation of damaged mitochondria has been found to influence mitochondrial mobility by modifying Miro. PINK1 phosphorylates Miro, facilitates its degradation in parkin dependent manner and promotes mitochondrial retrograde transport (Wang et al., 2011). Interestingly, Mfns have also shown to undergo parkin mediated ubiquitylation, thus promoting mitochondrial fission and possibly mitophagy (Poole et al., 2010; Ziviani et al., 2010).

1.6.3.2 Mitochondrial dynamics and neurodegenerative diseases

Several studies in past decade have linked impaired mitochondrial dynamics, mitochondrial transport defects, perturbation of mitochondrial quality control and mitochondrial dysfunction to the pathogenesis of various neurodegenerative and neurological disorders (Schon and Przedborski, 2011). Alzheimer's disease (AD) is characterised by the neuronal death, neurofibrillary tau tangles and beta-amyloid (A β) plaques in cerebral cortex (Braak and Braak, 1991). Impaired axonal transport is involved in axonal degeneration in AD patients and is marked by the presence of axonal swellings containing aggregated mitochondria along with abnormal accumulation of other organelles, microtubules and motor proteins (Stokin et al., 2005). Additionally, mitochondrial dysfunction including decreased mitochondrial respiration, ROS generation, and decreased mitochondrial size with fragmented cristae structures are observed in brains of AD patients and AD mouse models (Spuch et al., 2012). Accumulation of soluble A β oligomers results in generation of nitric oxide by activating neuronal nitric oxide synthase due to increased intracellular Ca²⁺ via the pathological activation of NMDA receptors (Li et al., 2009). It has been shown that enhanced mitochondrial fragmentation in cultured cortical neurons and AD patient brains is due to activation of Drp1 GTPase activity by S-nitrosylation in the presence of nitric oxid (Cho et al., 2009).

Parkinson's disease (PD) is another common neurodegenerative disease, characterized by postural instability, resting tremor and walking difficulties caused by the loss of dopaminergic neurons in the substantia nigra and presence of Lewy bodies mainly consisting of α -Synuclein protein; a presynaptic protein (Abou-Sleiman et al., 2006). Post-mortem PD brain tissues showed impaired complex I activity and an increase in markers of oxidative stress (Schapira et al., 1990). However, mitochondrial association with PD came from studies done on autosomal recessive familial PD associated genes *PINK1* and *Parkin*. Initial studies in *Drosophila*, *in vivo* and in S2R⁺

cells, revealed that loss of *PINK1* or *Parkin* results in increased mitochondrial fusion. *In vivo* *PINK1* or *Parkin* mutant animals showed swollen and disrupted mitochondria in flight muscle while *PINK1* RNAi or *Parkin* RNAi in S2R+ cells showed tubular networks (Greene et al., 2003; Poole et al., 2008; Ziviani et al., 2010). Importantly, the *in vivo* phenotypes can be rescued by the over expression of *Drp1* or *Fis1* or loss-of-function mutations in *Mfn(Marf)* and *OPA1* showing that the effects on mitochondrial morphology may at least partially be responsible for the organismal phenotypes (Poole et al., 2008; Yang et al., 2008). In fact, *Mfn1* and *Mfn2* are targets for Parkin-mediated ubiquitination and degradation which explains the enhanced mitochondrial fusion seen in *Drosophila* cells (Ziviani et al., 2010; Tanaka et al., 2010). However, the literature on the effects of *PINK1* and *parkin* on mitochondrial morphology in vertebrates is conflicting. For example, while *PINK1* knockdown in COS-7 cells showed increased number of cells with long tubular mitochondria and fibroblasts derived from PD patients carrying *Parkin* mutations showed increased mitochondrial branching (Mortiboys et al., 2008; Yang et al., 2008). Different groups have demonstrated that *PINK1* or *Parkin* RNAi in HeLa cells or neuroblastoma cells results in mitochondrial fragmentation, which was enhanced by *Drp1* overexpression and rescued by the expression of *Drp1* dominant negative mutant (Exner et al., 2007; Lutz et al., 2009). While others have found no change in morphology in MEFs from *PINK1* KO mouse (Morais et al., 2009).

The possible reason for these discrepant findings are unclear but could likely reflect the greater complexity in regulation of cell biological processes found in higher organisms than in *Drosophila*. For instance, vertebrates may have additional compensatory or regulatory mechanisms that may further affect mitochondrial morphology in response to downstream effects of loss of *PINK1* or *Parkin*. Additionally, some variation may derive from technical differences used between model systems; for example, the degree of RNAi knockdown versus genetic knock-out in mammalian cells, or the genetic heterogeneity and other 'life history' factors inherent in patient cells. Overall, several studies support that *PINK1/Parkin* pathway has an influencing effect on mitochondrial dynamics but the degree of influence may depend on subtle variation in cellular circumstances, such as basal stress level (e.g. oxidative stress, mitochondrial stress).

Huntington's disease (HD) is gradually developing neurodegenerative disease resulting in cognitive function failure. It is caused by an abnormal polyglutamine

expansion (PolyQ) in the Huntingtin (HTT) gene (Walker, 2007). HTT is involved in the trafficking of mitochondria, ER, Golgi vesicles and late endosomes by forming complexes with both retrograde and anterograde motor machinery of the cell (Caviston and Holzbaur, 2009). In cultured neurons, mutant HTT decreases mitochondrial bi-directional transport (Trushina et al., 2004). This is due to the association between mitochondria and the N-terminal region of mutant HTT containing abnormal polyglutamate expansions, thus affecting the complex formation of mitochondria with transport machinery (Orr et al., 2008). In addition, fibroblast derived from juvenile and adult-onset HTT patient and neuronal cultures from HTT rat model showed increased fragmentation and abnormal cristae arrangement due to enhanced Drp1 dephosphorylation by increased calcineurin activity in the presence of mutant HTT (Costa et al., 2010; Song et al., 2011). Furthermore, expression of mitochondrial fission proteins Drp1 and Fis1 increases as compared to pro-fusion proteins in the presence of mutant HTT (Shirendeb et al., 2011).

Lastly, amyotrophic lateral sclerosis (ALS) is another late onset neurodegenerative disorder that involves gradual loss of motor neurons and demise of affected individual within 3-5 years of diagnosis (Tandan and Bradley, 1985). Mutations in the antioxidant enzyme Cu/Zn superoxide dismutase-1 (SOD1) are associated with familial ALS (Shaw, 2005). Neurons from ALS patients and transgenic mice expressing mutant SOD1 showed impaired axonal mitochondrial transport (De Vos et al., 2007; Shi et al., 2010). Furthermore, mouse models carrying SOD1 pathogenic point mutation displayed low mitochondrial quantity as well as degenerating mitochondria in the axons and dendrites (Wong et al., 1995; Collard et al., 1995). TAR DNA-binding protein 43 (TDP43) is also associated with familial and sporadic cases of ALS and cytoplasmic inclusions composed of massive accumulation of mitochondria in the motor neuron cell bodies of transgenic mice overexpressing wild-type human TDP43 (Shan et al., 2010).

1.7 Charcot-Marie Tooth (CMT) Diseases

Charcot-Marie-Tooth diseases (CMT) are the group of most common inherited neuromuscular disorders, involving degeneration of peripheral motor and sensory neurons. CMT affects up to 1 in 1200 individuals and in Europe its prevalence is 40 in 100,000 (Skre, 1974; Braathen et al., 2011). Based on clinical and pathological findings CMT is broadly subdivided in two major categories of neuropathies: demyelinating

neuropathy (CMT1) and axonal neuropathy (CMT2). The pathological difference between these two forms is degeneration and loss of supporting Schwann cells with secondary axonal loss in peripheral nerves in CMT1 and degeneration of only axons in peripheral nerves in CMT2. However, some mixed forms of CMT also exist which show both demyelination and axonal defects. To date, around 30 genes have been linked to CMT (Bucci et al., 2012). The genetics of CMT1, CMT2 and intermediate forms and functions of the causative genes are summarised in **Table 1.1**. However, it is still unclear that how mutations in mostly ubiquitously expressed genes result in exclusive demyelination and axonal degeneration of motor and sensory neurons of peripheral nervous system.

The clinical symptoms include distal limb weakness starting with lower extremities (leg and foot) and later progresses into distal upper extremities (hands and arms) as the disease advances, muscle atrophy, sensory loss, decreased reflexes, foot deformities including hammer toes and pes cavus with stepping gait and postural tremor (Zuchner et al., 2005; Verhoeven et al., 2006). Often mobility impairment and frequent falls lead to wheelchair dependency. As the clinical presentations for both types of CMTs are quite similar therefore they can be distinguished by electrophysiological criteria for nerve conduction analysis of the affected individuals. Patients with CMT1 usually present motor nerve conduction velocity of less than 38 m/s and individuals presenting a mild decrease to normal motor nerve conduction velocity of more than 38 m/s are characterised under CMT2 (Harding and Thomas, 1980). Moreover, various intermediate forms of CMT have been reported displaying intermediate and/or heterogeneous motor nerve conduction velocity readings ranging from 25 to 45 m/s. Although, CMTs are non-fatal neuropathies but no doubt they affect the quality of life of the affected individuals. There are no treatments available apart from orthopaedic shoes, crutches, supportive braces, wheel chair and foot surgery (Zuchner et al., 2005).

Table 1.1: Genetics of CMT

CMT Type	CMT subtype	Gene/locus	Function	Inheritance	Reference
Demyelinating	CMT1A	PMP22: peripheral myelin protein 22	Myelination	AD/AR	Suter et al., 1992
Demyelinating	CMT1B	MPZ: myelin protein zero	Myelination	AD/AR	Hayasaka et al., 1993
Demyelinating	CMT1C	LITAF: lipopolysaccharide-induced tumor necrosis factor	Protein degradation	AD	Street et al., 2003
Demyelinating	CMT1D	EGR2: early growth response protein 2	Transcription of genes involved in myelination	AD/AR	Warner et al., 1998
Demyelinating	CMT1F	NEFL: neurofilament light chain	Neuronal cytoskeletal	AD	Zuchner et al., 2004
Demyelinating	CMT4A	GDAP1: ganglioside-induced differentiation-associated protein 1	Mitochondrial dynamics	AR	Baxter et al., 2002
Demyelinating	CMT4B1	MTMR2: myotubularin-related protein 2	Dephosphorylation of phosphoinositides	AR	Bolino et al., 2000
Demyelinating	CMT4B2	MTMR13: myotubularin-related protein 13	Dephosphorylation of phosphoinositides	AR	Senderek et al., 2003a
Demyelinating	CMT4C	SH3TC2: SH3 domain and tetratricopeptide repeats-containing protein 2	Membrane trafficking	AR	Senderek et al., 2003b
Demyelinating	CMT4D	NDRG1: N-myc downstream regulated gene 1	Membrane trafficking	AR	Kalaydjieva et al., 2000
Demyelinating	CMT4F	PRX: periaxin	Schwann cells and nerve myelination	AR	Guilbot et al., 2001
Demyelinating	CMTX1	GJB1: gap junction protein β 1	Gap junction architecture	X-linked	Bergoffen et al., 1993

Table 1.1: Genetics of CMT

CMT Type	CMT subtype	Gene/locus	Function	Inheritance	Reference
Axonal	CMT2A1	KIFB1: kinesin family member β 1	Axonal transport	AD	Zhao et al., 2001
Axonal	CMT2A2	Mfn2: mitofusin 2	Mitochondrial fusion	AD	Zuchner et al., 2004
Axonal	CMT2B	RAB7: RAS-associated protein RAB7	Endosomal trafficking	AD	Verhoeven et al., 2003
Axonal	CMT2C	TRPV4: transient receptor potential cation channel subfamily V member 4	Cation channel	AD	Landouere et al., 2010
Axonal	CMT2D	GARS: glycyl-tRNA synthetase	RNA processing	AD	Antonellis et al., 2003
Axonal	CMT2E	NEFL: neurofilament light chain	Neuronal cytoskeleton	AD	Mersiyanova et al., 2000
Axonal	CMT2F	HSP27: heat shock protein 27	Mitochondrial molecular chaperon, neurofilament assembly	AD	Evgrafov et al., 2004
Axonal	CMT2G	12q12-q13	Not determined	AD	-
Axonal	CMT2H/K	GDAP1: ganglioside-induced differentiation-associated protein 1	Mitochondrial dynamics	AD/AR	Baxter et al., 2002; Cuesta et al., 2002
Axonal	CMT2I/J	MPZ: myelin protein zero	Myelination	AD	Hattori et al., 2003
Axonal	CMT2L	HSP22: heat shock protein 22	Mitochondrial molecular chaperon	AD	Irobi et al., 2004
Axonal	CMT2M	AARS: alanyl-tRNA synthetase	Protein translation	AD	Latour et al., 2010
Axonal	CMT2B1	LMNA: lamin A/C	Chromatin structure and organisation	AR	De Sandre-Giovannoli et al., 2002
Axonal	CMT2B2	MED25: mediator complex subunit 25	Transcription	AR	Leal et al., 2009
Axonal	CMTX5	PRPS1: phosphoribosylpyrophosphate synthetase 1	Nucleotide biosynthesis	X-linked	Kim et al., 2007

Table 1.1: Genetics of CMT

CMT Type	CMT subtype	Gene/locus	Function	Inheritance	Reference
Intermediate	CMTA	10q24.1-25.1	Not determined	AD	-
Intermediate	CMTB	DNM2: dynamin 2	Vesicle budding	AD	Zuchner et al., 2005
Intermediate	CMTC	YARS: tyrosyl-tRNA synthetase	Protein translation	AD	Jordanova et al., 2006

AD; Autosomal dominant, AR; Autosomal recessive

1.7.1 Charcot-Marie Tooth type 2A2 and Hereditary motor and sensory neuropathy type VI

Charcot-Marie Tooth type 2A (CMT2A/CMT2A2) is a subtypes of CMT2 linked with mutations in *mitofusin 2 (Mfn2)* (Zuchner et al., 2004; Verhoeven et al., 2006). Mutations in *Mfn2* account for 20-40% of all CMT cases and ~20% of all CMT2 cases (Zuchner et al., 2005; Verhoeven et al., 2006). More than 60 mutations in *Mfn2* have been reported to be linked with CMT2A (Cartoni and Martinou, 2009) (**Table 1.2**). Mutations are spread throughout the protein (Zuchner et al., 2004; Verhoeven et al., 2006) (**Table 1.2**). Heterozygous missense mutations predominate, but nonsense mutations and small in-frame deletions have also been reported (Zuchner et al., 2004; Engelfried et al., 2006; Verhoeven et al., 2006; Zuchner et al., 2006; Polke et al., 2011) (**Table 1.2**). The mode of inheritance is mainly autosomal dominant (Zuchner et al., 2005; Chung et al., 2006; Verhoeven et al., 2006). However, families with homozygous or compound heterozygous mutations have also been reported (Nicholson et al., 2008; Vallat et al., 2008; Calvo et al., 2009; Polke et al., 2011) (**Table 1.2**). The age at onset is diverse even within and among families ranging from 1 year of age to the 6th decade of life (Zuchner et al., 2006) (**Table 1.2**). Most of the affected individuals present symptoms in the 1st or 2nd decade of life, though; many remain mildly affected or non-symptomatic indicating low disease penetrance (Zuchner et al., 2006). Early onset CMT2A with progressive optic nerve dysfunction results in visual impairment and is classified under Hereditary Motor and Sensory Neuropathy type VI (HMSNVI) (Verhoeven et al., 2006; Zuchner et al., 2006). Usually the visual impairment gets worse, however, a subset of HMSNVI patient have shown recovery of vision later in life (Zuchner et al., 2006).

Biopsies taken from CMT2A patients sural nerves have shown loss of axons and thick myelinated nerve fibers (Vallat et al., 2008). One report has shown that early onset cases show 70% reduction in myelinated fibers as compared to the late onset CMT2A (Chung et al., 2006). Though onion bulb formations which are the layers of Schwann cell proliferation around a regenerating nerve fiber are not typical feature of CMT2A as compared to CMT1, however few patients have also shown some pseudo-onion bulbs in the clusters of regenerating nerve fibers (Chung et al., 2006; Vallat et al., 2008). Sural nerve biopsies have shown small spherical mitochondria aggregated abnormally near the periphery of the degenerating axons (Verhoeven et al., 2006; Vallat et al., 2008).

Table 1.2: *Mfn2* mutations associated with CMT2A and HMSNVI

Mutation	Heterozygous/homozygous	Region	Domain	Transmission	Phenotype	Onset	References
Gln45Arg	Heterozygous	Exon 3	Upstream region of GTPase domain	Autosomal dominant	CMT2	Unknown	Bienfait et al., 2007
Val69Phe	Heterozygous	Exon 4	Upstream region of GTPase domain	Autosomal dominant	CMT2	5-15	Zuchner et al., 2004
Leu76Pro	Heterozygous	Exon 4	Upstream region of GTPase domain	Autosomal dominant	CMT2	Unknown	Zuchner et al., 2004; Verhoeven et al., 2006
Leu92Pro	Heterozygous	Exon 4	Upstream region of GTPase domain	Autosomal dominant	CMT2	<10	Chung et al., 2006; Verhoeven et al., 2006
Arg94Trp	Heterozygous	Exon 4	Upstream region of GTPase domain	Autosomal dominant, De novo, Sporadic	CMT2, optic atrophy	3-17	Zuchner et al., 2004; Chung et al., 2006; Verhoeven et al., 2006; Zuchner et al., 2006; Cho et al., 2007; Calvo et al., 2009; Casasnovas et al., 2010
Arg94Gln	Heterozygous	Exon 4	Upstream region of GTPase domain	De novo	CMT2	<10	Zuchner et al., 2004; Kijima et al., 2005; Verhoeven et al., 2006; Neusch et al., 2007; Casasnovas et al., 2010
Ala100Gly	Heterozygous	Exon 4	GTPase	Autosomal dominant	CMT2	10	Verhoeven et al., 2006
Arg104Trp	Heterozygous	Exon 4	GTPase	Autosomal dominant	CMT2, optic atrophy	4-10	Del Bo et al., 2008; Calvo et al., 2009
Thr105Met	Heterozygous	Exon 5	GTPase	De novo	CMT2	3-15	Zuchner et al., 2004; Lawson et al., 2005; Chung et al., 2006
Gly108Arg + Arg707Trp	Compound heterozygous	Exon 5 + Exon 18	GTPase + Upstream of HR2 domain	Autosomal recessive	CMT2	<10	Calvo et al., 2009
Pro123Leu	Heterozygous	Exon 5	GTPase	Autosomal dominant	CMT2	2	Verhoeven et al., 2006
Gly127Asp	Heterozygous	Exon 5	GTPase	De novo	CMT2	10-50	Chung et al., 2006
Gly127Val	Heterozygous	Exon 5	GTPase	-	CMT2	48	Engelfried et al., 2006
H128R	Heterozygous	Exon 5	GTPase	De novo	CMT2	<5	Calvo et al., 2009
S156I	Heterozygous	Exon 5	GTPase	Sporadic	CMT2	<10	Calvo et al., 2009

Table 1.2: *Mfn2* mutations associated with CMT2A and HMSNVI

Mutation	Heterozygous/homozygous	Region	Domain	Transmission	Phenotype	Onset	References
Ala164Val + Thr362Met	Compound heterozygous	Exon 6 + Exon 11	GTPase + Downstream region of GTPase domain	Autosomal recessive	CMT2	3	Nicholson et al., 2008
His165Asp	Heterozygous	Exon 6	GTPase	Autosomal dominant	CMT2	4-20	Zhu et al., 2005
His165Tyr	Heterozygous	Exon 6	GTPase	Autosomal dominant	CMT2	10	Verhoeven et al., 2006
His165Arg	Heterozygous	Exon 6	GTPase	Autosomal dominant	CMT2	5-50	Zhu et al., 2005; Chung et al., 2006; Verhoeven et al., 2006; Cho et al., 2007
Ile203Met	Heterozygous	Exon 6	GTPase	Autosomal dominant	CMT2	10-40	Casasnovas et al., 2010
Thr206Ile	Heterozygous	Exon 7	GTPase	De novo	CMT2, optic atrophy	2-4	Verhoeven et al., 2006; Zuchner et al., 2006
Ile213Thr	Heterozygous	Exon 7	GTPase	Autosomal dominant	CMT2	5-12	Lawson et al., 2005
Asp214Asn + Cys390Arg	Compound heterozygous	Exon 7+ Exon 11	GTPase + Downstream region of GTPase domain	Autosomal recessive	CMT2	3	Nicholson et al., 2008
Phe216Ser+ Deletion exon 7-8	Compound heterozygous	Exon 7-8	GTPase	Autosomal recessive	CMT2, optic atrophy	1-2	Polke et al., 2011
Phe223Leu	Heterozygous	Exon 7	GTPase	Unknown	CMT2	<10	Kijima et al., 2005
Thr236Met	Heterozygous	Exon 7	GTPase	Unknown	CMT2	<10	Kijima et al., 2005; Calvo et al., 2009
Val244Met	Heterozygous	Exon 8	GTPase	Unknown	CMT2	~1	Kijima et al., 2005; Calvo et al., 2009
Arg250Trp + Arg400Stop	Compound heterozygous	Exon 8 + Exon 12	GTPase + Downstream region of GTPase domain	Unknown	CMT2	4	Verhoeven et al., 2006
Arg250Gln	Heterozygous	Exon 8	GTPase	Unknown	CMT2	21	Verhoeven et al., 2006

Table 1.2: *Mfn2* mutations associated with CMT2A and HMSNVI

Mutation	Heterozygous/homozygous	Region	Domain	Transmission	Phenotype	Onset	References
Pro251Ala	Heterozygous	Exon 8	GTPase	Autosomal dominant	CMT2, tremor	8-50	Zuchner et al., 2004
Ser263Pro	Heterozygous	Exon 8	Downstream region of GTPase domain	Autosomal dominant	CMT2	10-50	Chung et al., 2006; Cho et al., 2007
Val273Gly	Heterozygous	Exon 9	Downstream region of GTPase domain	Autosomal dominant	CMT2	5-28	Lawson et al., 2005
Arg274Gln	Heterozygous	Exon 9	Downstream region of GTPase domain	Unknown	CMT2	13	Zuchner et al., 2004
Gln276Arg	Heterozygous	Exon 9	Downstream region of GTPase domain	Autosomal dominant	CMT2, optic atrophy	10	Zuchner et al., 2006; Calvo et al., 2009
Gln276His	Heterozygous	Exon 9	Downstream region of GTPase domain	Autosomal dominant	CMT2	11-40	Casasnovas et al., 2010
His277Arg	Heterozygous	Exon 9	Downstream region of GTPase domain	Autosomal dominant	CMT2	10-15	Verhoeven et al., 2006
His277Tyr	Heterozygous	Exon 9	Downstream region of GTPase domain	Autosomal dominant	CMT2	>10	Calvo et al., 2009
Arg280His	Heterozygous	Exon 9	Downstream region of GTPase domain	Autosomal dominant	CMT2	11-42	Zuchner et al., 2004; Chung et al., 2006; Verhoeven et al., 2006
Phe284Tyr	Heterozygous	Exon 9	Downstream region of GTPase domain	Unknown	CMT2	10-50	Kijima et al., 2005
Gly298Arg	Heterozygous	Exon 9	Downstream region of GTPase domain	Autosomal dominant	CMT2	11-40	Casasnovas et al., 2010
Glu308X + Arg519Pro	Compound heterozygous	Exon 9+ Exon 15	Downstream region of GTPase domain + Downstream of HR1 domain	Autosomal recessive	CMT2, optic atrophy	1-3	Polke et al., 2011
Glu347Val	Heterozygous	Exon 11	Downstream region of GTPase domain	Unknown	CMT2	<10	Engelfried et al., 2006
Ser350Pro	Heterozygous	Exon 11	Downstream region of GTPase domain	De novo	CMT2	3	Cho et al., 2007

Table 1.2: *Mfn2* mutations associated with CMT2A and HMSNVI

Mutation	Heterozygous/homozygous	Region	Domain	Transmission	Phenotype	Onset	References
Lys357Asn	Heterozygous	Exon 11	Downstream region of GTPase domain	De novo	CMT2	~1	Kijima et al., 2005
His361Tyr	Heterozygous	Exon 11	Downstream region of GTPase domain	De novo	CMT2, optic atrophy	1	Zuchner et al., 2006
Thr362Met	Heterozygous	Exon 11	Downstream region of GTPase domain	Autosomal dominant	CMT2	10-50	Chung et al., 2006
Thr362Met+ in frame Lys38 deletion	Compound heterozygous	Exon 11	Downstream region of GTPase domain	Autosomal recessive	CMT2, optic atrophy	1-3	Polke et al., 2011
Arg364Pro	Heterozygous	Exon 11	Downstream region of GTPase domain	Autosomal dominant	CMT2	<5	Calvo et al., 2009
Arg364Gln	Heterozygous	Exon 11	Downstream region of GTPase domain	Sporadic	CMT2	>10	Calvo et al., 2009
Arg364Trp	Heterozygous	Exon 11	Downstream region of GTPase domain	Autosomal dominant	CMT2, optic atrophy	1	Chung et al., 2006; Zuchner et al., 2006
Met376Thr	Heterozygous	Exon 11	Downstream region of GTPase domain	Autosomal dominant	CMT2	10-50	Chung et al., 2006
Met376Ile	Heterozygous	Exon 11	Downstream region of GTPase domain	Autosomal dominant	CMT2	22, 35	Engelfried et al., 2006; Verhoeven et al., 2006
Met376Val	Heterozygous	Exon 11	Downstream region of GTPase domain	Autosomal dominant	CMT2	11-40	Casasnovas et al., 2010
Leu379-Met381del	Heterozygous	Exon 11	Downstream region of GTPase domain	Autosomal dominant	CMT2	3	Verhoeven et al., 2006
Ala383Val	Heterozygous	Exon 11	Downstream region of GTPase domain	Autosomal dominant	CMT2	10-50	Muglia et al., 2007
Gln386Pro	Heterozygous	Exon 11	Downstream region of GTPase domain	De novo	CMT2	1.5	Verhoeven et al., 2006
Arg418Stop	Heterozygous	Exon 12	HR1	De novo	CMT2, optic atrophy	1-4	Zuchner et al., 2004; Zuchner et al., 2006

Table 1.2: *Mfn2* mutations associated with CMT2A and HMSNVI

Mutation	Heterozygous/homozygous	Region	Domain	Transmission	Phenotype	Onset	References
Glu424Gly	Heterozygous	Exon 12	HR1	Unknown	CMT2	<10	Kijima et al., 2005
Arg468His	Heterozygous	Exon 14	Downstream of HR1 domain	Autosomal dominant	CMT2	20-50	Engelfried et al., 2006; Casasnovas et al., 2010
Phe665Ser	Heterozygous	Exon 17	Downstream of HR1 domain	Autosomal dominant	CMT2	<10	Calvo et al., 2009
Val705Ile	Heterozygous	Exon 18	Upstream of HR2 domain	Unknown	CMT2	6	Engelfried et al., 2006
Arg707Trp	Homozygous	Exon 18	Upstream of HR2 domain	Autosomal dominant	CMT2	2	Nicholson et al., 2008
Leu710Pro	Heterozygous	Exon 18	Upstream of HR2 domain	Unknown	CMT2	6	Verhoeven et al., 2006
Trp740Cys	Heterozygous	Exon 19	HR2	Autosomal dominant	CMT2	<10	Calvo et al., 2009
Trp740Ser	Heterozygous	Exon 19	HR2	Autosomal dominant	CMT2	5-52	Zuchner et al., 2004; Verhoeven et al., 2006
Leu745Pro	Heterozygous	Exon 19	HR2	Autosomal dominant	CMT2	>10	Calvo et al., 2009
Met747Thr	Heterozygous	Exon 19	HR2	De novo	CMT2	<10	Calvo et al., 2009
Gln751Stop	Heterozygous	Exon 19	HR2	De novo	CMT2	4-5	Verhoeven et al., 2006
Leu753frame shift and stop codon at 764	Heterozygous	Exon 19	HR2	Unknown	CMT2	62	Engelfried et al., 2006

1.7.2 Mitochondrial morphology in patient derived fibroblasts

In recent year mitochondrial morphology has been analysed in fibroblasts derived from CMT2A patients. Loiseau et al studied mitochondrial morphology in patients carrying *Mfn2* heterozygous mutations *Mfn2*^{M21V}, *Mfn2*^{R364W} and *Mfn2*^{A160T} and reported normal mitochondrial network morphology. However, they reported energetic metabolic defects in patient fibroblasts. They showed reduced mitochondrial respiratory control ratio due to increased oligomycin-insensitive respiration, reduced membrane potential and reduced oxidative phosphorylation efficiency (ATP production/oxygen consumption) (Loiseau et al., 2007). In another report, fibroblasts from CMT2A patients carrying *Mfn2* GTPase domain mutations *Mfn2*^{T105M}, *Mfn2*^{I213T}, *Mfn2*^{F240I}, *Mfn2*^{V273G} and one mutation in the HR2 domain *Mfn2*^{L734V} were analysed for mitochondrial morphology and fusion capacity (Amiott et al., 2008). This report also showed normal mitochondrial morphology with efficient mitochondrial fusion occurring. Also they reported no difference in *Mfn2* expression levels, mtDNA content and respiratory capacity.

Recently, another group has shown that fibroblasts derived from CMT2A patient carrying *Mfn2* heterozygous mutation *Mfn2*^{R94Q} displayed enhanced fusion with increased branching and mitochondrial networks (Chevrollier et al., 2012). This is the first time any group has quantified the mitochondrial morphology using a computerized analysis (in this case Imaris FilamentTracer software) for the CMT2A fibroblasts. This report is in opposition to what Chan and colleagues showed by expressing *Mfn2*^{R94Q} in *Mfn2* null MEFs (Detmer and Chan, 2007a). It is also important to mention that MitoCharc mice carrying *Mfn2*^{R94Q} mutation has also shown no mitochondrial morphology defects in motor neuron soma and axon.

Another recent report has shown fragmentation of mitochondrial networks in fibroblasts carrying novel *Mfn2* heterozygous mutation *Mfn2*^{D210V}, however this mutation is associated with Optic atrophy ‘plus’ phenotype (Rouzier et al., 2012). This report has shown reduced *Mfn2* expression in patients carrying D120V mutation but not in patients carrying another classical mutation *Mfn2*^{A166T}. In addition *Mfn2*^{D120V} patients also carry multiple mtDNA deletions in muscles, thus adding *Mfn2* to the list of genes responsible for mitochondrial myopathy. Muscle biopsy showed enlarged swollen mitochondria with paracrystallin inclusions. Biochemical analysis from muscles and

fibroblasts showed respiratory impairment due to complex IV deficiency.

1.7.3 In-vitro analysis of CMT2A associated *Mfn2* mutations

PEG fusion assays carried out in double *Mfn* null MEFs showed that CMT2A associated mutations *Mfn2*^{R94Q}, *Mfn2*^{R94W}, *Mfn2*^{T105M}, *Mfn2*^{P251A} and *Mfn2*^{R280H} failed to induce mitochondrial fusion, however other common CMT2A mutation *Mfn2*^{V69F}, *Mfn2*^{L76P}, *Mfn2*^{R274Q} and *Mfn2*^{W740S} have normal fusion activity (Detmer and Chan, 2007a). As discussed earlier, either *Mfn1* or *Mfn2* knockout MEFs show fragmented and aggregated mitochondrial morphology. Interestingly *Mfn2*^{R94Q} expression rescued mitochondrial fragmentation in *Mfn2* null MEFs but not in *Mfn1* lacking MEFs. This indicates that CMT2A-associated *Mfn2* alleles (here *Mfn2*^{R94Q} which is unable to initiate fusion on its own) are able to form fusion capable complexes with wild-type *Mfn1* by forming *Mfn1*/*Mfn1* and *Mfn1*/*Mfn2* (CMT2A allele) complexes and not with wild-type *Mfn2* (Detmer and Chan, 2007a). Furthermore, overexpression of CMT2A-associated *Mfn2* mutations in dorsal root ganglion neurons results in mitochondrial aggregation in cell body and reduced number of mitochondria in distal axons (Baloh et al., 2007). Also, *Mfn1* overexpression in motor neurons rescues the deficient mitochondrial transport associated with *Mfn2*^{CMT2A} alleles (Misko et al., 2010).

It is still not clear that how *Mfn2* mutations cause axonal degeneration, it can also be presumed that low *Mfn1* expression in peripheral neurons may result in defective mitochondrial fusion and/or transport that could potentially result in many structural and metabolic complications.

1.7.4 Transgenic models for CMT2A

Transgenic mouse expressing *Mfn2* GTPase mutation T105M in motor neurons under the control of HB9 motor neuron promoter has been reported to show gait defects and severe muscle atrophy due to axonal degeneration (Detmer et al., 2008). Motor neurons showed improper mitochondrial distribution with few mitochondria in axons which also form occasional clumps. However, heterozygous *Mfn2*^{T105M} mice were asymptomatic with no muscle atrophy and motor neuron degeneration (Detmer et al., 2008). This is also in contrast to human disease as only a single copy of *Mfn2* mutants is sufficient to cause neuropathy in humans. Additionally, sural nerve biopsies from CMT2A patients have shown the aggregation of mitochondria in the distal part of axons

but *Mfn2*^{T105M} homozygous mice have shown few mitochondria in distal axon regions (Vallat et al., 2008; Funalot et al., 2009). Also, transgenic mice expressing *Mfn2*^{R94Q} mutation in neurons develop late-onset neuropathy showing locomotion impairments and gait defects. Histopathological analysis of sciatic nerves has shown an increased mitochondrial density in the distal part of axons in addition to decrease in axonal size (Cartoni et al., 2010). Likely explanations for increased density of mitochondria in distal axonal regions might be due to defective retrograde transport of mitochondria leading to accumulation of mitochondria in distal regions or an enhanced mitochondrial fission or both. In addition *Mfn2* knockdown in zebrafish results in developmental defects and motility impairments (Vettori et al., 2011). Recently, our group has also reported that loss of function mutations in *Mfn2* results in motor deficit in zebrafish probably due to impaired mitochondrial axonal transport (Chapman et al., 2013).

In the prospect of all the major advancement in the understanding the pathogenesis of CMT2A and HMSNVI it is still not clear how mutations in *Mfn2* result in the cell specific degeneration of peripheral motor and sensory neurons. There are many questions still needed to be answered for example is mitochondrial dynamics is disturbed in these patients, is mitochondrial axonal transport is altered, is mitochondrial quality control mechanisms are disturbed etc. Studying these mechanisms in-vivo in patient derived cells and animal models would aid in the better understanding of disease pathology and development of potential treatments.

1.8. *Drosophila melanogaster* as a model system

The fruit fly *Drosophila melanogaster* has been successfully used as a model organism in the fields of genetics, developmental biology, neurobiology and pathophysiology. As a result of collaboration between Berkeley *Drosophila* Genome Project and Celera genomics *Drosophila melanogaster* genome sequence was completed in 2000 (Celniker, 2000). Genome size is approximately 180 Mb encoding approximately 13600 genes (Adams et al., 2000). Interestingly, 60% of human disease genes have orthologues in *Drosophila* making them a powerful system to study disease genetics and pathology in-vivo (Celniker, 2000; Rubin and Lewis, 2000).

Drosophila melanogaster has only four pairs of chromosomes, three autosomes and one sex chromosome. Female flies are homozygous for X chromosome (X/X) with a ratio of 1. Males are considered hemizygous as they have only one X chromosome

(X/Y) and the ratio 0.5. Y chromosome contains few genes that are required for sperm differentiation (Bridges, 1916). Furthermore, recombination during meiosis is absent in male flies thus proving useful for genetic studies (Greenspan, 2004). The important genetic tools available in *Drosophila* are balancer chromosomes and phenotypic markers. Balancer chromosomes carry the normal sequence in a jumbled up manner that is due to a lot of inversions, chromosomes are unable to cross over with their homologues during meiosis. In addition balancer chromosomes also carry an easily identifiable marker (Greenspan, 2004). This is helpful in maintaining the stocks of homozygous lethal alleles in a heterozygous state without recombination.

Many molecular pathways and several aspects of cell biology including gene expression, neural connectivity, organogenesis, cell signalling and cell death are similar in both flies and humans. The main reason for studying human diseases using *Drosophila* as an in-vivo model is because unbiased genetic screens to identify and analyze the components of pathological pathways can be performed. Forward genetic screens and reverse genetic approaches are typical method to study disease pathology in flies. Large amount of screening is necessary in forward genetic approaches to isolate the mutant of interest and such screens are done easily using various standard protocols in small set up (Celotto and Palladino, 2005). In reverse genetic approach the human diseases are modelled in *Drosophila* either by making transgenic flies expressing human genes or by targeting loss of function in fly orthologues of respective gene. In this approach using transgenic flies with the help of UAS-GAL4 system one can down regulate or over-express any gene in tissue specific pattern to analyze the phenotype (Brand and Perrimon, 1993; Johnston, 2002). Furthermore, UAS-GAL4 system allows expression of fluorescent proteins to be expressed in various tissue compartments in addition to tagging cellular organelles and studying their physiology in live or fixed samples (Johnston, 2002).

On further practical basis *Drosophila* rearing needs less care and maintenance as flies can easily be grown on yeast agar food in small plastic vials or bottles. Flies have short generation time normally 10 days at 25°C and have easily recognizable morphology of all the developmental stages. Virgin adult females can be distinguished easily to collect and use in genetic crosses. People have successfully developed low cost, easily performed and highly informative various every day assays such as larval locomotion assay, adult climbing and flight assays and longevity analysis.

Over the past years *Drosophila melanogaster* has been used extensively and successfully to study neurodegeneration in various common neurodegenerative diseases such as Parkinson's disease, Alzheimer's disease and Huntington disease.

1.9 Aims and Objectives of the PhD Project

The aim of the PhD project was to further investigate the role of *Mfn2* in mitochondrial morphology. CMT2A and HMSNVI patient fibroblasts and *Drosophila melanogaster* were used as in-vivo model systems to study this cellular phenomenon. We aimed to test the hypothesis that pathogenic mutations in *Mfn2* could lead to alterations in mitochondrial morphology. Enhanced fusion leads to longer mitochondria often making connections with each other forming mitochondrial networks and increased fission results in fragmented mitochondria. This balance is maintained by mitochondrial fusion and fission factors which are tightly regulated, since mitochondrial dynamics is considered to be important for a plethora of cellular processes such as energy production, calcium signalling, calcium buffering and apoptosis. To examine the effects of mutant *Mfn2* on mitochondrial morphology, skin fibroblasts derived from CMT2A and HMSNVI patients carrying *Mfn2* heterozygous mutations were used. *Mfn2* is involved in mitochondrial outer membrane fusion, suggesting that mitochondrial fusion may be defective in CMT2A and HMSNVI; however this remains to be confirmed. There are a few studies reporting mitochondrial morphological abnormalities in sural nerve biopsies done for CMT2A and HMSNVI patients (Verhoeven et al., 2006; Vallat et al., 2008). However, these nerve cells are not easily and readily accessible and not ideal to study the mitochondrial morphology in a large number of patients to profile mitochondrial morphology defects in CMT2A and HMSNVI. In recent years, researchers have successfully used patient derived skin fibroblasts as cellular model to analyse mitochondrial morphology and bioenergetic defects for various neurodegenerative diseases (Auburger et al., 2012). These fibroblasts are also ideal cells to study mitochondrial morphology as they carry the genetic and environmental factors which the patients were exposed to in their lifetime. Thus these cells will help us to better understand the mitochondrial morphological defects if any present in CMT2A and HMSNVI patients and to carry out various cellular assays to quantify the defects.

The second objective was to characterise ethacrynic acid (EA), a potent mitochondrial fusion-inducing compound identified previously by Soltys and Gupta (Soltys and Gupta, 1994) and also identified in the drug screen performed as part of

my PhD. EA treatment results in increased mitochondrial length and mitochondrial networks in cultured cells. Soltys and Gupta suggested that the cysteine alkylating nature of EA might be responsible for the increased mitochondrial fusion. However, they did not characterise the cellular targets and mechanism through which EA promotes mitochondrial fusion. Therefore, in this project I wanted to extend this work by characterising EA and seeing its effect on mitochondrial morphology under increased mitochondrial fission. Also, as a part of on-going drug screen to identify the compounds affecting mitochondrial morphology and increasing mitochondrial fusion, we in the department wanted to develop a potential treatment for fusion defective disorders and/or a bench tool to study mitochondrial dynamics. Having such goals are important for commercial and economic growth of the department which is appreciated in SITraN.

The third objective of the project was to characterise *Drosophila* Mitofusin (Marf). *Drosophila* Marf has been studied before in various genetic interaction studies relating to the PINK1/Parkin pathway involved in mitochondrial dynamics (Poole et al., 2008; Ziviani et al., 2010). In the beginning of my PhD, involvement of Marf in fly development and locomotion was not characterised, therefore, we aimed to generate *Marf* transgenic and genetic mutants and study the effect on development and locomotion. Also, *Drosophila* provides an opportunity to study mitochondrial morphology in motor neurons easily, offering an additional opportunity to study cellular processes in intact animals under physiological conditions.

Chapter 2: Materials and Methods

2.1 Maintenance of tissue culture cell lines

2.1.1 Solutions

Fetal Calf serum (FCS)

10% FCS (Lonza), 10% FCS (Invitrogen)

L-glutamine

Stock concentration: 200mM L-glutamine (Lonza)

Working concentration: 2mM L-glutamine

1% Pen-Strep

Stock concentration: 10,000UI Penicillin and 10,000µg/ml Streptomycin (Lonza)

Working concentration: 100UI/ml penicillin, 100µg/ml streptomycin

Sodium Pyruvate Solution

Stock concentration: 100mM sodium Pyruvate Solution (Lonza)

Working concentration: 1mM sodium Pyruvate Solution

Minimum Essential Medium non essential amino acids

Stock concentration: 10mM non-essential amino acids (Lonza)

Working concentration: 0.1mM non essential amino acids

Minimum essential medium vitamins

Stock concentration: 10mM Minimum essential medium vitamins (Lonza)

Working concentration: 0.1mM Minimum essential medium vitamins

Minimum Essential Medium (MEM) for human fibroblasts culture

MEM with Earle's salts (Lonza) supplemented with 10% FCS (Lonza), 2mM L-

glutamine (Invitrogen), 1% Pen-Strep, 1mM sodium pyruvate, 0.1mM non essential amino acids and 0.1mM minimum essential medium vitamins.

Dulbecco's modified Eagle's medium (DMEM) media for CV14A cells culture

DMEM (Lonza) supplemented with 10% FCS (Invitrogen), 2mM L-glutamine (Invitrogen) and 1% Pen-Strep.

Ethylene diamine tetra acetate(EDTA)

0.5M EDTA, pH 8.0 made up in deionised water and autoclaved

Trypsin-EDTA

trypsin 0.25% with EDTA 0.02% (Sigma)

Poly-L-Lysin

5X Stock Solution made up adding 50ml deionised water, 1X used as working concentration.

Phosphate buffered saline (PBS)

PBS tablets (Sigma): 1 tablet dissolved in 200ml of deionised water yields 0.01 M phosphate buffer.

3.7% formaldehyde fixative

3.7% formaldehyde was made up in PBS from 37% formaldehyde (Sigma)

Cells freezing solution

90% FCS and 10% dimethylsulfoxide (DMSO)

2.1.2 CV14A cells

CV14A cells are green monkey fibroblasts stably transfected with mitochondrially targeted DsRed1 and were kindly provided by Dr. Kurt J. De Vos (De Vos et al., 2003).

2.1.2.1 Culture of CV14A fibroblasts

CV14A cells were seeded at a standard density (1×10^5 cells) in 75cm² flasks in Dulbecco's modified Eagle's medium (DMEM) supplemented with 10% fetal calf serum (Invitrogen), 2mM L-glutamine (Invitrogen) and 1% Pen-Strep and maintained at 37°C, under 5% CO₂ in air. Cultured CV14A cells show cytoplasmic prolongation (<60% confluency) scattered on the culture surface which would later show a fusiform morphology once the culture is confluent (>60% confluency). CV14A cells were passaged 1:8 twice a week.

2.1.2.2 Subculture of CV14A fibroblasts

Subculture (passage) of fibroblasts was done with 80% cellular confluency in the flask. After aspirating the culture medium, the cells were rinsed with phosphate buffered saline (PBS) twice and then 2ml of trypsin 0.25% with EDTA 0.02% (Sigma) was added and the flask is maintained in humidified incubator for 5 minutes or until the cells had fully detached. Cells detached from the plastic surface were observed with spherical morphology. 8ml complete medium was added to the flask to inhibit the enzymatic action of trypsin and 1/8 part of cells with media were split into a new flask. They were kept in an incubator at 37°C with 5% CO₂.

2.1.3 Human fibroblasts

The human fibroblasts used in this study were obtained from Prof. Frank Baas (Academic Medical Centre, Amsterdam, Netherlands) under informed consent.

2.1.3.1 Primary culture of human fibroblasts

Primary fibroblast cells were cultured continuously in minimum essential medium (MEM) with 10% fetal calf serum, 2mM L-glutamine, 1% PenStrep (100UI/ml penicillin, 100µg/ml streptomycin), 1mM sodium pyruvate, 0.1mM non-essential amino

acids and 0.1mM minimum essential medium vitamins. This glucose-containing culture medium was used for all measurements (both biochemical and morphological) unless otherwise stated.

2.1.3.2 Subculture of human fibroblasts

Subculture (passage) of fibroblasts was done with 80% cellular confluency in the flask. After aspirating the culture medium, the cells were rinsed with PBS twice and then 2ml of trypsin was added and the flask was maintained in humidified incubator for 5 minutes. 8ml complete medium was added to the flask to inhibit the enzymatic action of trypsin and 1/5 part of cells with media were split into a new flask. They were kept in an incubator at 37°C with 5% CO₂.

2.2. Quantification of mitochondrial morphology for human fibroblasts

2.2.1. Plating fibroblasts on 6 well plate

22mm coverslips were placed in 6 well plate and incubated at 37°C for 20 minutes in 0.1mg/ml poly-L-lysine (Sigma) prior to plating. Coverslips were washed twice in sterile H₂O. Human fibroblasts were grown in a 75cm² flask until they reached 80% confluency and were trypsinised as in section 2.1.3.2. The cell suspension was mixed well by gentle agitation of the flask. Before the cells have a chance to settle, 10µl of cell suspension was carefully added to the haemocytometer by gently resting the end of the Gilson tip at the edge of the chambers. 10X objective of the microscope used and cells were counted in all 4 sets of 16 corner squares. The cell count was determined and 3.2x10⁴ cells/ml were plated per well of a 6-well plate. Cultures were kept in an incubator at 37°C with 5% CO₂ overnight to establish for further experiments.

2.2.2 Preparation of Staining Solution

Human fibroblast mitochondria were ideally stained with thiol-reactive chloromethyl moiety containing cell permanent MitoTracker probes (Invitrogen). These probes passively diffuse across the plasma membrane and accumulate in active mitochondria and retain in the mitochondria even after fixation. The stock for MitoTracker Red CMXRos (Molecular Probes) was prepared by adding anhydrous dimethylsulfoxide (DMSO) to the lyophilized probe to make a final concentration of

1mM. This stock was always kept at -20°C.

2.2.3 Labelling mitochondria for visualisation with MitoTracker RED

Once the cells reached the desired confluency, fibroblasts were stained with 66nM MitoTracker Red CMXRos freshly prepared in prewarmed MEM media and incubated for 3 min at 37°C. Cells were subsequently washed 3 times with prewarmed fresh media for 1 min each at 37°C.

2.2.4. Live image acquisition

2.2.4.1. Mounting cells for live imaging

A square smaller than the size of 22x22mm coverslip was made in the middle of a chamber glass slide with high vacuum grease using a syringe. 200µl of media in which fibroblasts were growing was added in the chamber and the coverslip with cells was placed on it with cells face down in contact with the warm media. The edges of the coverslip were coated in wax made up of equal parts lanolin, vaseline and paraffin wax to prevent any air escaping and liquid leakage.

2.2.4.2 Image capture of cells for mitochondrial morphology analysis

The mounted slides were then placed under a 63X/1.25NA oil Antiflex Plan-Neofluar objective on an upright Manual Zeiss Axiophot microscope with phase contrast and DIC for transmitted light illumination. This microscope was equipped with DAPI, FITC and TRITC filter sets (Chroma Technology Corp) for conventional epifluorescence illumination with (100W HBO lamp), Lambda 10-2 filter wheel (Sutter Instrument Company) and a multiformat CCD camera C4880-80 (Hamamatsu). Images were taken using the modular imaging software Openlab (PerkinElmer). 566nm fluorescence (Dsred2mito/CMXRos) image was taken for approximately 50-60 cells per sample and per condition. The exposure time was set as low as possible whilst still maintaining visible MitoTracker staining. This was done to keep bleaching and phototoxicity to a minimum. Images were saved as 12-bit gray scale TIFF (tagged image file format) files. Prior to image acquisition, images of a graticule (Watson, UK) of standard distances were taken to calculate the scaling factor that converts pixels to microns.

2.2.5 Post-Imaging analysis using ImageJ

To study mitochondrial morphology in human fibroblasts mitochondrial aspect ratio, mitochondrial length, mitochondrial bifurcation ratio and mitochondrial network complexity were quantified using ImageJ software and following the procedure for mitochondrial morphology analysis as described by De Vos and Sheetz (De Vos and Sheetz, 2007) with some modifications which are described in the text.

2.2.5.1 Image processing to calculate mitochondrial aspect ratio and length

Mitochondrial aspect ratio is the ratio between the major and minor axis of the ellipse equivalent to the mitochondrion (De Vos and Sheetz, 2007).

$$AR = l_{\text{major}} / l_{\text{minor}}$$

Where major axis is the longitudinal length and minor axis is the equatorial length of the ellipse fitted to the mitochondrion. As the shape of mitochondria resembles an ellipse therefore aspect ratio is a reliable measurement of mitochondrial length, however aspect ratio is a parameter suitable for individual mitochondria.

Mitochondrial length is a direct measurement of individual mitochondrion length with reference to its height and width.

Images were transferred as TIFF files to a computer with ImageJ software (by W. Rasband (NIH, Bethesda, MD; <http://rsbweb.nih.gov/Imagej>) and plug-ins written by Kurt J. De Vos (De Vos and Sheetz, 2007). Each Image file was opened as a stack of 30 images. Each individual image in one stack represents individual cells therefore stack was converted into 30 individual images. All the raw images were 16-bit images.

In fibroblasts the mitochondria are organised in a large network near the centre of the cell, also touching the neighbouring mitochondria and can result in over estimated measurements. Therefore to analyse individual mitochondria, the networked mitochondria were removed to avoid these artifacts.

The various steps in image analysis are as follows:

i. Adjust Image Brightness/Contrast

Each individual raw image was opened in the ImageJ and the brightness and contrast was set to ensure even pixel intensity values across the entire image.

This was achieved using brightness/contrast control panel.

ImageJ: Image>Adjust>Brightness/Contrast

ii. Removing Networked Mitochondria

Filter the original image with a 15x15 Gaussian filter:

ImageJ: Process>Filters>Convolve>Gaus 15x15

```
  2 2 3 4 5 5 6 6 6 5 5 4 3 2 2
  2 3 4 5 7 7 8 8 8 7 7 5 4 3 2
  3 4 6 7 9 10 10 11 10 10 9 7 6 4 3
  4 5 7 9 10 12 13 13 13 12 10 9 7 5 4
  5 7 9 11 13 14 15 16 15 14 13 11 9 7 5
  5 7 10 12 14 16 17 18 17 16 14 12 10 7 5
  6 8 10 13 15 17 19 19 19 17 15 13 10 8 6
  6 8 11 13 16 18 19 20 19 18 16 13 11 8 6
  6 8 10 13 15 17 19 19 19 17 15 13 10 8 6
  5 7 10 12 14 16 17 18 17 16 14 12 10 7 5
  5 7 9 11 13 14 15 16 15 14 13 11 9 7 5
  4 5 7 9 10 12 13 13 13 12 10 9 7 5 4
  3 4 6 7 9 10 10 11 10 10 9 7 6 4 3
  2 3 4 5 7 7 8 8 8 7 7 5 4 3 2
  2 2 3 4 5 5 6 6 6 5 5 4 3 2 2
```

Threshold the resulting image to include the now blurred network:

ImageJ: Image>Adjust>Threshold

Apply the threshold; mitochondria show up black.

Select the networked mitochondria using the wand tool in ImageJ.

Restore the selection on the original image:

ImageJ: Edit>Selection>Restore Selection

Clear the selected region on the original image:

ImageJ:Edit>Clear

iii. Segmenting touching Mitochondria

Filter the original image with a 5x5 Mexican Hat filter:

ImageJ >Process>Filters>Convolve>MHat 5x5

```
0 0 -1 0 0
0 -1 -2 -1 0
-1 -2 16 -2 -1
0 -1 -2 -1 0
0 0 -1 0 0
```

iv. Producing 8-bit binary image:

Subtract the convolved image from the cleared image obtaining a 32-bit result:

ImageJ: Process>Image Calculator

Threshold the resulting image to include all mitochondria and apply.

Convert the threshold image to 8-bit:

ImageJ: Image>Type>8-bit

Threshold the 8-bit image and apply.

Using the resulting binary image, count the number of mitochondria, determine the area and the best fitting ellipse for each organelle per time point by particle analysis:

ImageJ: Analyze>Analyze Particles

v. Mitochondrial Aspect ratio calculation

Calculate aspect ratio by dividing the major axes over minor axes and then get the average aspect ratio per cell.

Aspect ratio=Major axis/Minor axis

vi. Mitochondrial Length calculation

Calculate the length of mitochondria by taking the bigger value from height and width using following formula.

Length=MAX(Width:Height)

2.2.5.2 Image processing for mitochondrial branching and networks

Fibroblasts commonly show enormous branching and large networks of mitochondria. Mitochondrial branching and networks are defined as the quantification of the form factor of mitochondrial dynamic morphology in a cell. To quantify branching and network morphology I followed the same procedure as described by De Vos and Sheetz, 2007.

i. Creating a skeleton image

The individual raw image was opened in the ImageJ and converted into binary image:

ImageJ>Process>binary>make binary

The binary image was then converted into skeleton:

ImageJ>Process>binary>skeletonise

The image skeleton allows quantification of mitochondrial branching and connectivity as it involves erosion of any foreground pixel touching the background pixels except where the foreground pixels have value above background pixels. This leaves behind a skeletal remnant that largely preserves the extent and connectivity of the original network.

ii. Bifurcation ratio and network complexity ratio calculations

Branching and networks can be estimated by counting the endpoints and the nodes of the mitochondrial network. For instance a single mitochondrion has two end points and single branch point.

After creating a skeleton binary image, end point and branch points were calculated using the Binary Connectivity plug-in written by G. Landini (<http://www.dentistry.bham.ac.uk/landining/software/software.html>).

ImageJ>Plugin>Morphology>Binary Connectivity

Apply the brightness and contrast.

ImageJ>Adjust>Brightness/Contrast>Auto

Look up the histogram for the graphic output and numeric results.

ImageJ>Process>Histogram>List

Numeric results were imported into Excel file and Branching or bifurcations was calculated by:

Bifurcation ratio=Bifurcations/Endpoints

Finally, network complexity ratio is calculated by:

Network complexity ratio = Sum(four-way+five-way+...)/endpoint

2.2.5.3. Statistical Analysis

All the statistical analyses were performed using Prism software. Normality of the data was tested with D'Agostino-Pearson omnibus K2 test. Then for normally distributed data sets one-way ANOVA was used to analyse the statistical difference with Tukey's post test for multiple comparisons. For non-normally distributed data sets non-parametric Kruskal-Wallis test followed by Dunn's multiple comparisons test was performed to determine the statistical significance.

2.3 Screen for mitochondrial fusion inducing compounds

2.3.1 Drug library for the screen

The drugs used in the screen were either taken from the literature search with relevance to their role on mitochondrial dynamics and/or also from the Spectrum Collection library of compounds details in result section 4.2 and Table 4.1.

2.3.1.1 Preparation of Drug Stocks

1000X stocks for all the drugs were prepared in DMSO or chloroform. Stocks were then aliquoted and kept at -20°C.

2.3.1.2 Plating CV14A cells on 24 well plate

13mm cover slips were placed in 24 well plates and incubated at 37°C for 20 minutes in 0.1mg/ml poly-l-lysine prior to plating. Coverslips were washed twice with sterile H₂O. CV14A cells were grown in a 75cm² flask until they reached 80% confluency and were trypsinised as in section 2.1.2.2. The cell count was determined and 4x10⁴ cells/well was plated in 24-well plate. Cultures were kept in an incubator at 37°C with 5% CO₂ overnight to establish for further experiments.

2.3.1.3 Addition of Drugs

The drugs were made up from stock solution in half fresh and half conditioned DMEM medium in which cells were growing at a range of concentrations mentioned in the text of result section 4.2.1 and Table 4.1 Drug treatments were for 15 minutes, 4 hours and 24 hour at 37°C with 5% CO₂.

2.3.1.4 Fixation and mounting of cells

CV14A cells were fixed with an aldehyde-based fixative. 3.7% formaldehyde in PBS was used. Cells were washed with PBS and incubated for 20 min at room temperature in 3.7% formaldehyde in PBS (Sigma). They were washed 2 times in PBS. 13mm coverslips carrying cells were then placed, cells face up on microscope slides. 50µl 50% glycerol/PBS was added to the coverslip and a 22x22mm glass coverslip placed on top. The edges were sealed with wax made up of equal parts lanolin, vaseline and paraffin wax.

2.3.1.5 Image capture of cells for mitochondrial morphology analysis

Slides were placed on the microscope set up and images were taken as shown in section 2.2.4.2 and later saved as stacks of TIFF files.

2.4 Cell Viability Assay

A widely used MTT colorimetric assay was performed to determine the effect of drugs on viability and growth of cells. MTT (3-(4,5-dimethylthiazol-2-yl)-2,5-diphenyl tetrazolium bromide) is a yellow tetrazole salt that enters the mitochondria and is reduced by mitochondrial succinate dehydrogenase to an insoluble formazan (purple) (Mosmann, 1983). The cells are then solubilised or lysed with an organic lysis solvent and the released coloured formazan reagent is measured spectrophotometrically. Since

reduction of MTT can only occur in metabolically active cells the level of activity is a measure of the viability of the cells.

2.4.1 MTT reagents

MTT solution was prepared at 5mg/ml in PBS and was filtered through a 0.2µm filter. The falcon was wrapped in aluminium foil as MTT is photosensitive and kept at 4°C.

Lysis solution: 100g SDS was dissolved in 200ml of dH₂O and stir overnight at 60°C. Next day 200ml of dimethyl formamide (DMF) was added to the solution and the pH was adjusted at 4.7 by adding few drops of 1M HCl: glacial acetic acid (1:1). The final volume was made up to 500ml by adding 50% DMF (DMF: H₂O, 1:1).

2.4.2 MTT Assay

Human fibroblasts were cultured in MEM media at the density of 4x10⁴ cells/well in 96-well flat bottom plate and were grown overnight at 37°C. On the following day 100µl of various drug concentrations were added to the cultures and incubated for 24 hours at 37°C. After 24 hours drug incubation, 10µl of 5mg/ml MTT solution was added in each well and incubated at 37°C for 2 hours. In the meantime lysis solution was warmed up to 37°C. MTT solution and media was aspirated and replaced with 100µl lysis solution. The plate was left on bench top plate shaker for 1 hour at room temperature. The optical density of the wells was read on spectrophotometer at a wavelength of 570nm.

2.5 Quantification of mitochondrial fusion

Poly-ethylene glycol (PEG) is a polyether and is an important reagent to study membrane fusion in-vitro (Lentz, 2007). In membrane fusion two initially distinct lipid bilayers merge their hydrophobic cores to form interconnected structure. These structures can be hemifused when only one leaflet of a bilayer is involved in fusion or fully fused where the internal contents of the two structures has completely mixed (Holopainen et al., 1999). PEG has shown its significance in promoting fusion via its ability to bind to a large number of water molecules present on lipid bilayer surfaces. This volume exclusion results in an osmotic force driving membranes into close contact

in a dehydrated region and promotes cell-cell fusion (Arnold et al., 1990; Burgess et al., 1992). Recently, PEG fusion assay has been used in several studies to measure mitochondrial fusion activity in cell hybrids (Chen et al., 2003; Chen et al., 2005; Detmer and Chen, 2007a).

2.5.1 PEG reagents

DMSO/PEG (Sigma) mix, DMEM +10%DMSO, 35mg/ml cycloheximide in DMSO, DMEM complete media+ 30µg/ml cycloheximide (made fresh every time).

2.5.2 PEG Fusion Assay

5x10⁴cell/well CV14A cells expressing mitochondrially targeted DsRED were co-cultured with 5x10⁴cells/well CV14A cells expressing mitochondrially targeted GFP, overnight on 13mm cover slips coated with poly-l-lysine in 24 well plates. The next day, media was removed and cells were fused for 1 minute with 200µl 10% DMSO/50% PEG solution. The cells were washed 3 times with DMEM+10%DMSO solution followed by one wash with DMEM complete media. Cells were then incubated for 30 minutes at 37°C in the presence of DMEM complete media+30µg/ml cycloheximide. Cycloheximide was included to prevent synthesis of new mitochondrially targeted DsRed or GFP in the fused cells. After 30 minutes incubation freshly prepared drug dilutions in DMEM complete media+30µg/ml cycloheximide were added to the cells for 4 hours. At the end of 4 hours drug incubation cells were fixed as discussed in section 2.3.1.4.

The cells were then scored for fusion under a 63X/1.25NA oil Antiflex Plan-Neofluar (Zeiss) objective on the upright Manual Zeiss Axiophot microscope.

2.6. Fis1 overexpression in CV14A cells

2.6.1 Plasmids used

Human myc-tagged Fis1 plasmid (hFis1) was a kind gift from Dr. Yisang Yoon (University of Rochester, USA) (Yoon et al., 2003). pCI-NEO empty vector (Promega), EGFP-C2 empty vectors (Clontec) and EGFP-peroxisome (Clontec) were gift from Dr. A.L Chapman.

2.6.2 DNA preparation and purification

Bacterial cultures of all the plasmids used were prepared from glycerol stocks by dipping the end of a sterile 10µl pipette tip into the appropriate frozen glycerol stock and placing in 5ml of LB broth containing 50µg/ml (final concentration) of the appropriate antibiotic. For hFis1 and pCI-NEO empty vector cultures were grown in presence of carbenicillin (50µg/ml final concentration). EGFP-cyto and EGFP-peroxi were grown in presence of Kanamycin (50µg/ml final concentration). The inoculated LB broth 5ml cultures were incubated overnight in the shaking incubator (200rpm) at 37°C.

2.6.3 Plasmid isolation using QIAprep Kit Method (Silicon based)

Overnight cultures were then centrifuged at 4000g for 10 minutes. The supernatant was discarded and the tubes were inverted on paper towels. 250µl of resuspension buffer A1 (4°C) was added and the pellet was resuspended by pipetting up and down. The homogenised mixture was transferred to a 1.5ml eppendorf tube and 250µl of lysis buffer A2 was added. The tubes were gently inverted 5-6 times in order to lyse the cells. 300µl of neutralising buffer A3 was added and mixed by inversion. The samples were centrifuged at 13000rpm for 10 minutes to pellet debris. The supernatant was loaded onto the spin column and a 2ml collection tube and centrifuged for 13000rpm for 1 minute. The flow through was discarded. 500µl of AW buffer was added to enhance the binding of plasmid to the membrane of the spin column and centrifuged for 1 minute at 13000rpm and the flow through was discarded. The column was washed with 600µl buffer A4 and the flow through was discarded after spinning at 13000rpm for 1 minute. Centrifugation was repeated for 2 minutes at 13000rpm to remove all traces of A4 solution. The column was placed in a clean 1.5 ml tube and 50µl of AE (elution buffer) was loaded on the column. The column was centrifuged at 13000rpm for 1 minute and the plasmid DNA eluted in the AE buffer was collected and stored at -20°C.

2.6.4 Quantification of plasmid DNA

Plasmid DNA was quantified using the Nanodrop Spectrophotometer ND-1000 (NanoDrop Technologies, Wilmington, USA). The nanodrop was first initiated with 2µl nuclease free water and subsequently blanked with 2µl elution buffer AE. 2µl sample

DNA was then used to assess the concentration in ng/ml.

2.6.5 Fis1 overexpression in CV14A cells for mitochondrial morphology analysis

2.6.5.1 Qiagen Effectene transfection

Effectene is a nonliposomal lipid reagent for DNA transfection into many sensitive cell lines and primary cells. CV14A cells were plated at 2.5×10^4 cells/well density on 13mm coverslips in 24 well plates as discussed in section 2.3.1.2. After 12-18 hours transfection was performed. 1 μ g DNA containing 3:1 ratio for gene of interest (hFis1 plasmid or empty vector plasmid) and reporter gene (GFP-cytoplasmic) was added in EC buffer (provided in the kit), followed by the addition of 8 μ l of enhancer making the total volume 120 μ l. This solution was mixed and vortexed for 1-2 seconds and incubated at room temperature for 5 minutes. After incubation 5 μ l of effectene transfection reagent was added, vortexed for 10 seconds and pipetted up and down gently, avoiding bubble formation, and incubated for 10 minutes at room temperature.

Lastly, serum free media was added making the volume 200 μ l. The transfection mix was vortexed for 10 seconds and incubated at room temperature for 10 minutes. In the meantime cells were washed with sterile PBS and 200 μ l fresh complete media was added. After incubation, 20 μ l of the transfection mix was added to each well of the plate and cells were kept in the 37°C incubator for 4 hours.

2.6.5.2 Drug addition

After 4 hours the transfection mix was aspirated and cells were given a wash with sterile PBS followed by the addition of various concentration of ethacrynic acid and 0.1% DMSO made in pre-warmed complete media (for details see Table 4.1). The plates were then incubated in 37°C incubator for 24 hours.

2.6.5.3 Cell fixation, Hoechst staining and Mounting

After 24 hours drug incubation CV14A cells were fixed as discussed in section 2.3.1.4. The fixed cells were then stained with Hoechst stain for nuclear morphology. Hoechst dyes are bisbenzimidazole derivatives and are commonly used to stain genomic DNA to visualise the morphology of the nucleus. Cells are stained with Hoechst 33258

(Molecular Probes) at the concentration of 0.2µg/ml in PBS for 10 min at room temperature in dark. Afterwards cells were washed twice with PBS to remove unbound dye. After Hoechst staining cells were mounted on the glass slides as discussed in section 2.3.1.4.

2.6.5.4 Assessment of mitochondrial morphologies

Assessment of mitochondrial morphology was conducted on samples which had been re-named/re-numbered so the investigator was blind to the experimental condition. For each condition 200 cells were scored under 63X/1.25NA oil Antiflex Plan-Neofluar (Zeiss) objective on upright Manual Zeiss Axiophot microscope.

2.6.6 Fis1 overexpression in CV14A cells for peroxisome morphology analysis

2.6.6.1 ExGen500 transfection

2.5×10^4 cell/well CV14A cells were plated in 24-well plate as discussed in section 2.3.1.2. 1 µg of DNA containing 3:1 ratio for gene of interest (hFis1 plasmid or empty vector plasmid) and reporter gene (GFP-peroxisome plasmid) was diluted in 20µl of 150mM NaCl. The mixture was vortex gently, 3.3µl of ExGen 500 (Fermentas) was added and vortex the solution immediately for 10 seconds. The transfection mix was then incubated for 10 minutes at room temperature. 20µl of the transfection mix (ExGen 500+DNA mixture) was added drop-wise to the cells in each well containing 200µl of culture media. Cells were incubated at 37°C for 4 hours, then 800µl of pre-warmed culture media was added and transfections were monitored 24 hours later.

2.6.6.2 Drug Addition

After allowing the transfection for 24 hours different concentrations of Ethacrynic acid were added to the cells. Cells were then incubated for next 24 hours in 37°C incubator.

2.6.6.3 Image Acquisition and Processing

After 24 hours drug incubation CV14A cells were fixed and mounted on the glass slides as discussed in section 2.3.1.4. Z-stack images were taken of the fixed cells

on Olympus FV1000 confocal microscope. 30 Z-stack images were taken for each condition.

2.6.6.4 Peroxisome count analysis using ImageJ

The maximum intensity Z-stack tiff image file was opened in the ImageJ and converted into Z-projection.

ImageJ>Image>Stacks>Z-project

The 5x5 Mexican Hat filter was applied to the 16-bit image

ImageJ >Process>Filters>Convolve>MHat 5x5

$$\begin{array}{ccccc} 0 & 0 & -1 & 0 & 0 \\ 0 & -1 & -2 & -1 & 0 \\ -1 & -2 & 16 & -2 & -1 \\ 0 & -1 & -2 & -1 & 0 \\ 0 & 0 & -1 & 0 & 0 \end{array}$$

Threshold was applied to the resulting image to include all the dots (peroxisome circularity).

ImageJ: Image>Adjust>Threshold

Convert the threshold image to 8-bit:

ImageJ: Image>Type>8-bit

Number of peroxisome per cell was calculated by applying particle analysis

ImageJ: Analyze>Analyze Particles>bare outlines>summary>count

2.7. Fly Stocks

Fly stocks including wild type w^{1118} and balancer stocks (*CyO/MKRS*, *Gla;TM6B*, *If/CyO;TM6B/MKRS*, *FM7.GFP*) were used from already existing stocks in the department and were originally obtained from the Bloomington *Drosophila* stock centre. GAL4 expressing lines including *da-GAL4*, *elav-GAL4*, *D42-GAL4* were obtained from the Bloomington *Drosophila* Stock. The UAS-RNAi lines; *UAS-Marf-IR(GD)* and *UAS-Marf-IR(KK)* were purchased from Vienna *Drosophila* RNAi Centre (VDRC).

The deficiency line *Df(1)Exel6239* used in EMS genetic screen, was from the Exelixis library, molecularly mapped based on the known position of the P-elements that were used to make the lines. *Df(1)G4e[L]H24i[R]* used in complementation assay was cytologically mapped deletion of DrosDel collection from the Bloomington *Drosophila* Stock Center (<http://www.drosdel.org.uk/coverage.php>). The attached XX duplication stock *C(1)DX y f/FM7h/Dp(1;Y)dx⁺* was generated by Dr. Alex Whitworth by combining compound X stock with *Dp(1;Y)dx⁺* stock sourced from Bloomington *Drosophila* Stock Center (<http://flystocks.bio.indiana.edu/>).

2.8 Fly Husbandry

All the flies were maintained in a humidified chamber (20-40% humidity) at 25°C or 18°C on 12 hour dark-light cycle. Flies were grown in 250ml bottles containing 25% filled standard yeast, cornmeal and agar medium. Stocks were grown at 18°C and the flies were transferred into fresh food every 3 weeks. The experimental crosses were kept at 25°C and were turned over every 3 days for maximum progeny collection. An experimental cross usually consists of 2 males and 5 females in a 10ml vial. However, crosses set up in bottles consist of 8-10 males and 16-20 females.

2.9 Behavioural Assays

All the behavioural experiments were performed in a genotype-balanced manner. Flies were reared in bottles, kept as mixed genders to allow mating, and kept with standard food at all times prior to testing, unless noted otherwise in the text. On the day of experiment the flies were allowed to acclimatize to the testing room for 2 hours before each experiment. The experiments were performed at the same time of the day.

All behavioural assays except larval locomotion assay were carried out at 25°C.

2.9.1 Larval locomotion assay

Drosophila larval crawling involves repeated, rhythmic, peristaltic contraction. During each peristaltic stride, muscle contractions are propagated from rear end of the body to the mouth, passing through all 11 segments one by one and pushing the larvae one step forward (Berrigan and Pepin, 1995). The larval locomotion assay was performed as described previously (Feiguin et al., 2009). Wandering third instar larvae were used for the assay. Individual larva was placed on a 100mm plate containing a matrix of 1% agarose and allowed to adapt for 30 seconds. The larva was then allowed to crawl across the dish for 2 minutes and under the stereoscope the peristaltic waves were counted. 20 larvae for each genotype were counted individually.

2.9.2 Climbing Assay

The climbing behaviour was assessed in a counter-current apparatus consisting of 6 chambers for two 18x150mm Pyrex test tubes joined by a sliding bridge (Benzer, 1967). Flies were set in a cohort of 20 adult flies and habituated for 2 hours in the 25°C room. Normally, 5 cohorts of 20 flies were tested each time. To start the assay, flies were introduced in lower tube of the first chamber of the apparatus and allowing 20seconds to reach the top of the chamber. With the help of sliding bridge the successful climbers were then shifted into the next chamber and the process repeated four times (making five in total). At the end the number of flies in each chamber was noted and climbing index was calculated based on the distribution of the flies across all the chambers (Greene et al., 2003).

2.9.3 Flight Assay

The same cohort of flies used in climbing assays were analysed in flight assays. Flight assays were usually carried out after climbing assays. Flies were dispensed downwards through a 64x465mm 1-litre graduated cylinder via funnel. The cylinder has been lined with an acetate sheet coated with vacuum grease. The sheet was divided vertically into 5 equal parts. During the free fall from the top the flies with the ability to fly adhere to the grease. Number of flies in each section was noted and given a score. The flies that are unable to fly land at the base of the cylinder and were given zero

score. The flight index was calculated based on the distribution of the flies across all the sections.

2.9.4 Longevity Assay

For longevity assay all the experimental flies were reared and the lifespan trials were conducted in a humidified chamber (20-40% humidity) at 25°C on 12 hour dark–light cycle. 0-24 hour's old flies were collected and kept in food vial at the density of 20 per vial with a proportion of 10 male and 10 female. 200 flies were used for each genotype. After every three days the flies were transferred to new vial containing fresh food and number of dead flies was scored. In experiments with Ethacrynic acid feeding the flies were kept in vials containing food and Ethacrynic acid or DMSO. The mortality was recorded daily for 30 days.

2.10 Neuromuscular Junction study

2.10.1 NMJ dissection

3rd instar wandering larvae were selected for neuromuscular junction study. Selected larvae were collected in a glass plate containing 1xPBS to wash away the food. A drop of cold 1xPBS was dropped on the sylgard dissection plate and an individual larva was placed in it. This will keep the larvae from drying and stun the larvae to restrict their active movements. Larva was pinned using minuten pins between posterior spiracles and in the head near the mouth hooks. Larval body wall muscles were carefully opened in the dorsal side using surgical spring scissors. Internal organs were removed with the help of forceps and the fillet was carefully washed with 1xPBS buffer. The cuticle was laterally expanded on both sides in order to see the nerve muscle interactions in all muscles of each segment.

2.10.2 Sample fixation, immunocytochemistry and mounting

The dissections were fixed in 4% paraformaldehyde (Sigma) in PBS for 20 minutes. The preparations were washed in PBS-0.1% Triton (PBST) for 3x5 minutes each. Samples were incubated for 2 hours at room temperature or overnight at 4°C with neuronal marker 1:200 dilution of anti-HRP (Jackson ImmunoResearch) in PBST. After primary antibody incubation samples were given 3xPBST quick washes, followed by

3x10 minutes PBST washes. The secondary anti-rabbit AlexaFluor594 (Molecular Probes) was incubated at 1:500 dilution in PBST for 2 hours room temperature or 4°C overnight. Samples were given 3xPBST quick washes, followed by 3x10 minutes PBST washes. After washes all the PBST was removed and replaced with 70% Glycerol+30%PBS solution to remove the air bubbles. The samples were left in the fridge for overnight or 3-4 hours at room temperature. Dissected larvae can be stored for up to one week at 4°C. Lastly the samples were mounted on glass slide with mowiol 4-88 (Sigma-Aldrich). A coverslip was placed on the top and the edges were sealed with nail varnish.

2.10.3 Muscle imaging and Bouton quantification

Bouton number and NMJ branches were acquired from longitudinal muscle 6/7 of hemisegment A3. All the observations were made by eye under epi-fluorescence microscope using 63X objective. Methods used for recording and quantification were same as discussed by Milton et al 2011 with minor modifications.

2.10.3.1 Normalized Bouton number

Bouton number is determined by counting every distinct anti-HRP stained swollen spherical structure at the neuromuscular junction. To minimise the effect of reduced developmental size between various genotypes we determined the muscle surface area as well to normalise all the calculations to the controls. Muscle surface area was calculated by imaging muscle 6/7 with a 10X objective Leica DC500 digital camera with a Leica DMLA microscope. Muscle surface area size was measured as drawing a straight line across the junction of muscle 6 and 7 (X) and then drawing a straight line parallel to the muscle extremes in the middle of muscle 6 and 7 (Y). X refers to length of the muscle and Y stands for width of the muscle. X and Y were determined by using measure>ImageJ. Area was then calculated by multiplying X and Y. Bouton numbers for testing genotypes were then determined by following formula:

Normalized bouton number for the test= actual bouton count for test/(average muscle surface area of test /average muscle surface area of control)

2.10.3.2 Branch Number

Branch number was defined as the divergent points or extensions on the presynaptic motor neuron.

2.10.3.3 Confocal imaging for mitochondrial morphology

Z-stack images were taken using a Carl Zeiss LSM510 confocal microscope using Plan-Apochromat 63X NA 1.4 oil objective. Images for the cell bodies, segmental nerve segments and synaptic boutons were taken from the fixed larvae samples to study mitochondrial morphology.

2.11 Culture S2R plus cells and incubation with EA

2.11.1 Cell Culture conditions

Drosophila Schneider S2 receptor plus (S2R⁺) cells were cultured in 75cm² flasks in Schneider's medium (Invitrogen) supplemented with 10% heat inactivated fetal bovine serum (Sigma) and 1% Penstrep (Invitrogen-Gibco). Cells were kept in a 25°C incubator with 5% CO₂. Cells were passaged twice a week by gently scrapping the adhered cells off the bottom of the flask with a sterile scraper. Then transfer 1ml of the suspended cells into a fresh flask with 9ml fresh media.

2.11.2 Plating S2R⁺ cells

2x10⁵ cells/well were plated into 8-well slide chambers with well surface area of 1.8cm². The cells were allowed to adhere overnight before drug treatment. The following day cells were stained with MitoTracker Red CMXRos (Molecular Probes) in DMSO with working concentration of 1.8μM diluted in fresh prewarmed MEM media and incubated for 3 minute at 25°C. Cells were washed 3 times with prewarmed fresh media for 1 minute each at 25°C.

2.11.3 Drug Incubation and Imaging

Various concentrations of ethacrynic acid (EA) were prepared in prewarmed Schneider's medium and added to cells (details see section 5.10.1). Cells were then incubated for 4 hours in 25°C incubator. After 4 hours cell were imaged live under the Carl Zeiss LSM510 confocal microscope using Plan-Apochromat 63X NA 1.4 oil

objective.

2.11.4 Feeding flies EA

Drosophila standard food was made with addition of 0.1% DMSO as vehicle and EA test concentrations. 50ml of drug food (carrying 50µl drug) was added to the 250ml standard bottles. The food bottles were covered with paper towels and left over night on the bench to settle. Following day, a thin coat of toothpaste-like suspension of live yeast in water containing 0.1% DMSO, or EA was added to the drug food. Flies were reared in the drug food bottles at 25°C. The progeny was collected and transferred to the 10ml vial containing drug food. The flies were kept at 25°C for aging.

2.11.5 Behavioural assays

Climbing and flight assays were carried out on EA fed 2 days and 15 days old flies in the same manner as discussed in section 2.9.2 and 2.9.3.

2.12 EMS mutagenesis screen for *Marf* mutant

Ethyl methane sulfonate (EMS), commercially known as methanesulfonic acid ethyl ester (Sigma) is a chemical mutagen which has been widely used by *Drosophila* geneticist to induce *de novo* DNA lesions. EMS is an alkylating agent; it introduces an ethyl group to O-6 position of guanine, thus creating O-6-alkylguanine. This alkylation leads to direct mispairing with thymine during replication and results in GC → AT transitions. These transitions can lead to missense or nonsense codons or may even destroy splice sites (Pastink et al., 1991; Bentley et al., 2000).

2.12.1 EMS mutagenesis method

200 newly emerged w^{1118} males were collected and aged separately from females for 1-3 days. 400-500 virgin females from $Dp(1;Y)dx^+$ stock were collected and aged 1-3 days. For optimum mating both males and females should be same age preferably females should be younger. 2 layers of small circles cut out of whatman 3mm paper were put in the bottom of 250ml empty food bottles. 2 bottles were prepared. Next day, starting early in the morning 100 males flies were placed in each of the bottle. Males were starved for 6 hours. After the period of starvation required concentration of EMS dissolved in 1% sucrose solution was dispensed carefully using 5ml syringe on the

whatman filter paper fitted at the bottom of the bottles. For example, for a final EMS concentration of 25mM EMS, we used 12µl of EMS (Sigma) in 5ml of sucrose and then dripped 2ml of the solution into each bottle. After use, the syringe was filled with 10% sodium thiosulphate solution used as decontaminant. Any left over EMS solution was also decontaminated by adding 10% sodium thiosulphate to the tube. After 24 hours of decontamination the liquid was poured down the drain of the hood and syringe and tubes were placed in plastic bags. Caution: always used double layer of gloves while handling EMS. Also this whole procedure was done in the designated hood in the room for mutagenesis. All the waste material was left in sealed plastic bags and put in hazard yellow bin which was then removed by the department safety officer. The males were then left in the hood overnight. Following day, mutagenized males were carefully transferred to new empty bottles containing whatman filter paper layers, carried to experimental lab and further, males rub off their feet on the whatman papers and get cleaned. After an hour, the males were then transferred to the bottles containing standard food and were allowed to recover for 24 hours at 25°C. EMS bottles were decontaminated and removed as discussed above. Next day, the $Dp(1;Y)dx^+$ females were added to the bottles. 100 w^{118} mutagenized males and 200-250 $Dp(1;Y)dx^+$ females. Crosses were kept at 25°C room and flies were transferred to new bottles every 24 hours for next 2 days. The parents were removed on 4th day of the experiment to prevent the getting several identical mutants derived from mutagenized germline stem cells as a result of spermatogenesis cease in males.

2.12.2 Isolation of EMS mutants

After 10 days the newly emerged F₁ males $w^{118}*/Dp(1;Y)dx^+$ were collected (* denotes the presence of newly induced mutations) and aged for 2-3 days. In mean time 600-800 $Df(1)Exel6239$ virgins were collected. Individual crosses were set in 10ml standard food vial by adding 1 $w^{118}*/Dp(1;Y)dx^+$ males and 2-3 $Df(1)Exel6239$ females. For 25mM EMS screen normally 500 individual crosses were set to get at least one or two lethal mutations/chromosome. All the crosses were kept at 25°C and parents were allowed to mate only for 24 hours. Please see result section for the number of individual crosses set for our EMS screens. Mutant lines were scored in F₂ for the absence of adult female $w^{118}*/Df(1)Exel6239$ genotype. Please see result section for details. The mutant lines were then kept as stable stocks by crossing them with *FM6* balancer.

2.12.3 Identification of EMS mutants

Mutant stocks $w^{1118}*/FM6$ were crossed with $FM7.GFP$ to isolate the mutant phenotype. Please see detail in result section.

2.12.4 DNA isolation and PCR for sequencing

2.12.4.1 Larvae genomic DNA extraction

Thirty 3rd instar and approximately hundred 1st instar larvae were used for each DNA preparation. The samples were collected according to the mutant phenotype. The samples were collected in an eppendorf and kept on ice. 400µl of lysis buffer (1M TrisHCl pH 7.5, 500mM EDTA pH 8.0, 40mM NaCl, 10% SDS) made in dH₂O was added in each tube keeping on ice. Larvae were squashed in lysis buffer using plastic homogenisers. The samples were then incubated for 30minutes at 65°C. Tubes were replaced to the room temperature and 800µl LiCl/KAc solution (6M NiCl, 5M KAc) was added in each tube. Tubes were inverted several times to mix and incubated for 10 minutes on ice. After incubation tubes were spun for 15 minutes at 14000rpm on bench top centrifuge at room temperature. Supernatant was transferred into a new eppendorf. 800µl isopropanol (Fisher Scientific) was added to precipitate the DNA. The samples were mixed by inverting the tubes gently and then centrifuged for 10 minutes at 14000rpm to obtain DNA pellet. Supernatant was discarded and tubes were given a quick spin. All the residual isopropanol was aspirated and discarded. The pellets were washed in 500µl of cold 70% ethanol. The samples were centrifuged at 14000rpm for 5 minutes and the ethanol was aspirated. Tubes were then given a quick spin again and all the residual ethanol was removed. The pellets were air dried for 20 minutes and resuspended in 50µl nuclease free water overnight at room temperature. DNA preps were stored at -20°C.

2.12.4.2 PCR for *Marf* DNA templates

Using the primer3 programme (http://biotools.umassmed.edu/bioapps/primer3_www.cgi), primers were designed to amplify *Marf* as overlapping amplicons of about 1.6-2.2kb, based on extended gene sequence obtained from *FlyBase*. All the designed primers were then purchased from Sigma. Details of the amplicon locations and sizes

were discussed in result section. The primers used are shown in **Table 2.1**.

The amplicons were amplified using Phusion DNA Polymerase (Finnzymes). 2µl DNA template was added to 20µl of PCR mix consisting of 4µl 5xPhusion HF buffer, 0.4µl 10mM dNTPs, 0.6µl 50mM MgCl₂, 1µl 1mM Forward primer, 1µl 1mM Reverse Primer, 0.2µl Phusion DNA Polymerase and 10.8µl nuclease free H₂O. The PCR tubes were placed in a PCR machine and run on a Touchdown PCR programme consisting of:

Cycle 1 (1x) Step 1: 98°C 2min (denaturation)

Cycle 2 (20x) Step 1: 98°C 30sec (denaturation)

Step 2: 68°C 30sec (annealing)

Decrease temperature after cycle 1 by 0.5°C every 1 cycle

Step 3: 72°C 1min 40sec (extension)

Cycle 3 (15x) Step 1: 98°C 30sec (denaturation)

Step 2: 58°C 30sec (annealing)

Step 3: 72°C 1min 40sec (extension)

Cycle 4 (1x) Step 1: 72°C 5min (final extension)

Table 2.1: Amplification and sequencing primers

Primer ID	Primer Sequence	Map Distance relative to <i>Marf</i>	Amplification	Sequencing
F1 (F1new)	GGCTAGTGTGACCATTTCCTAA	-230	YES	YES
F2	TCAACTCGATTTACGCACACA	321	-	YES
F3(MfnEcoR1)	ATGGCGGCCTACTTGAACCGC	909	YES	YES
R1(N)*	GATCTGGAGCGGTGATTTGT	1133	-	YES
F11	TACCCAACAGAAGCCAATCC	1241	YES	YES
F4	GAAGTACTGCAGCGGGATCA	1494	YES	YES
R2(N)*	CATTCGCCAGTTGTTTGATG	1773	YES	YES
F5(Mfn3F)	AGCAAGCCGAACATCTTCAT	2038	YES	YES
F12	AGGAGTGCATCTCGCAGAGT	2797	YES	YES
F10	AGGTGGAGGAGAAGGTGTCAA	3037	YES	YES
R3(Mfn3R)	AGTTCAATATGCCCTTCCATCC	3122	YES	YES
R7	GAAGCGTGAGATCAACGACA	3667	YES	YES
F7(MfnSeqQC)	ATCTACCTGTACGAGCGCCTCTC	3903	YES	YES
R4(N)*	AGGTCGACAATCATCTTGAGC	4009	-	YES
Xba(N)		4289	YES	YES
F8	GAAATCAGGCCGAAGACAAACA	4376	-	YES
R8	TATCGTTTTGATCGGGATCAC	5141	YES	YES
R5(N)*	TTCTGTGAACAAACACAAAATCA	5233	YES	YES

To determine the amplified product was correct size, the PCR products were run with Hyper Ladder I (Bioline) on a 1% agarose gel at 100V for 50 minutes. DNA bands were visualised using ultraviolet (UV) light.

The amplified DNA was always stored at 4°C.

2.12.4.3 Sequencing

The amplified genomic DNA amplicons were sent for purification and sequencing to the Core Genomic Facility in University of Sheffield. For sequencing 1pmol/μl dilutions of sequencing primers were used. The sequence data obtained from Genomic core facility was analysed using FinchTV to see the quality of data and later Sequencher® was used to align the sequencing data with extended *Marf* reference sequence from *Flybase* to generate contigs that covered the entire gene plus 200bps 5' and 3' intergenic regions.

2.12.5 Protein analysis for EMS mutants

2.12.5.1 Larvae protein extraction

The protein samples were collected from fifteen 3rd instar and fifty 1st instar larvae according to each mutant phenotype. The larvae were collected in an eppendorf tube and anaesthetised at -20°C for 10 minutes. The samples were homogenised in 75μl RIPA buffer (50mM Tris-HCl, 150mM NaCl, 1mM EDTA, 0.1%SDS) and 3μl Protease Inhibitor (11836170001, Roche). The samples were centrifuged at 13000rpm for 10 minutes and supernatant was collected.

2.12.5.2 Bradford Assay

Protein concentration was determined by performing standard Bradford assay (Bradford, 1976). Serial dilutions of Bovine Serum Albumin (BSA) (stock concentration: 10mg/ml) were prepared as follows:

1mg/ml (10μl of BSA (10mg/ml) + 90μl dH₂O)

2mg/ml (20μl of BSA (10mg/ml) + 90μl dH₂O)

4mg/ml (40μl of BSA (10mg/ml) + 90μl dH₂O)

Reaction mixture (diluted 1:4 with water) was prepared by adding 200ml Bradford reagent in 800ml dH₂O.

BSA working concentrations were prepared in the reaction mix as follows:

BSA working concentrations	Volume added from BSA working concentration	Reaction Mix
1mg/ml BSA	1µl	1ml
2mg/ml BSA	2µl	1ml
4mg/ml BSA	4µl	1ml

Note: 3 tubes for each dilution concentration were prepared to make standard curve.

1µl of the protein homogenates for each sample was added to 1ml of reaction mix. Tubes were incubated for 5 minutes at room temperature for colour development. Absorbance of each sample was measured at 595nm using UV-visible spectrophotometer. Standard curve was prepared using Excel and concentration of protein in each sample was calculated from the equation:

$$y = a(x)+b.$$

Here x = concentration of protein, y = absorbance at 595nm

All the concentrations were brought to the lowest value in the sample concentrations by adding RIPA buffer and PI mixture to load equal volume of protein on gel. Formula to calculate the amount of RIPA buffer and PI mixture in each protein sample:

Concentration of protein sample - final solution volume (e.g: 50µl) = amount of RIPA buffer and PI mixture

$$d-50 = f$$

2.12.5.2 Protein Analysis by Western Blotting

4XSDS loading dye (0.25M Tris-HCl (pH6.8), 8% SDS, 10% β-mercaptoethanol, 30% Glycerol, 0.02% Bromophenol blue) was added to the protein samples and boiled at 95°C for 8 minutes to denature the protein and break disulphide bonds. The samples were replaced on ice to stop the denaturing process. The protein

samples were always kept at -20°C. The denatured protein samples were separated by 8 % SDS-PAGE.

8% resolving gel recipe for 10ml:

4.6ml H₂O, 2.7ml 30% acrylamide, 2.5ml 1.5M TrisHCl (pH 8.8), 0.1ml 10%SDS, 0.1ml 10% Ammonium persulphate, 0.006ml TEMED.

Stacking gel recipe for 10ml:

6.8ml H₂O, 1.7ml 30% acrylamide, 1.25ml 0.5M TrisHCl (pH 6.8), 0.1ml 10%SDS, 0.1ml 10% Ammonium persulphate, 0.001ml TEMED.

The resolving and stacking gels were casted in 1.5mm thickness glass plates. 20µg protein/well was loaded and the gels were run in running buffer (25mM Tris, 192mM Glycine, 0.1% (w/v) SDS, pH8.3) at 60volts for stacking gel and 120volts for resolving gel to obtain optimum separation. The gels were transferred to polyvinylidene difluoride (PVDF) membrane (162-0177, BioRad) using the transfer buffer (25mM Tris, 192mM Glycine, 20% Methanol, pH8.3). Transfer time was 1 hour at 100volts.

The transferred membranes were given a quick wash with H₂O and blocked in in 5% blocking solution (PBST-0.2% Tween-20 with 5% (w/v) milk powder) for 1 hour to minimise the background binding of antibodies. The primary antibody used to detect Marf against N-terminal peptide, DTVDKSGPGSPLSRF (Ziviani et al., 2010) was used at 1:2000 dilutions in 5% blocking solution. Mouse anti-Complex V α (MS507, MitoSciences) was used as control in 1:5000 dilutions. Membranes were incubated with primary antibodies at 4°C overnight. The membrane were given 3xPBST washes each for 20 minutes and incubated with the HRP-conjugated secondary antibodies (1:5000) for 1 hour at room temperature. For Marf, anti-rabbit HRP (Jackson ImmunoResearch) and for Complex V α , anti-mouse HRP (MitoScience) were used. The membranes were washes thoroughly with 3xPBST 10 minutes each. Proteins on the membrane were detected using ECL-Plus Chemiluminescence (RPN2132, GE Health) and recorded on photo-reactive films (28906837, GE Healthcare).

Chapter 3: Mitochondrial morphology in
axonal neuropathies associated with
***Mfn2* mutations**

3.1 Introduction

The ideal model system to study the pathological effects of *Mfn2* pathogenic alleles are CMT2A patient derived motor or sensory neurons. However, these cells are not readily available but patient derived primary skin fibroblasts are easily available and already a well established model to study disease pathology for various common diseases (Connolly, 1998; Auburger et al., 2012). Skin fibroblasts present a disease model system where pathological mutations are expressed at physiological levels along with the aggregated cell damage according to the patient's age and polygenic and environmental risk factors faced by the patients (Connolly, 1998; Auburger et al., 2012). Patient skin fibroblasts have been used to study disease mechanisms in Parkinson's disease, Alzheimer's disease, amyotrophic lateral sclerosis and other neurological diseases (Huang et al., 1994; Mortiboys et al., 2008). Mitochondrial function, morphology and distribution have been studied in fibroblasts derived from CMT2A and HMSNVI patients (Loiseau et al., 2007; Amiott et al., 2008; Guillet et al., 2010; Chevrollier et al., 2012; Rouzier et al., 2012).

We studied mitochondrial morphology in CMT2A and HMSNVI patients carrying *Mfn2* mutations and observed mitochondrial morphology defects in HMSNVI patient fibroblasts.

3.2 Fibroblasts used in the study

Fibroblasts carrying *Mfn2* mutations used in this project were obtained from Professor Frank Baas (Academic Medical Centre, Amsterdam, Netherlands). *Mfn2* mutations were also characterised in his lab. We have 2 family members (Patient 1 and Patient 2) with Charcot-Marie-Tooth Type 2A (CMT2A). They carry a novel point mutation Q674P, reported for the first time here. The other patient (Patient 3) has hereditary motor and sensory neuropathy type VI (HMSNVI) patient carrying a point mutation R364W in highly conserved R3 region of *Mfn2* (Zuchner et al., 2006) (**Figure 3.1**). This patient showed severe form of axonal degeneration, muscle loss and optic atrophy and was wheelchair bound. The onset of CMT was at the age of 1 year old and developed bilateral optic atrophy at the age of 10. Also fibroblasts obtained from 3 unrelated, non-CMT individuals with wild type *Mfn2* were used as control.

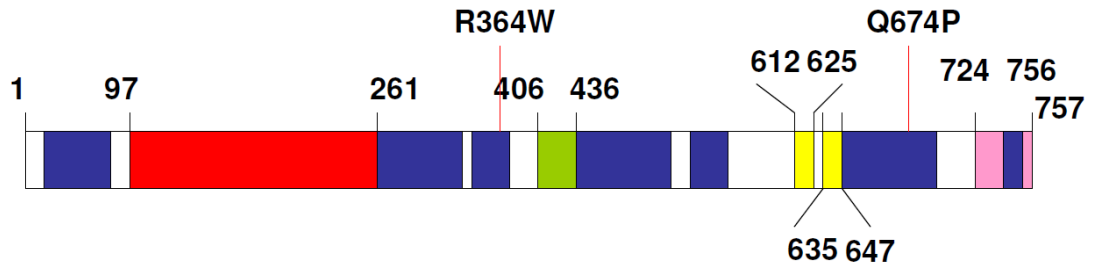


Figure 3.1: Location of *Mfn2*^{R364W} and *Mfn2*^{Q674P} in the gene. *Mfn2* mutations carried by CMT2A (Q674P present in R6 region) and HMSNVI (R364W present in R3 region) patients are indicated. GTPase domain: red box, HR1 domain: green box, yellow boxes: bi-partite transmembrane domain, HR2 domain: pink box. Blue boxes are the R regions (R1-R7) R-regions are the highly conserved regions among species including mammals, fruit fly and nematodes. (Adapted from Honda et al., 2005).

3.3 Mitochondrial morphology in CMT2A and HMSNVI patient fibroblasts

Primary fibroblasts were cultured using standard procedures and stained with MitoTracker Red CMXRos for live imaging as discussed in section 2.1.3. Mitochondria appeared as long tubular structures and loose networks in all the three control fibroblasts (**Figure 3.2**). CMT2A derived fibroblasts from Patient 1 and Patient 2 showed similar mitochondrial morphology as controls (**Figure 3.3**).

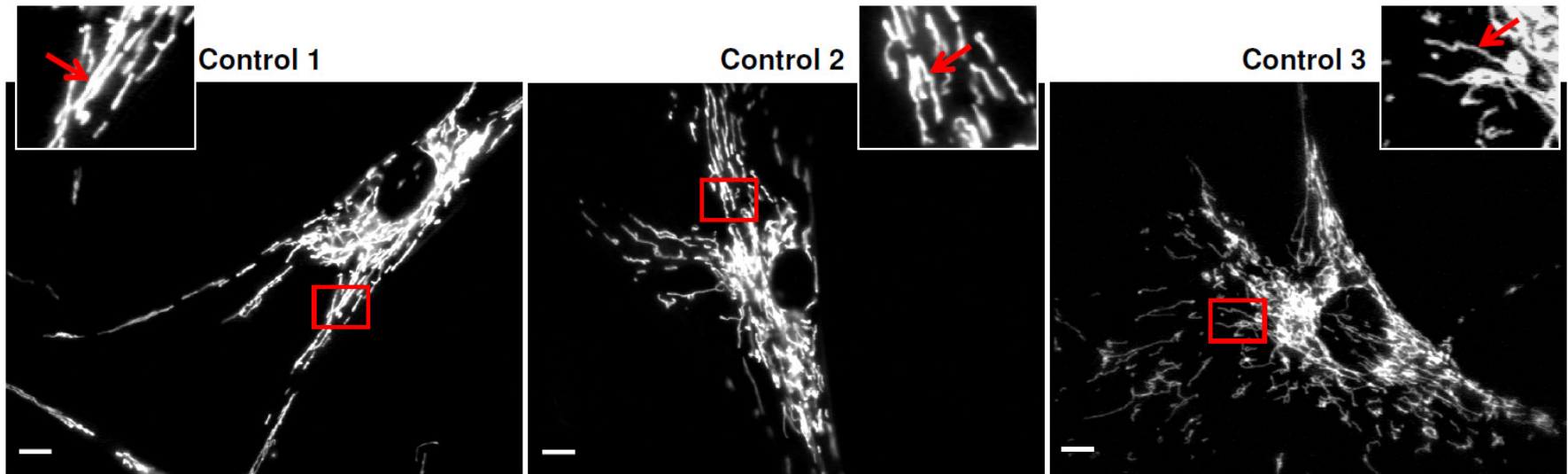


Figure 3.2: Mitochondrial morphology in Control fibroblasts. Primary fibroblasts were stained with MitoTracker Red (CMXRos) to visualize by fluorescence microscope. Control 1, Control 2 and Control 3 showed long tubular mitochondria (indicated with arrows in inset) and mitochondrial networks in perinuclear region. Scale bar = 10 μ m.

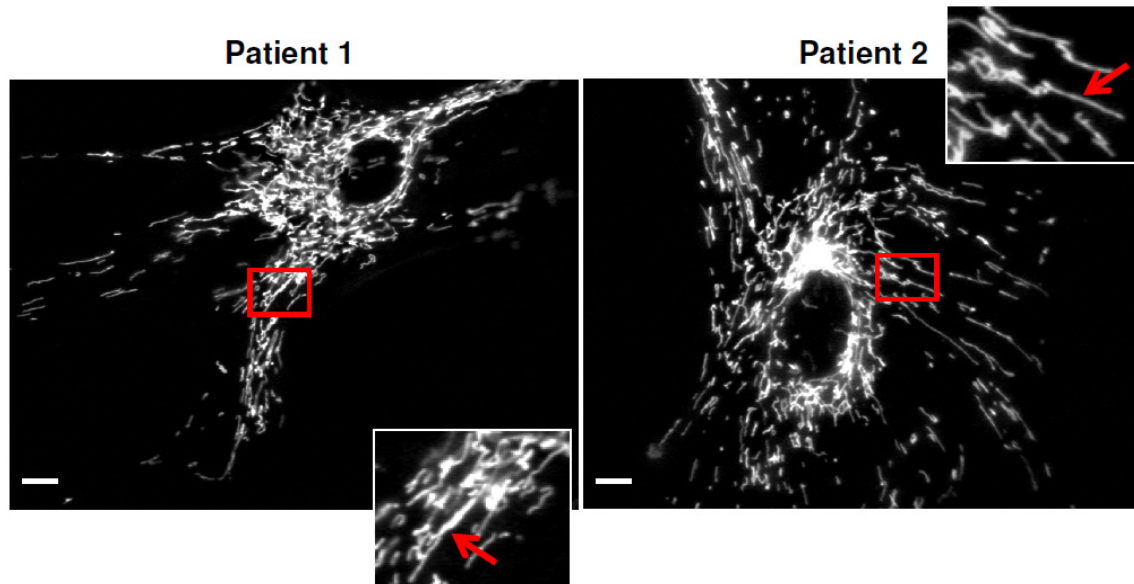


Figure 3.3: Mitochondrial morphology in CMT2A patient fibroblasts. Patient 1 and Patient 2 showed long tubular mitochondria (indicated with arrows in inset) and mitochondrial networks around perinuclear region. Scale bar = 10 μ m.

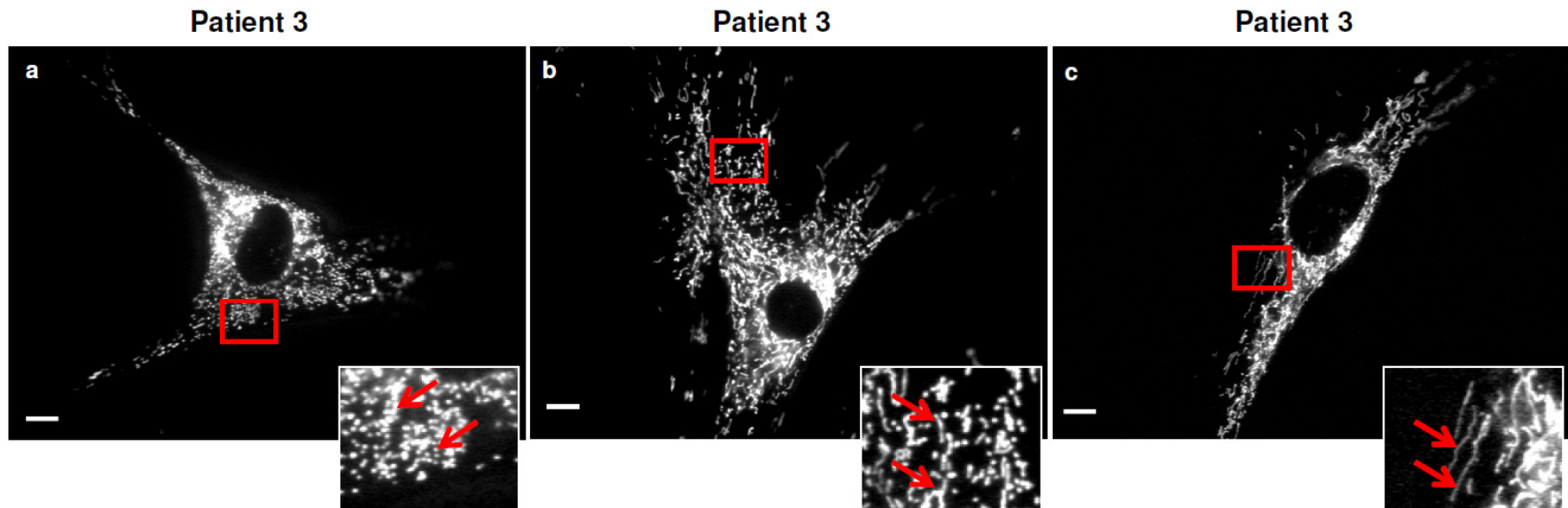


Figure 3.4: Mitochondrial morphology in HMSNVI patient fibroblasts. Patient 3 fibroblasts showed different mitochondria morphologies including fibroblasts with fragmented spherical mitochondria (a) (indicated with arrows in inset), small tubule shaped mitochondria with few branch points (b) (indicated with arrows in inset) and long tubular mitochondria with occasional branching (also considered as normal mitochondria morphology) (c) (indicated with arrows in inset). Scale bar = 10 μ m.

In contrast, Patient 3 showed variable mitochondrial morphologies across the cell samples. Fibroblasts with fragmented spherical disconnected mitochondria were predominantly present along with cells harbouring small rod shaped mitochondria with few branch points with neighbouring mitochondria (**Figure 3.4**). However, fibroblasts with normal mitochondria carrying long tubular mitochondria and mitochondria forming connections with neighbouring mitochondria were also present (**Figure 3.4**).

To quantify these different mitochondrial morphologies across the patients we carried out two different analyses; subjective analysis and a computational analysis using ImageJ software.

3.3.1 Subjective analysis for mitochondrial morphology

Images of MitoTracker Red stained cells were taken for each of the samples. Scoring was performed once the investigator had been blinded to the sample ID. Each cell was scored as one of three categories: Small and spherical shaped mitochondria lacking connections with neighboring mitochondria were categorized as fragmented mitochondria. Small rods shaped mitochondria with less frequent branching were categorized as small tubular mitochondria. Generally, in fibroblasts mitochondria appear as long filamentous tubules dispersed throughout the cytosol and mitochondrial networks in the perinuclear region. Such morphology was categorized as normal mitochondrial morphology in our subjective analyses (**Figure 3.2**). Mitochondrial morphology was scored from 50-60 cells per experiment from 3 independent experiments and the percentage of cells that showed normal mitochondrial morphology (**Figure 3.2**, **Figure 3.3**, **Figure 3.4c**) or fragmented mitochondria (**Figure 3.4a**) or small tubular mitochondria (**Figure 3.4b**) was calculated.

Patient 1 and Patient 2 showed zero fibroblasts with fragmented mitochondria, however Patient 3 showed significantly high percentage of fibroblasts with fragmented mitochondria as compared to the controls (**Figure 3.5A**). Patient 3 also showed significantly higher percentage of fibroblasts with small tubular mitochondria. A small percentage of cells with small tubular mitochondria were also observed in Control 2 and Control 3. Patient 2 also showed few cells with small mitochondrial tubules but the difference was insignificant as compared to the controls (**Figure 3.5B**). Patient 3 showed significantly less fibroblasts with normal mitochondrial morphology (**Figure 3.5C**).

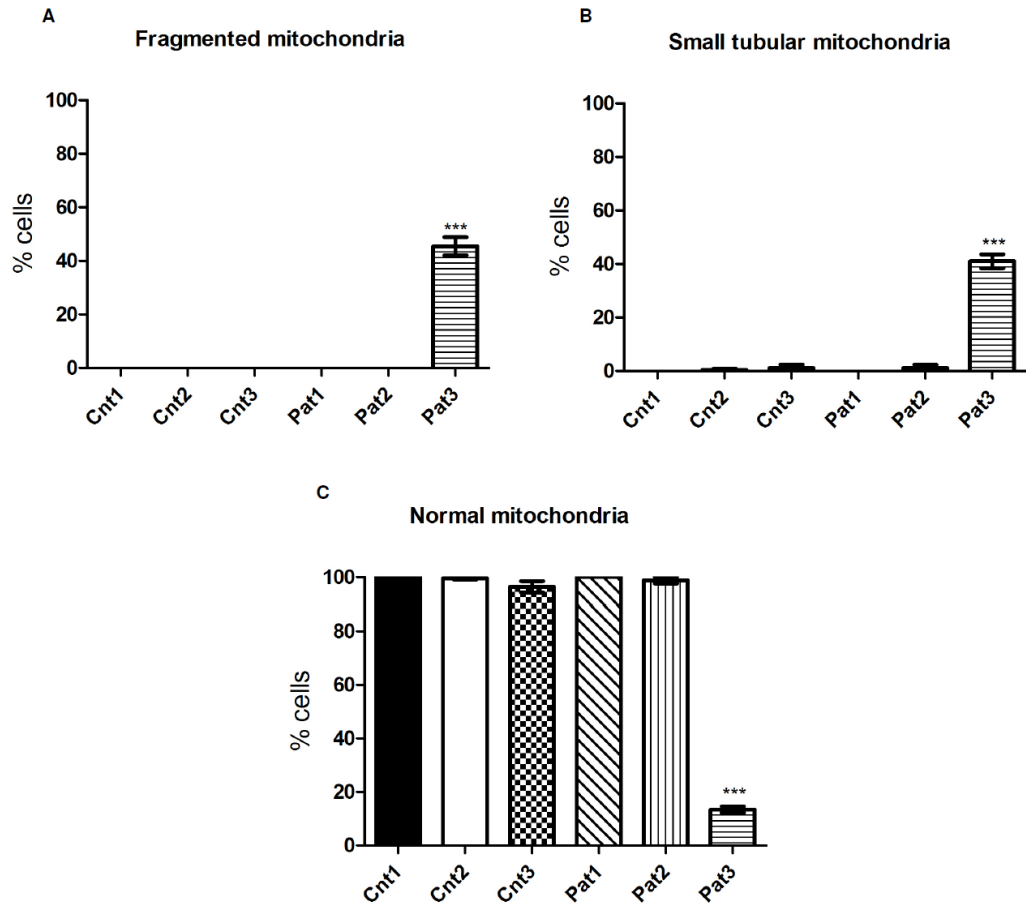


Figure 3.5: Subjective analysis for mitochondrial morphology. Fibroblasts were scored blindly for fragmented (A), small tubules (B) and normal mitochondrial morphologies (C). Control 1: black bar, Control 2: white bar, Control 3: dotted bar, Patient 1: angled striped bar, Patient 2: vertical striped bar and Patient 3: horizontal striped bar. Data is presented as mean±standard error. Statistical significance was determined by one-way ANOVA followed by Tukey’s multiple comparison. (***) $P < 0.001$.

3.3.2 Mitochondrial morphology analysis using ImageJ Software

Image analysis was done with the open-source image analysis programs ImageJ (developed by W. Rasband, National Institutes of Health, Bethesda, MD; <http://rsb.info.nih.gov/ImageJ>) and the plugins written by K. De Vos. To quantify mitochondrial morphology in fibroblasts different mitochondrial shape attributes were selected see section 2.2.5.1 and 2.2.5.2.

3.3.2.1 Patient 3 fibroblasts showed reduced mitochondrial aspect ratio and length

Mitochondria appear as long tubular structures and extensive networks forming in fibroblasts. To determine the shape of individual mitochondria segregating from the connected mitochondrial structures mitochondrial aspect ratio and mitochondrial length was determined using ImageJ software as discussed in section 2.2.5.1. Patient 1 and Patient 2 showed normal aspect ratios as compared to controls (**Figure 3.6A**). However, Patient 3 showed significantly reduced aspect ratio as compared to controls. Next mitochondrial length was measured and quantified for each sample. Mitochondrial length for Patient 1 and Patient 2 also appeared comparable to all three controls. Patient 3 showed significantly smaller mitochondria with reduced mitochondrial length (**Figure 3.6B**).

3.3.2.2 Patient 3 fibroblasts showed reduced mitochondrial bifurcation ratio and network ratio

Branching and network mitochondrial morphology, typical in fibroblasts was measured as bifurcation ratio and network complexity ratio (see section 2.2.5.2). Patient 1 showed normal bifurcation ratio as compared to controls (**Figure 3.6C**). Patient 2 showed significantly lower bifurcation ratio as compared to Control 1 and Control 2, however the difference was insignificant as compared to Control 3. Patient 3 showed significantly reduced bifurcation ratio compared to all controls (**Figure 3.6C**). The overall network complexity ratio for Patient 1 was in normal range with controls (**Figure 3.6D**). Patient 2 presented lower network complexity as compared to Control 2 only (**Figure 3.6D**). Patient 3 showed significantly reduced network complexity ratio (**Figure 3.6D**).

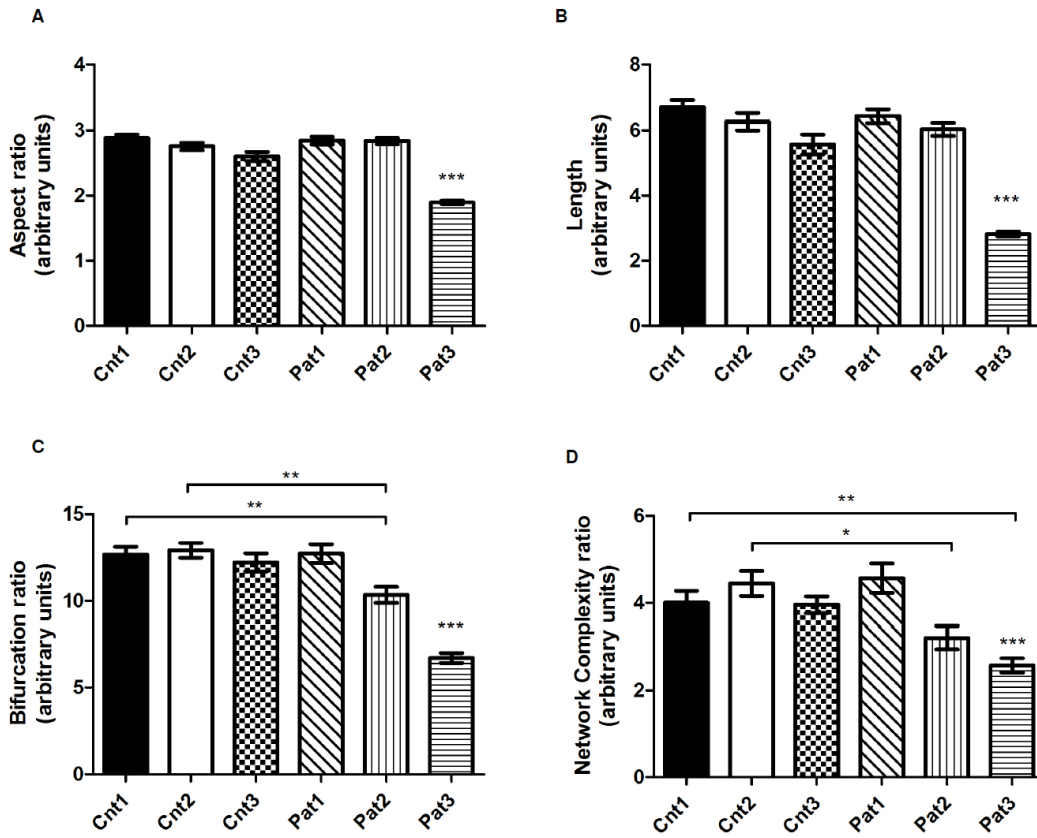


Figure 3.6: ImageJ analysis of the mitochondrial morphology. (A) Aspect Ratio. (B) Length. (C) Bifurcation ratio. (D) Network complexity ratio. 15 images were analysed for each genotype. N = 3. Data is presented as mean±standard error. Statistical significance was determined with Kruskal-Wallis non-parametric analysis and Dunn’s pair-wise comparison (***) $P < 0.001$, ** $P < 0.01$, * $P < 0.05$).

3.4. Discussion

Our results showed that fibroblasts derived from the HMSNVI patient (Patient 3) carrying a heterozygous *Mfn2*^{R364W} mutation showed fragmented mitochondrial morphology with reduced mitochondrial aspect ratio, mitochondrial length, bifurcation ratio and network complexity ratio. CMT2A patients (Patient 1 and 2) harbouring heterozygous *Mfn2*^{Q674P} mutation showed normal mitochondrial morphology. However, computational analysis highlighted the subtle mitochondrial morphology defects in Patient 2, showing reduced mitochondrial bifurcation ratio and network complexity ratio. Due to limitation of number of HMSNVI and CMT2A patients we can not make conclusive result that the defected morphology we saw in this Patient 3 is typical to *Mfn2* pathogenic mutations or is just a novel case due to some other underlying pathology in this patient. Furthermore, ImageJ analysis proved to be useful tool to quantify the mitochondrial morphology efficiently.

Two previous studies have shown normal mitochondrial morphologies in CMT2A patient fibroblasts and are comparable to the normal mitochondrial morphology observed in our CMT2A patients (Loiseau et al., 2007; Amiott et al., 2008). Appearance of normal mitochondrial morphology in CMT2A fibroblasts suggests that disease-associated *Mfn2* alleles are able to form fusion competent complexes with *Mfn1*. As *Mfn2* CMT2A associated alleles restore normal mitochondrial morphology in *Mfn2* knockout mouse embryonic fibroblasts by forming *Mfn1/Mfn1* and *Mfn1/Mfn2* (CMT2A allele) hetero oligomeric complexes (Detmer and Chan, 2007a).

HMSNVI patient (Patient 3) carrying a heterozygous *Mfn2*^{R364W} mutation was first discussed by Zuchner et al (Zuchner et al., 2006). According to their findings, Patient 3 was 10 years old and disease onset was at 1 year age (Zuchner et al., 2006). This individual presented severe muscular atrophy, sensory impairments, reduced visual acuity and was restricted to a wheelchair at an early age. The individual also presented with respiratory insufficiency. The severity of the clinical symptoms presented by this patient is consistent with significantly fragmented mitochondrial morphology observed in the skin fibroblast derived from this patient. The fragmented mitochondrial morphology seen in Patient 3 suggests defective mitochondrial fusion and inability of *Mfn1/Mfn1* and *Mfn1/Mfn2* (CMT2A allele) hetero oligomeric complexes to maintain a normal mitochondrial fusion. Previously, Loiseau et al also studied mitochondrial

morphology in a patient harbouring heterozygous *Mfn2*^{R364W} mutation and reported normal mitochondrial morphology in fibroblasts (Loiseau et al., 2007). This patient was a 31 years old man, who was 20 at the onset of his initial symptoms and has moderate ankle weakness, normal gait, normal motor conduction velocity and no optic atrophy. The difference seen in clinical phenotypes and mitochondrial morphology in these two patients carrying the same mutation highlights the degree of variability presented by the CMT2A and HMSNVI patients and suggests the existence of disease modifying factors. These factors could possibly be a mutation in other gene/genes, which can exacerbate the disease and result in severe early onset or reduce the effects of mutation, thereby reducing disease penetrance. Alternatively the modifying factor could be environmental such as exposure to a currently unidentified neurotoxic factor. As discussed earlier *Mfn2* associates directly and indirectly with other cellular proteins and pathways and these interactions play their role in mitochondrial dynamics. Mutations in any of the interacting proteins can exaggerate the deleterious effects of *Mfn2* mutations itself in a subset of patients with early onset and severe neuropathy.

Furthermore, Patient 3 is not a novel case showing fragmented mitochondrial morphology as recently another study has also shown fragmentation of mitochondrial networks in fibroblasts carrying *Mfn2* mutation D210V. However, this mutation is associated with Optic atrophy ‘plus’ phenotype as the patient presented with optic atrophy as initial clinical complication with the development of sensorineuropathy and muscular atrophy (Rouzier et al., 2012). This report showed reduced *Mfn2* expression in patient fibroblasts which might lead to reduced mitochondrial fusion. In our opinion, it might be possible as low levels of Mfn1/Mfn2 (normal copy) and Mfn1/Mfn2 (mutation allele) complexes are being formed in less abundance and Mfn1/Mfn1 complexes are unable to fulfil the requirement for normal mitochondrial morphology. We also know that *Mfn2* deficient MEFs and mice have shown fragmented mitochondrial morphology and metabolic defects and recently *Mfn2*^{R94W} knock-in mice showed fragmented mitochondria in MEFs (Chen et al., 2003; Chen et al., 2007; Strickland et al., 2014).

Inter and intra familial variabilities in disease penetrance have been reported in many studies showing family members with severe, mild and asymptomatic individuals, individuals with early onset, rapidly progressive severe neuropathy and individuals with late onset, slowly progressive mild sensory neuropathy (Muglia et al., 2007; Del Bo et al, 2008; Klein et al., 2011). Such variabilities support the incomplete penetrance of *Mfn2* mutations and highlight the importance of interacting gene/genes affecting the

disease phenotype. We could also investigate the haploinsufficiency by determining the expression level of Mfn2 mRNA and protein in our patient fibroblasts as compared to controls. In addition, heterozygous patients carrying more than one mutation are also reported (Polke et al., 2011). Additionally, we have recently showed that zebrafish with a null mutation develop symptoms consistent with CMT which supports the loss of function as disease mechanism (Chapman et al., 2013).

Chapter 4: Effect and role of Ethacrynic
Acid on mitochondrial fusion

4.1 Introduction

Mitochondrial fusion and fission are essential for mitochondrial function and are also involved in fundamental cellular processes, including development, apoptosis, and ageing. However, the role of mitochondrial fusion and fission in cell function and survival is still poorly understood. Most commonly used approaches to study mitochondrial dynamics are either to knockdown gene expression using RNAi methods or use dominant-negative mutants affecting the expression of pro-fusion and pro-fission proteins. We know that changes in mitochondrial morphology occur within minutes to hours but the changes due to genetic manipulations take much longer time to be detected. There is a need to identify compounds that produce changes in mitochondrial morphology on the time scale of minutes to hours to study these cellular processes more conveniently and such approaches might also help to provide novel insight into these dynamic processes. One of the known mitochondrial fusion-inducing compounds is ethacrynic acid (EA) identified by Soltys and Gupta (Soltys and Gupta, 1994).

EA is an α,β -unsaturated ketone which acts as a cysteine alkylator and is able to deplete cellular glutathione without an increase in reactive oxygen intermediates (ROIs) (Ciaccio et al., 1994; Seyfried et al., 1999; Rizzardini et al., 2003). The known cellular targets of EA alkylation are adenylate cyclase coupled G-proteins, sodium potassium chloride (Na-K-2Cl) cotransporter and ATP-dependent Cl⁻ transporter, and it was previously clinically tested as diuretic (Kunugi et al., 1991; Palfrey and Leung, 1993). In cultured cells, EA treatment induced end-to-end fusion resulting in increased mitochondrial length and end to side fusion to form a mitochondrial reticulum (Soltys and Gupta, 1994). However, in the presence of 0.5mM dithiothreitol, a sulfhydryl reagent, EA was unable to produce mitochondrial reticulum. This suggested that EA induced mitochondrial fusion could be mediated by cellular thiols (Soltys and Gupta, 1994). However, a saturated EA analogue; Dihydro-EA which lacks the central α,β -unsaturated ketone structure did not induce mitochondrial fusion in cells, suggesting that the α,β -unsaturated ketone group is responsible for EA toxicity and unique fusion inducing nature (Bowes and Gupta, 2005). Gupta and colleagues also tested a well-known cysteine alkylator N-ethylmaleimide and found that it produced a similar mitochondrial reticulum as observed in cells treated with EA (Bowes and Gupta, 2005). This suggests that induction of mitochondrial fusion by EA is not due to glutathione depletion but could possibly be due to the cysteine alkylating nature of the compound (Bowes and Gupta, 2005). Thus it is possible that EA induces mitochondrial fusion by

modifying critical cysteine residue(s) in proteins involved in mitochondrial dynamics (Bowes and Gupta, 2005).

We wanted to further characterise EA, in order to understand how it causes increased mitochondrial fusion in cells. I wanted to determine whether EA could be developed as a potential treatment for diseases where there are mutations in mitochondrial fusion factors such as CMT2A, or whether it would simply be a useful tool compound to study mitochondrial dynamics in laboratory assays. Our working hypothesis was that EA induce mitochondrial fusion by acting as a cysteine alkylator. This is possible by two distinct mechanisms: either EA is inhibiting a negative regulator/repressor of the fusion machinery or it is inactivating positive regulators important for fission (**Figure 4.1**). However, as this investigation is the part of larger drug screening project being carried out to identify the compounds affecting mitochondrial morphology, we included other compounds in the screen as discussed in the following result sections.

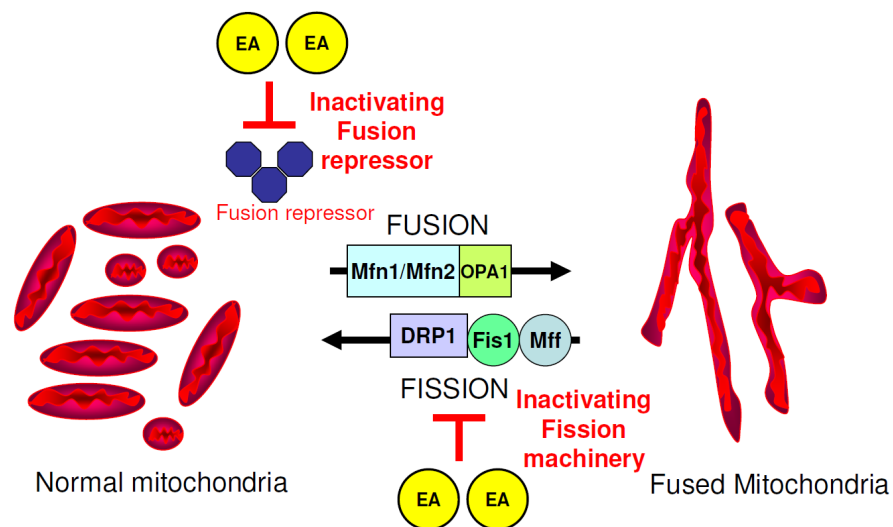


Figure 4.1: Schematic of EA working hypothesis. EA is acting as a protein inactivator by alkylating essential cysteine residue(s) of either pro-fission proteins (Drp1, Fis1, Mff or an unknown protein) or fusion repressor/s.

4.2 Background and initial compound screen

Dr. Andrew Grierson in Academic Neurology, University of Sheffield carried out primary screen in fibroblasts derived from a hereditary motor and sensory neuropathy type VI (HMSNVI) patient carrying a *Mfn2*^{R364W} mutation to identify compounds affecting mitochondrial morphology. He used 2000 compounds from the SPECTRUM Collection and 4 compounds identified from published work suggesting their involvement in mitochondrial dynamics and/or transport. He used a single dose of each compound and observed its effect on the mitochondrial morphology as mitochondrial fusion enhancer. From this primary screen 10 potential candidates were identified, and were further studied by me in a secondary screen carried out in CV14A cells (**Table 4.1**).

4.2.1 Effect of candidate compounds on mitochondrial morphology in CV14A cells

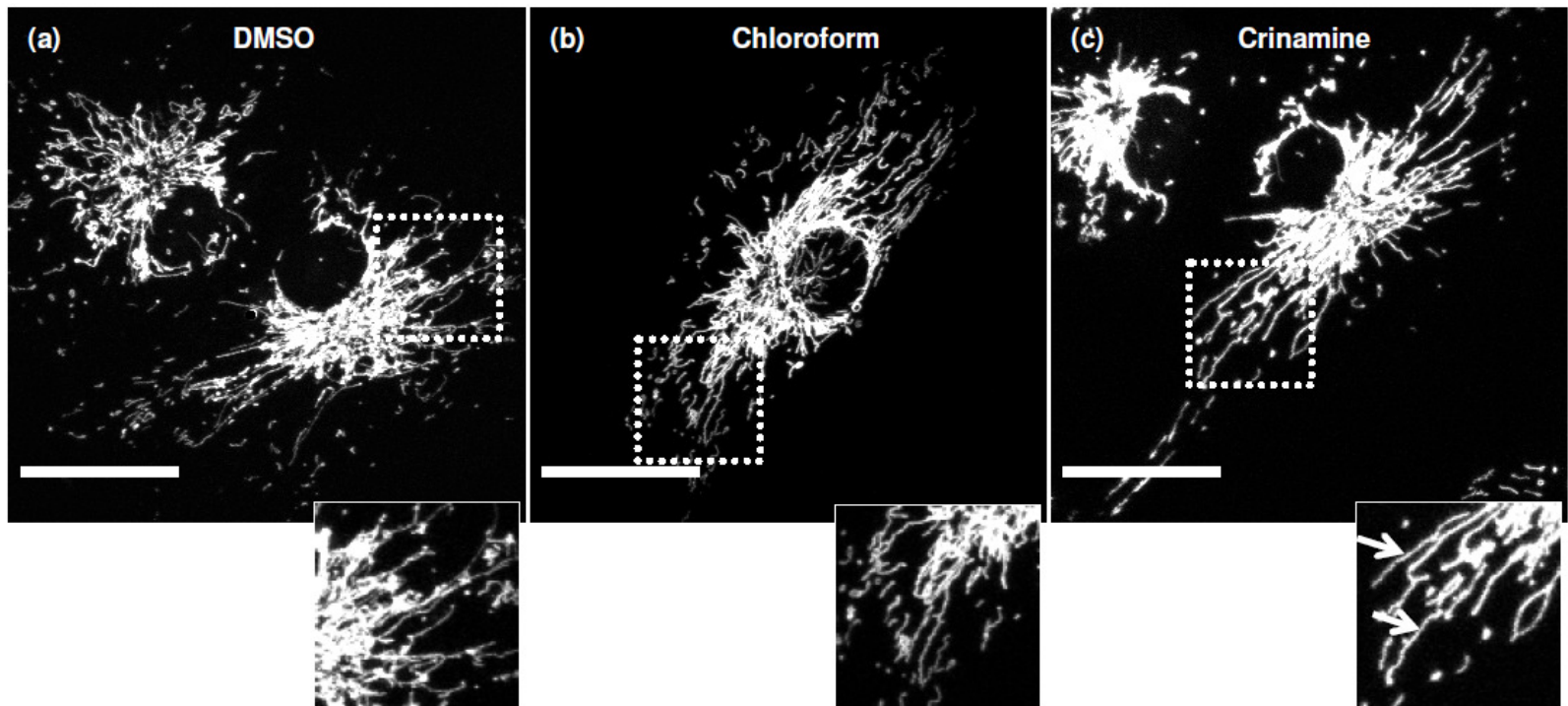
CV14A cells stably expressing DsRed1mito were used for the secondary screen. These cells normally have mitochondrial networks around the nuclear region with long rod shaped mitochondria reaching to the cell periphery. CV14A cells also contain few spherical mitochondria. Cells were plated 18-20 hours prior to incubation with test compounds. Serial dilutions of all the compounds were made in DMEM media. Each compound was tested at the concentrations shown in **Table 4.1** for incubation periods of 15 minutes, 4 hours and 24 hours on three separate occasions. Positive hits were defined as compounds that gave increased mitochondrial length and networks (also defined as mitochondrial reticulum) morphology. Mitochondrial morphology of cells was scored as increased fusion or no increase in fusion; however, scoring was not done blind and formal statistical tests were not applied.

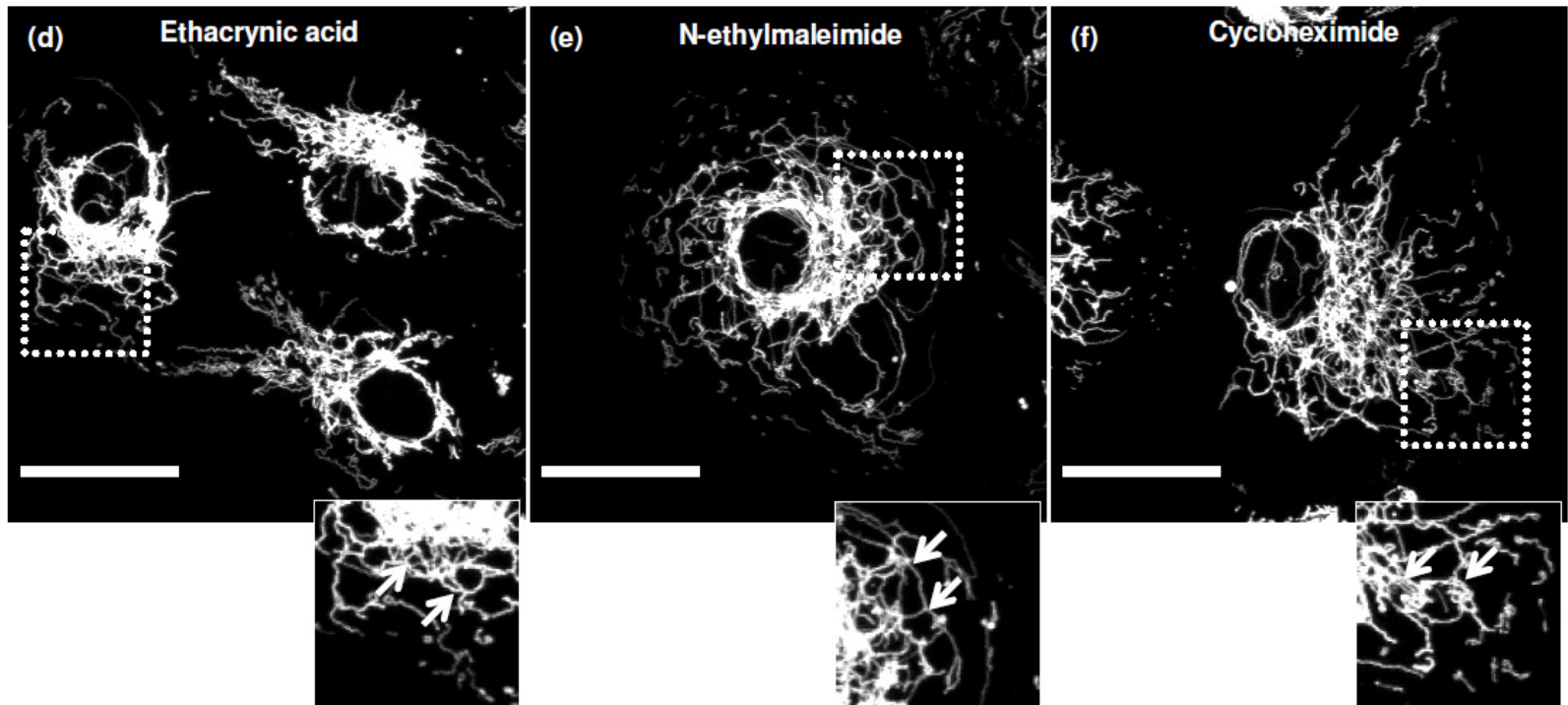
0.1% DMSO and 0.1% chloroform were used as vehicles. CV14A cells incubated with 0.1% DMSO or 0.1% chloroform showed normal mitochondrial morphology with perinuclear mitochondrial networks and long and small rod shaped mitochondria near the cell periphery designated as normal mitochondrial morphology in these cells (**Figure 4.2**). In 15 minute drug incubation experiment, cells showed increased mitochondrial network morphology or typical mitochondrial reticulum formation only with 165 μ M EA. However, 4 hour drug incubation showed increased mitochondrial fusion with EA, NEM and cycloheximide. Mitochondrial reticulum

formation was seen with 41 μ M EA, 83 μ M EA, 165 μ M EA, 2 μ M N-ethylmaleimide (NEM) and 100 μ M cycloheximide. However, long incubation of 24 hours proved to be an ideal time frame to characterise the effects of all the compounds on mitochondrial morphology (**Table 4.1** and **Figure 4.2**). Cells incubated with EA (2.6-81 μ M) showed increased mitochondrial networks in a dose dependent manner. 165 μ M EA proved to be toxic as cells rounded up and detached from cover slip. NEM (0.2-2 μ M) and cycloheximide (10-100 μ M) also showed extensively interconnected mitochondrial networks after 24 hours incubation (**Figure 4.2**). All the mitochondria in the cell appeared to have joined together making continuously interconnected reticulum with EA and NEM. However with cycloheximide few separated mitochondria near cell periphery were also observed in addition to the central mitochondrial reticulum. Also, crinamine (10 μ M) showed long tubular mitochondria as compared to controls but no mitochondrial reticulum was seen in the cells (**Figure 4.2**). Podophylotoxin acetate, a microtubule inhibitor, showed a unique mitochondrial morphology with less branching or network formation but more curly large and small mitochondrial rods (**Figure 4.2**). Dopamine HCl (1-100 μ M), β -Sitosterol (2.5-250 μ M) and 12-Methoxy-4,4 bisnor-5 α -8,11,13-podocarpatrien-3-ol (12 Methoxy) (10 μ M), showed no obvious effects on mitochondrial morphology and mitochondria appeared similar to the controls (**Figure 4.2**). Mitochondria in dynasore (5-500 μ M) treated cells lack any connections and appeared as small rods distributed throughout the cytoplasm (**Figure 4.2**). MTMA bromide (3-300 μ M) showed small round and aggregated mitochondria in the entire cell lacking any mitochondrial branching (**Figure 4.2**). The secondary screen identified EA, NEM, cycloheximide and crinamine as positive hits for increased mitochondrial fusion morphology observed in CV14A cells. However, NEM and crinamine were excluded from further analysis (see the discussion section for details).

Table 4.1: Compounds tested in secondary drug screen.

COMPOUND	SOURCE	PUTATIVE FUNCTION	REFERENCE	CONCENTRATIONS USED	EFFECT ON MITOCHONDRIAL MORPHOLOGY
Crinamine	Spectrum Collection	Unknown	-	10 μ M	Increased fusion, longer mitochondria
Ethacrynic acid	Literature Search	Cysteine alkylator, GSH depletion	Soltys and Gupta, 1994, Bowes and Gupta, 2005	1.3 μ M, 2.6 μ M, 5 μ M, 10 μ M, 21 μ M, 41 μ M, 83 μ M, 165 μ M	Increased fusion, mitochondrial reticulum formation
N-ethylmaleimide	Literature Search	Cysteine alkylator	Bowes and Gupta, 2005	0.2 μ M, 2 μ M, 20 μ M	Increased fusion, mitochondrial reticulum formation
Cycloheximide	Spectrum Collection	Protein synthesis inhibitor	-	1 μ M, 10 μ M, 100 μ M	Increased fusion, mitochondrial reticulum formation
Dynasore	Literature Search	Dynamin inhibitor	Macia et al., 2006	5 μ M, 50 μ M, 500 μ M	Reduced fusion, small mitochondrial rods/tubules
Podophylotoxin acetate	Literature Search	Microtubule inhibitor	Gupta, 1983	1 μ M, 10 μ M, 100 μ M	Reduced fusion, curly large and small mitochondria rods
MTMA bromide	Spectrum Collection	Unknown	-	3 μ M, 30 μ M, 300 μ M	Reduced fusion, small round aggregated mitochondria
β -Sitosterol	Spectrum Collection	interact with phosphoglycerol	-	2.5 μ M, 25 μ M, 250 μ M	No effect
Dopamine HCl	Spectrum Collection	Catecholamine neurotransmitter	-	1 μ M, 10 μ M, 100 μ M	No effect
12-Methoxy-4,4 bisnor-5 α -8,11,13-podocarpatrien-3-ol	Spectrum Collection	Unknown	-	10 μ M	No effect





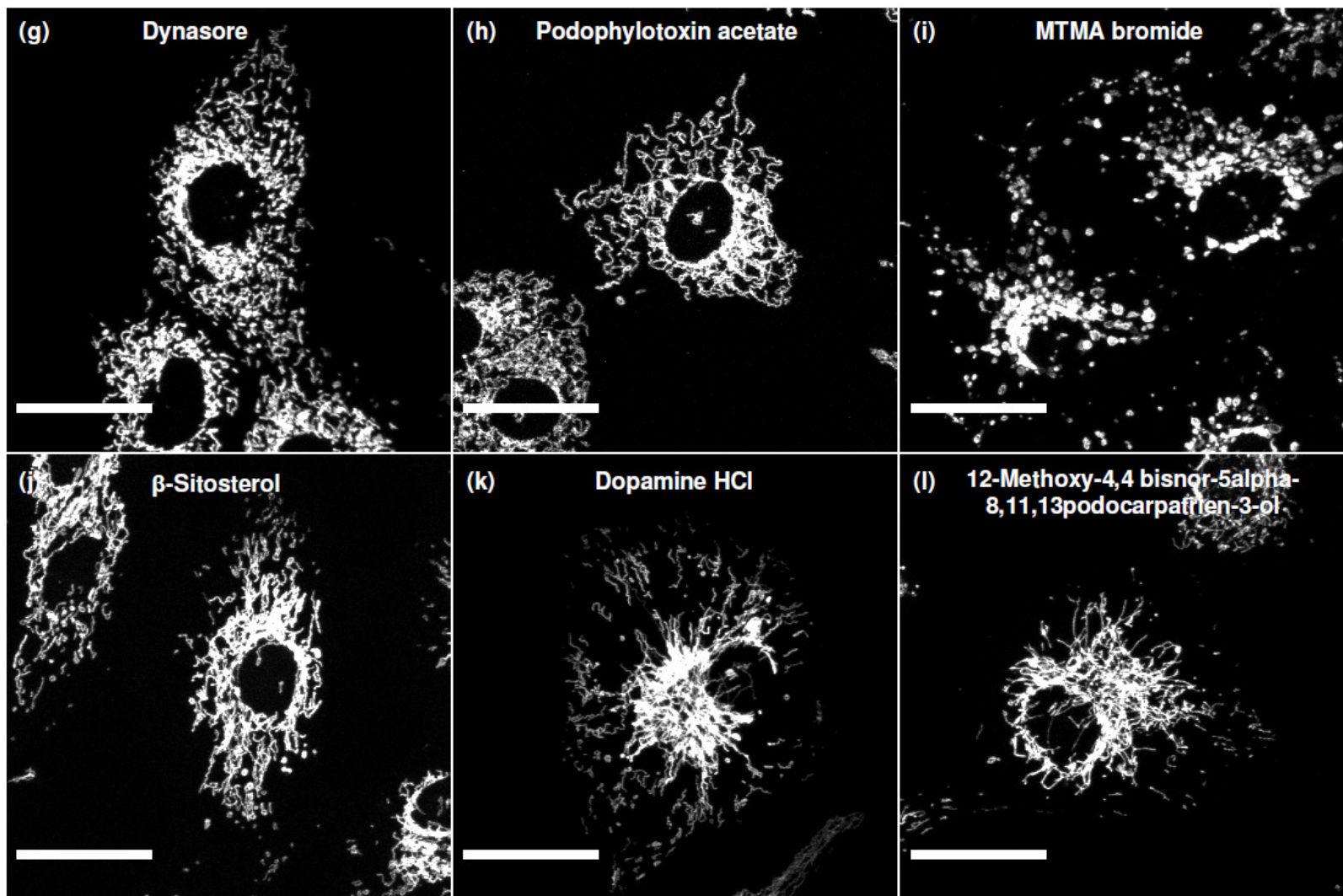


Figure 4.2: Screen for mitochondrial fusion inducing compounds in CV14A cells. Representative images of each compound showing its effect on mitochondrial morphology after 24 hours incubation are shown. (a) 0.1% DMSO and (b) 0.1% Chloroform used as vehicles. (c) Crinamine 10 μ M (arrows indicate long tubular mitochondria) (d) Ethacrynic Acid 41 μ M (arrows indicate mitochondrial reticulum formation, increased branching) (e) N-ethylmaleimide 2 μ M (arrows indicate mitochondrial reticulum formation) (f) Cycloheximide 10 μ M (arrows indicate mitochondrial reticulum formation) (g) Dynasore 10 μ M, (h) Podophylotoxin acetate 10 μ M, (i) MTMA bromide 10 μ M, (j) β -Sitosterol 25 μ M, (k) Dopamine HCl 10 μ M, (l) 12-Methoxy-4,4 bisnor-5 α -8,11,13-podocarpatrien-3-ol 10 μ M. Scale bar = 10 μ m.

4.2.2 Analysis of compound toxicity for EA, NEM and Cycloheximide

MTT (3-(4,5-dimethylthiazol-2-yl)-2,5-diphenyl tetrazolium bromide) assay was used to analyse cytotoxicity of the compounds. The principle of the assay is the reduction of MTT salt by mitochondrial succinate dehydrogenase in metabolically active cells (Mosmann, 1983). *Mfn2*^{R364W} patient fibroblasts were incubated with various concentrations of EA, NEM and cycloheximide for 24 hours. 0.1% DMSO was used as control. Cytotoxicity was calculated as cell survival with drug relative to the cell survival with 0.1% DMSO (vehicle). *Mfn2*^{R364W} patient fibroblasts treated with lower doses of EA showed a trend towards increased cell survival but this effect was not statistically significant relative to the control (**Figure 4.3A**). Cell survival declined at concentrations higher than 10µM EA with significant reduction at concentration of 41µM, 83µM and 165µM EA (**Figure 4.3A**). In CV14A cells, EA showed less toxicity. Cell survival declined above 83µM EA but the effect was not significant as compared to control (**Figure 4.3B**). However, these cells showed significant decrease in cell survival with 165µM EA (**Figure 4.3B**). Furthermore, in *Mfn2*^{R364W} patient fibroblasts NEM showed significant decrease in relative cell survival in a dose dependent manner (**Figure 4.3C**). Also, cycloheximide showed significantly reduced cell survival relative to the control in *Mfn2*^{R364W} patient fibroblasts but this remains constant without further decrease at higher doses (**Figure 4.3D**).

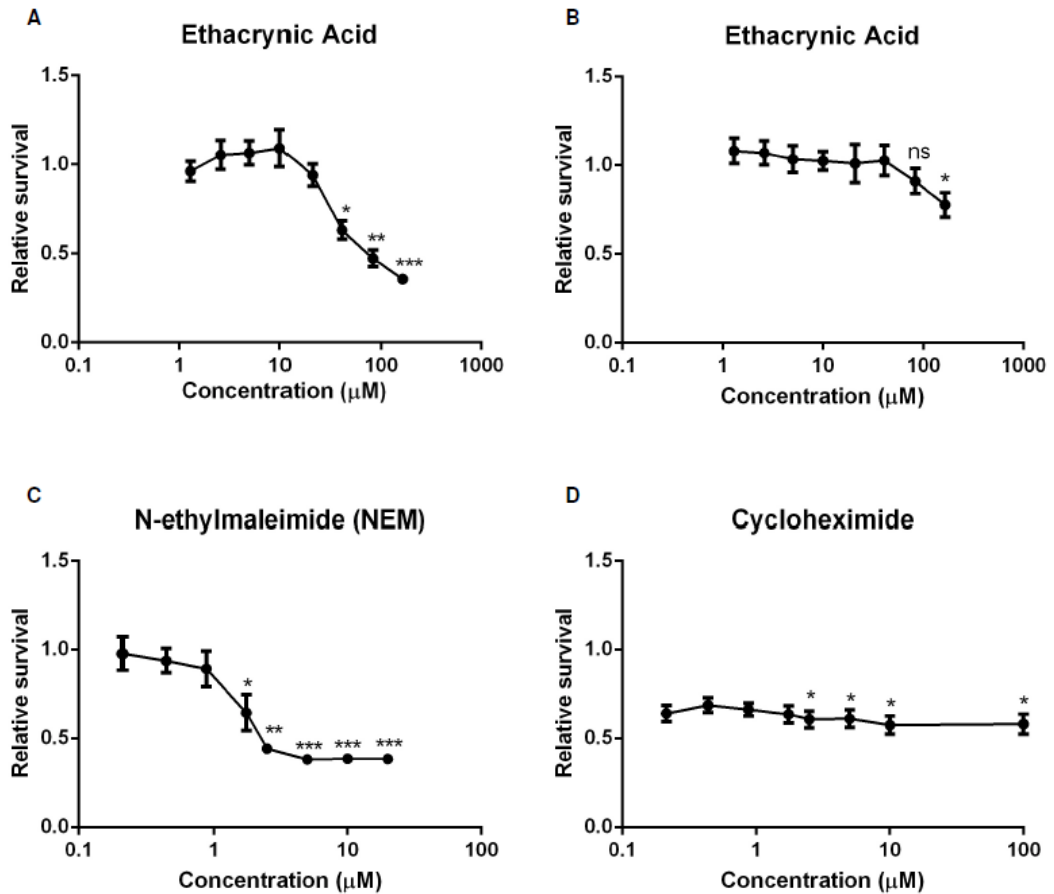


Figure 4.3: MTT assay. (A) Relative cell survival of *Mfn2*^{R364W} patient fibroblasts after 24 hours treatment with ethacrynic acid. (B) Relative cell survival of CV14A cells after 24 hours treatment with ethacrynic acid. (C) Relative cell survival of *Mfn2*^{R364W} patient fibroblasts after 24 hours treatment with N-ethylmaleimide. (D) Relative cell survival of *Mfn2*^{R364W} patient fibroblasts after 24 hours treatment with cycloheximide. N = 3 independent experiments. Statistical significance was determined by student t-test (****P* < 0.001, ***P* < 0.01, **P* < 0.05).

4.3 PEG fusion assay for EA and Cycloheximide

The fusion activity of EA and cycloheximide was tested in polyethylene glycol (PEG) mitochondrial fusion assay see section 2.5.2. In this assay, CV14A cells containing either DsRed1mito or GFPmito were co-cultured and PEG was transiently applied to fuse the cells. This is followed by incubation with the respective drug along with cycloheximide. Addition of cycloheximide is a part of the standard protocol to prevent synthesis of new fluorescent molecules in the fused cells. Cellular fusion results in the formation of bi or multi-nucleated cell hybrids. These hybrids allow cytoplasmic mixing where DsRed1mito and GFPmito labelled mitochondria interact and undergo fusion which can be seen as mixing of the both fluorescent tags. To quantify fusion activity the hybrids between the two cell lines were visually evaluated and scored. The scoring criteria used are shown in **Figure 4.4A**, with 0% fusion in cells where no overlapping or co-localised fluorescent DsRed and GFP signals were present. Less than 50% fusion was scored for hybrids where less than half of the cell has shown co-localised DsRed and GFP fluorescent. Cell hybrids showing half or more than half of mitochondrial population with DsRed+GFP co-localisation were scored as more than 50% fusion activity. Full or 100% fusion was scored for cell hybrids that exhibited a complete overlay of mito-DsRed and mito-GFP.

After 4 hours of incubation, CV14A cells were fixed as shown in section 2.3.1.4, and 50-60 cell hybrids were scored blindly for each concentration. Cells incubated with 0.1% DMSO showed majority of cells with 0% and less than 50% fused cells and no cell hybrids with full fusion were observed (**Figure 4.4B**). Cells incubated with EA showed increase in cell hybrids with increased mitochondrial mixing in dose dependent manner (**Figure 4.4B**). Number of cells with more than 50% fusion and 100% fusion increased with the increase in EA concentration. With 165 μ M EA only 6% of cell population showed zero fusion (**Figure 4.4B**). The two experiments performed for EA are two biological replicates and statistical analysis was performed. However, we suggest in order to determine formal statistical significance this assay has to be repeated with at least 3 biological replicates which is considered as standard. Therefore, at this point the PEG fusion assay results are preliminary but indicate that ethacrynic acid is increasing fusion in cells at higher concentrations.

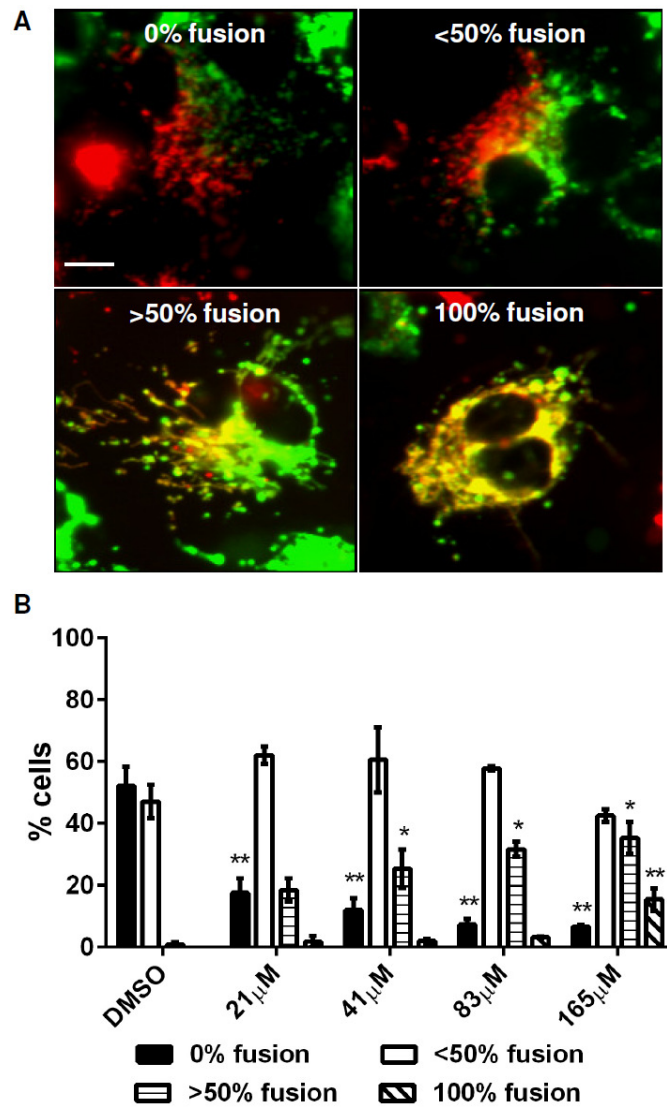


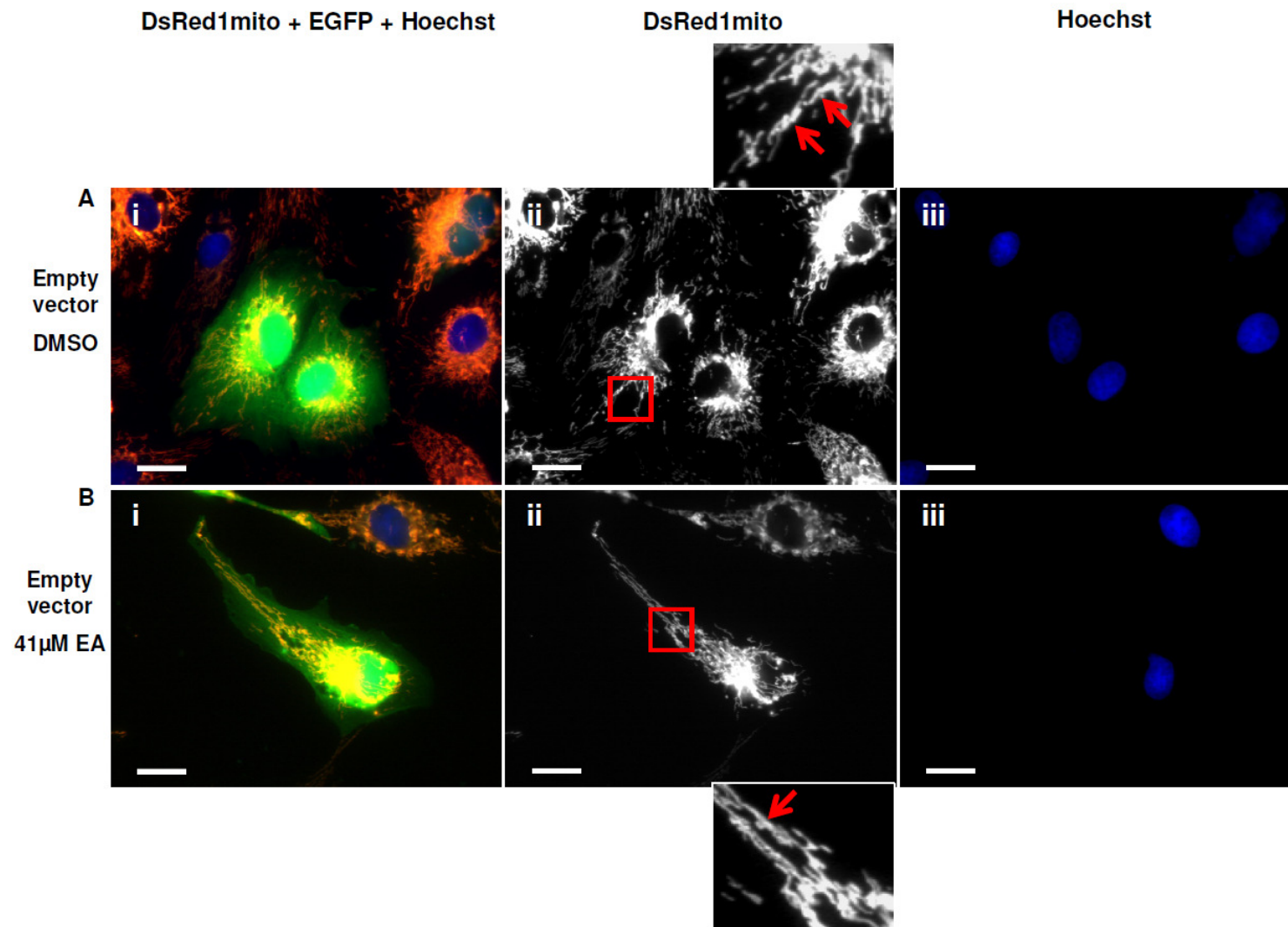
Figure 4.4: Mitochondrial fusion assay. PEG fusion of CV14A cells stably expressing mito-DsRed1mito and GFPmito. (A) Representative images for the fusion scoring criteria. Following 4 hours of drug incubation cells were scored for 0% fusion, less than 50% fusion, more than 50% fusion and full or 100% fusion. Scale bar = 5 μ m (B) PEG fusion assay for EA. Data is presented as mean \pm standard error. n = 50 cells, N = 2 independent experiments. Statistical significance was determined by student t-test (** $P < 0.01$, * $P < 0.05$).

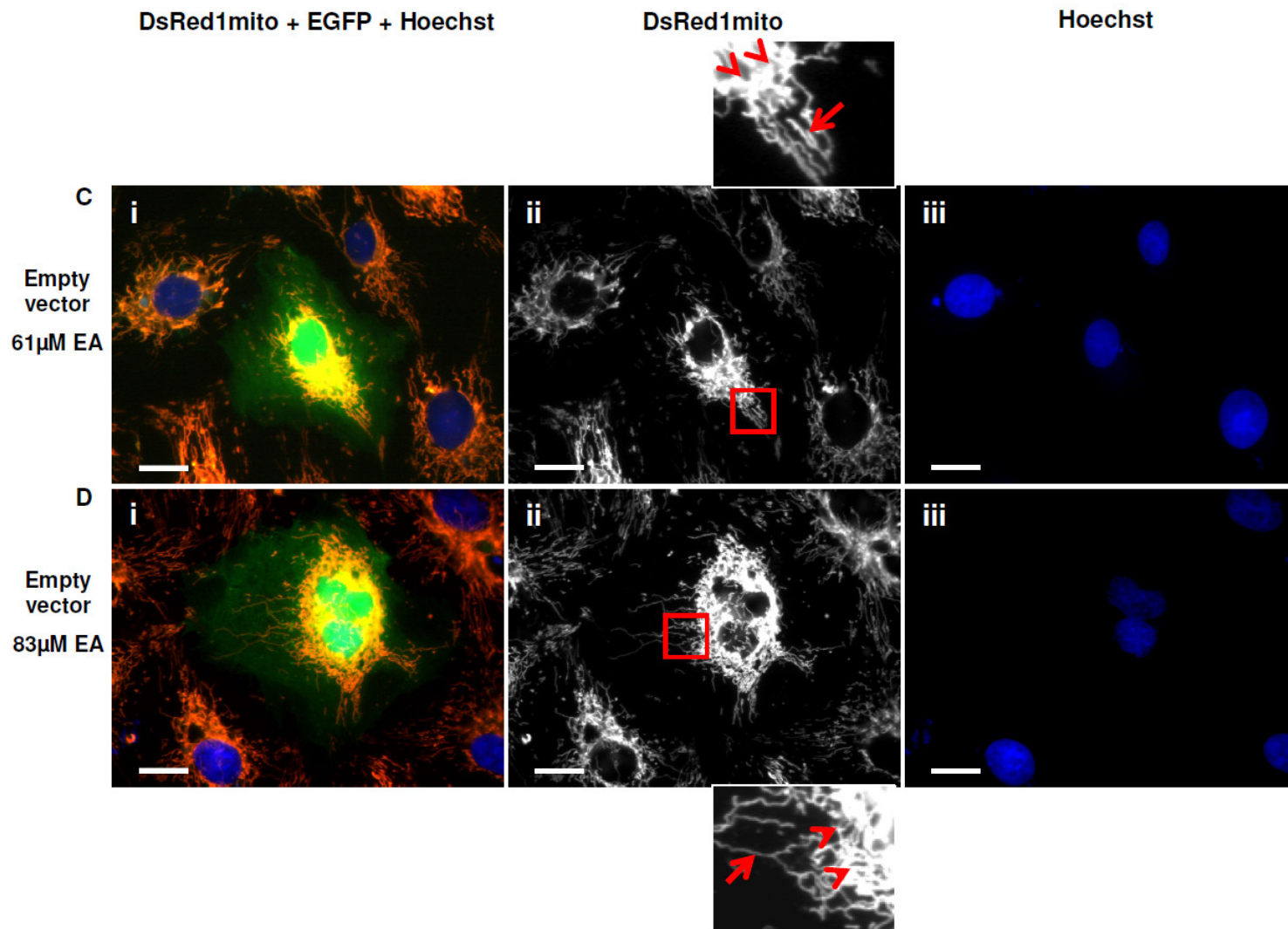
Cycloheximide was excluded from the PEG assay and further characterisation due to specific limitations of the PEG assay protocol and additional reasons as mentioned in discussion section.

4.4.1 Fis1 overexpression assay to observe the effect of EA on mitochondrial morphology

Fis1 was overexpressed in CV14A cells to induce mitochondrial fragmentation and test whether EA can inhibit Fis1 mediated mitochondrial fission or not. Fis1 was chosen to overexpress rather than Drp1 because Fis1 is a mitochondrial outer membrane protein and acts as an anchor for cytosolic Drp1. Hence, more Fis1 on the mitochondrial outer membrane results in more Drp1 recruitment to fission sites. Also, overexpression of Fis1 has been shown to fragment mitochondrial networks suggesting increased mitochondrial fission (Yoon et al., 2003).

CV14A cells stably expressing DsRed1mito were used to assess the effect of hFis1 overexpression on mitochondrial morphology (for details see section 2.6.5). **Figure 4.5** demonstrates the principle of the assay. CV14A cells were transfected with either pCI-NEO empty vector and EGFP-C2 vector (**Figure 4.5 A-D (i-iii)**), or myc-tagged hFis1 plasmid and EGFP-C2 vector (**Figure 4.5 E (i-iii)**). 0.5 μ g and 0.75 μ g Fis1 were used to see the effect of increasing Fis1 expression on mitochondrial morphology. EGFP was used to identify the transfected cells and 1:3 ratio of EGFP: Fis1 is used to confirm co-transfection. 4 hours post transfection 0.1% DMSO (vehicle) or 21 μ M, 41 μ M and 83 μ M EA was added to all the conditions. **Figure 4.5 A-D** is showing the effect of 0.1% DMSO or various concentrations of EA on mitochondrial morphology in pCI-NEO empty vector transfected cells. **Figure 4.5 E** is a representative image for 0.75 μ g Fis1 overexpression induced fragmentation of mitochondrial network morphology in CV14A cells treated with 0.1% DMSO. After 24 hours cells were fixed, stained with Hoechst for nuclear morphology and scored for mitochondrial morphologies as shown in **Figure 4.6**. Mitochondrial morphology was classified as clustered, fragmented, small tubules and normal in CV14A cells. Mitochondrial morphology was classified as clustered if mitochondria were clustered around the nucleus forming small aggregates, with the presence of few fragmented mitochondria not spread in the cytoplasm (**Figure 4.6. A**). Small spherical mitochondria spread in the cytoplasm were categorised under fragmented mitochondrial morphology (**Figure 4.6 B**).





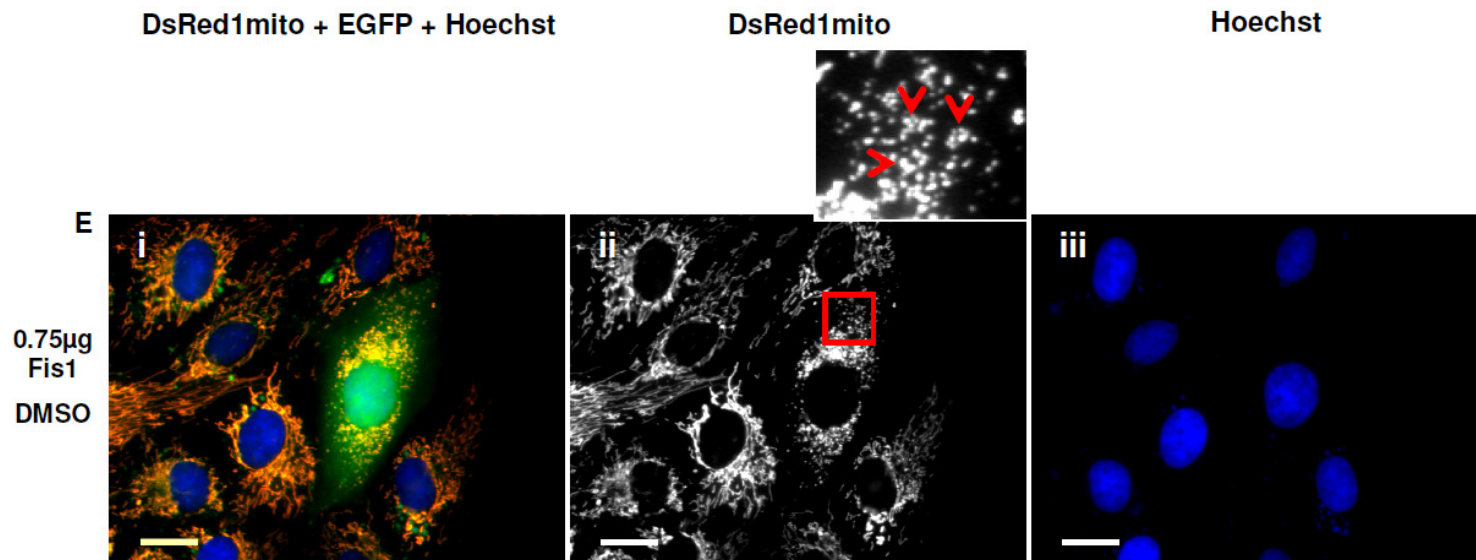


Figure 4.5: Fis1 overexpression assay for mitochondrial morphology. CV14A cells stably expressing DsRed1mito were transfected with EGFP-C2 vector and pCI-NEO empty vector (A,B,C,D) and EGFP-C2 and 0.75 μ g myc-tagged hFis1 (E). (i) DsRed1mito+EGFP+Hoechst merged (ii) DsRed1mito (iii) Hoechst staining for nuclei images. A (i-iii) CV14A cells treated with 0.1% DMSO showing normal mitochondria (indicated with arrow in inset) with loose networks (indicated with arrowhead in inset). B (i-iii) CV14A cells treated with 41 μ M EA for 24 hours post transfection with empty vector show few long tubular mitochondria. (indicated with arrow in inset). C (i-iii) CV14A cells treated with 61 μ M EA for 24 hours post transfection show long tubular mitochondria (indicated with arrow in inset) and increased mitochondrial networks (indicated with arrowheads in inset). D (i-iii) CV14A cells treated with 83 μ M EA for 24 hours post transfection show long tubular mitochondria (indicated with arrow in inset) and extensive mitochondrial reticulum morphology (indicated with arrowheads in inset). E (i-iii) CV14A cells treated with 0.1% DMSO for 24 hours post transfection with 0.75 μ g Fis1 show fragmented spherical mitochondria (indicated with arrowheads). Scale bar = 10 μ m.

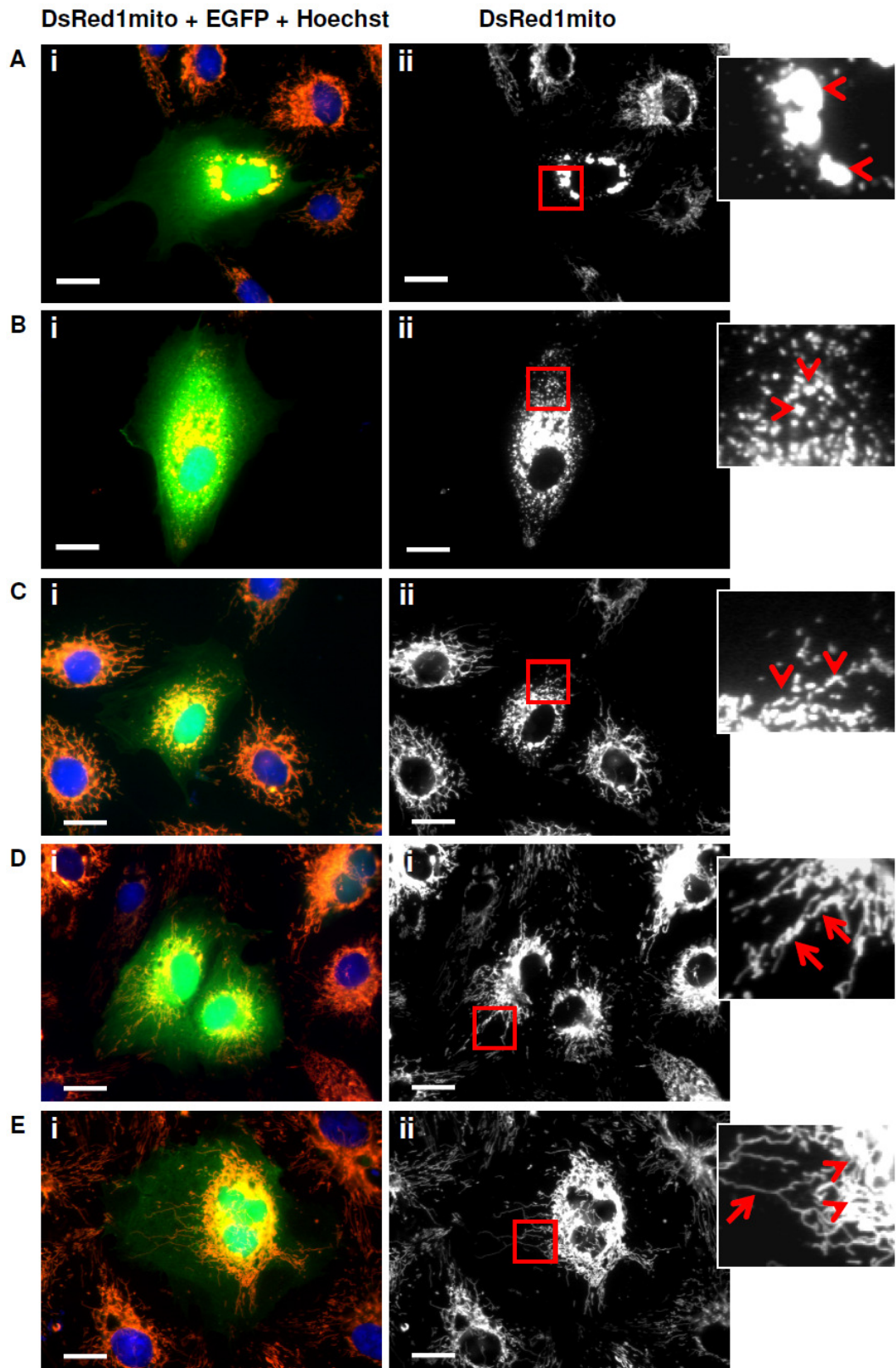


Figure 4.6: Classification of mitochondrial morphology for Fis1 overexpression assay. Representative images of CV14A cells showing various mitochondrial morphologies observed in Fis1 assay. A (i,ii) clustered mitochondria (indicated with arrowheads in inset). B (i,ii) Fragmented mitochondria (indicated with arrowheads in inset). C (i,ii) small tubular mitochondria. (indicated with arrowheads in inset). D (i,ii), E (i,ii) normal/fused mitochondria (In insets arrows indicate long tubular mitochondria and arrowheads indicate mitochondrial networks or reticulum). Scale bar = 10 μ m

Mitochondria which were larger than fragmented mitochondria and appear as small rods were categorised as small tubular mitochondria (**Figure 4.6 C**). The normal/fused mitochondrial category was elaborate as it included mitochondria larger than small tubules and present near cell periphery and mitochondria forming loose network around the nucleus (**Figure 4.6 D**) and extensively fused mitochondrial reticulum morphology; a typical of EA effect (**Figure 4.6E**). EA effects were considered as normal mitochondrial morphology because the principle of the experiment was to see the rescue effect of EA on increased mitochondrial fission rather than to quantify increased mitochondrial fusion induced by EA. Fis1 overexpression significantly increased mitochondrial clustering and fragmentation in a dose dependent manner in both 0.5 μ g and 0.75 μ g Fis1 suggesting increased mitochondrial fission (**Figure 4.7**). However, EA treatments showed reduced mitochondrial clustering and fragmentation and increase in cells with normal/fused mitochondrial morphology, in a dose dependent manner (**Figure 4.7**). Though, small tubular mitochondria were not significantly affected across the EA treatments (**Figure 4.7**). This assay showed that increased mitochondrial fission induced by Fis1 overexpression was rescued by EA treatment and resulted in increased number of cells with either normal mitochondrial morphology or enhanced mitochondrial fusion morphology.

Overexpression of Fis1 induces mitochondrial mediated apoptosis (James et al., 2003; Yoon et al., 2003). Hence, in Fis1 overexpression assay, nuclear morphology of the cell was also studied to test the effect of EA on cell toxicity. Apoptosis is characterised morphologically by condensation and fragmentation of nuclei and cells. Therefore, nuclear morphologies were categorically scored for apoptotic nuclei, mild condensed nuclei and normal nuclei. Cells showing completely fragmented nuclei were categorised as apoptotic nuclei, nuclei which were slightly condensed were scored as mild condensed nuclei and normal nuclei were scored for smoothly membrane bound nucleus. Cells with apoptotic nuclei increased with Fis1 overexpression and the proportion was significantly increased with 0.75 μ g Fis1 in the presence of 0.1% DMSO (**Figure 4.8**). Mild condensed nuclear morphology was also significantly increased with Fis1 overexpression and high EA doses 61 μ M and 83 μ M. However, 41 μ M EA did not show increased apoptotic and mild condensed nuclei in pCI-NEO empty vector or Fis1 transfected cells (**Figure 4.8**). This assay showed that Fis1 induced apoptosis and 41 μ M EA significantly reduced this effect, however at higher doses EA led to enhanced cell death.

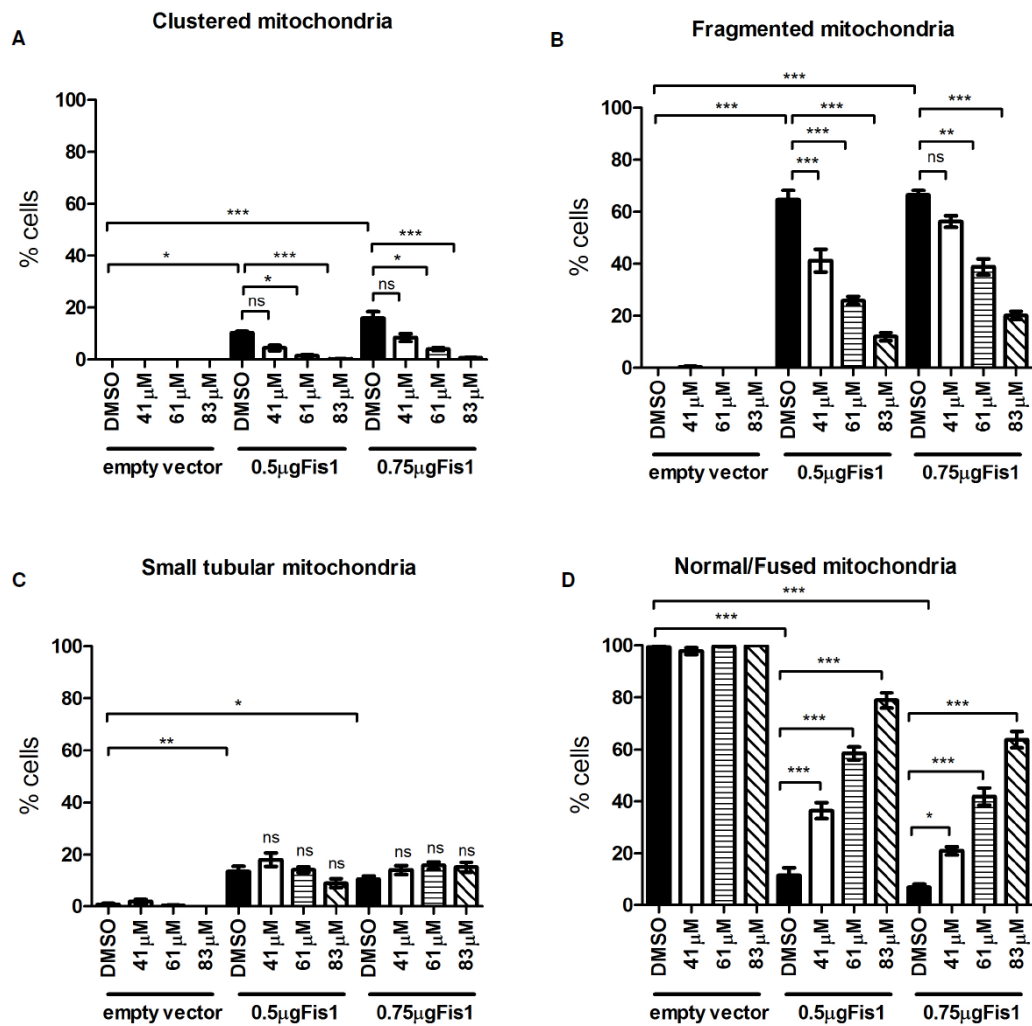


Figure 4.7: Mitochondrial morphology in CV14A cells overexpressing hFis1 and incubated with EA. CV14A cells transfected with pCI-NEO empty vector and/or 2 concentrations of myc-tagged hFis1 (0.5 μ g Fis1 and 0.75 μ g Fis1) for 4 hours and later incubated with 0.1% DMSO and 41 μ M, 61 μ M and 83 μ M EA for 24 hours. 200 cells were scored blindly for each condition. n = 200 cells, N = 3 independent experiments. Data is presented as mean \pm standard error. Statistical significance was determined by one-way ANOVA followed by Tukey's multiple comparison. (***) $P < 0.001$, (**) $P < 0.01$, (*) $P < 0.05$.

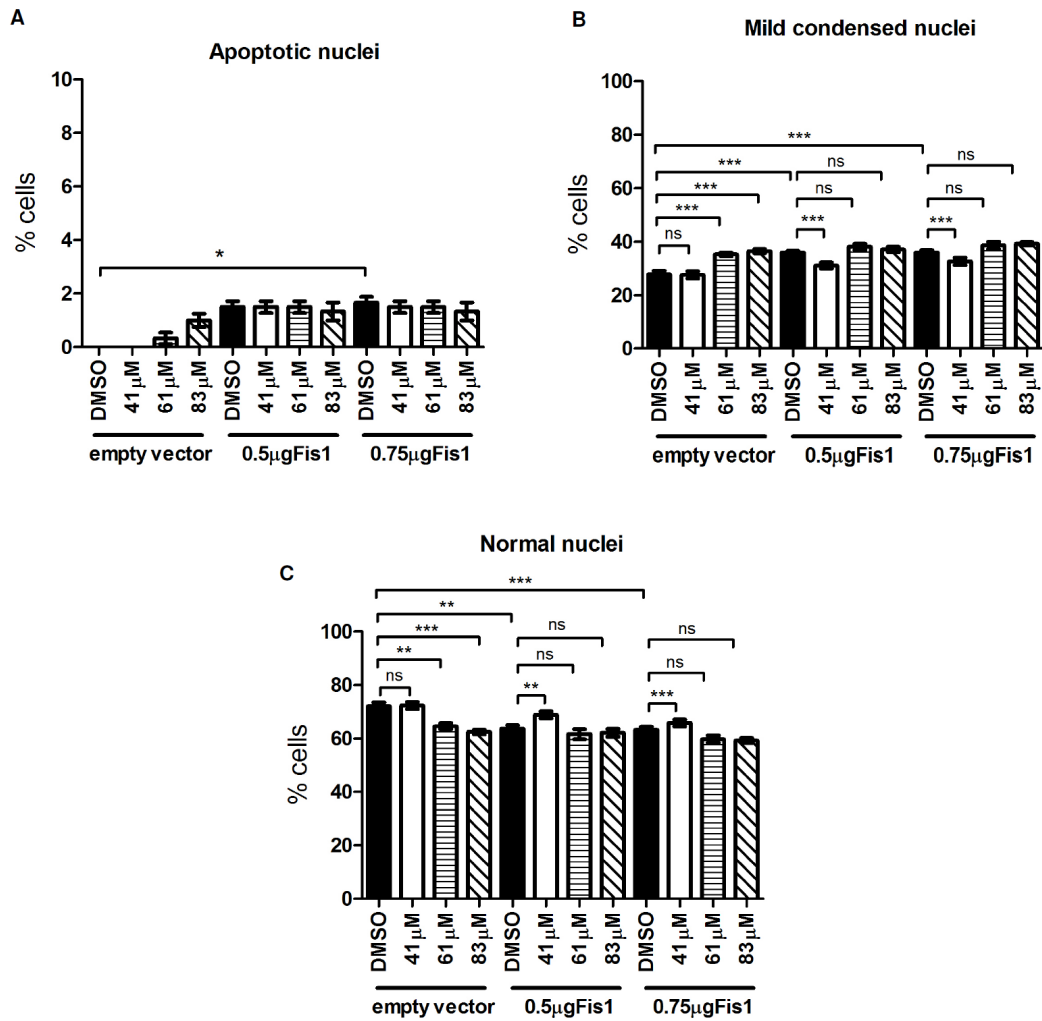


Figure 4.8: Nuclear morphology in CV14A cells overexpressing hFis1 and incubated with EA. CV14A cells were scored for (A) apoptotic, (B) mild condensed and (C) normal nuclei. 200 cells were scored blindly for each condition. $n = 200$ cells, $N = 3$ independent experiments. Data is presented as mean \pm standard error. Statistical significance was determined by one-way ANOVA followed by Tukey's multiple comparison. (***) $P < 0.001$, (**) $P < 0.01$, (*) $P < 0.05$).

4.4.2 Fis1 overexpression assay to observe the effect of EA on peroxisome morphology

To further investigate whether EA is acting as an inhibitor for the fission machinery, we took advantage of peroxisome proliferation and studied the effects of EA on peroxisome number. CV14A cells were transfected with either pCI-NEO empty vector and EGFP-peroxisome (**Figure 4.9A-C(i-i')**), or 0.75 μ g myc-tagged hFis1 plasmid and EGFP-peroxisome (**Figure 4.9A-C(ii-ii')**) as discussed in section 2.6.6 and treated with either 0.1% DMSO or 83 μ M and 124 μ M EA for 24 hours. The peroxisome numbers for all the conditions were quantified using ImageJ particle analysis plugins as discussed in sections 2.6.6.4. CV14A cells transfected with empty vector showed small spherical peroxisomes spread throughout the cytoplasm under DMSO incubation. Peroxisome number was significantly increased in cells overexpressing Fis1 (**Figure 4.10**). Particle analysis showed the number of peroxisomes did not change in EA treated cells transfected with empty vector however; peroxisome number was significantly reduced in cells overexpressing Fis1 and treated with 83 μ M EA 124 μ M EA (**Figure 4.10**).

It is important to mention that 124 μ M EA was only used to investigate the possible dose dependent decrease of peroxisome number, since lower EA concentrations such as 41 μ M did not show any effect on peroxisome number with empty vector and Fis1 overexpression (data not shown). Incubation of CV14A cells with 124 μ M EA for 24 hours showed 50% cell death in MTT assays, however, to see the effect of EA on peroxisome numbers the higher dose was included only to investigate whether EA produces a stronger effect beyond 83 μ M. The results are considered preliminary as they are from one experiment and require further repetition to draw conclusive results. It is difficult to suggest that why peroxisome number does not change in mock transfected cells treated with EA. This is discussed further in the discussion section.

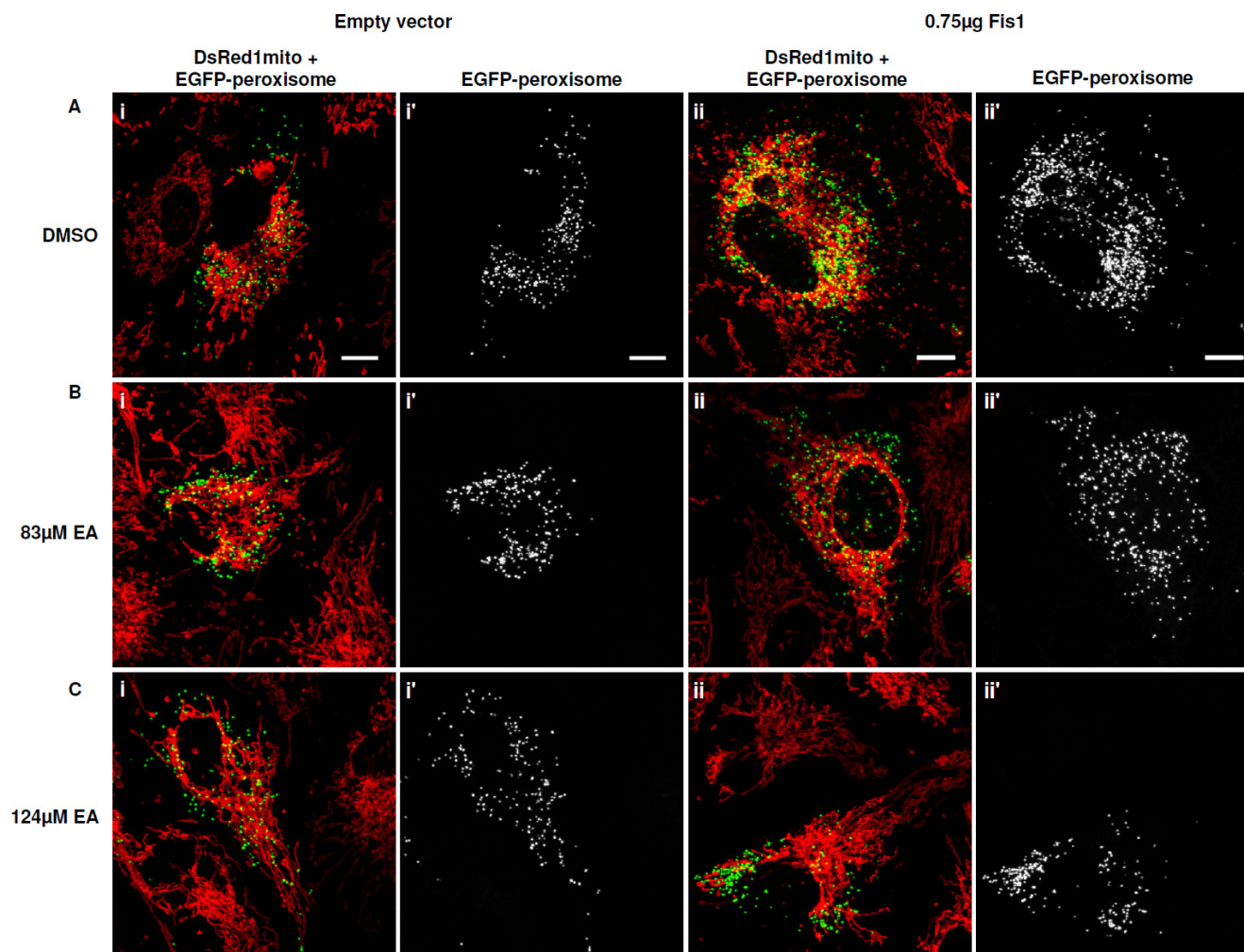


Figure 4.9: Fis1 overexpression assay for peroxisome number. CV14A cells stably expressing DsRed1mito were transfected with EGFP-peroxisome and pCI-NEO empty vector (A,B,C i-i') and EGFP-peroxisome and 0.75 μ g myc-tagged hFis1 (A,B,C ii,ii'). Panel A shows cells treated with 0.1% DMSO for 24 hours. Panel B shows cells treated with 83 μ M EA for 24 hours. Panel C shows cells treated with 124 μ M EA for 24 hours. Scale bar = 5 μ m.

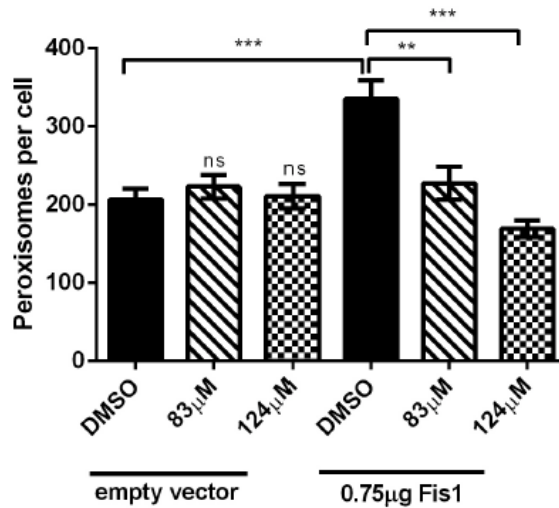


Figure 4.10: Peroxisome number analysis in Fis1 overexpression assay. Data is presented as mean \pm standard error. n = 30 cells. N = 1 Statistical significance was determined by one-way ANOVA followed by Tukey's multiple comparison. (***) $P < 0.001$, (**) $P < 0.01$).

4.5 Effect of EA on the mitochondrial morphology in fibroblasts derived from Patient 3 carrying *Mfn2*^{R364W} mutation

As shown in chapter 3, HMSNVI patient derived fibroblasts carrying *Mfn*^{R364W} heterozygous mutation have fragmented mitochondria lacking branching and network morphology. This phenotype is indicative of reduced mitochondrial fusion in these fibroblasts. Screening for fusion inducing compounds, could identify molecules that can be developed into a potential treatment for mitochondrial fusion deficient disorders. As mentioned earlier that the primary compound screen was done on fibroblasts derived from patient 3 carrying *Mfn2*^{R364W} mutation. I further quantified the effect of EA on the mitochondrial morphology in these patients using subjective and ImageJ analysis discussed in section 2.2.5.1 and 2.2.5.2.

Fibroblasts derived from control 1, control 2 and patient 3 carrying *Mfn2*^{R364W} mutation were incubated with either 0.1% DMSO or 83 μ M EA for 4 hours (**Figure 4.11**). Images taken from live cells were scored for fragmented, small tubules, normal and fused mitochondrial morphology as discussed in section 3.3.1. Fused mitochondrial morphology was included to evaluate the fusion inducing ability of EA on mitochondrial morphology in controls as well as patient fibroblasts.

In the presence of 0.1% DMSO, control 1 and control 2 showed a comparable percentage of cells with normal mitochondria. Furthermore, control fibroblasts showed zero cells with fragmented and small tubular mitochondria under normal conditions (**Figure 4.12**). However, in the presence of 0.1% DMSO, Patient 3 fibroblasts showed significantly high percentage of cells with fragmented mitochondria and cells with small tubular mitochondria (**Figure 4.12**). With 83 μ M EA 4 hours incubation an over all increase in mitochondrial fusion was observed in control fibroblasts (**Figure 4.12**). Both controls showed significantly high percentage of cells with increased mitochondrial connections with neighbouring mitochondria producing mitochondrial reticular morphology also known as mitochondrial reticulum (**Figure 4.12**). Interestingly, with 83 μ M EA incubation for 4 hours, Patient 3 fibroblasts showed a shift in the mitochondrial fragmented morphology spectrum to significantly increased number of cells with normal and fused mitochondrial morphology (**Figure 4.12**). Mitochondria appear as long filaments and often displaying the connections with neighbouring mitochondria to form few networks.

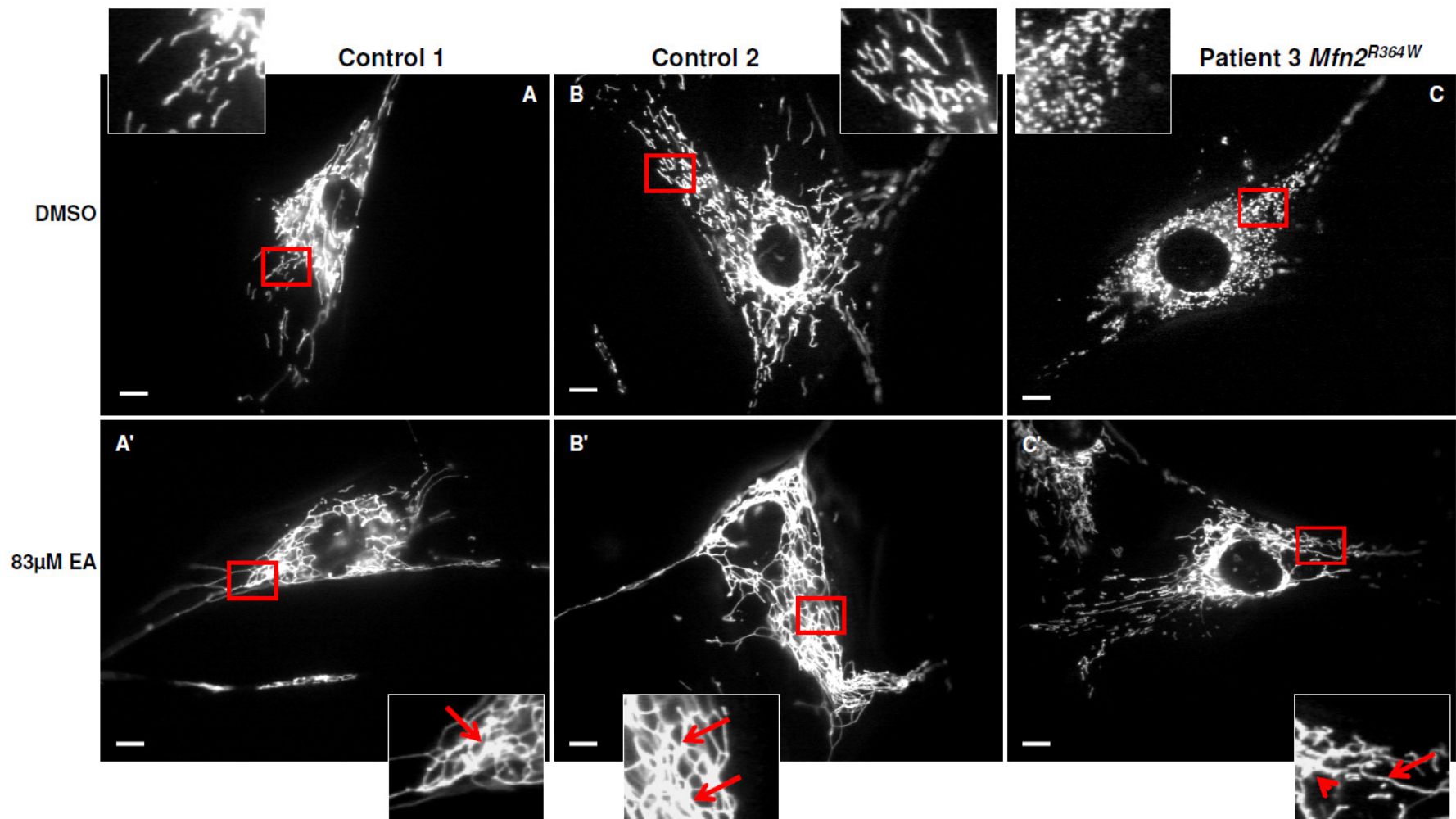


Figure 4.11: Mitochondrial morphology in Patient 3 *Mfn2*^{R364W} fibroblasts incubated with EA. Fibroblasts were treated with either 0.1% DMSO or 83μM EA for 4 hours. (A) Control 1 and (B) Control 2 show long tubular mitochondria and mitochondrial loose networks in perinuclear region (C) Patient 3 *Mfn2*^{R364W} fibroblasts show fragmented mitochondria dispersed in the cytoplasm (A') Control 1 fibroblasts treated with 83μM EA. In inset arrow indicate the mitochondrial connections producing mitochondrial reticulum. (B') Control 2 fibroblasts treated with 83μM EA. In inset arrows indicate the mitochondrial connections producing mitochondrial reticulum. (C') Patient 3 fibroblasts treated with 83μM EA. In inset arrow indicate long mitochondrial filament and arrowhead indicate the mitochondrial branching. Scale bar = 10μm.

In the presence of 83 μ M EA percentage of cells with fragmented mitochondria and cells with small tubular mitochondria was also significantly reduced as compared to DMSO treated ones (**Figure 4.12**).

ImageJ analysis for mitochondrial aspect ratio, length, bifurcation ratio and network complexity ratio was carried out to quantify the difference in the mitochondrial morphologies observed with DMSO and EA treatment (for analysis details see section 2.2.5). Patient 3 showed significantly reduced aspect ratio as compared to controls in the presence of 0.1% DMSO, however in the presence of 83 μ M EA Patient 3 showed significant increase in mitochondrial aspect ratio (**Figure 4.13**). With 83 μ M EA, Control 1 presented slightly reduced aspect ratio and Control 2 showed significantly reduced mitochondrial aspect ratio, and no effect on mitochondrial length was observed in control fibroblasts (**Figure 4.13**). The reduction in aspect ratio is most likely due to increase in mitochondrial connectivity among the mitochondrial population which is shown as significant increase in bifurcation ratio and network complexity ratio in controls (**Figure 4.13**). Furthermore, with 83 μ M EA, Patient 3 fibroblasts showed significant increase in mitochondrial length, bifurcations and network complexity ratio (**Figure 4.13**).

In conclusion, these analyses demonstrated that EA has shown an enhanced mitochondrial fusion effect in both controls and patient fibroblasts. We have shown that in the presence of EA an overall increase in the number of cells showing normal and fused mitochondrial network morphology was observed. Also, ImageJ analysis demonstrated significant increase in mitochondrial aspect ratio, length, branch formation and network complexity. Hence, our results suggest that EA is rescuing the fragmented mitochondrial morphology in Patient 3 fibroblasts.

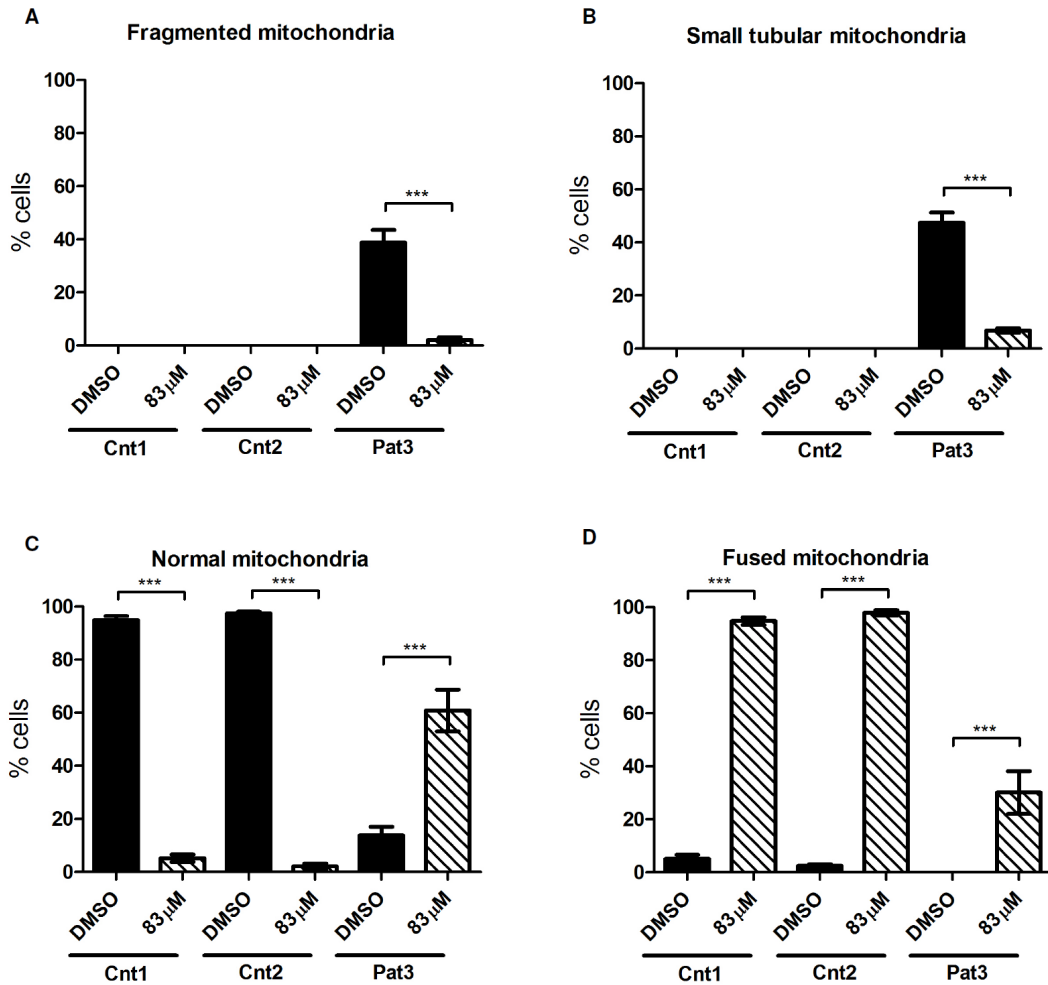


Figure 4.12: Subjective analysis of mitochondrial morphology in Patient 3 *Mfn2*^{R364W} fibroblasts incubated with EA. 0.1% DMSO used as vehicle. Cnt1: control 1, Cnt2: control 2, Pat3: patient 3 *Mfn2*^{R364W}. Data is presented as mean \pm standard error. n = 50-60 cells, N = 3 independent experiments. Statistical significance was determined by one-way ANOVA followed by Tukey's multiple comparison. (***) $P < 0.001$).

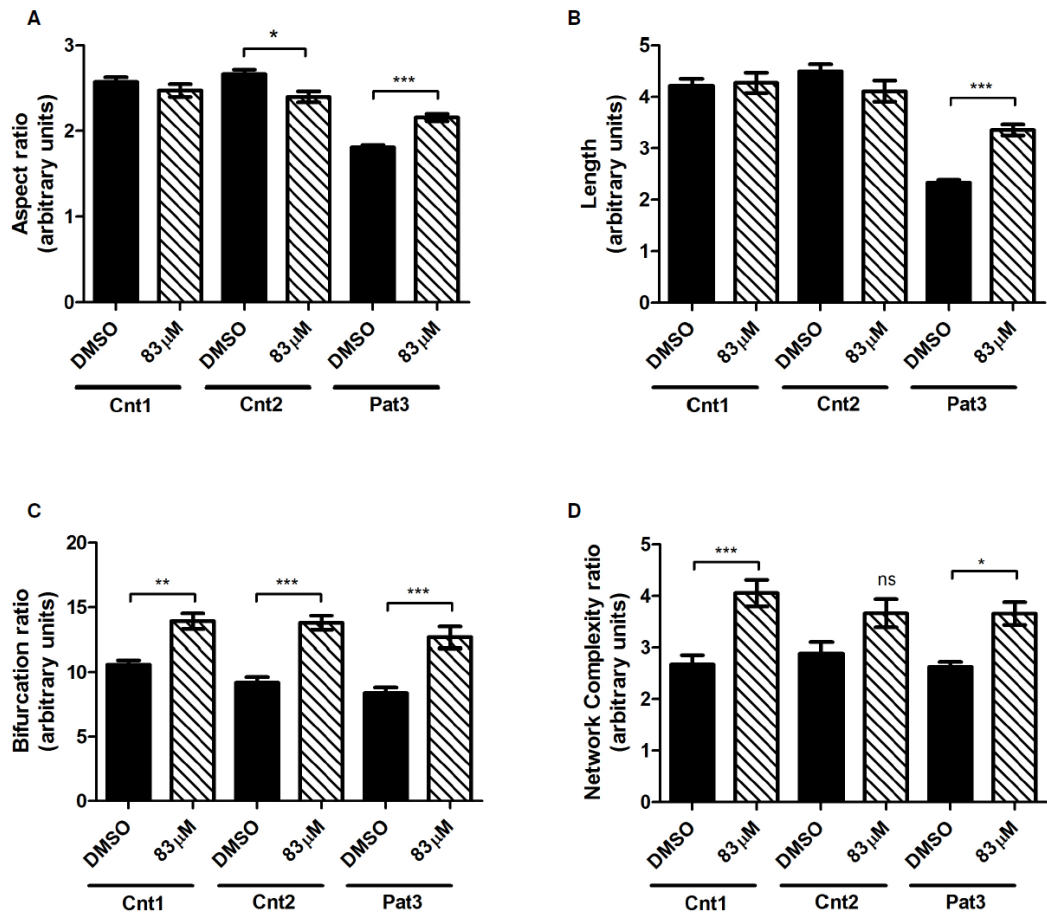


Figure 4.13: ImageJ analysis of mitochondrial morphology in Patient 3 *Mfn2*^{R364W} fibroblasts incubated with EA. 0.1% DMSO used as vehicle. Cnt1: control 1, Cnt2: control 2, Pat3: patient 3 *Mfn2*^{R364W}. Data is presented as mean±standard error. n = 50-60 cells, N = 3 independent experiments. Statistical significance was determined with Kruskal-Wallis non-parametric analysis and Dunn's pair-wise comparison (****P* < 0.001, **P* < 0.05).

4.6 Discussion

Primary drug screen including 2000 compounds from the Spectrum Collection and 4 compounds from literature search were tested for their ability to affect mitochondrial morphology in skin fibroblasts obtained from HMSNVI patient carrying heterozygous *Mfn2*^{R364W} mutation. Following the primary screen, positive compounds were tested for their ability to increase mitochondrial fusion in CV14A cells. The scoring for the effect of each dose of the compounds with the 3 incubation periods (15 mins, 4 hours and 24 hours) on mitochondrial morphology was done once, however, the scoring was not done blind. Hence, the results are considered preliminary for the secondary screen. However, the increase in mitochondrial fusion morphology was strong enough for us to continue with the compounds that scored as positive candidates in the initial results. Nevertheless, the results need to be improved by replicating the incubations times with blind scoring of mitochondrial fusion. From the secondary screen EA, NEM, cycloheximide and crinamine came out as positive hits for the increased mitochondrial fusion in cells, however, NEM and crinamine were excluded from further analysis. NEM was excluded because it is well-known non-specific cysteine alkylator with cellular targets in various cellular pathways (Glick and Rothman, 1987; Mseeh et al., 2002). The effect of NEM on mitochondrial morphology might be non-specific as it may be interacting with other pathways not directly involved in mitochondrial dynamics and the increased mitochondrial fusion observed in cells might reflect the secondary effects of such interactions. Also, NEM was included in the study as a comparison with EA to see how it behaves in our cells since Bowes and Gupta used NEM as another cysteine alkylator to see its effect on mitochondria along with EA (Bowes and Gupta, 2005). Crinamine is a natural product and was obtained at the standard concentration of 10 μ M from Spectrum library. Crinamine was excluded from further characterisation due to the lack of availability of the compound and also because another group in Canada communicated with us that they are already working on the effects of this compound on mitochondrial dynamics. Cycloheximide also showed increased mitochondrial fusion in CV14A cells but was dropped from further validation because of various reasons as discussed later in the text. As a result, from secondary screen EA was considered as candidate compound for studying its effect on mitochondrial morphology and further characterisation for how it is increasing mitochondrial fusion in cells.

MTT assay was performed to determine cytotoxicity and cell viability for EA, NEM and cycloheximide. The rationale for testing toxic effects of positive hits on cell survival was to determine drug doses that can be used in further cell based assays to characterise the compounds without toxic effects. In MTT assay EA showed an increase in cell survival in *Mfn2^{R364W}* patient fibroblasts and 50% inhibitory concentration (IC₅₀) was in between 41µM and 83µM for 24 hours incubation. However, CV14A cells showed much less toxicity with EA. The difference in the toxicity of EA in patient fibroblasts and CV14A cell is presumed to be the sensitivity of patient cells. It might be because patient fibroblasts may perhaps be under stress which makes them more sensitive to cytotoxicity of EA. Also, EA showed a typical dose dependent decrease in cell survival in both patient and CV14A cells that is supportive to consider it as potential drug. The toxic levels of EA found in CV14A cells were in concordance with Gupta and colleagues who showed that short exposure (2 hours) had no toxic effect in Chinese hamster cells with higher EA concentrations (Soltys and Gupta, 1994). However, long term exposure of EA (6-7days) showed adverse effects on colony formation by showing IC₅₀ at approximately 40µM EA (Soltys and Gupta, 1994). In MTT assay NEM showed high toxicity level and 50% cells were dead past 1.75µM NEM after 24 hours incubation. Furthermore, cycloheximide did not show high toxicity with higher concentrations but it failed to produce a drug like response in MTT assay. This suggests that increasing the concentration of cycloheximide in the assays would not influence its effect on cells and therefore it would be difficult to establish a reliable concentration for the optimal effect to be studied. We know that the MTT assay involves the reduction of MTT salt by mitochondrial succinate dehydrogenase in metabolically active cells (Mosmann, 1983). There are various other tests such as the lactate dehydrogenase (LDH) assay and ATP quantification to analyse compound/drug toxicity and effect on cell viability. However, we used MTT assay because it was already in use in our lab to test the toxicity and cell survival. Though, one question that arises is, whether the effect of compounds on cell survival could be due to effects on mitochondria? It is ought to be considered that the drugs screened in this project were selected because they modify mitochondrial morphology and we do not expect such changes in morphology to lead to toxicity. However, it could be that toxicity causes changes in mitochondrial morphology but such change is typically pro-fission not pro-fusion (DeVos et al., 2005).

The PEG fusion assay was performed to test the ability of EA and cycloheximide to induce mitochondrial fusion in cells in-vitro. The rationale was to investigate whether the increase in mitochondrial fusion is the primary effect of the compounds and not a phenomenon that occur secondary to some other process in the cell. The PEG fusion assay protocol included addition of 107 μ M cycloheximide to inhibit new protein synthesis before the addition of compounds being tested for fusion induction (Chen et al., 2003). It is an important step as it prevents the synthesis of new mitochondrially targeted DsRed1 and GFP fluorophores in the fused cells and makes it possible to show that the increased fusion is the result of drug action on mitochondrial dynamics rather than production of more DsRed1mito and GFPmito in the cells. For EA our results have shown a significant increase in mitochondrial fusion in a dose dependant manner. As stated in result section, this assay needs further replication. However, data from the two biological replicates suggests that EA is able to induce mitochondrial fusion in-vitro and the increase in mitochondrial fusion is not a result of any other process going on in cells under EA exposure. These are novel findings as previous work done on characterisation of EA has not measured its ability to induce mitochondrial fusion in in-vitro conditions.

However, testing cycloheximide for its ability to induce fusion in PEG fusion assay was problematic because of the addition of cycloheximide in initial steps to inhibit protein synthesis. Therefore, we decided to exclude cycloheximide from further characterisation. Also, cycloheximide is a known protein synthesis inhibitor; therefore its broad activity would make it a hard choice to be developed into a potential drug as well as a bench tool to study the mitochondrial dynamics specifically. There is a report in the published literature suggesting that stress as a result of protein inhibition by cycloheximide results in the activation of SLP2, which in turn leads to mitochondrial hyperfusion (Tondera et al., 2009). SLP2 is believed to stabilize the OPA1-L isoform under stress facilitating the hyper fusion of mitochondria and increased production of ATP (Merkwirth et al., 2008; Tondera et al., 2009). This process is thought to be cell's resistance response to the stress. However, they did not show the effect on mitochondrial morphology in longer incubations with cycloheximide. Similarly, such findings are also not performed in my studies but it is suggested that longer exposure on mitochondrial morphology with cycloheximide is necessary to see what happens in long term stress conditions. Does mitochondrial fragmentation render cells unable to cope with continued stress exposure? Normally, mitochondrial fission is the result of any

stress a cell is experiencing; however, elongated mitochondria were seen in tobacco cells in hypoxic conditions and in HeLa cells generating ATP by oxidative phosphorylation instead of glycolysis (Van Gestel and Verbelen, 2002; Rossignol et al., 2003). Furthermore, our MTT assay results also support the idea of excluding cycloheximide from further investigation as it resulted in 50% loss of cell viability at all the tested concentrations.

To investigate how EA is able to increase mitochondrial fusion in cells we followed our working hypothesis that EA is acting by either inactivating the essential cysteine residue/s in mitochondrial fission machinery or in mitochondrial fusion repressor factor. For this, we used an easy approach to manipulate normal mitochondrial dynamics by increasing mitochondrial fission by overexpressing Fis1. EA showed significant increase in mitochondrial fusion in cells overexpressing Fis1 as compared to control cells. Fis1 overexpression assay was an alternative readout assay to show that EA increases mitochondrial fusion, however this assay does not reveal whether EA is pro fusion or anti fission. Possible assays that could give an unbiased answer for identifying EA cellular targets are seeing the effect of EA in fission machinery knockout models (Drp1 knockout) or fusion machinery knockouts (Mfn1 and Mfn2 knockout and Opa1 knockout models). Based on the hypothesis that EA is inactivating a fission factor, we can assume that in cells lacking Drp1 EA will be unable to show increased mitochondrial fusion and possibly the fusion level would be same as in DMSO (vehicle) treated cells. The emphasis of our discussion is more on Drp1 as a major candidate for EA action because it is the main GTP protein involved in membrane scission using GTP hydrolysis (Smirnova et al., 1998; Mozdy et al., 2000; Smirnova et al., 2001). Other members of fission machinery such as Fis1 and Mff are the anchoring proteins for Drp1 and facilitate the dimerization of Drp1 at fission sites. These anchoring proteins are not involved in the membrane severing in mitochondrial fission and their expression in Drp1 mutant backgrounds does not rescue mitochondrial fission (Breckenridge et al., 2008; Otera et al., 2010). In addition to Fis1 and Mff other anchoring proteins MiD49 or MiD51 mediate Drp1 recruitment to the fission sites in the absence of Fis1 and Mff (Loson et al., 2013). Cells expressing dominant-negative Drp1 mutant *Drp1*^{K38A}, which is GTPase dead form, have shown increased mitochondrial network morphology (Smirnova et al., 1998; Smirnova et al., 2001). We assume that EA inactivates its target by alkylating the functional cysteine residue(s). Drp1 has in total 9 cysteines; N-terminal GTP-binding domain has one cysteine, middle domain has

6 cysteines, insert B has 1 cysteine and the C-terminal GTPase effector (GED) domain also has 1 cysteine. The GED domain is involved in mediating GTPase activity to sever the mitochondrial membranes (Pitts et al., 2004; Zhu et al., 2004). Additionally, an intra-molecular association has been identified between the GED domain folding back to interact in *cis* as well as in *trans* with the GTP-middle domains of Drp1 (Zhu et al., 2004). These intra- and inter-molecular associations have been thought to promote Drp1 dimerization and enhance its GTPase activity (Pitts et al., 2004; Zhu et al., 2004). More to the point, S-nitrosylation of cysteine 644 in the GED domain enhances the dimerization of Drp1, increased GTPase activity and showed fragmented neuronal mitochondria and neurotoxicity (Cho et al., 2009). A similar report to our study has also shown increased mitochondrial network morphology in cells when incubated with 15 deoxy- $\Delta^{12,14}$ -prostaglandin J2 (15d-PGJ2) peptide for 2 hours. It is believed that 15 deoxy- $\Delta^{12,14}$ -prostaglandin J2 (15d-PGJ2) peptide acts by thiol modification of cysteines in target proteins (Mishra et al., 2010). Based on our hypothesis, the second possibility is that EA is inactivating an anti-fusion factor or fusion repressor. There could be various candidates which are involved in negative regulation of mitochondrial fusion either acting directly or indirectly. It is known that Drp1 undergoes various post-translational modifications for its activation and translocation from the cytoplasm to the mitochondrial outer membrane to start mitochondrial fission (Chang and Blackstone, 2007; Karbowski et al., 2007). Hence, any of the kinases involved in its activation could possibly be inactivated by EA. Additionally; another interesting side to the story would be if EA is acting on components of the PINK1/Parkin pathway. We know that Mfn1 and Mfn2 are targets for Parkin mediated degradation upon dissipation of membrane potential (Ziviani et al., 2010). In order to investigate whether EA may be acting on the PINK1/Parkin pathway, it could be tested in cells overexpressing Parkin or PINK1 to look for effects on expression levels of normal and ubiquitinated forms of Mfn1 and Mfn2.

Furthermore, Fis1 overexpression induced mitochondrial fission morphology could primarily be rescued by expressing mitochondrial fusion factors such as Mfn1, Mfn2 and OPA1. It is suggested that in future, it would be interesting to add these conditions in parallel to EA treatment of cells overexpressing Fis1. Also, it would be interesting to see the effect of EA in *Drp1* knockout cells and in *Mfn1* and *Mfn2* double knockout and *Opal* knockout cells. Such studies would help further dissect the pathway EA is acting to promote mitochondrial fusion in cells. However, it is difficult to

separate out whether EA is inhibiting fission machinery or it is inactivating a fusion inhibitor or repressor. Therefore, it is suggested to take a direct approach and see the effect of EA on Drp1 GTPase activity if EA is alkylating cysteine residue/s in Drp1 and rendering it inactive.

EA showed significant increases in mitochondrial fusion in HMSNVI patient fibroblasts carrying *Mfn2*^{R354W} mutation. *Mfn2*^{R364W} is a heterozygous mutation giving one mutated allele and one wild type allele. It is clear from previous studies that pathogenic *Mfn2* alleles can make fusion competent complexes with the wild type alleles and with *Mfn1* (Detmer and Chan, 2007a). Our results indicate an increase in mitochondrial fusion in *Mfn2*^{R364W} patient cells when treated with EA. Therefore, it can be assumed that EA might be blocking fission, and as a result fusion continues to take place, this leads to an increased number of cells with normal and branched mitochondrial morphology. Although 100% rescue of the fragmented mitochondrial morphology of *Mfn2*^{R364W} cells was not observed, however, a significant number of cells with increased mitochondrial aspect ratio, length and branching were present after EA treatment. This suggests the occurrence of fusion might be facilitated by the formation of fusion competent complexes of *Mfn1/Mfn1*, *Mfn2*^{wild type}/*Mfn2*^{R364W} and *Mfn1/Mfn2*^{wild type} and *Mfn1/Mfn2*^{R364W}. *Mfn2*^{R364W} mutation has not been tested for its ability to be fusion competent, therefore at this point we can not be sure of its mitochondrial fusion competence and testing the fusion ability was beyond the scope of present study. However, fusion competency can be analysed with the PEG fusion assay co-culturing *Dsred1mito* and *GFPmito* cells expressing *Mfn2*^{R364W} heterozygous mutation. This would be a valuable assay for the characterization of this mutation.

Furthermore, peroxisomes use the same mitochondrial fission machinery including primarily Drp1, Fis1 and Mff for division and multiplication (Kobayashi et al., 2007; Gandre-Babbe and van der Blik, 2008). Our preliminary results have shown significant increase in peroxisome number in Fis1 overexpressing cells and are presumably due to increased proliferation of peroxisomes. After EA incubation for 24 hours the peroxisome number was significantly decreased in cells overexpressing Fis1. Peroxisome number did not change in mock treated cells (empty vector) and no larger or bloated peroxisomes were seen, suggesting the non-fusing nature of peroxisome. Peroxisome fusion is still a grey area and the majority of scientific evidence suggests that peroxisomes do not fuse to form larger structures (Motley and Hettema, 2007). Like fission machinery components, mitochondrial fusion factors such as *Mfn1*, *Mfn2* and

OPA1 were not identified to be present on peroxisomes, however, it has been reported that moving peroxisomes interact with each other while motile and form transient contacts but such connections are not considered as fusion events (Schrader et al., 2000). For division and proliferation peroxisomes form elongated tubular structures with constrictions which look like beads on a string (Schrader et al., 1998; Kobayashi et al., 2007). Pex11 has the major role in elongation and tubulation of peroxisomes (Schrader et al., 1998). The beads on a string like morphology represent the elongation of single peroxisomes and not the fusion of neighbouring peroxisomes to form longer structures. Drp1 is recruited to the constriction sites on the elongated peroxisome to initiate membrane scission (Kobayashi et al., 2007). *Drp1* knockdown cells showed peroxisomes with beads on a string like morphology showing failure of membrane scission (Koch et al., 2004). We did not see bloated peroxisomes or beads on a string like morphology with EA treatment; we only observed reduction in peroxisome number. It is difficult to make conclusion from one experiment about how EA is causing the reduction in number without giving bloated peroxisomes or beads on string like morphology. However, it could be suggested that EA action does not occur to a detectable level unless increased number of Drp1 is present on peroxisomes as a result of Fis1 overexpression. Hence for this reason, EA was unable to show obvious effect on peroxisome number under basal levels of fission machinery. Moreover, failure to see the beads on string like morphology could be due to limitations of microscopy, or because the effects of EA on Drp1 are not equivalent to the effects seen in *Drp1* knockout cells. Therefore, in future studies it would be helpful to use 3D confocal imaging techniques to study the peroxisomal morphology more carefully. Finally, due to limitations of our data we cannot make any conclusion about how EA is acting on peroxisomes and why we only see an effect of EA in Fis1 overexpressing cells.

To conclude, we have shown that EA is able to increase mitochondrial fusion in CV14A cells and *Mfn2*^{R364W} patient fibroblasts. We have also shown that EA is able to induce mitochondrial fusion in PEG fusion assay. EA has shown increased mitochondrial fusion in cells overexpressing Fis1 and preliminary assays show that EA is able to reduce the number of peroxisomes in cells overexpressing Fis1. Mitochondrial fusion and fission are highly regulated processes and many factors have indirect link to the actual process. Consequently, there are number of candidates and their inactivation could result in increase in mitochondrial fusion. Hence, it is an interesting avenue for

further research in order to progress our understanding of how EA is increasing mitochondrial fusion in cells.

Chapter 5a: Characterisation of
***Drosophila melanogaster* Marf**

5.1. Introduction

Drosophila melanogaster has been used as a successful animal model for various common neurodegenerative diseases such as Alzheimer's disease, Parkinson's disease, amyotrophic lateral sclerosis and Huntington's disease (Wittmann et al., 2001; Auluck et al., 2002; Gunawardena et al., 2003; Iijima et al., 2004; Clark et al., 2006; Park et al., 2006). Modelling a human neurodegenerative disease in *Drosophila melanogaster* allows several advantages for studying molecular and cellular pathology of the disease. In this respect, fruit fly offers researchers a system to analyse neuronal structure and physiology in an intact animal. Mfn2 is a profusion factor present in the outer mitochondrial membrane and is associated with common inherited neurodegenerative diseases such as CMT2A and HMSNVI (Zuchner et al., 2004; Verhoeven et al., 2006). *Drosophila* has Fzo and Marf for mitochondrial outer membrane fusion. However, *fzo* expression is restricted to male testis only (Hales and Fuller, 1997). Marf is considered as the main profusion factor as it is expressed ubiquitously and shares a higher percentage of sequence homology to mammalian Mfn1 and Mfn2 (Hwa et al., 2002). In this project, *GAL4/UAS* system was used in conjunction with inducible RNA interference (RNAi) to knockdown Marf expression in different fly tissues and study the effect on fly development, locomotion and mitochondrial morphology. RNAi is cell-autonomous in *Drosophila* and targeted expression of RNAi using the *GAL4-UAS* system can be achieved for cell or tissue specific gene knockdown (Gunsalus and Piano, 2005). The method of RNAi knockdown involves the expression of an interfering RNA containing inverted repeat sequences (>200bps) that form hairpin double-stranded RNAs (dsRNA) homologous to sequences of the target transcript. These hairpin dsRNAs are processed by the enzyme Dicer into short interfering RNA (siRNA) (21-23bps). These siRNAs are then incorporated into a group of proteins called the RISC (RNA-Inducing Silencing Complex) that uses the antisense strand of the siRNA to bind to and degrade the corresponding mRNA. *GAL4-UAS* is a bipartite system in flies involving separate transgenic stocks for *GAL4*-driver flies and *UAS-IR* flies. The *GAL4*-driver fly carries a promoter controlling the expression of yeast transcription factor GAL4, which allows tissue specific expression. The *UAS-IR* fly holds a transgene containing inverted repeat sequences (IR) of the target gene under the control of the *GAL4* upstream activating sequence (*UAS*). A cross between these two transgenic lines results in a tissue specific binding of *GAL4* on the promoter region of

UAS to activate the formation of hairpin dsRNA, which results in sequence specific gene silencing.

5.2. Characterisation of Marf and its role in *Drosophila melanogaster* development, locomotion and mitochondrial dynamics

5.2.1 Marf RNAi lines

Two UAS-RNAi lines designed to knockdown *Marf* were obtained from Vienna *Drosophila* RNAi Centre (VDRC). P-element generated RNAi line: *Marf*^{RNAiGD}, (*UAS-Marf-IR(GD)* (ID40478)) was the first line used. The inverted repeat sequence to generate the short hairpin formation targets the exon 6 (**Figure 5.1A**). This RNAi line has one predicted off target Dmel/CG3188, a protein with unknown function, and low to moderate expression in larval and adult midgut, hindgut, malphigian tubules, adult heart, adult spermathecae and adult carcass. The 2nd RNAi line: *Marf*^{RNAiKK}, (*UAS-Marf-IR(KK)* (ID105261)), was from a library of newly generated RNAi lines using site specific integration of transgene with phiC31 integrase. *Marf*^{RNAiKK} targets exon 2 and 3 of *Marf* and has no predicted off target effects (**Figure 5.1B**).

5.2.2 Characterisation of lethal phase of Marf knockdown in basic tissues

To characterise the lethal phase for *Marf* knockdown we drove the RNAi expression in all tissues using ubiquitous *da-GAL4* driver, in muscles using *Dmef-GAL4* driver, in all neurons using *elav-GAL4* driver and in motor neurons using *D42-GAL4* driver (**Table 5.1**). A benign RNAi control; *y*-RNAi was used in the assays for comparison for non-specific effects of RNAi. *y*-RNAi control showed normal developmental cycle under ubiquitous-*GAL4*-driven *y* knockdown, muscles-*GAL4*-driven *y* knockdown, neuronal-*GAL4*-driven *y* knockdown and motor neuron-*GAL4*-driven *y* knockdown flies (**Figure 5.2**). Ubiquitous-*GAL4*-driven *Marf*^{RNAiGD} showed developmental failure arresting at 3rd instar larval stage (**Figure 5.2**). These larvae were smaller than control larvae (data not shown) and had life span up to 28-30 days post embryonic stage (**Table 5.1**). Similarly, ubiquitous-*GAL4*-driven *Marf*^{RNAiKK} also presented developmental arrest by 3rd instar larval stage (**Figure 5.2**).

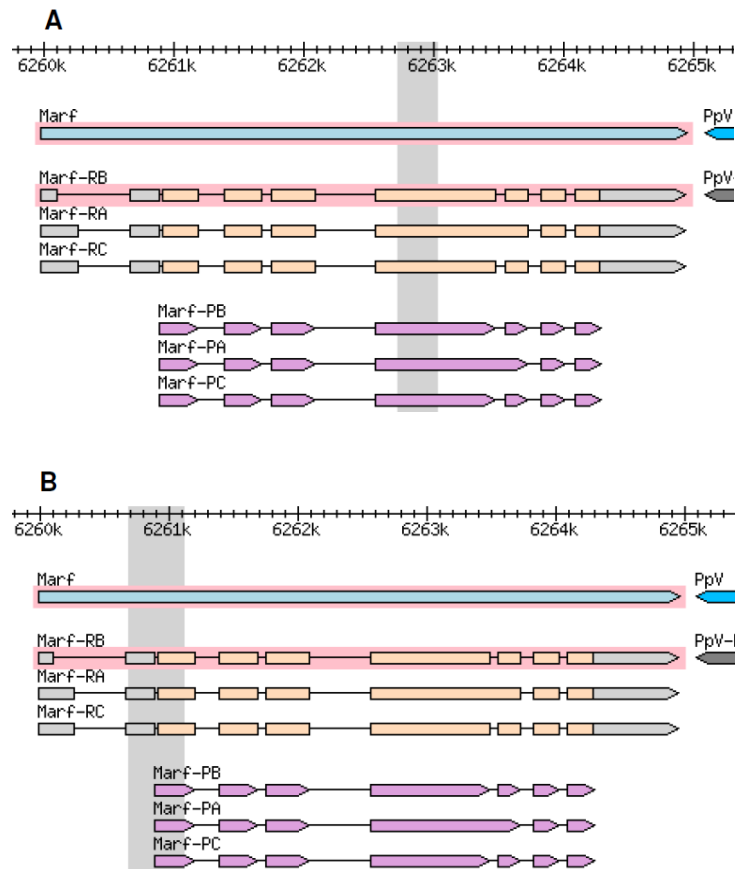


Figure 5.1: RNAi lines. GD line: *UAS-Marf-IR(GD)* and KK line: *UAS-Marf-IR(KK)* used in this study. *GBrowse* indicating the targeting sequences for the short hairpin sequences. (A) *UAS-Marf-IR(GD)* has inverted repeat sequences for hairpin formation targeting the exon 6 of *Marf*. (B) *UAS-Marf-IR(KK)* has inverted repeat sequences for hairpin formation targeting the exon 2 and 3 of *Marf*.

Table 5.1: Phenotypes for *Drosophila melanogaster* *Marf* knockdowns.

GAL4	Expression	Phenotype
<i>da</i>	Ubiquitous	3 rd instar larval arrest
<i>Dmef</i>	Muscle	pupal lethality
<i>elav</i>	All neurons	viable, weak, immotile
<i>D42</i>	Motor neurons	viable, active

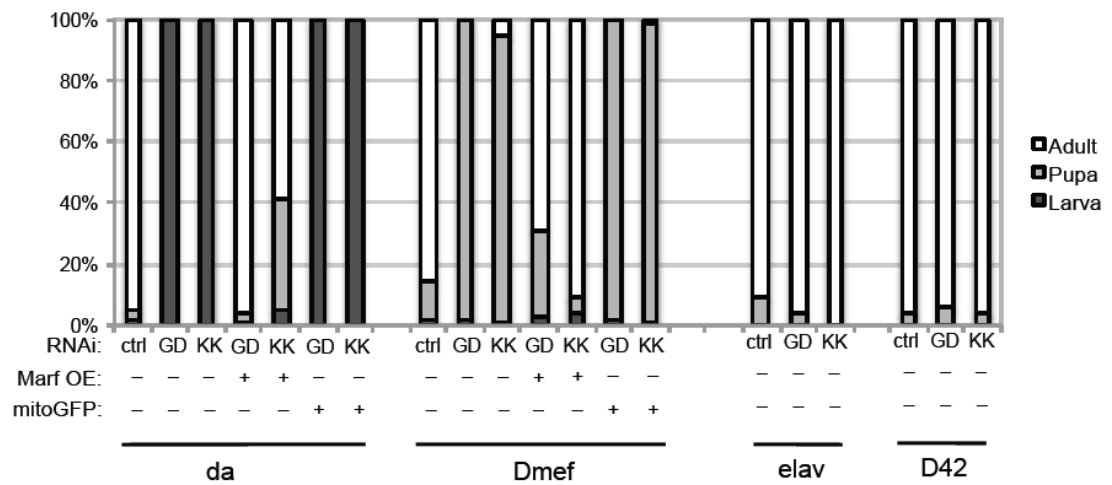


Figure 5.2: Lethal phase of *Marf* knockdowns. *da*: *da-GAL4*: ubiquitous expression, *Dmef*: *Dmef-GAL4*: muscle expression, *elav*: *elav-GAL4*: all neurons expression, *D42*: *D42-GAL4*: motor neurons expression. ctrl: *UAS-y-IR*; used as control. GD: *UAS-Marf-IR(GD)*. KK: *UAS-Marf-IR(KK)*. *Marf* OE: *UAS-Marf* overexpression. *UAS-Marf* transgenic lines; *UAS-Marf-IR(GD)*, *UAS-Marf(1)* have *UAS-Marf* transgene on chromosome 1 and *UAS-Marf-IR(KK)*, *UAS-Marf(3)* have *UAS-Marf* on chromosome 3. mitoGFP: *UAS-Marf-IR*, *UAS-mitoGFP*.

To verify that these phenotypes were due to loss of *Marf* function and not an off-target effect, *Marf* was re-expressed using a *UAS-Marf* overexpression transgene, although this transgene may also be affected by the RNAi. As expected, re-expression of *Marf* in ubiquitous-*GAL4*-driven *Marf* knockdown was sufficient to almost completely rescue the developmental arrest for both *GD* and *KK* lines (**Figure 5.2**). Importantly, as a control for the dilution effect of RNAi in the presence of two UAS transgenes we also tested development in fly line carrying *Marf^{RNAi}* in combination with UAS-mitochondrial green fluorescent protein (GFP) reporter transgene. Ubiquitous-*GAL4* driven *Marf* down regulation for both *GD* and *KK* lines carrying UAS-mitochondrial GFP showed similar developmental arrests as seen in the presence of single UAS transgene (**Figure 5.2**). This suggests that halted developmental defect was likely due to *Marf* knock down and *Marf* plays a vital role in *Drosophila* normal developmental process.

Subsequently, we explored the affect of *Marf^{RNAi}* in muscles on *Drosophila* development. Muscle-*GAL4*-driven *Marf* knockdown showed normal development up to pupal stage but fail to develop further and showed pupal lethality (**Table 5.1, Figure 5.2**). The majority of animals showed pupal lethality, however, a few escapers were seen in *KK* line (**Figure 5.2**). Again, the pupal lethality was rescued by muscle-*GAL4* re-expression of *Marf* in muscle-*GAL4*-driven *Marf^{RNAi}* in both *GD* and *KK* lines (**Figure 5.2**). These findings also suggested that the developmental defects were due to the down regulation of *Marf* in fly muscles and optimum levels of *Marf* in muscles are significant for normal developmental cycle. Subsequently, we wanted to assess the relative effect of *Marf^{RNAi}* in nervous system and independently in motor neurons only. Neuronal-*GAL4*-driven *Marf* knockdown for both *GD* and *KK* lines showed viable adults, however, the flies were weak and immotile (**Table 5.1, Figure 5.2**). In contrast, motor neuron-*GAL4*-driven *Marf* knockdown flies showed viable active adults for both *Marf^{RNAiGD}* and *Marf^{RNAiKK}* lines (**Table 5.1, Figure 5.2**). The rescue experiments were not performed in these assays since the knockdowns did not affect viability. Nevertheless, our results suggest that *Marf* is important for normal developmental process for *Drosophila* and its ubiquitous loss is lethal. Also, these results are consistent with recent report describing *Marf* genetic mutants (Sandoval et al., 2014)

5.2.3 Western blot analysis for *Marf* RNAi effectiveness

The effectiveness of the RNAi to knockdown *Marf* was analysed by western blots against Marf protein. At the beginning of the project no suitable antibodies for Marf were available, therefore we began by raising an antibody to the protein. This was done through a commercial outsource. Anti-Marf was raised in rabbit against N-terminal peptide, DTVDKSGPGSPLSRF (Ziviani et al., 2010). Protein expression analysis was done to analyse the effectiveness of ubiquitous-*GAL4*-driven *Marf*^{RNAi}, *Marf* rescue lines and *Marf*^{overexpression}. Control larvae showed predicted size Marf band (91.4-94.1 kDa), which was absent in ubiquitous-*GAL4*-driven *Marf* knockdown larvae for both GD and KK lines (**Figure 5.3A**). This band was also absent in larvae carrying ubiquitous-*GAL4*-driven *Marf*^{RNAi} and *UAS-mitochondrial GFP* but reappeared upon the re-expression of *UAS-Marf* (**Figure 5.3A**). Interestingly, the Marf band appeared more intense in ubiquitous-*GAL4*-driven *Marf*^{RNAiKK} and *Marf*^{overexpression line3} as compared to ubiquitous-*GAL4*-driven *Marf*^{RNAiGD} and *Marf*^{overexpression line1} (**Figure 5.3A**). At the present it can be suggested that this difference of band intensity could probably be due to different levels of *Marf* expression in both lines. Additionally, the Marf band appeared similar in intensity in ubiquitous-*GAL4*-driven *Marf*^{overexpression} for both line 1 and line 3. In conclusion, immunoblotting showed the efficacy of *Marf*^{RNAiGD} and *Marf*^{RNAiKK} lines to attenuate Marf expression.

We also wanted to see the expression levels of Marf throughout fly developmental stages, therefore, protein samples were extracted from embryo, early larval stage (1st and 2nd instar), 3rd larval instar, pupae and adult flies. In the control blot, predicted size Marf band (91.4-94.1kDa) was present in all the developmental stages (**Figure 5.3B**). Blots showed moderate Marf expression in embryonic and early larval stages and high Marf expression in late larval stage, pupae and adults in control (**Figure 5.3B**). In addition, Marf expression in ubiquitous-*GAL4*-driven *Marf*^{RNAi} during the early stages of development to the arrested 3rd instar larval stages was also analysed. Early and late ubiquitous-*GAL4*-driven *Marf*^{RNAiGD} larvae showed absence of the Marf band (**Figure 5.3B**), Marf band was present in embryonic stages for both ubiquitous-*GAL4*-driven *Marf*^{RNAiGD} and ubiquitous-*GAL4*-driven *Marf*^{RNAiKK}. Appearance of Marf in embryonic stages is possibly due to the known inefficiency of RNAi in embryonic stages. In the case of ubiquitous-*GAL4*-driven *Marf*^{RNAiKK}, very weak Marf band was present during early larval stages but the band disappeared in 3rd instar larval stage (**Figure 5.3B**).

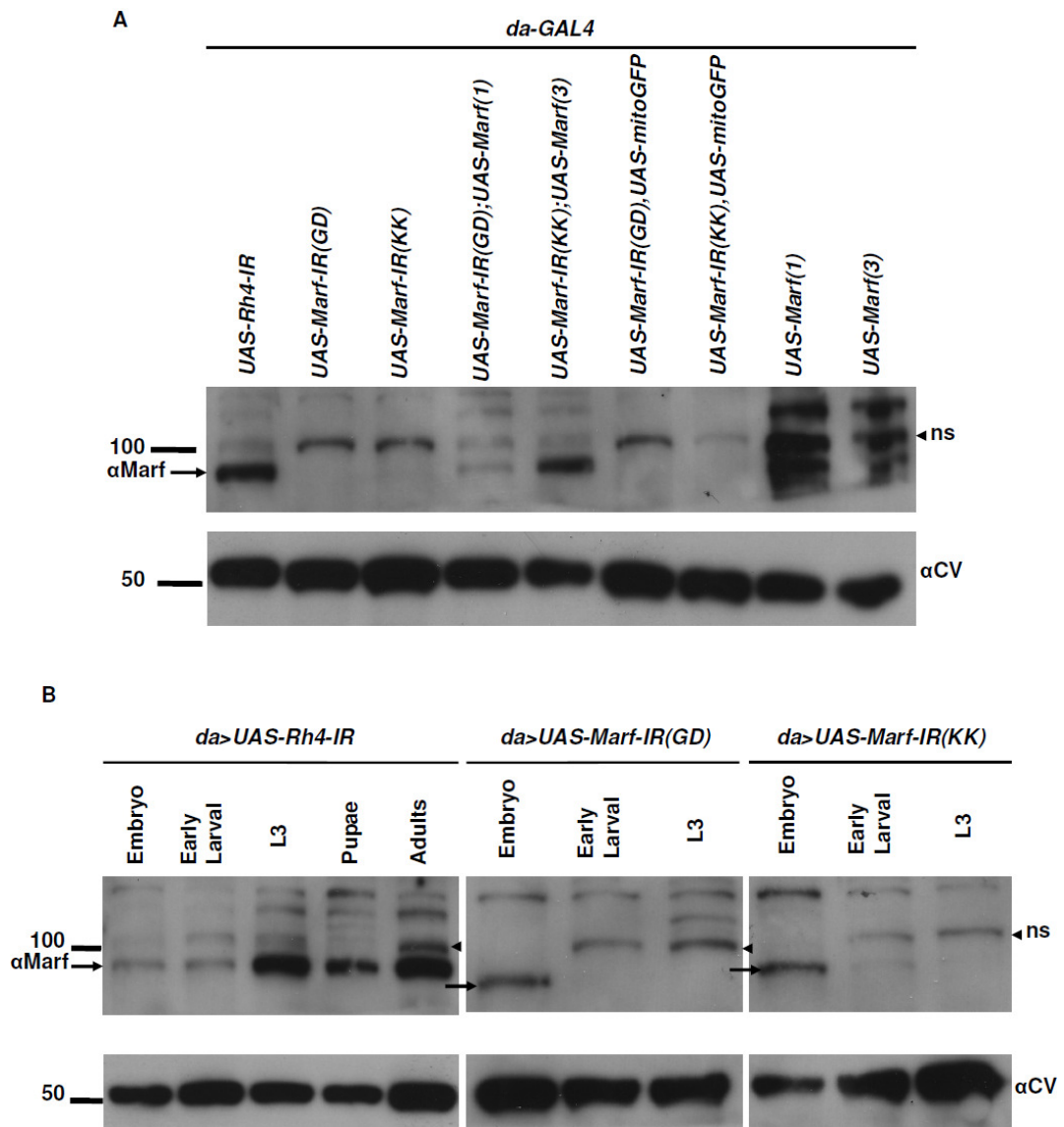


Figure 5.3: Western blot analysis for *Marf* RNAi effectiveness. (A) Expression analysis for *Marf* ubiquitous knockdown, rescue and overexpression. *da-GAL4>UAS-Rh4-IR* used as control (lane 1). *Marf* band (91.4-94.1kDa) (indicated with arrow) is absent in *da-GAL4>UAS-Marf-IR(GD)* (lane 2) and *da-GAL4>UAS-Marf-IR(KK)* (lane 3). *Marf* band is present in *da-GAL4>UAS-Marf-IR(GD);UAS-Marf(1)* (lane 4) *da-GAL4>UAS-Marf-IR(KK);UAS-Marf(3)* (lane 5). *Marf* band is absent in *da-GAL4>UAS-Marf-IR(GD),UAS-mitoGFP* (lane 6) and *da-GAL4>UAS-Marf-IR(KK),UAS-mitoGFP* (lane 7). Intense *Marf* band present in *Marf* overexpression lines: *da-GAL4>UAS-Marf(1)* (lane 8) and *da-GAL4>UAS-Marf(3)* (lane 9).

(B) Western blot analysis for Marf expression during development. (Blot 1) *da-GAL4>UAS-Rh4-IR* controls (Lane 1: embryo, Lane 2: early larval stages (1 and 2), Lane 3: 3rd instar larval stage, Lane 4: pupal stage, Lane 5: adult stage). Marf band present in all lanes at 91.4-94.1 kDa (indicated with arrow) with an increase in band intensity through the later developmental stages. *da-GAL4>UAS-Marf-IR(GD)*; Marf band is present in embryonic stage (Lane 1, indicated with arrow), and not visible in larval stages (Lane 2 and 3). *da-GAL4>UAS-Marf-IR(KK)*; Marf band is present in embryonic stage (Lane 1, indicated with arrow), faint Marf band present in early larval stages (Lane 2), Marf band disappeared in 3rd instar larval stage (Lane 3). ns: non specific band. Complex V was used as loading control (westerns run by Joe Pogson).

5.2.4 Locomotion defects in *Marf* ubiquitous knockdown larvae

Drosophila larvae exhibit forward movement by contracting the body wall muscles in successive segments from posterior to anterior creating a peristaltic wave pushing the body forward. Such movement has been extensively studied to detect locomotory defects in larvae (Feiguin et al., 2009). To find motility defects in the *Marf* ubiquitous knockdown larvae, the numbers of peristaltic waves for every 2 minutes were recorded for 3rd instar larvae. Both ubiquitous-*GAL4*-driven *Marf*^{RNAiGD} and *Marf*^{RNAiKK} larvae showed significantly reduced peristaltic movement as compared to the controls (**Figure 5.4**). Larvae obtained from cross between ubiquitous-*GAL4*-driver line and transgenic line carrying *Marf*^{RNAiGD} and *UAS-mitochondrial GFP*, also showed significantly reduced peristaltic movements (**Figure 5.4**). Interestingly, the defective larval locomotion was rescued in the rescue line where *Marf* was re-expressed in ubiquitous-*GAL4*-driven *Marf*^{RNAi} (**Figure 5.4**). These results suggest that loss of *Marf* interferes with normal larval locomotion. However, since a benign RNAi control, such as *y*^{RNAi} or *Rh4*^{RNAi}, is absent therefore this data should be interpreted cautiously.

5.2.5 Survival rate for *Marf* nervous system and motor neuron knockdowns

The longevity assay was performed to establish the role of *Marf* in adult survival. 0-24 hour old flies were collected, kept in food vials in humidified chamber at 25°C and survival was recorded for 30 days. Neuronal-*GAL4*-driven *Marf* knockdown flies showed significantly reduced survival (**Figure 5.5A**). Neuronal-*GAL4*-driven *Marf*^{RNAiGD} adult flies were severely affected and showed a median life of 2 days (**Figure 5.5A**), whereas *Marf*^{RNAiKK} adult flies showed slightly longer life span with a median survival of 12 days (**Figure 5.5A**). However, motor neuron-*GAL4*-driven *Marf* knockdown flies showed relatively variable survival rates (**Figure 5.5B**). Motor neuron-*GAL4*-driven *Marf*^{RNAiGD} adult flies presented median survival of 15 days (**Figure 5.5B**), and motor neuron-*GAL4*-driven *Marf*^{RNAiKK} adult flies showed normal survival rate with very few deaths over the periods of 30 days (**Figure 5.5B**).

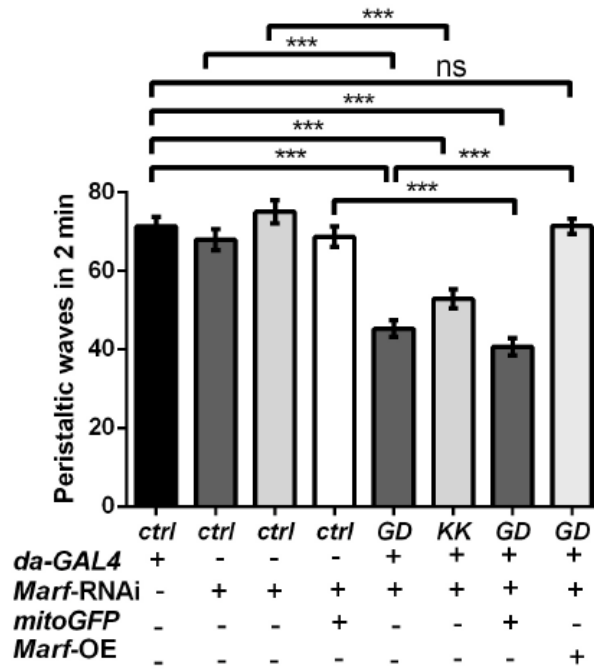


Figure 5.4: Larval locomotion assay for *Marf* ubiquitous knockdowns. $n = 20$ for each genotype. Controls out crossed with w^{1118} . Black control bar: *da-GAL4*/+, dark grey control bar: *UAS-Marf-IR(GD)*/+, light grey control bar: *UAS-Marf-IR(KK)*/+, white control bar: *UAS-Marf-IR(GD),UAS-mitoGFP*/+. Data is presented as mean±standard error. Significance was determined by one-way ANOVA with Tukey's multiple comparison test (***) $P < 0.001$.

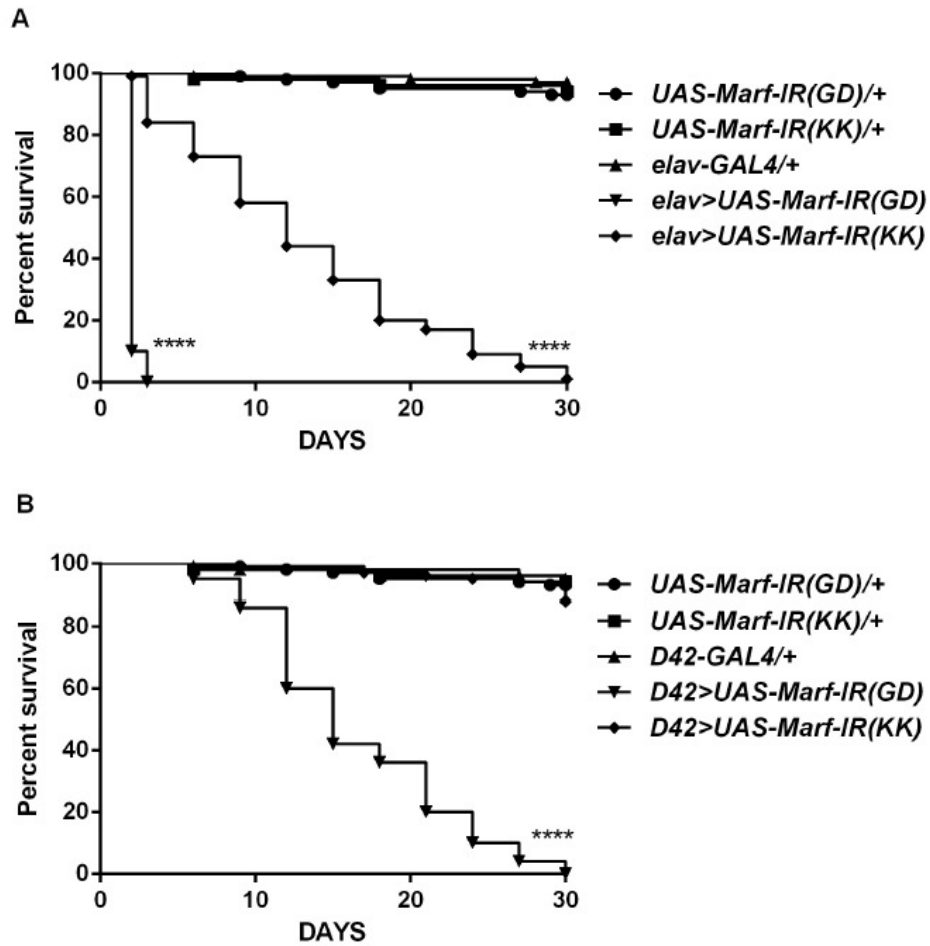


Figure 5.5: Survival curves for *Marf* nervous system and motor neuron knockdown flies.

The number of flies scored from each cross was >100. (A) *elav-GAL4>UAS-Marf-IR(GD)* and *elav-GAL4>UAS-Marf-IR(KK)* showed significantly reduced life span. (B) *D42-GAL4>UAS-Marf-IR(GD)* showed reduced survival. *D42-GAL4>UAS-Marf-IR(KK)* showed normal survival. Each data point represents percent survival. All statistical analyses were performed by χ^2 analysis using log-rank Mantel-Cox test and log rank test for trend (****P<0.0001).

The difference in survival observed between the *GD* and *KK* lines for motor neuron *Marf* knockdowns is difficult to explain. One possible suggestion can be an off target effect associated with *Marf*^{*RNAiGD*} transgene and/or possibly reduced expression of *Marf*^{*RNAiKK*} transgene in motor neurons. Future work could test for off-target effects by assessing whether re-expression of *Marf* can rescue these phenotypes. Our results suggest that *Marf* expression have an effect on fly survival but the limitation of the data to draw conclusion is the absence of benign RNAi as control in this assay. The effect of *Marf* down regulation in nervous system and motor neurons on fly survival could be a false positive effect of UAS-RNAi it self. Hence we are unable to distinguish between the effect of UAS-RNAi on fly survival and the effect due to ablation of a necessary gene such as *Marf* on fly survival.

5.2.6 Locomotion defects in *Marf* nervous system knockdown and motor neuron knockdown flies

Climbing and flight ability of the flies were tested to assess locomotion defects in nervous system and motor neuron knockdown adult flies. 100 flies for each genotype in cohorts of 20 flies (approximately equal proportion of males and females) were tested in climbing assays followed by flight assays. Nervous system-*GAL4*-driven *Marf*^{*RNAiGD*} flies were unable to perform in the climbing test and showed 0.00 climbing index (**Figure 5.6**). Similarly, nervous system-*GAL4*-driven *Marf*^{*RNAiKK*} flies also showed poor climbing with significantly reduced climbing index as compared to the controls (**Figure 5.6**). The climbing deficit was successfully rescued in nervous system-*GAL4*-driven *Marf*^{*RNAiGD*} flies with the re-expression of *Marf* (**Figure 5.6**) (Data for locomotion assays for *Marf* overexpression flies is presented in Appendix A). Re-expression of *Marf* increased the climbing ability of nervous system-*GAL4*-driven *Marf*^{*RNAiKK*} flies but the effect was significantly lower than control flies (**Figure 5.6**). Motor neuron-*GAL4*-driven *Marf*^{*RNAi*} flies also showed significantly reduced climbing as compared to the control flies (**Figure 5.6**). However, the climbing defect was significantly rescued in these flies with re-expression of *Marf* in motor neurons (**Figure 5.6**). Moreover, flies carrying both *Marf*^{*RNAi*} and *UAS*-mitochondrial *GFP* transgene were also included in the assays as transgene dilution test sample. These flies showed similar climbing defects as seen in nervous system and motor neuron *Marf*^{*RNAi*} flies (**Figure 5.6**).

In the flight assay, both nervous system-*GAL4*-driven *Marf*^{*RNAiGD*} and *Marf*^{*RNAiKK*} flies showed significantly reduced flight ability as compared to the control (**Figure 5.7**).

The flight defect was significantly rescued for both *GD* and *KK* lines with re-expression of *Marf* (**Figure 5.7**). Additionally, both motor neuron-*GAL4*-driven *Marf*^{*RNAiGD*} and *Marf*^{*RNAiKK*} flies showed significantly reduced flight ability (**Figure 5.7**) and was significantly rescued with *Marf* re-expression (**Figure 5.7**). Flies carrying both *Marf*^{*RNAiGD*} and *UAS*-mitochondrial *GFP* also showed significantly reduced flight ability. However, flies with motor neuron-*GAL4*-driven *Marf*^{*RNAiKK*} and *UAS*-mitochondrial *GFP* transgene showed normal flight ability (**Figure 5.7**). Also, the difference between the flight ability of *GD* and *KK* lines was statistically significant. The difference in flight ability of these two transgenic lines is difficult to rationalise but could possibly be due to the consistently weaker effect of the *Marf*^{*RNAiKK*} being further titrated by the presence of a second *UAS* transgene.

In conclusion, our data indicate that *Marf* plays a role in *Drosophila* locomotion and that down regulation of *Marf*, either in nervous system or in motor neurons significantly inhibits motor ability.

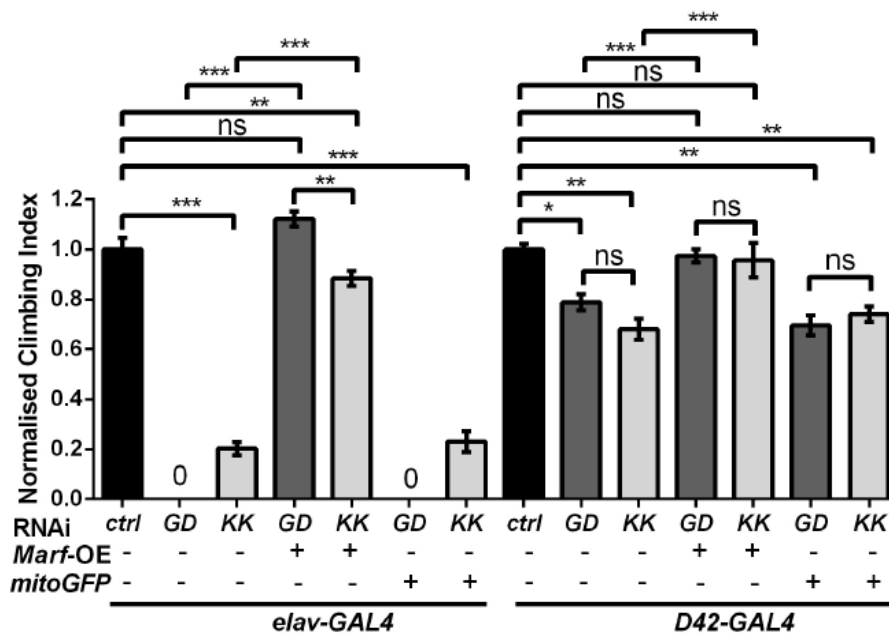


Figure 5.6: Climbing assay for *Marf* knockdown flies. n = 100 for each genotype. RNAi: *UAS-Marf-IR*. *Marf-OE*: *UAS-Marf*. ctrl: *UAS-y-IR*. *mitoGFP*: *UAS-Marf-IR,UAS-mitoGFP*. ctrl: *UAS-y-IR*. GD: *UAS-Marf-IR(GD)*. KK: *UAS-Marf-IR(KK)*. Data is presented as mean \pm standard error. Significance was determined with Kruskal-Wallis non-parametric analysis and Dunn's pair-wise comparison (***) $P < 0.001$, (**) $P < 0.01$, (*) $P < 0.05$).

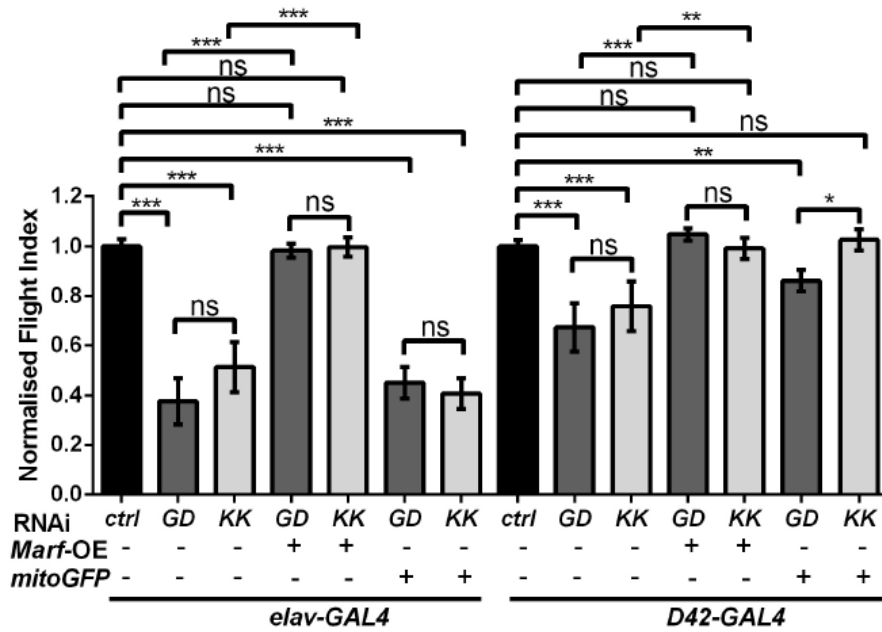


Figure 5.7: Flight assay for *Marf* knockdown flies. n = 100 for each genotype. RNAi: *UAS-Marf-IR*. *Marf-OE*: *UAS-Marf*. ctrl: *UAS-y-IR*. *mitoGFP*: *UAS-Marf-IR,UAS-mitoGFP*. ctrl: *UAS-y-IR*. GD: *UAS-Marf-IR(GD)*. KK: *UAS-Marf-IR(KK)*. Data is presented as mean±standard error. Significance was determined with Kruskal-Wallis non-parametric analysis and Dunn's pair-wise comparison (*** $P < 0.001$, ** $P < 0.01$, * $P < 0.05$).

5.2.7 Mitochondrial morphology and neuromuscular junction structure analysis in *Marf* motor neuron knockdown and *Marf* motor neuron overexpression larvae

Mitochondrial morphology in motor neurons of *Drosophila* was analysed to gain insight into the effect of *Marf* knockdown in motor neurons. Mitochondrial morphology was observed in the cell bodies of the motor neurons present in the ventral ganglion, in axonal part of segmental nerves in abdominal segment A2 and in the boutons of the neuromuscular junctions innervating muscle 6/7 in abdominal segment A3. Anti-HRP was used to stain the motor neuron membranes and *UAS-mitochondrial GFP* transgene under the control of motor neuron-*GAL4* driver was used as mitochondrial marker. Motor neuron-*GAL4*-driven *Marf*^{*RNAiGD*} larvae showed heterogeneous mitochondrial morphology in cell bodies. Mitochondria appeared fragmented in various cell bodies unlike filamentous and loose mitochondrial networks present in control cell bodies (**Figure 5.8b**). Cell bodies of motor neuron-*GAL4*-driven *Marf*^{*overexpression*} larvae showed elongated mitochondria forming tangles of highly interconnected mitochondrial mass (**Figure 5.8c**). Axons projecting from the ventral ganglion of motor neuron-*GAL4*-driven *Marf*^{*RNAiGD*} larvae showed increased population of small mitochondria as compared to control (**Figure 5.9b**). Motor neuron-*GAL4*-driven *Marf*^{*overexpression*} larvae showed various elongated thread like- mitochondria in addition to normal mitochondrial population in axons (**Figure 5.9c**). The last part of the motor neuron studied for mitochondrial morphology was the neuromuscular junction (NMJ) where motor neurons innervate the muscles (**Figure 5.10**). Typical NMJ has several spherical structures called boutons which are the sites where neurotransmitters are released to induce muscle contraction. Each bouton harbours a number of small mitochondria to meet the energy requirement during synaptic transmission. We noticed no difference in the mitochondrial morphology in boutons of motor neuron-*GAL4*-driven *Marf*^{*RNAiGD*} larvae (**Figure 5.11c,c',d,d'**). However, noticeably few mitochondria were present in the boutons of motor neuron-*GAL4*-driven *Marf*^{*overexpression*} (**Figure 5.11e,e',f,f'**). These findings suggest a possible mitochondrial morphology defects in these larvae. The confocal images are representative of many analysed samples, but the changes were not able to be quantified satisfactorily. Nevertheless, we feel that this qualitative assessment fairly represents the reproducible effects observed.

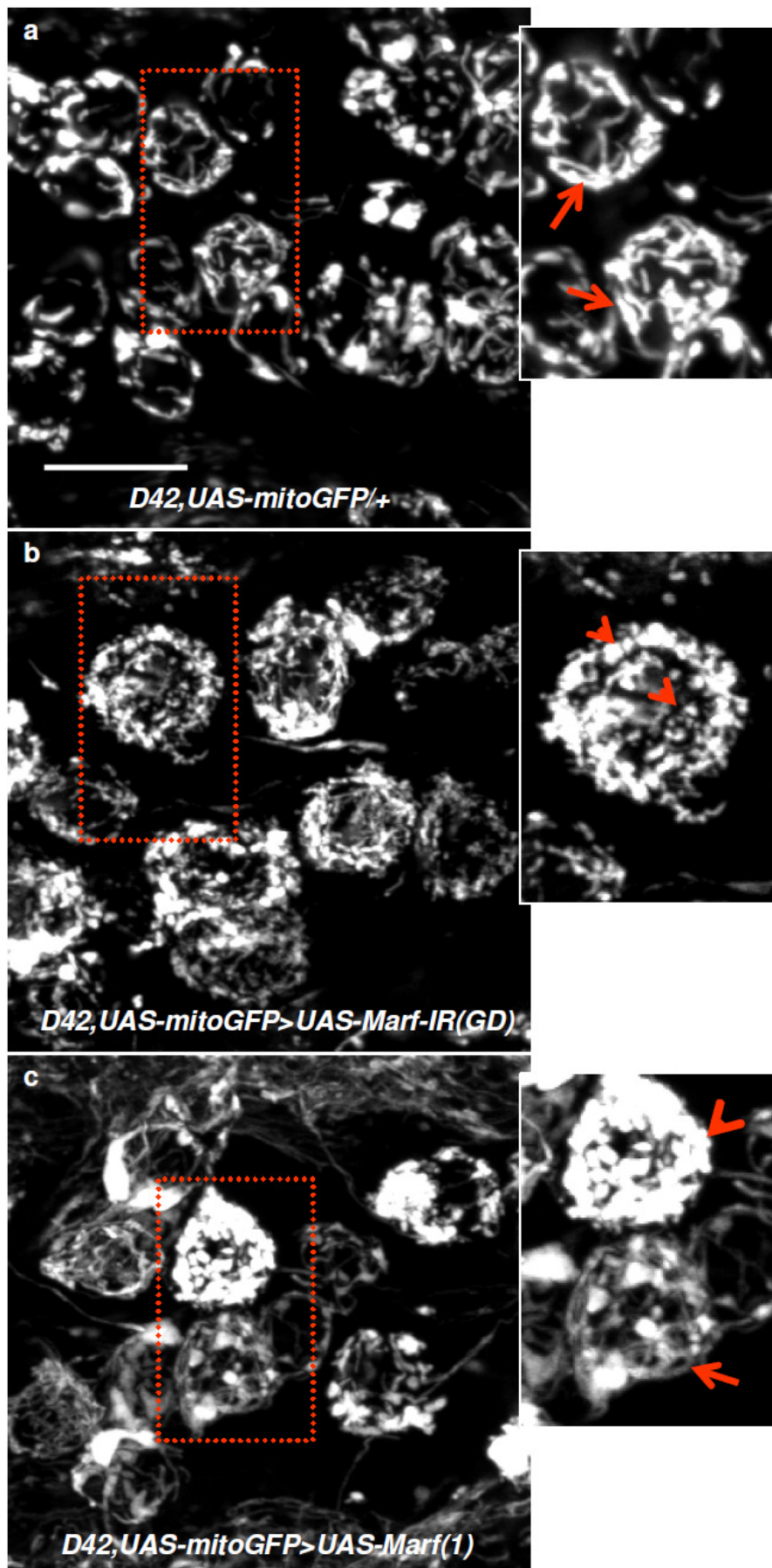


Figure 5.8: Mitochondrial morphology in cell bodies of *Drosophila* larvae motor neurons.

Representative confocal images from cell bodies of motor neurons present in ventral ganglion of 3rd instar larvae. (a) In *D42-GAL4,UAS-mitoGFP/+* (control) larvae showed typical loose mitochondrial networks morphology (indicated with arrows in the inset). (b) *D42-GAL4,UAS-mitoGFP>UAS-Marf-IR(GD)* larvae showed fragmented (indicated with arrowheads in inset) mitochondria and longer mitochondria. (c) *D42-GAL4,UAS-mitoGFP>UAS-Marf(1)* larvae showed elongated mitochondria and extensive mitochondrial networks (indicated with arrow in inset) and clumping of mitochondrial networks (indicated with arrowhead in inset). Scale bar = 10µm.

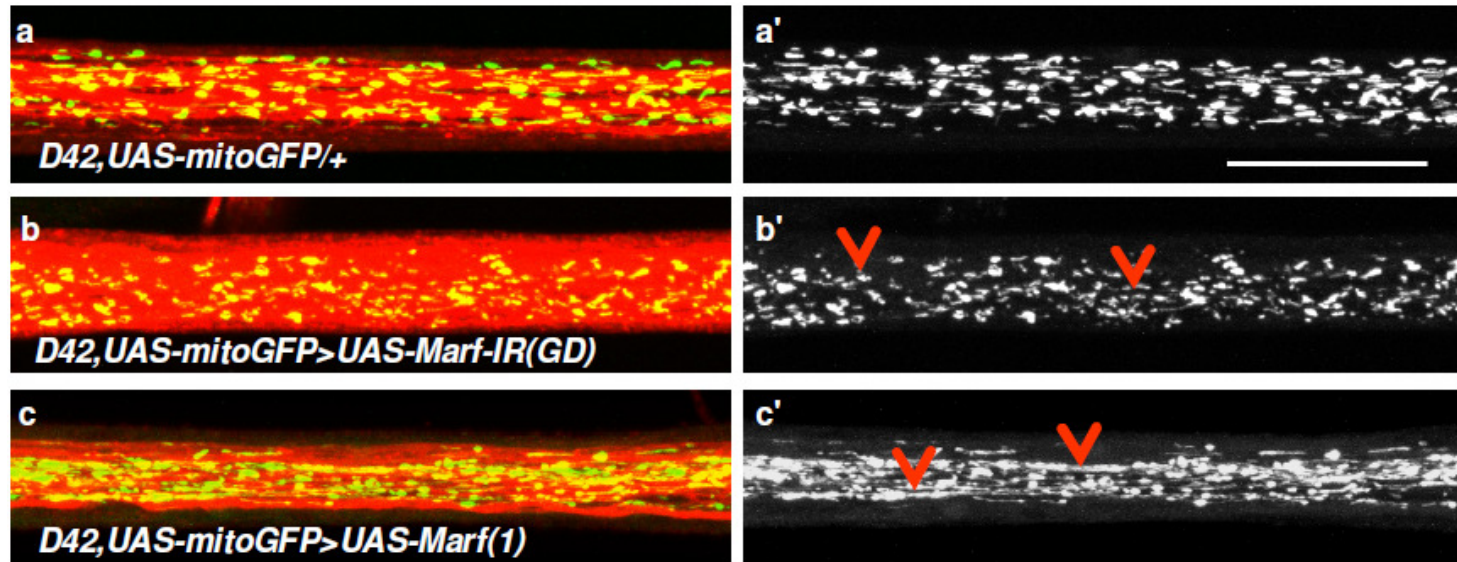


Figure 5.9: Mitochondrial morphology in axons of *Drosophila* larvae motor neurons. Representative confocal images from the axonal part of segmental nerve of 3rd instar larvae. Axonal membranes were labelled with HRP (red) and mitoGFP (green) to label the mitochondria. (a,a') Mitochondria appeared as small tubules and spheres in *D42-GAL4,UAS-mitoGFP/+*. (b,b') *D42-GAL4,UAS-mitoGFP>UAS-Marf-IR(GD)* larvae showed large number of fragmented mitochondria (indicated with arrowheads). (c,c') *D42-GAL4,UAS-mitoGFP>UAS-Marf(1)* mitochondria appeared elongated and form long thread-like structures (indicated with arrowheads) Scale bar = 20 μ m.

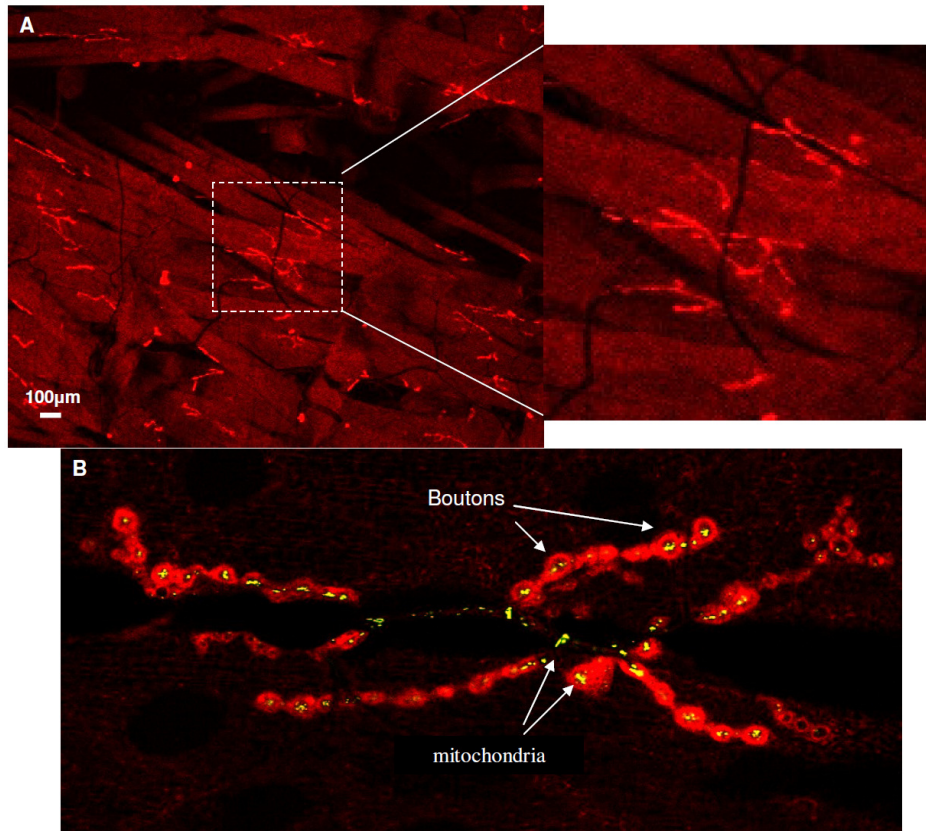


Figure 5.10: *Drosophila melanogaster* neuromuscular junctions. (A) Image showing various neuromuscular junctions in body wall muscles of 3rd instar larvae. Magnified inset image showing the neuromuscular junction of muscle 6/7. Neuromuscular junctions were stained with anti-HRP. (B) Typical structure of neuromuscular junction innervating muscle 6/7 in abdominal segment A3 of 3rd instar larvae. Boutons appear as round structure containing small spherical mitochondria (labelled with mitoGFP). Scale bar = 100µm.

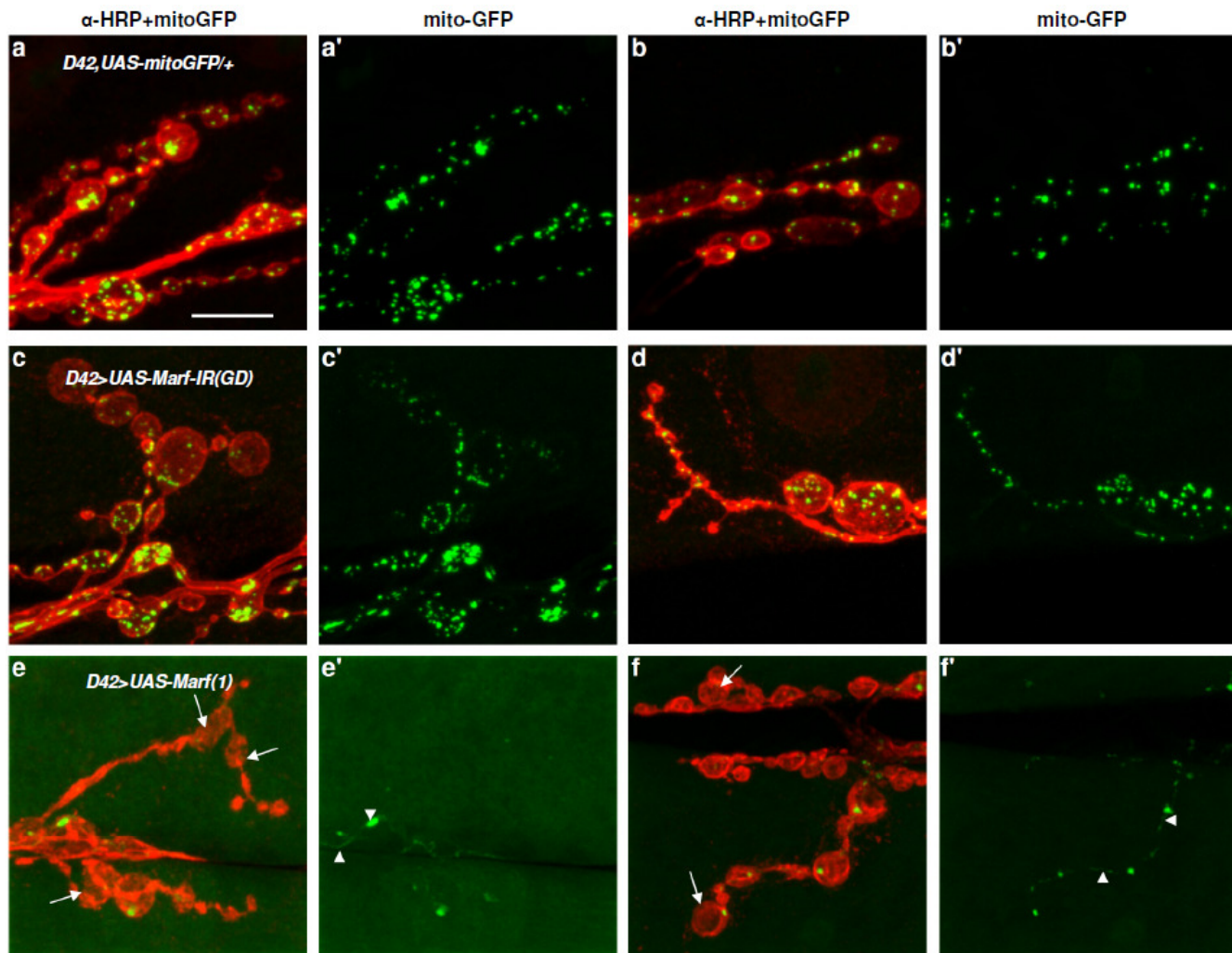


Figure 5.11: Mitochondrial morphology in neuromuscular junctions of *Drosophila* larvae motor neurons. Representative confocal images of synaptic boutons at muscles 6 and 7 (abdominal segment A3) in 3rd instar larvae. Two representative confocal images for each genotype are shown. Neuronal membranes stained with anti-HRP and mitochondria tagged with mitoGFP. (a,a',b,b') *D42-GAL4,UAS-mitoGFP/+* larvae showed small spherical mitochondria in the boutons. (c,c',d,d') *D42-GAL4,UAS-mitoGFP>UAS-Marf-IR(GD)* larvae also showed small spherical mitochondria. (e,e',f,f') *D42-GAL4,UAS-mitoGFP>UAS-Marf (1)* larvae showed few mitochondria in the boutons and majority appeared devoid of any mitochondria (indicated with arrows), mitochondria showed occasional clumps (indicated with arrowheads). Scale bar = 10µm.

Bouton number and synapse branching are the two common measurements of neuromuscular junction development in the *Drosophila* larvae (Verstreken et al., 2005). The number of boutons was assessed as percentage of bouton count normalized to muscle surface area relative to controls (see section 2.10.3). Motor neuron-*GAL4*-driven *Marf*^{RNAiGD} larvae showed no increase in bouton count compared to controls while motor neuron-*GAL4*-driven *Marf*^{overexpression} larvae presented a significant increase in relative bouton count (**Figure 5.12A**). Branch count per synapse was unaffected in motor neuron-*GAL4*-driven *Marf*^{RNAiGD} larvae. In addition, motor neuron-*GAL4*-driven *Marf*^{overexpression} larvae showed small increase in branch count per synapse, however the difference was not statistically significant as compared to control (**Figure 5.12B**). Due to the absence of benign UAS RNAi control from the data we have limitations in extracting the conclusion from the results. Still, considering the results presented in thesis as preliminary, it is suggested that Marf is important for the normal mitochondrial morphology and for the development of neuromuscular structure in flies. The affect seen on NMJ structure could be secondary to the disruptive mitochondrial dynamics as a result of *Marf* down regulation or overexpression in these larvae.

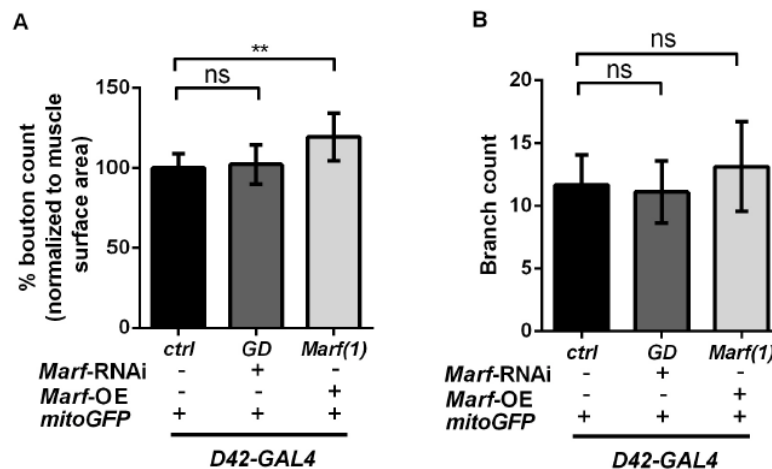


Figure 5.12: Structure analysis of neuromuscular junctions in *Drosophila* larvae. (A) Percent bouton count for motor neuron *Marf*^{RNAiGD} and motor neuron *Marf*^{overexpression} 3rd instar larvae. (B) The number of branches per synapse for motor neuron *Marf*^{RNAiGD} and motor neuron *Marf*^{overexpression} 3rd instar larvae. $n = 20$ animals for each genotype, (** $P < 0.01$).

5.2.8 Effects of Ethacrynic acid on *Marf* knockdown flies

We hypothesised that the locomotory deficit observed in *Marf* knockdown flies may be due to reduced mitochondrial fusion occurring in these flies. Since treatment with Ethacrynic acid (EA) showed increased mitochondrial fusion in CV14A cells and also reduced the increased mitochondrial fragmentation in Fis1 overexpressing CV14A cells and *Mfn2*^{R364W} patient fibroblasts (Chapter 4). Hence, we assumed that feeding EA to *Marf* knockdown flies might reduce the observed locomotory deficit.

5.2.8.1 Ethacrynic acid promotes mitochondrial fusion morphology in *Drosophila* S2R⁺ cells

Drosophila S2R plus (S2R⁺) cells were incubated with EA to see whether EA can produce similar effects as seen in CV14A cells and in patient fibroblasts. It was done primarily to determine that the mechanism through which EA increases the mitochondrial fusion in mammalian cells is conserved in flies or not. S2R⁺ cells were incubated with 0.1% DMSO as vehicle and 3 concentrations of EA; 21µM, 41µM and 83µM for 4 hours. In the presence of 0.1% DMSO S2R⁺ cells showed small tubular mitochondria with occasional connections with neighbouring mitochondria (**Figure 5.13a**). Interestingly, EA showed a dose dependent increase in mitochondria fusion in S2R⁺ cells. With 21µM EA mitochondrial morphology appeared similar to cells in 0.1% DMSO (**Figure 5.13b**) but in presence of 41µM EA cells showed longer mitochondria with increased connection and networks (**Figure 5.13c**). Additionally, mitochondria appeared as aggregated clumps with 83µM EA (**Figure 5.13d**), a phenotype very similar to that observed in *Drp1* RNAi S2R⁺ cells (Ziviani et al., 2010; Pogson et al., 2014). Since this assay was performed to verify the conserved mechanism of EA, and a consistent pattern emerged, these effects were not quantified. Hence, these are qualitative observations on a limited number of cells, and while representative, without quantification no firm conclusions can be drawn.

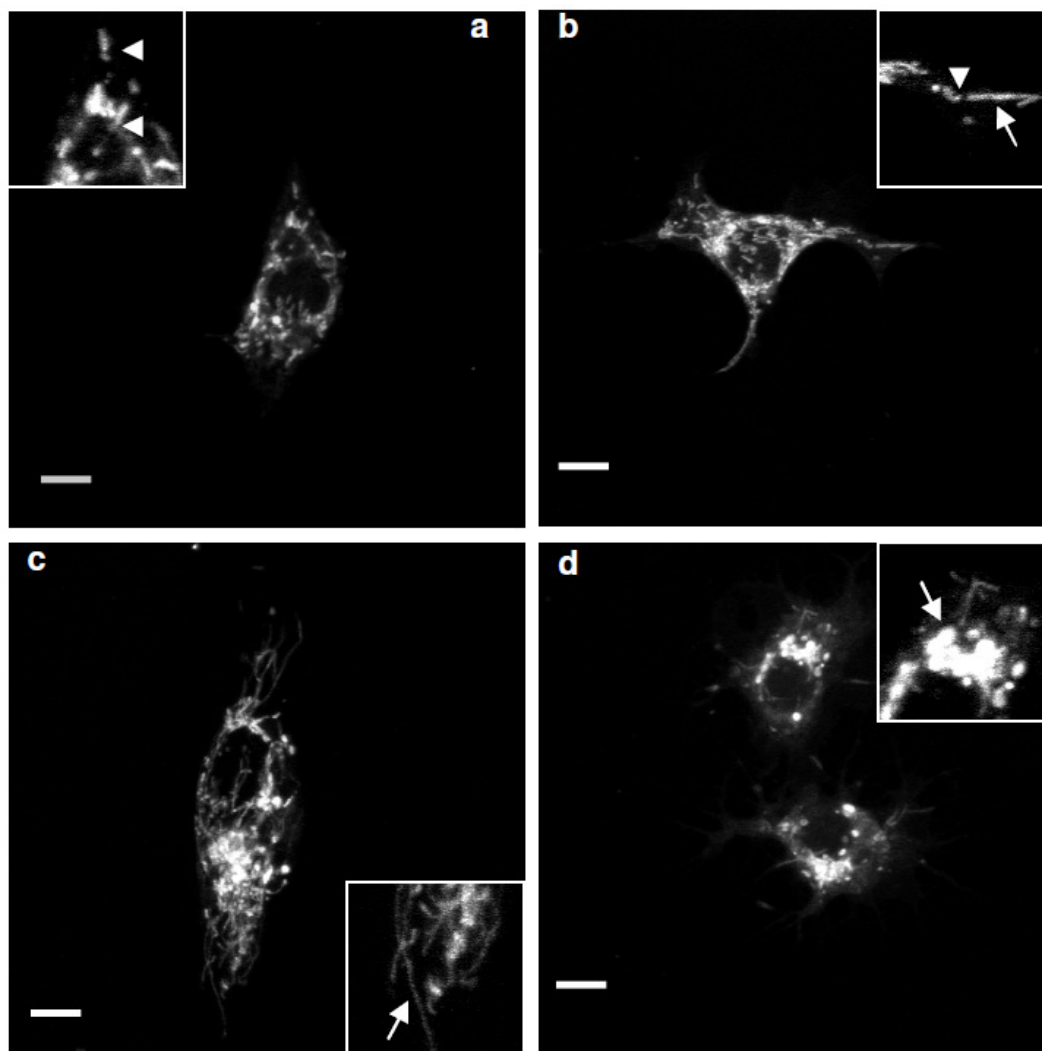


Figure 5.13: Mitochondrial morphology in S2R⁺ cells incubated with EA. Representative confocal images with magnified insets. MitoTracker was used to visualize mitochondrial morphology in live cells. (a) 0.1% DMSO treated S2R⁺ cells showed small tubular mitochondria (indicated with arrowheads). (b) 21 μ M EA showed small tubular mitochondria (indicated with arrowhead) and long tubular mitochondria (indicated with arrow). (c) 41 μ M EA showed long tubular mitochondria (indicated with arrow). (d) 83 μ M EA showed highly fused aggregated mitochondria (indicated with arrow) mostly with perinuclear location. Scale bar = 5 μ m.

5.2.8.2 Effect of Ethacrynic acid on *Marf* nervous system knockdown and *Marf* motor neuron knockdown

Flies were raised on normal food supplemented with 0.1% DMSO or 0.33mM EA and 1.65mM EA. These high concentrations of EA were used to ensure an optimal uptake of drug by the flies as no effect was observed with lower concentrations (data not shown). Additionally, EA reached its maximum solubility in DMSO with 1.65mM concentration. In 2 days old flies, EA failed to rescue the reduced climbing and flight ability in nervous system-*GAL4*-driven *Marf*^{RNAi} flies (**Figure 5.14**). In contrast, increase in climbing ability of motor neuron-*GAL4*-driven *Marf*^{RNAi} flies in a dose dependent manner was observed, with a significant increase in presence of 1.65mM EA (**Figure 5.14A**). However, increase in climbing was also observed in control flies treated with EA. Therefore, it cannot be concluded as rescue effect of EA on the climbing deficit of motor neuron-*GAL4*-driven *Marf*^{RNAi} flies, but simply increase in the locomotory activity of flies. Furthermore, EA treated motor neuron-*GAL4*-driven *Marf*^{RNAi} flies did not show significant increase in flight (**Figure 5.14B**). Moreover, 15 days old motor neuron-*GAL4*-driven *Marf*^{RNAiGD} flies raised and aged on EA supplemented food tend to show slightly better climbing as well as flight in the presence of EA as compared to flies kept on DMSO food, but the difference was non-significant as compared to control (**Figure 5.14B**). 15 days old motor neuron-*GAL4*-driven *Marf*^{RNAiKK} flies raised and aged on EA supplemented food failed to show obvious effects (**Figure 5.14B**).

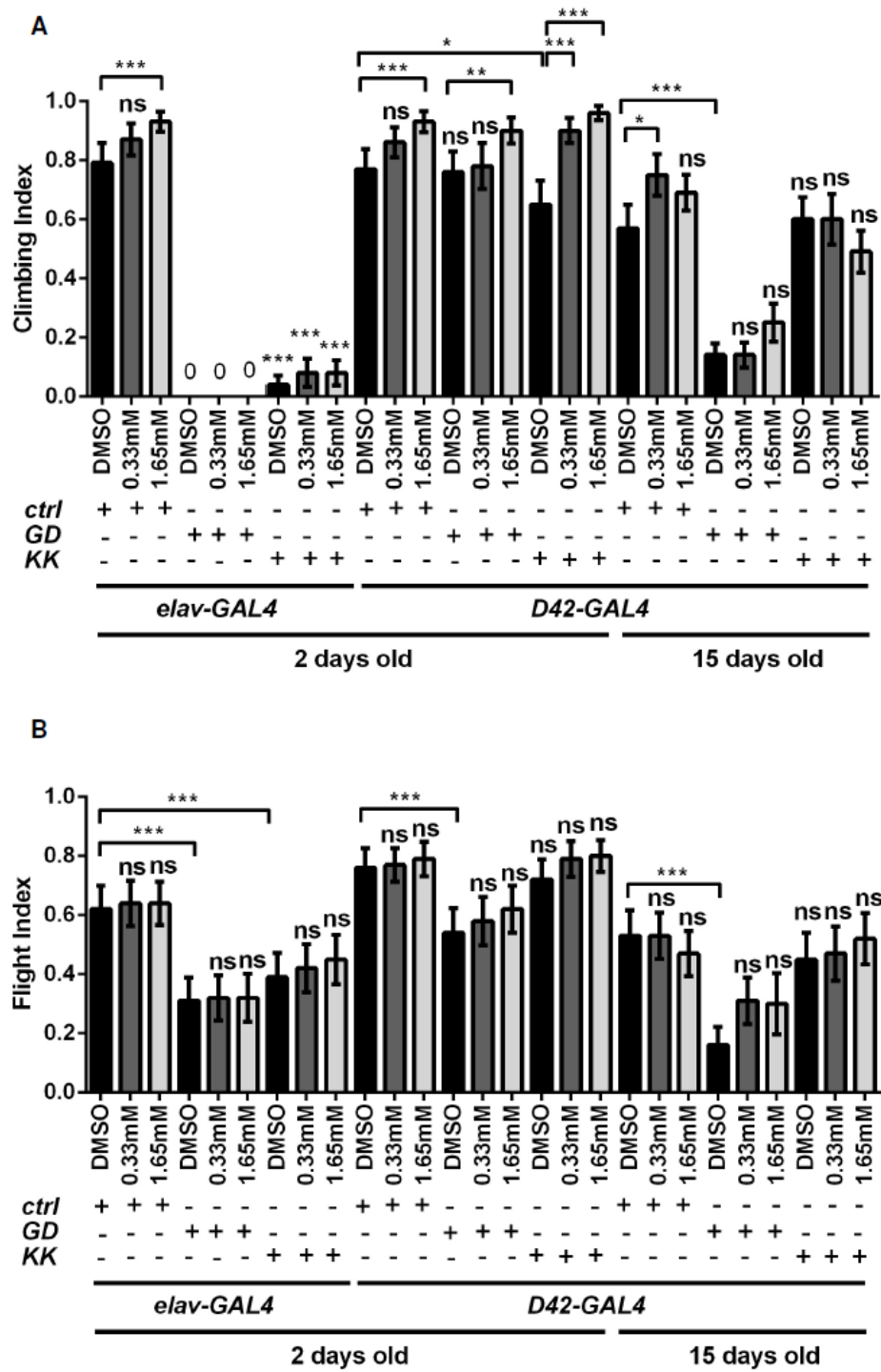


Figure 5.14: Locomotion assays for 2 days old and 15 days old *Marf^{RNAi}* flies fed on EA. (A) Climbing assay. (B) Flight assay. 0.1% DMSO was used as vehicle and 0.33mM and 1.65mM EA used. *ctrl*: *UAS-Rh4-IR*, *GD*: *UAS-Marf-IR(GD)*, *KK*: *UAS-Marf-IR(KK)*. n = 100 flies for each genotype per condition except 15 days old *D42-GAL4>UAS-Marf-IR(GD)*. n = 30-50 flies. Data is presented as mean ± standard error. Significance was determined by one-way ANOVA with Tukey's multiple comparison test (*) $P < 0.001$, ** $P < 0.01$, * $P < 0.05$).**

5.3 Discussion

To characterise the role of Marf on *Drosophila* development and locomotion we took advantage of down regulating *Marf* by RNAi using spatially controlled *GAL4* drivers. The data presented in the thesis showed that ubiquitous *Marf^{RNAi}* and muscle specific *Marf^{RNAi}* is lethal. Our data further demonstrated that Marf is essential for *Drosophila* locomotion, as nervous system *Marf^{RNAi}* and motor neuron *Marf^{RNAi}* flies showed severe mobility deficits. In addition, preliminary results suggested that normal levels of Marf in motor neurons are important for maintaining the typical mitochondrial morphology and distribution in larval motor neurons. Perturbing the normal Marf levels by *Marf^{RNAi}* and *Marf^{overexpression}* showed mitochondrial morphology and distribution defects and reduced bouton count in *Marf^{overexpression}* larvae. Also, we showed that mitochondrial fusion inducing compound EA has no effect on mobility deficits of nervous system *Marf^{RNAi}* and motor neuron *Marf^{RNAi}*.

Drosophila melanogaster larvae spend most of their time foraging inside the food substrate. In the late third instar stage, they leave the food and start to wander in search of adequate place to pupariate and undergo metamorphosis (Truman et al., 1994). However, ubiquitous-*GAL4*-driven *Marf^{RNAi}* larvae never entered into wandering stage remained inside or on top of the food, showed slow locomotion and the majority died at this foraging stage. We have shown that these larvae presented an extended time at 3rd instar stage. Previously, a similar delayed developmental phenotype with prolonged larval stages were reported in genes encoding other mitochondrial proteins including *mitochondrial transcription factor B2 (TFB2M)* (Adan et al., 2008), *polymerase gamma subunit β gene (pol γ - β)* (Iyengar et al., 2002) and *polymerase gamma subunit α gene (tamas)* (Iyengar et al., 1999). Ubiquitous *TFB2* RNAi and *tamas* mutant larvae both showed larval foraging stage for 30 days and more. This phenotype is similar to what we observed in ubiquitous *Marf^{RNAi}* larvae. *Pol γ - β* mutant larvae enter normally into the wandering larval stage but pupariation was delayed by 2-3 days and larvae died before eclosion (Iyengar et al., 2002). Also, ubiquitous *TFB2^{RNAi}*, *tamas* and *Pol γ - β* larvae were smaller in size as observed in ubiquitous *Marf^{RNAi}* larvae. Recently, two new reports have shown similar 3rd instar larval arrest in ubiquitous *Marf* knockdowns and in *Marf* genetic mutants obtained by EMS mutagenesis (Debattisti et al., 2014; Sandoval et al., 2014). Possible reasons for prolonged larval feeding stage and smaller larval size could be reduced cell growth and cell proliferation during larval stages. During the larval stages, larvae keep on feeding until they attain a critical weight at the 3rd instar

stage (Mirth et al., 2005). At this point larvae juvenile hormone levels decline and prothoracicotropic hormone (PTTH) levels are increased in hemolymph. PTTH acts on the prothoracic gland and triggers the synthesis of the molting hormone ecdysone. Ecdysone and its active metabolite 20-hydroxyecdysone (20E) (collectively known as ecdysteroid) allow transition from the feeding stage to the wandering stage and then pupation and metamorphosis. Reduced levels of ecdysteroid were found in experimentally delayed pupariation (Berreur et al., 1979). Interestingly, Sandoval and colleagues have shown that *Marf* is critical for cholesterol storage and ecdysone synthesis in the ring gland of *Drosophila* and further reported reduced levels of 20E in *Marf* genetic mutants (Sandoval et al., 2014). Thus, the larval arrested phenotype of ubiquitous-*GAL4*-driven *Marf*^{RNAi} larvae reported here could possibly be the outcome of lower 20E levels in ring glands of these larvae. Now, if *Marf* is critical for fly development then why does growth halt at a late larval stage and not earlier? One possible explanation could be the maternal contribution for *Marf* gene product which would likely be sufficient to continue development through zygotic, embryonic and larval stages. Furthermore, we know the polytene nature of all larval tissues except nervous system and imaginal tissues during fly development. The polytene cells have only G and S phase and do not divide but the diploid cells of imaginal tissues that later develop into adult fly divide continuously and rigorously throughout the larval stages to achieve critical weight (Fain and Stevens, 1982). Interestingly, reduced cell number of imaginal discs prevents the release of ecdysone at the beginning of wandering 3rd instar. Furthermore, arrested larval phenotype is typical to many mitochondrial proteins thus it also suggests failure of cells to cope with metabolic demand due to OXPHOS impairments (Iyengar et al., 2002; Adan et al., 2008). Also, *Mfn2* knockout mice have shown reduced number of cells and endo-replication cycles in polyploid trophoblast giant cells of placenta resulting in midgestation lethality (Chen et al., 2003). The high metabolic activities of trophoblast cells make them particularly vulnerable to defective mitochondrial fusion, which is responsible for maintaining a healthy population of mitochondria that are efficient in oxidative phosphorylation (Chen et al., 2003). Recently, Sandoval et al showed that *Marf* is involved in storage of free cholesterol in lipid droplets and suggested an inter-organellar interaction between endoplasmic reticulum and mitochondria for lipid vacuole formation. They further reported OXPHOS impairment in the *Marf* genetic mutants however they did not show that this defect is a secondary defect due to defective cholesterol storage or is due to some other factors (Sandoval et al., 2014).

Our data showed that Marf is critical for fly locomotion as both nervous system *Marf* knockdown flies and motor neuron *Marf* knockdown flies presented reduced climbing and flight which were rescued with the re-expression of *Marf*. These findings suggest that Marf is required in neuronal tissues and its loss induces motility deficits of neurological origin. Other mitochondrial shaping factors such as OPA1 and Drp1 mutants and mitochondrial trafficking factors such as Miro and Milton mutants also showed locomotive defects (Stowers et al., 2002; Guo et al., 2005). In addition, zebrafish carrying pathogenic *Mfn2* mutations showed slower swimming ability and defects in axonal transport of mitochondria (Chapman et al., 2013).

Furthermore, we saw mitochondrial fragmented morphology in neuronal cell bodies of motor-neuron-*GAL4*-driven *Marf*^{RNAiGD} larvae but the mitochondrial morphology defect was not clear in axonal segments and in boutons and might be due to the low expression of *D42-GAL4* driver. Debattisti and colleagues have reported prominent mitochondrial morphology defects in motor neurons, however, they reported these defects in strong *Marf* knockdown mutants such as ubiquitous-*GAL4*-driven *Marf*^{RNAi} and nervous system-*GAL4* driven *Marf*^{RNAi} larvae (Debattisti et al., 2014). Besides, *Marf*^{RNAiKK} line was not included in our data presented in this thesis rendering the data presented here as preliminary. However, it is suggested to include it in future work to make a comparison between the lines. In addition, elongated and highly fused mitochondrial morphology in motor neuron cell bodies in motor neuron-*GAL4*-driven *Marf*^{overexpression} larvae suggests increased mitochondrial fusion in these cells. The absence of mitochondria in boutons of these larvae imply that excess fusion is possibly disrupting transport of elongated mitochondria as mitochondrial transport machinery is unable to move large mitochondria. We know that *Drp1* mutants also showed few mitochondria in boutons (Verstreken et al., 2005). Additionally, mitochondrial transporting protein Milton and Miro also lack mitochondrial population in axons and boutons of the mutant larvae suggesting loss of mitochondrial transport (Stowers et al., 2002; Guo et al., 2005). It was shown in chick peripheral axons that either overexpressing *Mfn1* or inhibiting *Drp1* by RNAi resulted in long immotile mitochondria (Amiri and Hollenbeck, 2008).

In addition, we did not see any NMJ structure defect with *Marf* knockdown in motor neurons but we saw increase in bouton count in *Marf* overexpression larvae. Sandoval et al have reported few mitochondria in neuromuscular junction boutons of *Marf* mutants and severe reduction in size of boutons and doubling in the number of

boutons (Sandoval et al., 2014). *Marf* genetic mutant larvae also presented quick running down of neurotransmission in the motor neurons depicting a reserve pool mobilization defect and reduced local ATP levels (Sandoval et al., 2014). This defect was also reported in *Drp1* mutants that show normal bouton morphology (Verstreken et al., 2005). Sandoval and colleagues have suggested that this defect might be due to reduced number of mitochondria in distal regions of axons resulting in local energy deficiency due to reduced ATP production and increased ROS in their motor neurons (Sandoval et al., 2014). The increased bouton number in our motor neuron *Marf* overexpression larvae might also be due to increased oxidative stress as we have observed few mitochondria in the boutons but it needs to be shown. It has been reported previously that the reduced number of mitochondria present in neuromuscular junction could lead to Ca^{2+} homeostasis impairment leading to enhanced oxidative stress, which then results in activation of synapse growth pathways resulting in synaptic overgrowth (Milton et al., 2011; Vincent et al., 2012). However, motor neuron *Marf* overexpression flies showed normal climbing and flight (see appendix) which is different from *drp1*, *milton* or *miro* mutants that showed locomotion defects. A possible explanation could be that the adult flies may have sufficient ATP supply from few mitochondria present in synapses together with up-regulation of local glycolysis under oxidative stress to perform normal locomotion activities (Hansson et al., 2004, Adan et al., 2008). However, this question needs to be further addressed in depth by measuring the oxidative stress in the neuromuscular junctions of *Marf^{RNAi}* and *Marf^{overexpression}* larvae. Also, live imaging to study the axonal transport of mitochondria in *Marf* knockdown, and overexpression could provide a more precise view on mitochondrial defects. To conclude our data is still preliminary as it lacks the benign RNAi control and *Marf^{RNAiKK}* line. Also, ideally the mitochondrial morphology seen in motor neuron cell bodies, axons and boutons needs to be quantified to obtain conclusive results, however, technical and time constraints precluded further study to complete this.

Lastly, the effect of mitochondrial fusion inducing compound EA on the locomotory defects in nervous system and motor neuron *Marf* RNAi flies was assessed. While the effect of EA improved the climbing defect, we cannot conclude that this was due to a reversal of the loss of *Marf* since it also enhanced climbing in control as well by an unknown mechanism. This effect to climbing ability is difficult to explain, but possible reasons can be that EA is somehow providing more energy and/or EA is interacting with other cellular processes in addition to enhancing mitochondrial fusion.

Moreover, we have not monitored how much drug gets into the fly's system, so further assays using colour dyes in the food can be done to see how much food along with EA is taken up by the larvae. Although we failed to see any clear improvement of *Marf*^{RNAi} flies with EA it would be interesting to see the mitochondrial morphology in the motor neurons of *Marf*^{RNAi} larvae and see whether EA is able to increase mitochondrial fusion *in vivo*.

In conclusion, in concordance with the recently published reports by Debattisti et al and Sandoval et al on *Marf* mutants, the data in this thesis support that Marf is important for *Drosophila* normal development, its absence resulting in severe developmental defects, and that Marf plays critical role *Drosophila* locomotive abilities.

Chapter 5b: : EMS genetic screen for
Drosophila melanogaster Marf

5.4 Introduction

Drosophila melanogaster provides an excellent genetic model organism for the generation, recovery and identification of new mutations. Over the years, various approaches have been used to induce *de novo* mutations in fly genome but Ethyl methane sulfonate (EMS) mutagenesis has become established as a successful approach providing low toxicity and high mutagenesis efficiency (Bentley et al., 2000). EMS is an alkylating agent which adds an ethyl group to O⁶ position of guanine, thus creating O⁶-alkylguanine which mispairs with thymine during replication and results in GC → AT transitions in DNA (Pastink et al., 1991). 75-100% EMS induced lesions result in missense or nonsense mutations or may even destroy splice sites (Pastink et al., 1991; Bentley et al., 2000). Occasionally small deletions, transversions and frame shift mutations can also be recovered but in small proportions (Vogel and Natarajan, 1979). DNA alkylation is linearly dependent on the EMS dose used in a screen (Aaron and Lee, 1978; Ayaki et al., 1985). For a typical mutagenesis protocol using 25-50mM EMS, it is predicted that a new mutation is induced every 150-300kb of the genome (Greenspan, 2004; Bokel, 2008). EMS treatment induces mutations in all chromosomes; it only produces lesions in one chromosomal strand (Ashburner and Bergman et al., 2005; Bokel, 2008). Additionally, with the availability of the *Drosophila* genome sequence it has become easier to accurately map and identify the mutations generated in EMS screen.

Drosophila Marf is present on the X chromosome. To isolate new mutation on a locus on X chromosome is not straight forward and requires additional genetic manipulations to a conventional EMS screen. Being hemizygotic *Drosophila* males carry only one copy of X chromosome, therefore male flies carrying a mutation in a vital gene on X chromosome cannot survive unless there is a wild-type copy of the gene duplicated elsewhere in the genome (Greenspan, 2004). Advancements in fly genetics provide us with a unique tool known as compound X chromosomes. Compound X-chromosomes also known as attached X[^]X chromosomes have both arms of X chromosome attached to one centromere. X[^]X stocks are kept as both males and females carrying a Y chromosome which during segregation is inherited by the sons from their mothers only (Greenspan, 2004; Bokel, 2008). To rescue the male flies bearing a lethal mutation on the X chromosome, a duplication of the region of interest on X-chromosome must be present in the genome, for example may be on Y chromosome of the X[^]X chromosome stock. As a result of which, during meiosis this duplication

carrying Y chromosome segregates away from the attached X of the mother and the sons bearing lethal mutations can be recovered in next generation (Cook et al., 2010). Bloomington *Drosophila* Stock Centre has an on going project to construct interchromosomal duplications of the X chromosome called Bloomington Duplication Project (<http://flystocks.bio.indiana.edu/Browse/dp/BDSC-Dps.php>). The approach taken to generate these duplications is by translocation of large segments of the X chromosome on to the tips of Y chromosomes (Cook et al., 2010). Another useful advancement for mapping and characterising new mutations are the available deficiency chromosomes from Bloomington *Drosophila* Stock Center (<http://www.drosdel.org.uk/>) (Parks et al., 2004; Ryder et al., 2007). The deficiency chromosomes can be used in *trans* with newly induced mutation to identify interacting loci and characterizing complementing alleles.

The main disadvantages of RNAi are off-target effects and it does not completely eliminate a protein expression. So, to study the knockout effect of *Marf* in *Drosophila* we aimed to isolate a genetic mutant through EMS mutagenesis. Ideally, from such mutagenesis an allelic series may be isolated. This would generate a number of genetic mutants which could be useful for comparison and complementation among the mutants. It is known that EMS generally results in missense or nonsense mutations and occasionally it may even destroy splice sites, therefore we aimed at isolating either missense or nonsense mutations for *Marf*.

5.4.1 Forward Genetic screen for *Marf* using EMS mutagenesis

5.4.1.1 Complementation test for *Df(1)Exel6239* used in EMS screen

Df(1)Exel6239 was used to map the mutations on the EMS mutagenized chromosome. The chromosomal break points for *Df(1)Exel6239* are at 5F2-6B2 on *Drosophila* X chromosome (**Figure 5.15**). It completely deletes 21 genes including *Marf* (**Table 5.3**). Before starting the EMS screen we wanted to verify that the *Df(1)Exel6239* is approximately mapping the same region and true to the position by performing complementation with another deficiency chromosome overlapping the same region. *Df(1)G4e[L]H24i[R]* is a cytologically mapped deficiency for 5E3-5E8;6B. Complementation assay showed that both the deficiencies fail to complement each other suggesting they are overlapping (**Figure 5.16**).

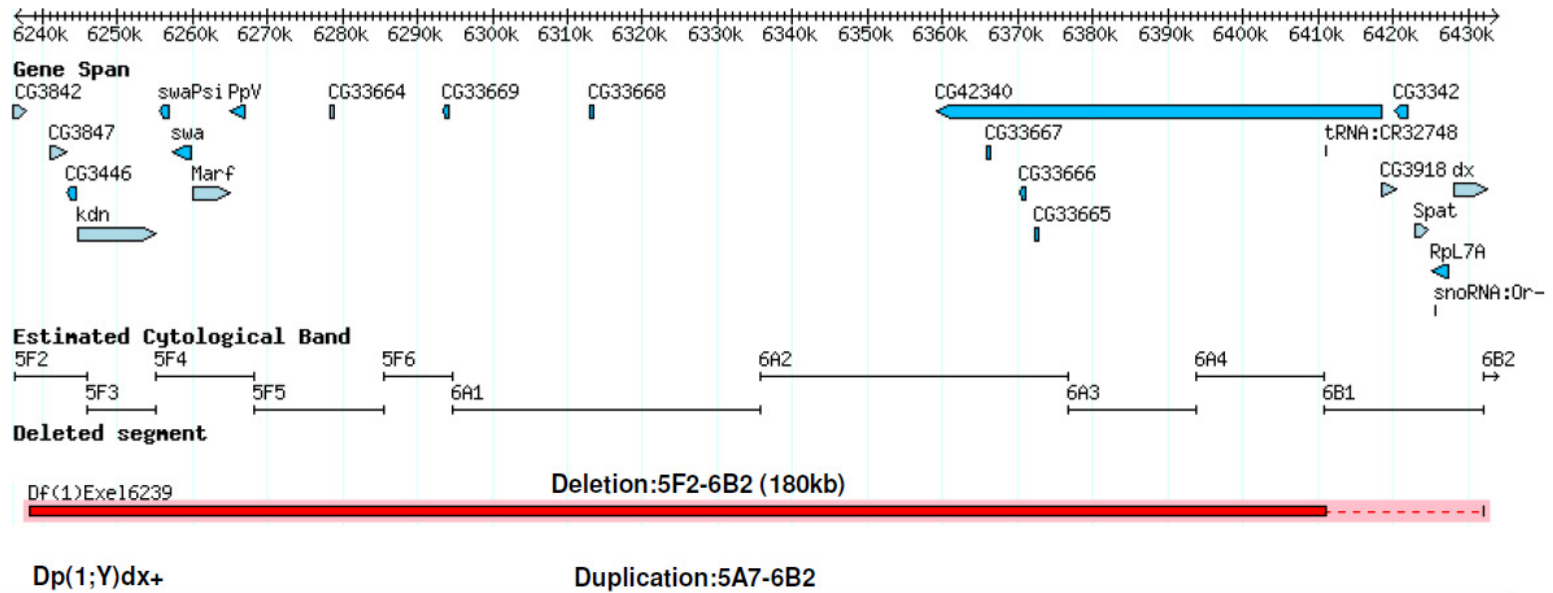


Figure 5.15: Genomic map for the *Df(1)Exel6239* deficiency chromosome showing the deleted 180kb region and the genes in the region. The deficiency maps to 5F2-6B2 on X-Chromosome. Duplicated region spanning from 5A7-6B2 is also indicated. This overlay also shows that duplication covers the deleted region in the deficiency chromosome.

Table 5.3: Genes deleted in *Df(1)Exel6239* deficiency chromosome.

Gene Deleted	Gene Size (kb)	Molecular Functions	Biological Processes involved	Reference
CG3847	2.138	Zinc ion binding; nucleic acid binding	Unknown	FlyBase Curators et al., 2004; Ryder, 2004
CG3446	1.077	NADH dehydrogenase activity	Mitochondrial electron transport, NADH to ubiquinone	Sardiello et al., 2003
kdn	5.9115	Citrate (Si)-synthase activity	Tricarboxylic acid cycle	FlyBase Curators et al., 2004; Ryder, 2004
swa Ψ	1.466	Unknown	Unknown	Chao et al., 1991, Ryder, 2004
swa	2.292	mRNA binding	mRNA localization	Stephenson et al., 1988
Marf or Mfn	4.979	GTPase activity	Mitochondrial fusion, mitochondrion organization	Hwa et al., 2002; Deng et al., 2008
PpV	1.851	Protein serine/threonine phosphatase activity	G1/S transition of mitotic cell cycle	Mann et al., 1993
CG33664	0.618	Unknown	Unknown	Chintapalli et al., 2007
CG33669	0.646	Unknown	Unknown	Chintapalli et al., 2007
CG33668	0.618	Unknown	Unknown	Chintapalli et al., 2007
CG42340	10.565	Potassium channel activity	Potassium ion transmembrane transport	Wang et al., 2004
CG33667	0.683	Unknown	Unknown	Chintapalli et al., 2007
CG33666	0.640	Unknown	Unknown	Chintapalli et al., 2007
CG33665	0.683	Unknown	Unknown	Chintapalli et al., 2007
tRNA:CR32748	0.073	UUC codon-amino acid adaptor activity	Protein translation	Ryder 2004, Lowe 2002
CG3342	1.783	Unknown	Unknown	Chintapalli et al., 2007
Spat	1.779	Alanine-glyoxylate transaminase activity	Glyoxylate catabolic process	Han and Li, 2002
CG3918	1.879	Zinc ion binding; nucleic acid binding	Unknown	Page et al., 2005
RpL7A	2.270	Structural constituent of ribosome	Centrosome organization and duplication, mitotic spindle elongation and organization	Goshima et al., 2007; Muller et al., 2010
snoRNA:Or-CD10	0.0067	Unknown	Unknown	Yuan et al., 2003; Huang et al., 2005
dx	4.573	Protein binding	Notch signaling pathway	Matsuno et al., 1995; Matsuno et al., 2002

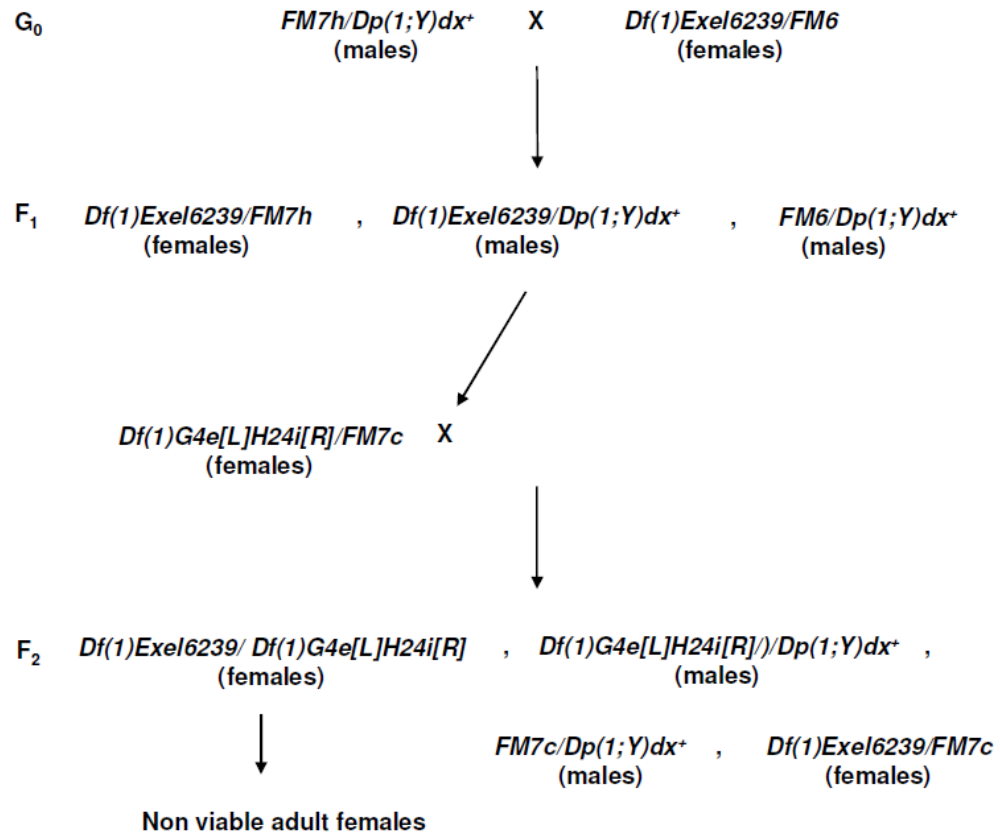


Figure 5.16: Crossing scheme for deficiency chromosomes complementation assay. *Df(1)Exel6239/FM6* females were crossed with *FM7h/Dp(1;Y)dx⁺* males. *Df(1)Exel6239/Dp(1;Y)dx⁺* males from F_1 progeny were crossed with *Df(1)G4e[L]H24i[R]/FM7c* females. *FM7c* is a balancer chromosome. In F_2 absence of *Df(1)Exel6239/Df(1)G4e[L]H24i[R]* adult female flies showed the deficiency chromosomes do not complement.

5.4.1.2 Isolation of EMS mutants

To isolate a genetic mutant for *Marf* we conducted F₃ EMS screen targeting the X chromosome. Males were collected from a w^{1118} stock (previously isogenised) and aged for 1-3 days, see **section 2.12.1**. These males were exposed to certain concentration of EMS for 24 hours. After recovery mutagenized w^{1118} males were crossed with $X^X/Dp(1;Y)dx^+$ females (G₀). This $Dp(1;Y)dx^+$ duplication stock carries an interchromosomal duplication of X chromosome segment 5A7-6B2 on the Y chromosome (<http://flybase.org/reports/FBab0028754.html>). $Dp(1;Y)dx^+$ duplication spans the *Marf* region as *Marf* is mapped to cytological region 5F4-5F4 on X chromosome (**Figure 5.15**) (<http://flybase.org/reports/FBgn0029870.html>). $Dp(1;Y)$ chromosome show typical Y-linked inheritance by behaving as normal Y chromosome in the crosses. Therefore, lethal mutation bearing $w^{1118}*/Dp(1;Y)dx^+$ males were recovered in F₁ progeny (Note: * indicates newly induced mutations). The F₁ mutagenized X chromosomes were tested against *Df(1)Exel6239* deficiency of the X chromosome by single pairing of individual $w^{1118}*/Dp(1;Y)dx^+$ males with 3-4 *Df(1)Exel6239/FM6* females (**Figure 5.17**).

Since characterisation of the *Marf*^{RNAi} showed loss of *Marf* is lethal, we predicted that genetic mutations in *Marf* would also be lethal. Therefore, F₂ progeny was scored for the absence of $w^{1118}*/Df(1)Exel6239$ adult females which could potentially uncover a lethal *Marf* mutation. The lethality of $w^{1118}*/Df(1)Exel6239$ was scored by the absence of females lacking the FM6 balancer which carries the *B^l* (bar eye/kidney shaped eye) marker or mutation (**Figure 5.17**). F₂ included females $w^{1118}*/Df(1)Exel6239$ which did not show red bar eye and female flies $w^{1118}*/FM6$ with bar shaped eye and red eye colour. The heterozygous females were then backcrossed with FM6 males to generate a stable stock. The other progeny in F₂ cross include *FM6/Dp(1;Y)dx⁺* males and *Df(1)Exel6239/Dp(1;Y)dx⁺* males (**Figure 5.17**).

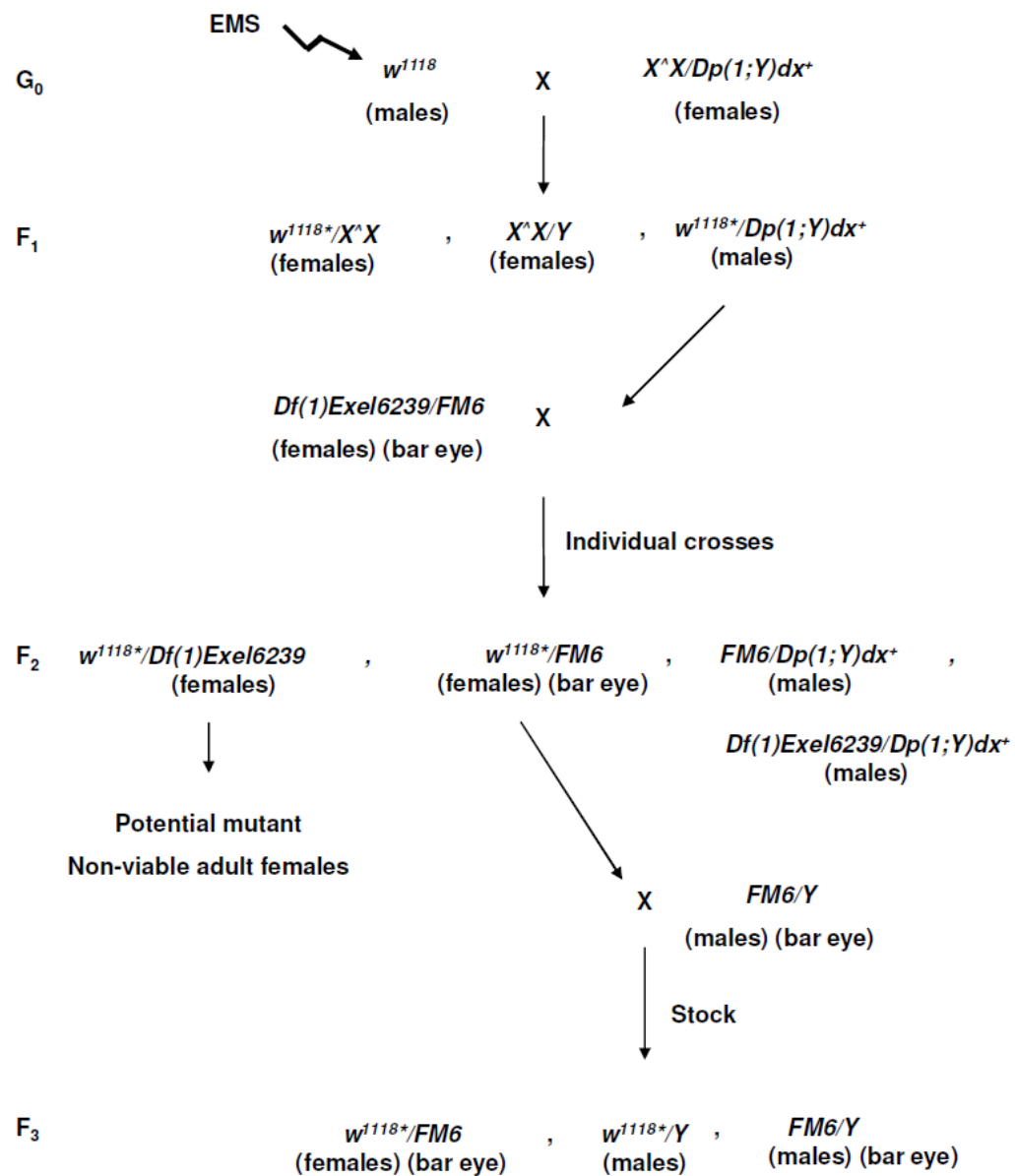


Figure 5.17: Crossing scheme for EMS mutagenesis. w^{1118} males were fed with EMS in 1% sucrose. These mutagenized w^{1118} males were crossed with $X^X/Dp(1;Y)dx^+$ females (G₀). $w^{1118^*}/Dp(1;Y)dx^+$ males from F₁ were set up in individual crosses with $Df(1)Exel6239/FM6$ females. F₂ progeny contains homozygous mutation bearing genotype $w^{1118^*}/Df(1)Exel6239$ females and heterozygous $w^{1118^*}/FM6$ females along with other genotypes including $FM6/Dp(1;Y)dx^+$ males and $Df(1)Exel6239/Dp(1;Y)dx^+$ males. Stable stocks for mutants were generated by crossing $w^{1118^*}/FM6$ females with $FM6$ males.

We performed 5 rounds of EMS screening (**Table 5.4**). In first EMS mutagenesis screen, 25mM EMS was used to mutagenize w^{1118} males from a previously isogenised stock. In F₁, 349 individual crosses with *Df(1)Exel6239* females were set up. This screen gave 85% viable crosses but recovered no lethal mutations over *Df(1)Exel6239*. During such random mutagenesis scheme it can be useful, though not essential, to monitor the mutagenesis rate. Since we were aiming for mutagenesis targeting the X chromosome, we can also monitor the incidental occurrence of mutants for known X chromosome genes such as *yellow (y)*. However, we did not observe any obvious y mutants (data not shown), suggesting that the mutation rate was very low. As the effect of EMS increases linearly with increase in concentration, we doubled the concentration in next 2 rounds of the screen. In the first 50mM EMS screen, 500 individual crosses for F₁ were set up. This gave 69.2% cross viability with no screen hit. In the second 50mM EMS screen, with 500 individual crosses for F₁, the cross viability was slightly lower 68.4%. However, in this screen line 112 came up as a potential hit. To achieve less male lethality and more viable crosses, in the fourth screen we used 40mM EMS for mutagenesis. In this screen we set up 550 individual crosses and achieved 63.6% viable crosses. This screen was more successful as 5 hits, namely line 52, line 91, line 149, line 189 and line 407, were obtained. We repeated the 40mM EMS for the fifth screen and set up 546 individual crosses but the percentage of viable crosses was lower 60.1%. Unfortunately, this screen failed to achieve any hits.

5.4.1.3 Characterisation of EMS screen hits

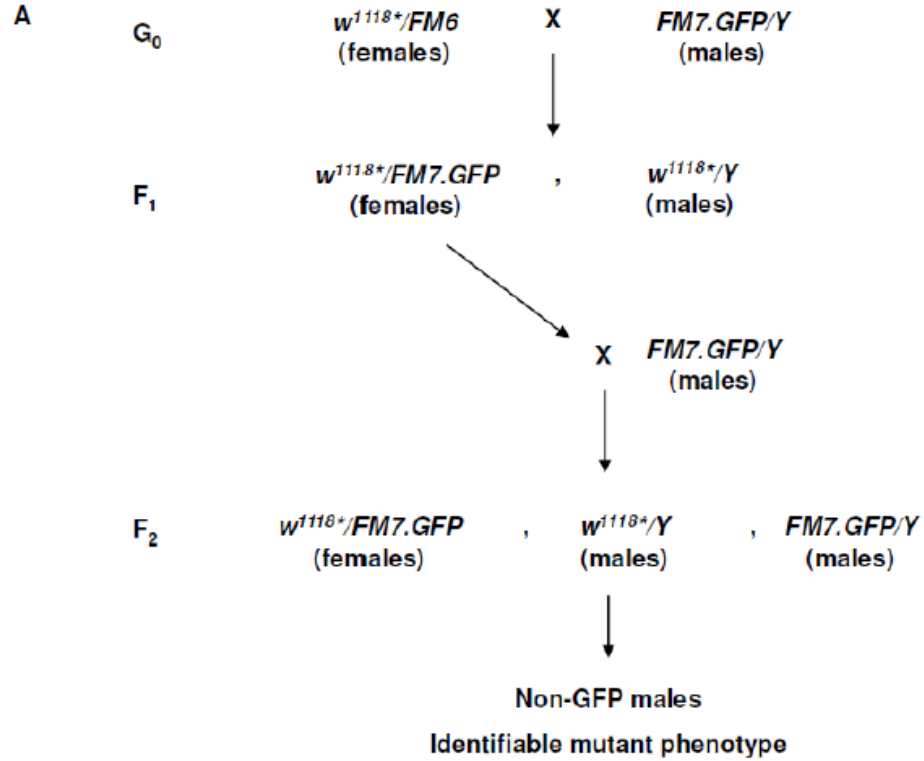
To characterise the mutant phenotype we needed to distinguish the homozygous mutant in early developmental stages from the siblings. In order to achieve this we used *FM7.GFP* balancer. Heterozygous $w^{1118*}/FM6$ females were crossed with *FM7.GFP* males to bring in the *FM7.GFP* balancer in place of *FM6* in F₁ progeny. Males and females carrying *FM7.GFP* were then crossed to generate a stable stock and isolate the w^{1118*} mutant males (**Fig 5.18A**). Mutant lines were characterised according to the phenotypes presented by the hemizygous males (**Fig 5.18B**). Line 112 showed 3rd instar larval lethality for the majority, however, a few pupate but die before eclosion. Line 52 and line 91 both showed embryonic lethality as we were unable to locate any non-GFP 1st instar larvae. Line 149 showed 3rd instar larval lethality. Line 189 and line 407 both showed early larval lethality.

Table 5.4: EMS mutagenesis screens results.

Screen	1	2	3	4	5
EMS concentration (mM)	25mM	50mM	50mM	40mM	40mM
Individual crosses (F1 males x deficiency females)	349	500	500	550	546
Viable crosses	297	346	342	350	328
Viable crosses %	85%	69.2%	68.4%	63.6%	60.1%
Lethal lines recovered	-	-	1 (112)	5 (52, 91, 149, 189, 407)	-

5 EMS screens were carried out. 3rd screen using 50mM EMS gave one potential hit: line 112.

4th screen using 40mM EMS resulted in 5 potential hits: line 52, line 91, line 149, line 189 and line 407.



B

Line #	Phenotype
112	Majority 3 rd instar larval lethals, few pupate but die before eclosion
52	Embryonic lethal
91	Embryonic lethal
149	3 rd instar larval lethal
189	Early larval lethal
407	Early larval lethal

Figure 5.18: Characterisation of EMS screen hits. (A) Crossing scheme to identify mutant phenotypes. $w^{1118^*}/FM6$ females from the stable stocks were crossed with $FM7.GFP$ males. F₁ $w^{1118^*}/FM7.GFP$ females were crossed with $FM7.GFP$ males to generate a stable stock. (B) The non-GFP w^{1118^*}/Y males phenotypes for each of the mutant line were observed from embryonic stages to their lethality and mutant phenotypes characterised.

5.5 Complementation assay for EMS mutants

To establish whether the mutations are allelic, we performed complementation tests based on female lethality where two mutated X chromosomes appear together in F_1 . Crosses were set between males of each mutant line carrying the $Dp(1;Y)dx^+$ duplication with females of other mutant lines as shown in **Figure 5.19**. Complementation was scored on the basis of presence of non-balancer adult female flies. Three complementation groups were identified. Lines 112 and 149 failed to complement each other. Similarly, lines 52 and 91, and lines 189 and 407 also proved to be alleles of same gene by not complementing each other (**Table 5.5**).

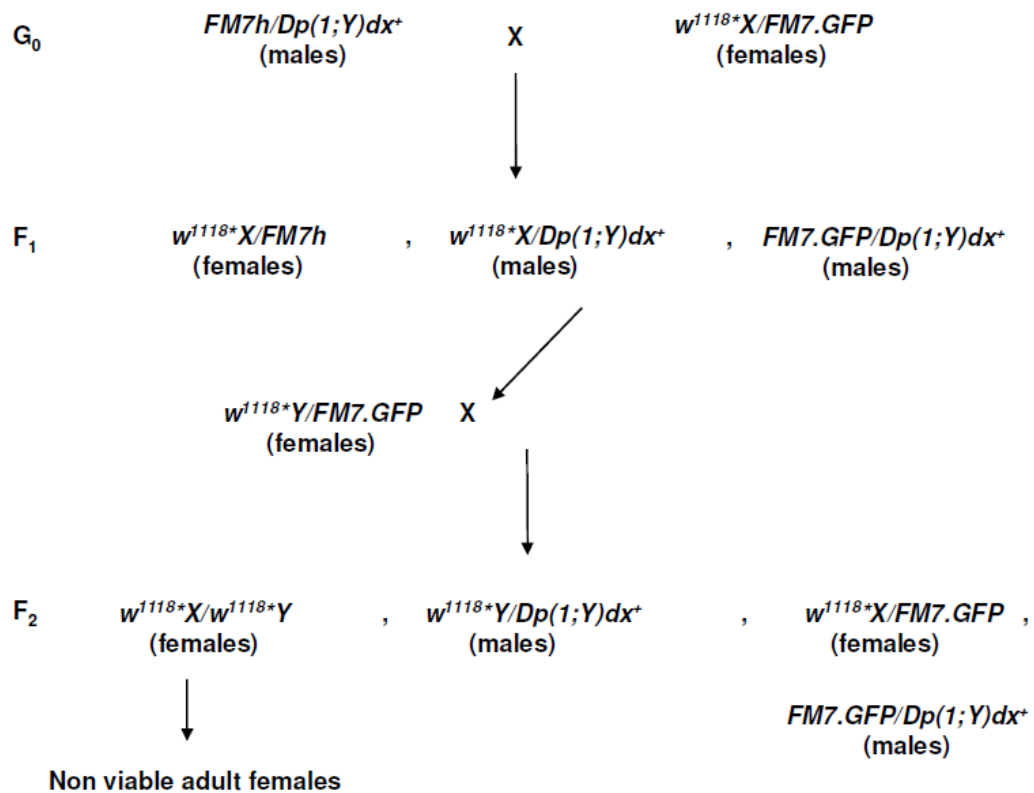


Figure 5.19: Crossing scheme for mutant lines complementation assay. $w^{118}X/FM7.GFP$ females were crossed with $FM7h/Dp(1;Y)dx^+$ males. $w^{118}X/Dp(1;Y)dx^+$ males from F_1 progeny were crossed with $w^{118}Y/FM7.GFP$ females. In F_2 absence of adult $w^{118}X/w^{118}Y$ female flies showed the deficiency chromosomes do not complement. In cases where two mutations complement each other adult female flies with both mutagenized X chromosomes were present. X and Y are used as examples.

Table 5.5: Complementation Table for EMS mutant lines.

		Females					
		52	91	112	149	189	407
Males	52		X	V	V	V	V
	91	X		V	V	V	V
	112	V	V		X	V	V
	149	V	V	X		V	V
	189	V	V	V	V		X
	407	V	V	V	V	X	

V stands for viable adult progeny and X stands for non-viable adult progeny.

5.6 Sequencing of *Marf* in EMS mutants

To identify any putative base changes in the *Marf* gene, genomic DNA was isolated from the w^{1118*} male 3rd instar larvae for line 112 and 149, 1st and 2nd instar for line 189 and 407 and control w^{1118} 3rd instar larvae as detailed in section 2.12.5. Genomic DNA was amplified as amplicons of 2kb for F1-R2, 1.6kb for F4-R3 and 2.2kb for F10-R5, 2.4kb for F11-R7, 1.6kb for F12-Xba and 1.24kb for MfnSeqQC(F7)-R8 (**Fig 5.20, Figure 5.21**). Wild-type w^{1118} genomic DNA was used as control and analysed first. Polymorphisms from the reference sequence were identified in the progenitor stock and so were ignored. Analysing the sequence data for lines 112, 149, 189 and 407, no additional base change was observed in *Marf* gene sequence apart from the pre-existing polymorphism observed in wild-type larvae. It can be presumed that EMS may have hit other vital genes in the deficiency region 5F2-6B2. CG42340, *kdn* and *dx* could be an easy target to be hit by EMS because of their large sizes. The deleted region also contains a tRNA:CR32748 gene which despite its very small size is an important gene involved in protein translation. However, a mutation in any of the other genes in the deficiency region is also possible.

5.7 Protein analysis of *Marf* in EMS mutants

Protein samples from control and mutant larvae were isolated to see protein quantity in mutants. Western blot analysis showed correct banding pattern for Marf in all the mutant lines (**Figure 5.22**). However, it showed reduced Marf levels in all mutant lines. It is presumed that maybe the mutations in the mutant lines are somehow affecting the protein levels of Marf. However, more likely chances are the limitation of presented data as it is produced from one blot due to time constraint. Therefore, for conclusive results to see that the mutations are affecting the protein level or not could only be obtained with the repetitions of the western analysis.

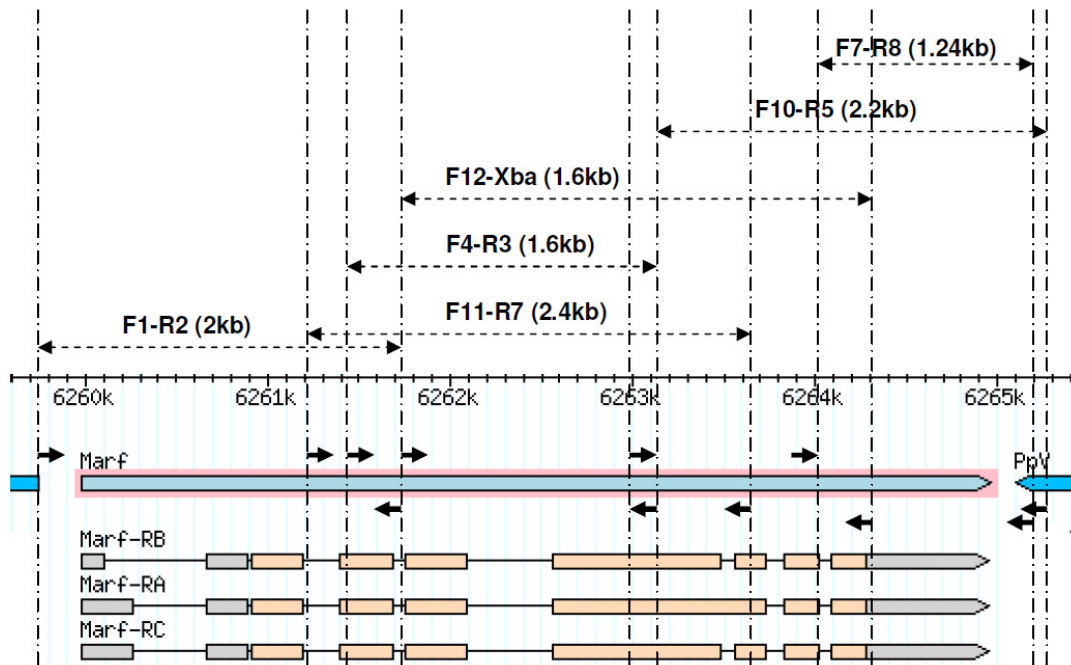


Figure 5.20: *Marf* overlapping amplicons PCR strategy. Amplicon F1-R2 is 2kb, F11-R7 is 2.4kb, F4-R3 is 1.6kb, F12-Xba is 1.6kb, F10-R5 is 2.2kb and F7-R8 is 1.24kb.

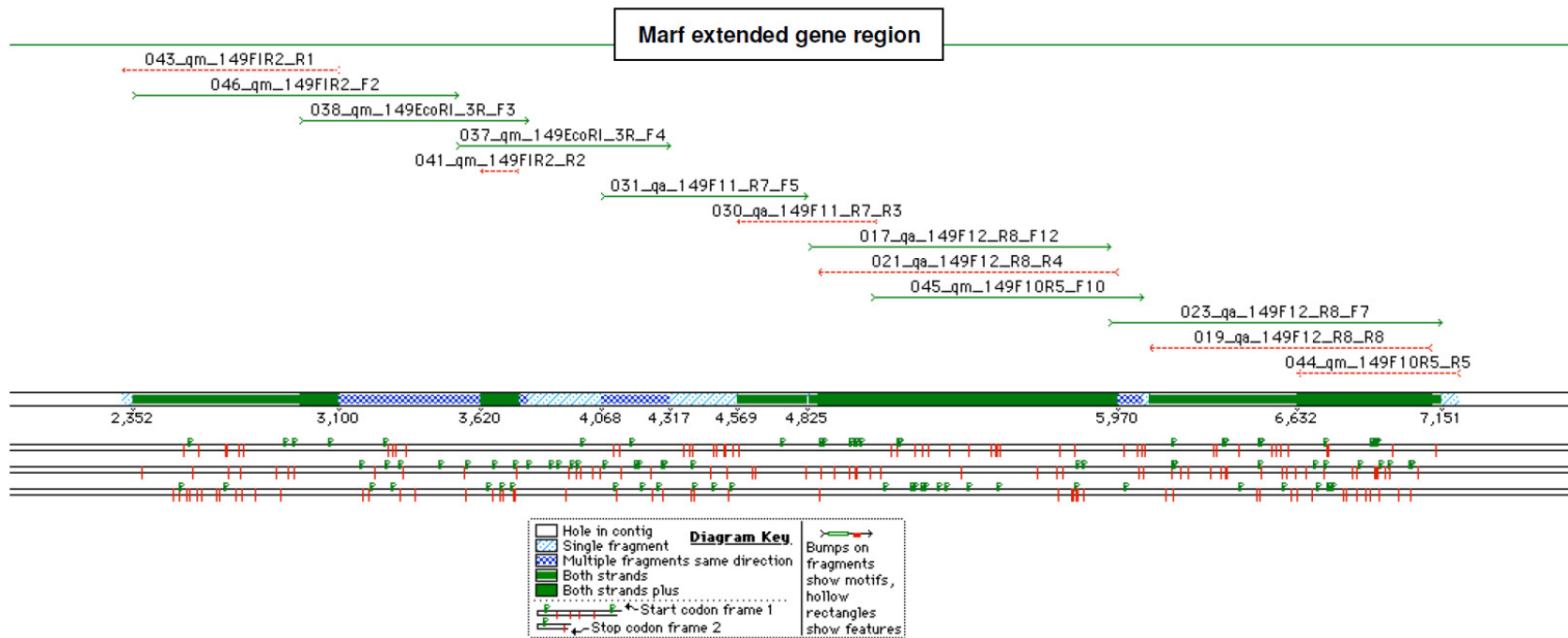


Figure 5.21: Sequencher® generated contig showing the sequencing coverage of control w^{1118} *Marf* entire gene plus 200 bps 5' and 3' intergenic regions.

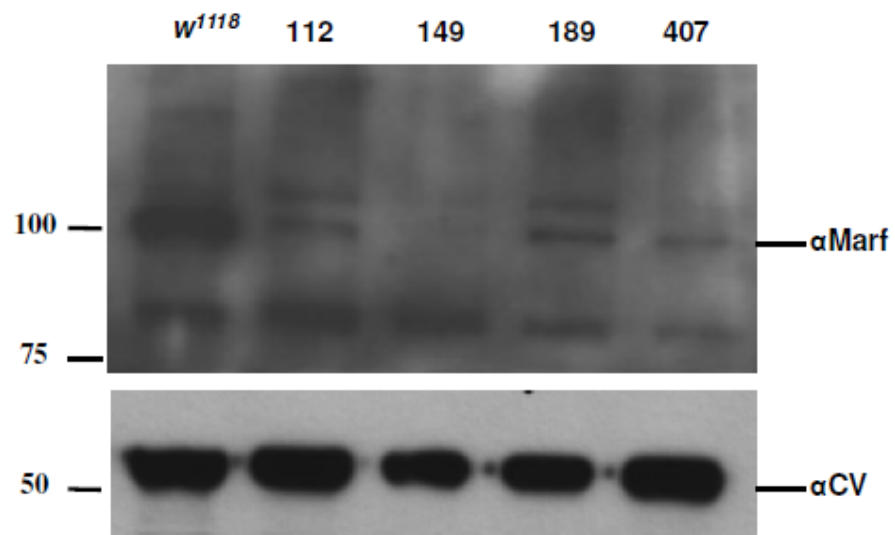


Figure 5.22: Western blot for EMS mutants. 20μg protein samples were loaded in each lane. Marf band about 91.4-94.1kDa was observed in all the lanes. *w¹¹¹⁸* is the wild type control. Complex V 50kDa was used as loading control.

5.8 Discussion

EMS mutagenesis is advantageous as it generates irreversible mutations in the genome and can generate a range of mutations including nonsense and missense mutations. However, EMS mutagenesis is laborious and the random nature of the mutagenesis makes it unpredictable in isolating desired mutations.

The EMS screens performed in this project were intended to be a small scale pilot screen to explore feasibility but in the end it was decided that it would take too much time investment to achieve the goal. Therefore, we did not proceed on further to achieve the statistically calculated number of flies needed to be screened to achieve the 1:1000 lethal mutation rates. Also, as EMS causes mutations throughout the genome, this can complicate subsequent analysis. It is beneficial for the starter stock for any genetic screen to be isogenized before hand to ensure that identified base changes are a result of EMS mutagenesis. Isogenization results in identical homologous chromosome pairs. The starter *w¹¹¹⁸* stock that we used in EMS screens was a previously isogenised stock obtained from Bloomington *Drosophila* Stock Center; however, over time it may have acquired additional polymorphisms. These may even be present heterogeneously in the stock. Indeed, we found a number of polymorphisms present in *Marf* nucleotide sequence as compared to the reference sequence from Flybase. While we did not identify any putative coding mutations in our screens, the possibility that the starting stock may contain heterogeneous polymorphisms may have confounded subsequent analysis of putative *Marf* mutants. Moreover, while these polymorphisms are clearly benign to the animal, as the starting stock was fully viable and fertile, it is possible that other such polymorphisms in the genome combined with the *Marf* mutations caused by EMS could be non-viable. This could be one possible explanation for the failure to obtain a genetic mutant for *Marf* in our screens. Furthermore, we obtained less viable F₁ crosses with higher EMS concentration such as 40mM and 50mM EMS. The major possibility is EMS toxicity and male sterility due to higher EMS concentrations (Bokel, 2008). For an EMS screen it is always better to start with a large number of males flies as EMS toxicity kills around 10% of G₀ males and many surviving suffer sterility as well. Recently, Sandoval et al, have reported the allelic series of *Marf* generated by EMS mutagenesis (Sandoval et al., 2014; Yamamoto et al., 2014). It was a large screen for generating chemically induced mutations in X-chromosome (Yamamoto et al., 2014). They looked at 33887 lines and identified 5857 lethal stock with 165 genes targeted, as compared to our small scale screen using only 500 lines for each screen

performed over a smaller region of deficiency chromosome. Additionally, they used lower EMS concentrations 7.5-10mM to avoid additional mutations in the genome (Yamamoto et al., 2014). Therefore, presumably the possible reasons for the failure of getting any *Marf* mutant in our EMS screen could be higher concentrations of EMS (25-50mM) used to mutagenize wild type males and less number of individual crosses (F₁).

We characterised the mutant phenotype from hemizygous w^{1118*} males. *Drosophila* males carry only one X chromosome therefore a lethal mutation in a gene would exert its effect in similar manner as in homozygotic females. However, the disadvantage is that the mutant phenotype seen in hemizygous w^{1118*} males would be due to the ‘most severe’ mutation and so may mask other mutations/phenotypes of interest. Here we only made a brief assessment of hemizygous males since we were specifically searching for coding mutations in *Marf* which we did not find in our limited screen. If a more extensive screen would be planned, it would indeed be advantageous to characterise isolated mutants in trans to a deficiency. In addition to nonsense mutations, EMS also generates missense mutations and small deletions. Such mutations could be interesting as loss of function mutations. The majority of *Mfn2* mutations associated with CMT2A are missense mutations leading to disease pathology. Most of these mutations are unable to restore fusion suggesting a loss of function or haploinsufficiency (Zuchner et al., 2006; Detmer and Chan, 2007a). However, the moderate size of *Marf* and the presence of few codons mutable to stop codons make it a hard target for our small scale screening strategy, though by scaling up the screening genomes and using lower EMS concentrations may be useful for further screens.

EMS is a classic mutagenesis method to obtain missense and null mutations, however, several site specific mutagenesis techniques, such as P-element mobilisation, homologous recombination, transcription activator-like effector nucleases (TALENs), zinc finger nucleases (Zfns) and clustered regularly interspaced short palindromic repeats (CRISPR)/CRISPR-associated (Cas) system, have evolved in past few years (Liao et al., 2000; Bibikova et al., 2002; Liu et al., 2012; Bassett et al., 2013;). These newer mutagenesis systems provide highly efficient methods to generate loss-of-function mutations in desired locations in genome, if one intends to generate genetic mutants for gene of interest.

Chapter 6: General Discussion

The dynamic processes of mitochondrial fusion and fission result in mitochondria as long tubular mitochondria and interconnected mitochondrial networks or small fragmented units or a combination of both morphologies present in a cell. A balance between mitochondrial fusion and fission in the cell regulates the steady state level of mitochondrial morphology. Mitochondrial fusion allows maintenance of mtDNA and mixing of essential proteins and nutrients, whilst mitochondrial fission is permissive for selective removal of damaged mitochondria through mitophagy and allows distribution of mitochondria within the cell. A cell can show different mitochondrial morphologies at various stages of the cell cycle and cell processes to meet the diverse energy demands. Long and interconnected mitochondrial networks provide easy access of energy to various neighbouring cellular components such as endoplasmic reticulum to maintain Ca^{2+} homeostasis and to Golgi complex for the synthesis of membranes, to liposomes for liposynthesis. Whereas, small mitochondria are motile energy units that are easily transported to the distant regions of the cell to meet the local energy demand or can be transported back to the cell soma for recovery or degradation in case of damage.

Primarily three large GTPases are involved in mitochondrial fusion; namely Mfn1 and Mfn2 which mediate outer mitochondrial membrane fusion which is followed by inner mitochondrial fusion mediated by OPA1. These fusion processes are carried out in a SNARE-like mechanism involving GTP hydrolysis. Unlike Mfn1, Mfn2 plays a part in various other cellular functions such as apoptosis, cell oxidative metabolism, cell cycle regulation, axonal mitochondrial transport, mitochondrial and endoplasmic reticulum tethering, Ca^{2+} uptake by mitochondria and endoplasmic reticulum stress (Neuspiel et al., 2005; de Brito and Scorrano, 2008; Sebastian et al., 2012; Debattisti et al., 2014). Mitochondrial fission also requires a cytosolic GTPase from the dynamin family, Drp1, which is recruited to the fission sites to initiate the membrane severing process. The association of mutations in mitochondrial fusion and fission proteins with neurodegenerative diseases highlight the importance of these mitochondrial processes in cell function. The pathological mechanisms for neurodegeneration linked to effective mitochondrial dynamics are still not clear. Oxidative stress due to impaired OXPHOS, enhanced excitability of glutamate receptors or enhanced intracellular Ca^{2+} levels pose a high risk for neurodegeneration. One way or other mitochondria are either directly or indirectly involved in maintenance of these cellular processes. Therefore, defective balance between mitochondrial fusion and fission can lead to oxidative stress in all cell

types. Neurons are particularly sensitive to imbalanced mitochondrial dynamics as it affects the intracellular distribution of mitochondria. The cell transport machinery is unable to transport larger mitochondria to synapses leading to loss of synaptic mitochondria, low ATP production and impaired Ca^{2+} buffering (Verstreken et al., 2005). Loss of fusion results in complications such as accumulation of damaged mitochondria with impaired OXPHOS and also increases ER stress (Debattisti et al., 2014).

Mutations in *Mfn2* are associated with peripheral axonal neuropathy CMT2A and its subtype HMSNVI (Zuchner et al., 2004; Zuchner et al., 2006). The disease mechanisms by which these mutations are causing the neurons to die are still unclear, and variability in disease severity has been reported in patients. It is important to establish how these mutations alter the normal function of *Mfn2*, for example whether the resulting protein is partially active or completely non-functional, and what effect such mutations actually have on mitochondrial morphology and functioning. The occurrence of CMT2A patients with compound heterozygous mutations supports loss of function as a possible mechanism. There are varying reports from patient data and from mouse models for CMT2A in relation to *Mfn2* expression levels, mitochondrial fusion capacity and ATP production (Detmer and Chan, 2007a; Amiott et al., 2008; Rouzier et al., 2012). *Mfn2* knockout MEFs show fragmented and aggregated mitochondrial morphology which was rescued by the expression of CMT2A pathogenic mutation *Mfn2*^{R94Q}. However, it failed to rescue fragmented mitochondrial morphology in *Mfn1* knockout MEFs indicating CMT2A-associated *Mfn2* alleles (here *Mfn2*^{R94Q} which is unable to initiate fusion on its own) are able to form fusion capable complexes with *Mfn1* (*Mfn1/Mfn2* (CMT2A allele) complexes) and not with wild-type *Mfn2* (Detmer and Chan, 2007a). However, in a PEG fusion assay CMT2A mutations had different effects on fusion ability as *Mfn2*^{R94Q}, *Mfn2*^{R94W}, *Mfn2*^{T105M}, *Mfn2*^{P251A} and *Mfn2*^{R280H} failed to induce mitochondrial fusion but *Mfn2*^{V69F}, *Mfn2*^{L76P}, *Mfn2*^{R274Q} and *Mfn2*^{W740S} showed normal fusion activity (Detmer and Chan, 2007a). It is difficult to say from the cellular assays that CMT2A mutations are all non functional but they appear to have variable capacity of being fusion efficient. In the case of transgenic mouse models, mice carrying *Mfn2*^{T105M} mutations showed gait defects and neurodegeneration with mitochondrial accumulation in axons of motor neurons (Detmer et al., 2008). Also, transgenic mice overexpressing *Mfn2*^{R94Q} in neurons develop late-onset neuropathy and increased mitochondrial density in the distal part of axons (Cartoni et al., 2010).

Recently, knock-in homozygous *Mfn2*^{R94W} mice die prematurely and showed fragmented mitochondria in MEFs, however heterozygous pups showed mild peripheral neuropathy (Strickland et al., 2014). Due to lack of other CMT2A genetic mouse models it is still not easy to interpret the pathophysiology of *Mfn2* heterozygous mutation scenario of human disease in transgenic mice overexpressing the mutations. On the other hand patient skin cells carrying the pathogenic mutations at endogenous levels also have reported contradictory results regarding mitochondrial morphology defects (Amiott et al., 2008; Chevrollier et al., 2012; Rouzier et al., 2012). This might be because patients carry heterozygous mutations, the effect of which is subtle and most pronounced in the primary affected cells, which are peripheral motor and sensory neurons.

The most widely used tools to study the pathophysiology of any disease are animal and cellular models. These systems provide insights into disease mechanisms but the physiological expression levels of pathogenic mutations are difficult to achieve in a model animal. Also, the endogenous cellular damage due to environmental factors exposure, other affected genes and individual's age are not easily represented in model organisms hence limiting the translation of a disease in a model system. The ideal scenario is to study the disease in affected cells but sometimes the affected cells such as neurons, glia, heart cells, are not easily accessible to study disease pathology. Hence, readily available patient skin fibroblasts have been used extensively in the past decade to study disease mechanisms as they are easily available to study and are exposed to the same genetic and environmental factors as the affected cells. In this thesis we have reported mitochondrial morphology defects in HMSNVI patient fibroblasts carrying *Mfn2*^{R364W} mutation. Fibroblasts from this patient showed significantly reduced mitochondrial aspect ratio, length, bifurcation ratio and network complexity. However, cells from two other CMT2A patients with *Mfn2*^{Q674P} mutation showed normal mitochondrial morphology (**Chapter 3**). The reasons for using patient fibroblasts to study the mitochondrial morphology was easy availability, robust culturing and established assays with significant number of published data using them as successful cellular system to study mitochondrial morphology for CMT2A and other neurological disorders (Huang et al., 1994; Amiott et al., 2008; Mortiboys et al., 2008). The effect on mitochondrial morphology we observed in the HMSNVI patient is quite pronounced; however, one should be cautious about drawing firm conclusions as this data from only one patient. Also, as discussed earlier in section 3.4 the defect we saw could be due to

some other factor influencing the fragmented mitochondrial morphology in fibroblasts. The question still remains as to whether the mitochondrial morphology we saw in patient fibroblasts is typical of what is happening in the affected motor and sensory neurons or not. Interestingly, now researchers are developing new techniques to study the issues of disease pathology in the affected cells (Saporta et al., 2011). The successful generation of motor neurons from patient derived fibroblasts to study ALS using induced pluripotent stem cell (iPSC) technology is an excellent example of such developments (Dimos et al., 2008). This technology involves reprogramming of skin fibroblasts obtained from patients into pluripotent stem cells (Saporta et al., 2011). These pluripotent stem cells are then differentiated into various lineages including neurons and glia (Dimos et al., 2008; Ebert et al., 2009; Liu et al., 2010; Ogawa et al., 2011). Recently, motor neurons derived from fibroblasts of 45 years old CMT2A patient carrying *Mfn2*^{R364W} heterozygous mutation have shown normal mitochondrial morphology but slower mitochondrial axonal movement (Saporta et al., 2015). Here one can suggest that the reduction in mitochondrial transport could be independent of mitochondrial fusion defect and is due to the pathology of disease. However, Saporta and colleagues have reported that these defects are subtle compared to what has been shown in motor neurons of mice expressing *Mfn2* disease alleles. The possible reason might be heterozygous expression of *Mfn2* mutation in patients (Saporta et al., 2015). Moreover, CMT2A patient iPSC-derived motor neurons were in a hyperexcitable state and had higher sodium current densities. They suggested that hyperexcitability of motor neurons might be causing axonal degeneration due to failure of sodium potassium channels and increased intracellular Ca²⁺, however this still needs to be shown in affected neurons. Nevertheless, it is an intriguing and growing area for model systems; therefore a suggestion for the future is to reprogram CMT2A and HMSNVI patient fibroblasts used in this thesis into motor neurons to further investigate what is happening in neurons. In addition, axonal transport studies can be done to find out any defective mitochondrial axonal transport in patient cells. Such studies in iPSC-derived motor neurons should be based on a large cohort of patient derived samples to allow comparison of several different *Mfn2* mutations.

Furthermore, it would be interesting to perform genetic studies in *Mfn2*^{R364W} fibroblasts to see whether over-expressing *Mfn2* rescues the fragmented mitochondrial morphology. Also, reducing *Drp1* levels using RNAi in these cells might reduce the number of fragmented mitochondria. This would suggest that the defective

mitochondrial morphology is due to the pathogenic Mfn2 allele making Mfn2 inactive and giving fragmented mitochondria through over-active mitochondrial fission genes. Such experiments would give insight into the cause of defective mitochondrial dynamics as previous studies on fibroblasts from CMT2A patients have not reported such genetic interactions.

We also undertook a drug screen to find potent fusion inducing compounds. The objective was to either develop a drug for cases where mitochondrial fusion appears affected, such as patients with *Mfn2* mutations or *OPA1* mutations, or to characterise a bench tool to study mitochondrial dynamics in cellular assays. We have shown that EA increases mitochondrial fusion in different cultured cell lines (**Chapter 4**). However, we were unable to characterise the cellular target of EA due to time constraints. It is worth mentioning that performing a drug discovery screen based on phenotypic analysis is useful however it could also be that the particular phenotype we are looking at is not due to the activation or deactivation of only one protein. We have shown that EA is able to promote mitochondrial fusion in the presence of Fis1 overexpression suggesting it might be acting on mitochondrial fission machinery factor and rendering it inactive. Therefore in future work, we suggest measurement of Drp1 GTPase activity under EA treatment to test for Drp1 function. Drp1 is major fission mediator and requires its GTPase activity to sever the mitochondrial membranes. Therefore, this assay will give us insight into the possibility that EA acts on Drp1 and renders it non-functional. Furthermore, we suggest using proteomic approaches to identify the binding partners of EA. Such advancements have been widely used by biochemists and biologists to identify the molecular targets for the small molecules and drugs.

Drosophila has been widely used as an animal model to study various neurological diseases. Despite the fact that there are obvious limitations of modelling a human disease in *Drosophila*, various functional studies can be done in flies as biological processes are well conserved between vertebrates and invertebrates. In this thesis, we studied the role of Marf, the orthologue of mammalian Mfn2, in fly development and locomotion. We have shown that Marf is vital for *Drosophila* viability and locomotion (**Chapter 5**). Recently, two other studies have also reported that Marf is important for fly development and Marf depletion showed larval lethality (Debattisti et al., 2014; Sandoval et al., 2014). These studies have also reported intriguing new functions for Marf in the maintenance of endoplasmic reticulum morphology and synthesis and storage of ecdysone in fly ring glands (Debattisti et al., 2014; Sandoval et

al., 2014). Debattisti and colleagues have shown that *Marf*^{RNAi} caused endoplasmic reticulum and mitochondrial fragmentation, and hMfn2 but not hMfn1 rescued ER morphology suggesting fly Marf has both functions in maintenance of ER as well as mitochondrial morphology. Sandoval and colleagues showed that larval lethality is probably due to the defective ecdysone synthesis which is necessary for larval development into pupae in flies. Ecdysone is specific for insects but these findings suggest that Mfn2 could possibly be involved in steroid synthesis in vertebrates. Additionally, Sandoval and colleagues have proposed a model suggesting that Marf has an active role in lipid droplet formation and steroidogenesis. The reduced lipid droplets and ecdysone levels seen in ring glands of Marf mutants was partially rescued by expression of hMfn2 as cells showed normal lipid droplet formation but reduced ecdysone levels in ring glands (Sandoval et al., 2014). However, coexpression of hMfn1 and hMfn2 rescues the defects completely but not Mfn1 alone. Sandoval and colleagues suggested that in flies Marf may interact with some other factor to promote steroid synthesis which is accomplished by hMfn1 and hMfn2 complex together. However, such findings need to be verified in mammalian systems as it would help to figure out how Marf is acting differently in fly ring glands and why its function was not solely rescued by either hMfn1 or hMfn2.

It is clear that Mfn2 has diverse functions as mutations in this gene resulted in reduced mitochondrial fusion, mitochondrial axonal transport disruption, mitochondrial-ER interaction failure, ER fragmentation and defective steroid (ecdysone in flies) synthesis (Detmer and Chan 2007; de Brito and Scorrano, 2008; Misko et al., 2010; Sandoval et al., 2014). However, it still remains unclear how Mfn2 mutations result in selective degeneration of long axons of motor and sensory neurons in peripheral nervous system. Mfn2 is a ubiquitously expressed protein, however high levels have been reported in heart cells, neurons and skeletal muscles. There are various models suggesting the degeneration or ‘dying back’ of long axons is possibly due to energy deficiency in distal axonal regions and synapses. This lack of energy might possibly be due to lack of mitochondrial population in those regions. In human motor nerves these axons are about a meter long and require highly organised and efficient mitochondrial transport machinery. CMT2A patient biopsies have shown clustering of small spherical mitochondria in the distal regions of axons (Vallat et al., 2008; Calvo et al., 2009). Similarly, cultured sensory neurons expressing CMT2A associated Mfn2 mutations and/or loss of Mfn2 (*Mfn2*^{-/-}) showed mitochondrial clustering in proximal axonal

segments, reduced density of mitochondria in distal regions, slower anterograde and retrograde mitochondrial mobility with prolonged pauses in axons (Baloh et al., 2007; Misko et al., 2010). This suggests that the possible reason for axonal degeneration in CMT2A and HMSNVI might be mitochondrial distribution defect rather than mitochondrial fusion defect. Additionally, various morphology analysis done on CMT2A derived fibroblasts including our data showed no obvious and dramatic mitochondrial fusion deficiency in these patients (Loiseau et al., 2007; Amiott et al., 2008; Guillet et al., 2009; Chevrollier et al., 2012; Rouzier et al., 2012). Also, reduced levels of OPA1 result in defective fusion and no affect on mitochondrial transport in cultured neurons (Chen et al., 2005; Misko et al., 2010). Therefore one can speculate that it might be Mfn2's role promoting axonal mitochondrial transport as being majorly affected in axonal neuropathies rather than its role as pro-fusion factor. It has been shown that Mfn2 interacts with Miro 2 and Milton 1 and mediates mitochondrial transport in axons (Misko et al., 2010). It is suggested that Mfn2:Miro2:Milton1 complex regulates mitochondrial motor transport activity as Mfn2^{-/-} or Miro^{-/-} neurons showed mitochondria spend increased time paused in the axons (Misko et al., 2010). This study has claimed that disruption in transport does not appear to be a consequence of attenuated fusion thus suggesting a fusion independent role for Mfn2 in the regulation of mitochondrial motility (Misko et al., 2010). A recent study by the same group has shown axonal degeneration in neurons expressing disease associated Mfn2 mutations due to improper distribution of mitochondria in the axons (Misko et al., 2012). This defect was partially rescued by either expressing Mfn1 or treatment with sodium channel blocker; tetrodotoxin (Misko et al., 2012). One can suggest the low expression of Mfn1 in these cells could potentially be the reason that peripheral motor and sensory neurons are specifically sensitive. Additionally, previously our group has also reported significantly reduced axonal transport of mitochondria in a zebrafish Mfn2 loss of function model (Chapman et al., 2013). These findings support the essential role of Mfn2 in axonal transport of mitochondria and implicate a possible mechanism that is disrupted in CMT2A patients leading to motor and sensory neuronal loss. At the present it still needs to be shown that how Mfn2 pathogenic mutations disrupt the Mfn2:Miro:Milton complex in the axons. It has been reported that Mfn2 mutant alleles lose their ability to maintain the tethering of mitochondria and endoplasmic reticulum (de Brito and Scorrano, 2009). The increased local Ca²⁺ levels due to fragmented ER and lost mitochondrial bridging might be playing a role in stopping of Mfn2:Miro:Milton complex by disrupting Miro connection with microtubules (de Brito

and Scorrano, 2009; Misko et al., 2012). However, expression of Mfn1 in neurons resulted in rescue of Ca²⁺ homeostasis and mitochondrial axonal transport (Misko et al., 2012). Further, the stoppage of mitochondria might result in hypoxic conditions in distal regions where synapse is taking place and resulting in local energy deficiency due to absence or late arrival of mitochondria (Misko et al., 2012). The recent study done on motor neurons derived from CMT2A patient fibroblasts have shown normal mitochondrial morphology but slower mitochondrial axonal movement supporting the idea of mitochondrial axonal transport impairments (Saporta et al., 2015). However, the precise mechanism of how these pathogenic mutations are halting mitochondrial movement remains unclear.

Moreover, a simple in vivo model such as *Drosophila* would allow the rapid testing of potential drugs. However, in this study *Drosophila* has proved to be a difficult model. The reasons for our inability to see EA effect in adult flies are unclear but could indicate that there might be less drug entering the animal system or drug being not metabolised into its active form to act on its target(s). We have seen similar effect on mitochondrial morphology in fly cells as seen in mammalian cells, which suggests that the protein target sites are conserved in flies, however, why we were unable to see the effect on fly phenotype is unclear. If time had allowed we could have dissected the larvae and looked at the mitochondrial morphology in motor neurons to assess whether EA had affected mitochondrial morphology in vivo. It is also suggested that zebrafish *Mfn2* mutants should be fed EA and see the affect of drug on their swimming defects. As an advantage, *Mfn2* fish mutants develop normally into adult and most functional studies including axonal transport of mitochondria and effect of EA on it can be studied easily.

In summary, in this thesis we have shown that Marf is essential for *Drosophila* development and locomotion. Additionally, CMT2A patients showed normal mitochondrial morphology and HMSNVI patient showed severely fragmented mitochondria. The reason for the different effects remains unknown and needs to be studied in large cohorts for a clearer overall picture. Analysing mitochondrial morphology and axonal transport in the patient iPSC-derived motor and sensory neurons would also be informative for effects in the disease-relevant cell type. We have also successfully tested EA fusion ability in various cellular assays, however, despite showing increased mitochondrial fusion morphology in patient fibroblasts EA was not able to rescue the *Marf* knockdown flies. This might be because mitochondrial axonal

transport, not mitochondrial fusion, is the most important process that is defective in these mutants. Further work is needed to elucidate the role of Marf/Mfn2 in mitochondrial transport in healthy and disease conditions.

Appendix A:

Table 1: Phenotypes for *D.melanogaster* *Marf* overexpression

GAL4	Expression	Phenotype
<i>da</i>	Ubiquitous	early 3 rd instar larval arrest
<i>elav</i>	All neurons	viable, active
<i>D42</i>	Motor neurons	viable, active

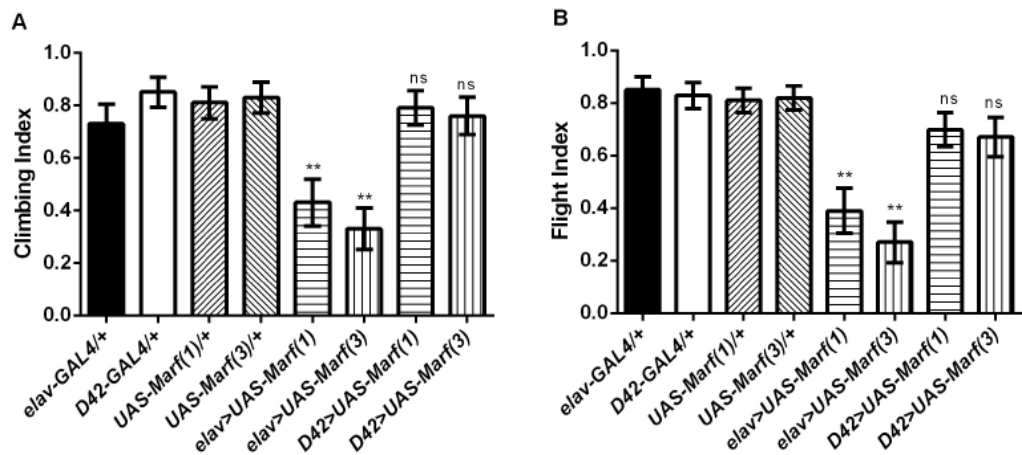


Figure A1: Locomotion assays for *Marf* overexpression. (A) Climbing assay. (B) Flight assay. *Marf* overexpression in nervous system *elav-GAL4>UAS-Marf(1)* and *elav-GAL4>UAS-Marf(3)* resulted in adult flies with reduced climbing and flight ability. *Marf* overexpression in motor neurons *D42-GAL4>UAS-Marf(1)* and *D42-GAL4>UAS-Marf(3)* flies showed normal climbing and flight. All controls were out crossed with *w¹¹¹⁸* flies. $n = 100$ for each genotype. Data is presented as mean \pm standard error. Significance was determined with Kruskal-Wallis non-parametric analysis and Dunn's pair-wise comparison (** $P < 0.01$).

Bibliography:

- Aaron CS, Lee WR. Molecular dosimetry of the mutagen ethyl methanesulfonate in *Drosophila melanogaster* spermatozoa: linear relation of DNA alkylation per sperm cell (dose) to sex-linked recessive lethals. *Mutat Res* 1978;49:27-44.
- Abou-Sleiman PM, Muqit MM, Wood NW. Expanding insights of mitochondrial dysfunction in Parkinson's disease. *Nat Rev Neurosci* 2006;7:207-18.
- Adams MD, Celniker SE, Holt RA, Evans CA, Gocayne JD, Amanatides PG, et al. The genome sequence of *Drosophila melanogaster*. *Science* 2000;287:2185-95.
- Adan C, Matsushima Y, Hernandez-Sierra R, Marco-Ferreres R, Fernandez-Moreno MA, Gonzalez-Vioque E, et al. Mitochondrial transcription factor B2 is essential for metabolic function in *Drosophila melanogaster* development. *J Biol Chem* 2008; 283:12333-42.
- Alexander C, Votruba M, Pesch UE, Thiselton DL, Mayer S, Moore A, et al. OPA1, encoding a dynamin-related GTPase, is mutated in autosomal dominant optic atrophy linked to chromosome 3q28. *Nat Genet* 2000;26:211-15.
- Amiott EA, Lott P, Soto J, Kang PB, McCaffery JM, DiMauro S, et al. Mitochondrial fusion and function in Charcot-Marie-Tooth type 2A patient fibroblasts with mitofusin 2 mutations. *Exp Neurol* 2008;211:115-27.
- Amiri M, Hollenbeck PJ. Mitochondrial biogenesis in the axons of vertebrate peripheral neurons. *Dev Neurobiol* 2008;68:1348-61.
- Antonellis A, Ellsworth RE, Sambuughin N, Puls I, Abel A, Lee-Lin SQ, et al. Glycyl tRNA synthetase mutations in Charcot-Marie-Tooth disease type 2D and distal spinal muscular atrophy type V. *Am J Hum Genet* 2003;72(5):1293-99.
- Arnold K, Zschoernig O, Barthel D, Herold W. Exclusion of poly(ethylene glycol) from liposome surfaces. *Biochim Biophys Acta* 1990;1022:303-10.
- Ashburner M, Bergman CM. *Drosophila melanogaster*: a case study of a model genomic sequence and its consequences. *Genome Res* 2005;15(12):1661-67.
- Auburger G, Klinkenberg M, Drost J, Marcus K, Morales-Gordo B, Kunz WS, et al. Primary skin fibroblasts as a model of Parkinson's disease. *Mol Neurobiol* 2012;46(1):20-27.
- Auluck PK, Chan HY, Trojanowski JQ, Lee VM, Bonini NM. Chaperone suppression of α -Synuclein toxicity in a *Drosophila* model for Parkinson's disease. *Science* 2002; 295:865-68.
- Ayaki T, Oshima K, Yoshikawa I. Linear relationship between lethal mutation yield and intake of ethyl methanesulfonate in *Drosophila melanogaster*. *Environ Mutagen* 1985;7:147-53.
- Bach D, Naon D, Pich S, Soriano FX, Vega N, Rieusset J, et al. Expression of Mfn2, the Charcot-Marie-Tooth neuropathy type 2A gene, in human skeletal muscle:

effects of type 2 diabetes, obesity, weight loss, and the regulatory role of tumor necrosis factor alpha and interleukin-6. *Diabetes* 2005;54:2685-93.

Baloh RH, Schmidt RE, Pestronk A, Milbrandt J. Altered axonal mitochondrial transport in the pathogenesis of Charcot-Marie-Tooth disease from mitofusin 2 mutations. *J Neurosci* 2007;27:422-30.

Bassett AR, Tibbit C, Ponting CP, Liu JL. Highly efficient targeted mutagenesis of *Drosophila* with the CRISPR/Cas9 system. *Cell Rep* 2013;4:220-28.

Baxter RV, Ben Othmane K, Rochelle JM, Stajich JE, Hulette C, Dew-Knight S, Hentai F, et al. Ganglioside-induced differentiation-associated protein-1 is mutant in Charcot-Marie-Tooth disease type 4A/8q21. *Nat Genet* 2002;30(1):21-22.

Bentley A, MacLennan B, Calvo J, Dearolf CR. Targeted recovery of mutations in *Drosophila*. *Genetics* 2000;156:1169-73.

Benzer S. Behavioral mutants of *Drosophila melanogaster* isolated by countercurrent distribution. *Proc Natl Acad Sci USA* 1967;58:1112-19.

Bereiter-Hahn J. Behaviour of mitochondria in the living cell. *Int Rev Cytol* 1990;122:1-63.

Bereiter-Hahn J, Voth M. Dynamics of mitochondria in living cells: shape changes, dislocations, fusion, and fission of mitochondria. *Microsc Res Tech* 1994;27:198-219.

Bergoffen J, Scherer SS, Wang S, Scott MO, Bone LJ, Paul DL, et al. Connexin mutations in X-linked Charcot-Marie-Tooth disease. *Science* 1993;262(5142):2039-42.

Berreuer P, Porcheron P, Berreuer-Bonnenfant J, Simpson P. Ecdysteroid levels and pupariation in *Drosophila melanogaster*. *J Expt Zool* 1979;2:347-52.

Berrigan D, Pepin DJ. How maggots move: allometry and kinematics of crawling in larval diptera. *J Insect Physiol* 1995;41:329-37.

Bibikova M, Golic M, Golic KG, Carroll D. Targeted chromosomal cleavage and mutagenesis in *Drosophila* using zinc-finger nucleases. *Genetics* 2002;161:1169-75.

Bienfait HM, Baas F, Koelman JH, de Haan RJ, van Engelen BG, Gabreels-Festen AA, et al. Phenotype of Charcot-Marie-Tooth disease Type 2. *Neurology* 2007;68(20):1658-67.

Bokel C. EMS screens: from mutagenesis to screening and mapping. *Methods Mol Biol* 2008;420:119-38.

Bolino A, Muglia M, Conforti FL, LeGuern E, Salih MA, Georgiou DM, et al. Charcot-Marie-Tooth type 4B is caused by mutations in the gene encoding myotubularin-related protein-2. *Nat Genet* 2000;25(1):17-19.

- Bowes TJ, Gupta RS. Induction of mitochondrial fusion by cysteine-alkylators ethacrynic acid and N-ethylmaleimide. *J Cell Physiol* 2005;202:796-804.
- Braak H, Braak E. Neuropathological staging of Alzheimer-related changes. *Acta Neuropathol* 1991;82:239-59.
- Braathen GJ, Sand JC, Lobato A, Heyer H, Russel MB. Genetic epidemiology of Charcot-Marie-Tooth in the general population. *Eur J Neurol* 2011;18:39-48.
- Bradford MM. A rapid and sensitive method for the quantitation of microgram quantities of protein utilizing the principle of protein-dye binding. *Anal Biochem* 1976;72:248-54.
- Brand AH, Perrimon N. Targeted gene expression as a means of altering cell fates and generating dominant phenotypes. *Development* 1993;118:401-15.
- Braschi E, Zunino R, McBride HM. MAPL is a new mitochondrial SUMO E3 ligase that regulates mitochondrial fission. *EMBO Rep* 2009;10:748-54.
- Breckenridge DG, Stojanovic M, Marcellus RC, Shore GC. Caspase cleavage product of BAP31 induces mitochondrial fission through endoplasmic reticulum calcium signals, enhancing cytochrome c release to the cytosol. *J Cell Biol* 2003;160:1115-27.
- Breckenridge DG, Kang BH, Kokel D, Mitani S, Staehelin LA, Xue D. *Caenorhabditis elegans* drp-1 and fis-2 regulate distinct cell-death execution pathways downstream of ced-3 and independent of ced-9. *Mol Cell* 2008;31:586-97.
- Bridges CB. Non-Disjunction as Proof of the Chromosome Theory of Heredity (Concluded). *Genetics* 1916;1:107-63.
- Bridgman PC. Myosin-dependent transport in neurons. *J. Neurobiol* 2004;58:164-74.
- Bucci C, Bakke O, Progida C. Charcot-Marie-Tooth disease and intracellular traffic. *Prog Neurobiol* 2012;99:191-225.
- Burgess SW, MaIntosh TJ, Lentz BR. Modulation of poly(ethylene glycol)-induced fusion by membrane hydration: importance of interbilayer separation. *Biochemistry* 1992;31:2653-61.
- Cai Q, Gerwin C, Sheng ZH. Syntabulin-mediated anterograde transport of mitochondria along neuronal processes. *J Cell Biol* 2005;170:959-69.
- Calvo J, Funalot B, Ouvrier RA, Lazaro L, Toutain A, De Mas P, et al. Genotype-phenotype correlations in Charcot-Marie-Tooth disease type 2 caused by mitofusin 2 mutations. *Arch Neurol* 2009;66:1511-16.
- Cartoni R, Leger B, Hock MB, Praz M, Crettenand A, Pich S, et al. Mitofusins 1/2 and ERRalpha expression are increased in human skeletal muscle after physical exercise. *J Physiol* 2005;567:349-58.

- Cartoni R, Martinou JC. Role of mitofusin 2 mutations in the physiopathology of Charcot-Marie-Tooth disease type 2A. *Exp Neurol* 2009;218:268-73.
- Cartoni R, Arnaud E, Medard JJ, Poirot O, Courvoisier DS, Chrast R, et al. Expression of mitofusin 2(R94Q) in a transgenic mouse leads to Charcot-Marie-Tooth neuropathy type 2A. *Brain* 2010;133:1460-69.
- Casasnovas C, Banchs I, Cassereau J, Gueguen N, Chevrollier A, Martinez-Matos JA, et al. Phenotypic spectrum of MFN2 mutations in the Spanish population. *J Med Genet* 2010;47(4):249-56.
- Caviston JP, Holzbaur EL. Huntingtin as an essential integrator of intracellular vesicular trafficking. *Trends Cell Biol* 2009;19:147-55.
- Celniker SE. The *Drosophila* genome. *Curr Opin Genet Dev* 2000;10:612-16.
- Celotto AM, Palladino MJ. *Drosophila*: a "model" model system to study neurodegeneration. *Mol Interv* 2005;5:292-303.
- Chang CR, Blackstone C. Cyclic AMP-dependent protein kinase phosphorylation of Drp1 regulates its GTPase activity and mitochondrial morphology. *J Biol Chem* 2007;282:21583-87.
- Chapman AL, Bennett EJ, Ramesh TM, De Vos KJ, Grierson AJ. Axonal Transport Defects in a Mitofusin 2 Loss of Function Model of Charcot-Marie-Tooth Disease in Zebrafish. *PLoS One* 2013;8(6):e67276.
- Chen H, Detmer SA, Ewald AJ, Griffin EE, Fraser SE, Chan DC. Mitofusins Mfn1 and Mfn2 coordinately regulate mitochondrial fusion and are essential for embryonic development. *J Cell Biol* 2003;160:189-200.
- Chen H, Chomyn A, Chan DC. Disruption of fusion results in mitochondrial heterogeneity and dysfunction. *J Biol Chem* 2005;280:26185-92.
- Chen H, McCaffery JM, Chan DC. Mitochondrial fusion protects against neurodegeneration in the cerebellum. *Cell* 2007;130:548-62.
- Chen H, Vermulst M, Wang YE, Chomyn A, Prolla TA, McCaffery JM, et al. Mitochondrial fusion is required for mtDNA stability in skeletal muscle and tolerance of mtDNA mutations. *Cell* 2010;141:280-89.
- Chen YA, Scheller RH. SNARE-mediated membrane fusion. *Nat Rev Mol Cell Biol* 2001;2:98-106.
- Chevrollier A, Cassereau J, Ferre M, Alban J, Desquiret-Dumas V, Gueguen N, et al. Standardized mitochondrial analysis gives new insights into mitochondrial dynamics and OPA1 function. *Int J Biochem Cell Biol* 2012;44:980-88.
- Chintapalli VR, Wang J, Dow JA. Using FlyAtlas to identify better *Drosophila melanogaster* models of human disease. *Nat Genet* 2007;39:715-20.

- Cho DH, Nakamura T, Fang J, Cieplak P, Godzik A, Gu Z, et al. S-Nitrosylation of Drp1 mediates beta-amyloid-related mitochondrial fission and neuronal injury. *Science* 2009;324:102-105.
- Cho KI, Cai Y, Yi H, Yeh A, Aslanukov A, Ferreira PA. Association of the kinesin-binding domain of RanBP2 to KIF5B and KIF5C determines mitochondria localization and function. *Traffic* 2007;8:1722-35.
- Choi SY, Huang P, Jenkins GM, Chan DC, Schiller J, Frohman MA. A common lipid links Mfn-mediated mitochondrial fusion and SNARE-regulated exocytosis. *Nat Cell Biol* 2006;8:1255-62.
- Chung KW, Kim SB, Park KD, Choi KG, Lee JH, Eun HW, et al. Early onset severe and late-onset mild Charcot-Marie-Tooth disease with mitofusin 2 (MFN2) mutations. *Brain* 2006;129:2103-18.
- Ciaccio PJ, Jaiswal AK, Tew KD. Regulation of human dihydrodiol dehydrogenase by Michael acceptor xenobiotics. *J Biol Chem* 1994;269:15558-62.
- Cipolat S, Martins de Brito O, Dal Zilio B, Scorrano L. OPA1 requires mitofusin 1 to promote mitochondrial fusion. *Proc Natl Acad Sci USA* 2004;101:15927-32.
- Cipolat S, Rudka T, Hartmann D, Costa V, Serneels L, Craessaerts K, et al. Mitochondrial rhomboid PARL regulates cytochrome c release during apoptosis via OPA1-dependent cristae remodelling. *Cell* 2006;126:163-75.
- Clark IE, Dodson MW, Jiang C, Cao JH, Huh JR, Seol JH, et al. *Drosophila* pink1 is required for mitochondrial function and interacts genetically with parkin. *Nature* 2006;441:1162-66.
- Cohen MM, Leboucher GP, Livnat-Levanon N, Glickman MH, Weissmann AM. Ubiquitin-proteasome-dependent degradation of a mitofusin, a critical regulator of mitochondrial fusion. *Mol Biol Cell* 2008;19:2457-64.
- Collard JF, Cote F, Julien JP. Defective axonal transport in a transgenic mouse model of amyotrophic lateral sclerosis. *Nature* 1995;375:61-64.
- Connolly GP. Fibroblast models of neurological disorders: fluorescence measurement studies. *Trends Pharmacol Sci* 1998;19(5):171-77.
- Cook RK, Deal ME, Deal JA, Garton RD, Brown CA, Ward ME et al. A new resource for characterizing X-linked genes in *Drosophila melanogaster*: systematic coverage and subdivision of the X chromosome with nested, Y-linked duplications. *Genetics* 2010;186:1095-109.
- Costa V, Giacomello M, Hudec R, Lopreiato R, Ermak G, Lim D, et al. Mitochondrial fission and cristae disruption increase the response of cell models of Huntington's disease to apoptotic stimuli. *EMBO Mol Med* 2010;2:490-503.
- Cribbs JT, Strack S. Reversible phosphorylation of Drp1 by cyclic AMP-dependent protein kinase and calcineurin regulates mitochondrial fission and cell death. *EMBO Rep* 2007;8:939-44.

- Cuddeback SM, Yamaguchi H, Komatsu K, Miyashita T, Yamada M, Wu C, et al. Molecular cloning and characterization of Bif-1. A novel Src homology 3 domain-containing protein that associates with Bax. *J Biol Chem* 2001;276:20559-65.
- Cuesta A, Pedrola L, Sevilla T, García-Planells J, Chumillas MJ, Mayordomo F, et al. The gene encoding ganglioside-induced differentiation-associated protein 1 is mutated in axonal Charcot-Marie-Tooth type 4A disease. *Nat Genet* 2002;30(1):22-25.
- Da Cruz S, Parone PA, Gonzalo P, Bienvenut WV, Tondera D, Jourdain A, et al. SLP-2 interacts with prohibitins in the mitochondrial inner membrane and contributes to their stability. *Biochim Biophys Acta* 2008;1783:904-111.
- Davies VJ, Hollins AJ, Piechota MJ, Yip W, Davies JR, White KE, et al. Opal deficiency in a mouse model of autosomal dominant optic atrophy impairs mitochondrial morphology, optic nerve structure and visual function. *Hum Mol Genet* 2007;16:1307-18.
- de Brito OM, Scorrano L. Mitofusin 2 tethers endoplasmic reticulum to mitochondria. *Nature* 2008;456:605-10.
- de Brito OM, Scorrano L. Mitofusin-2 regulates mitochondrial and endoplasmic reticulum morphology and tethering: the role of Ras. *Mitochondrion* 2009;9(3):222-26.
- de Duve C. The origin of eukaryotes: a reappraisal. *Nat Rev Genet* 2007;8:395-403.
- De Sandre-Giovannoli A, Chaouch M, Kozlov S, Vallat JM, Tazir M, Kassouri N, et al. Homozygous defects in LMNA, encoding lamin A/C nuclear-envelope proteins, cause autosomal recessive axonal neuropathy in human (Charcot-Marie-Tooth disorder type 2) and mouse. *Am J Hum Genet* 2002;70(3):726-36.
- De Vos KJ, Sable J, Miller KE, Sheetz MP. Expression of phosphatidylinositol (4,5) bisphosphate-specific pleckstrin homology domains alters direction but not the level of axonal transport of mitochondria. *Mol Biol Cell* 2003;14:3636-49.
- De Vos KJ, Allan VJ, Grierson AJ, Sheetz MP. Mitochondrial function and actin regulate dynamin-related protein 1-dependent mitochondrial fission. *Curr Biol* 2005;15:678-83.
- De Vos KJ, Chapman AL, Tennant ME, Manser C, Tudor EL, Lau KF, et al. Familial amyotrophic lateral sclerosis-linked SOD1 mutants perturb fast axonal transport to reduce axonal mitochondria content. *Hum Mol Genet* 2007;16:2720-28.
- De Vos KJ, Sheetz MP. Visualization and quantification of mitochondrial dynamics in living animal cells. *Methods Cell Biol* 2007;80:627-82.
- Debattisti V, Pendin D, Ziviani E, Daga A, Scorrano L. Reduction of endoplasmic reticulum stress attenuates the defects caused by *Drosophila* mitofusin depletion. *J Cell Biol* 2014;204(3):303-12.

- Del Bo R, Moggio M, Rango M, Bonato S, D'Angelo MG, Ghezzi S, et al. Mutated mitofusin 2 presents with intrafamilial variability and brain mitochondrial dysfunction. *Neurology* 2008;71:1959-66.
- Delettre C, Lenaers G, Griffoin JM, Gigarel N, Lorenzo C, Belenguer P, et al. Nuclear gene OPA1, encoding a mitochondrial dynamin-related protein, is mutated in dominant optic atrophy. *Nat Genet* 2000;26:207-10.
- Delivani P, Adrain C, Taylor RC, Duriez PJ, Martin SJ. Role for CED-9 and Egl-1 as regulators of mitochondrial fission and fusion dynamics. *Mol Cell* 2006;21:761-73.
- Deng H, Dodson MW, Huang H, Guo M. The Parkinson's disease genes pink1 and parkin promote mitochondrial fission and/or inhibit fusion in *Drosophila*. *Proc Natl Acad Sci USA* 2008;105:14503-08.
- Detmer SA, Chan DC. Complementation between mouse Mfn1 and Mfn2 protects mitochondrial fusion defects caused by CMT2A disease mutations. *J Cell Biol* 2007a;176:405-14.
- Detmer SA, Chan DC. Functions and dysfunctions of mitochondrial dynamics. *Nat Rev Mol Cell Biol* 2007b;8:870-79.
- Detmer SA, Vande Velde C, Cleveland DW, Chan DC. Hindlimb gait defects due to motor axon loss and reduced distal muscles in a transgenic mouse model of Charcot-Marie-Tooth type 2A. *Hum Mol Genet* 2008; 17:367-75.
- DeVay RM, Dominguez-Ramirez L, Lackner LL, Hoppins S, Stahlberg H, Nunnari J. Coassembly of Mgm1 isoforms requires cardiolipin and mediates mitochondrial inner membrane fusion. *J Cell Biol* 2009;186:793-803.
- Dimos JT, Rodolfa KT, Niakan KK, Weisenthal LM, Mitsumoto H, Chung W, et al. Induced pluripotent stem cells generated from patients with ALS can be differentiated into motor neurons. *Science* 2008;321:1218-21.
- Dorn GW 2nd, Clark CF, Eschenbacher WH, Kang MY, Engelhard JT, Warner SJ, et al. MARF and Opa1 control mitochondrial and cardiac function in *Drosophila*. *Circ Res* 2011;108:12-17.
- Duvezin-Caubet S, Koppen M, Wagener J, Zick M, Israel L, Bernacchia A, et al. OPA1 processing reconstituted in yeast depends on the subunit composition of the m-AAA protease in mitochondria. *Mol Biol Cell* 2007;18:3582-90
- Ebert AD, Yu J, Rose FF, Mattis VB, Lorson CL, Thomson JA, et al. Induced pluripotent stem cells from a spinal muscular atrophy patient. *Nature* 2009;457:277-80.
- Ehse S, Raschke I, Mancuso G, Bernacchia A, Geimer S, Tondera D, et al. Regulation of OPA1 processing and mitochondrial fusion by m-AAA protease isoenzymes and OMA1. *J Cell Biol* 2009;187:1023-36.

- Engelfried K, Vorgerd M, Hagedorn M, Haas G, Gilles J, Epplen JT, et al. Charcot-Marie-Tooth neuropathy type 2A: novel mutations in the mitofusin 2 gene (MFN2). *BMC Med Genet* 2006;7:53.
- Escobar-Henriques M, Westermann B, Langer T. Regulation of mitochondrial fusion by the F-box protein Mdm30 involves proteasome-independent turnover of Fzo1. *J Cell Biol* 2006;173:645-50.
- Eura Y, Ishihara N, Yokota S, Mihara K. Two mitofusin proteins, mammalian homologues of FZO, with distinct functions are both required for mitochondrial fusion. *J Biochem* 2003;134:333-44.
- Eura Y, Ishihara N, Oka T, Mihara K. Identification of a novel protein that regulates mitochondrial fusion by modulating mitofusin (Mfn) protein function. *J Cell Sci* 2006;119:4913-25.
- Evgrafov OV, Mersiyanova I, Irobi J, Van Den Bosch L, Dierick I, Leung CL, et al. Mutant small heat-shock protein 27 causes axonal Charcot-Marie-Tooth disease and distal hereditary motor neuropathy. *Nat Genet.* 2004;36(6):602-06.
- Exner N, Treske B, Paquet D, Holmstrom K, Schiesling C, Gispert, et al. Loss-of-function of human PINK1 results in mitochondrial pathology and can be rescued by parkin. *J Neurosci* 2007;27:12413-18.
- Fain MJ, Stevens B. Alterations in the cell cycle of *Drosophila* imaginal disc cells precede metamorphosis. *Dev Biol* 1982;92:247-58.
- Feiguin F, Godena VK, Romano G, D'Ambrogio A, Klima R, Baralle FE. Depletion of TDP-43 affects *Drosophila* motoneurons terminal synapsis and locomotive behavior. *FEBS Lett* 2009;583:1586-92.
- FlyBase Curators, Swiss-Prot Project Members, InterPro Project Members. Gene Ontology annotation in FlyBase through association of InterPro records with GO terms, 2004.
- Frank S, Gaume B, Bergmann-Leitner ES, Leitner WW, Robert EG, Catez F, et al. The role of dynamin-related protein 1, a mediator of mitochondrial fission, in apoptosis. *Dev Cell* 2001;1:515-25.
- Fritz S, Rapaport D, Klanner E, Neupert W, Westermann B. Connection of the mitochondrial outer and inner membranes by Fzo1 is critical for organellar fusion. *J Cell Biol* 2001;152:683-92.
- Fritz S, Weinbach N, Westermann B. Mdm30 is an F-box protein required for maintenance of fusion-competent mitochondria in yeast. *Mol Biol Cell* 2003;14:2303-13.
- Funalot B, Magdelaine C, Sturtz F, Ouvrier R, Vallat JM. Ultrastructural lesions of axonal mitochondria in patients with childhood-onset Charcot-Marie-Tooth disease due to MFN2 mutations. *Bull Acad Natl Med* 2009;193:151-60;discussion 160-61.

- Gandre-Babbe S, van der Blik AM. The novel tail-anchored membrane protein Mff controls mitochondrial and peroxisomal fission in mammalian cells. *Mol Biol Cell* 2008;19:2402-12.
- Glick BS, Rothman JE. Possible role for fatty acyl-coenzyme A in intracellular protein transport. *Nature* 1987;326(6110):309-12.
- Goshima G, Wollman R, Goodwin SS, Zhang N, Scholey JM, Vale RD, et al. Genes required for mitotic spindle assembly in *Drosophila* S2 cells. *Science* 2007;316:417-21.
- Greene JC, Whitworth AJ, Kuo I, Andrews LA, Feany MB, Pallanck LJ. Mitochondrial pathology and apoptotic muscle degeneration in *Drosophila* parkin mutants. *Proc Natl Acad Sci USA* 2003;100:4078-83.
- Greenspan RJ. Fly Pushing. The theory and practice of *Drosophila* Genetics. 2nd Edition. 2004.
- Griffin EE, Graumann J, Chan DC. The WD40 protein Caf4p is a component of the mitochondrial fission machinery and recruits Dnm1p to mitochondria. *J Cell Biol* 2005;170:237-48.
- Griparic L, van der Wel NN, Orozco IJ, Peters PJ, van der Blik AM. Loss of the intermembrane space protein Mgm1/OPA1 induces swelling and localized constrictions along the lengths of mitochondria. *J Biol Chem* 2004;279:18792-98.
- Griparic L, Kanazawa T, van der Blik AM. Regulation of the mitochondrial dynamin-like protein OPA1 by proteolytic cleavage. *J Cell Biol* 2007;178:757-64.
- Guilbot A, Williams A, Ravise N, Verny C, Brice A, Sherman DL, et al. A mutation in periaxin is responsible for CMT4F, an autosomal recessive form of Charcot-Marie-Tooth disease. *Hum Mol Genet* 2001;10(4):415-21.
- Guillet V, Gueguen N, Verny C, Ferre M, Homedan C, Loiseau D, et al. Adenine nucleotide translocase is involved in a mitochondrial coupling defect in MFN2-related Charcot-Marie-Tooth type 2A disease. *Neurogenetics* 2010;11:127-33.
- Gunawardena S, Her LS, Bruschi RG, Laymon RA, Niesman IR, Gordesky-Gold B, et al. Disruption of axonal transport by loss of huntingtin or expression of pathogenic polyQ proteins in *Drosophila*. *Neuron* 2003;40:25-40.
- Gunsalus KC, Piano F. RNAi as a tool to study cell biology: building the genome-phenome bridge. *Curr Opin Cell Biol* 2005;17:3-8.
- Guo X, Macleod GT, Wellington A, Hu F, Panchumarthi S, Schoenfield M, et al. The GTPase dMiro is required for axonal transport of mitochondria to *Drosophila* synapses. *Neuron* 2005; 47:379-93.
- Gupta RS. Podophyllotoxin-resistant mutants of Chinese hamster ovary cells: cross-resistance studies with various microtubule inhibitors and podophyllotoxin analogues. *Cancer Res* 1983;43(2):505-12.

- Hales KG, Fuller MT. Developmentally regulated mitochondrial fusion mediated by a conserved, novel, predicted GTPase. *Cell* 1997; 90:121-29.
- Han Q, Li J. Comparative characterization of *Aedes* 3-hydroxykynurenine transaminase/alanine glyoxylate transaminase and *Drosophila* serine pyruvate aminotransferase. *FEBS Lett* 2002;527:199-204.
- Han XJ, Lu YF, Li SA, Kaitsuka T, Sato Y, Tomizawa K, et al. CaM kinase I alpha-induced phosphorylation of Drp1 regulates mitochondrial morphology. *J Cell Biol* 2008;182:573-85.
- Hansson A, Hance N, Dufour E, Rantanen A, Hultenby K, Clayton DA, et al. A switch in metabolism precedes increased mitochondrial biogenesis in respiratory chain-deficient mouse hearts. *Proc Natl Acad Sci USA* 2004;101:3136-41.
- Harder Z, Zunino R, McBride H. Sumo1 conjugates mitochondrial substrates and participates in mitochondrial fission. *Curr Biol* 2004;14:340-45.
- Harding AE, Thomas PK. The clinical features of hereditary motor and sensory neuropathy types I and II. *Brain* 1980;103:259-80.
- Hattori N, Yamamoto M, Yoshihara T, Koike H, Nakagawa M, Yoshikawa H, et al. Demyelinating and axonal features of Charcot-Marie-Tooth disease with mutations of myelin-related proteins (PMP22, MPZ and Cx32): a clinicopathological study of 205 Japanese patients. *Brain* 2003;126(Pt 1):134-51.
- Hayasaka K, Himoro M, Wang Y, Takata M, Minoshima S, Shimizu N, et al. Structure and chromosomal localization of the gene encoding the human myelin protein zero (MPZ). *Genomics* 1993;17(3):755-58.
- Head B, Griparic L, Amiri M, Gandre-Babbe S, van der Bliek AM. Inducible proteolytic inactivation of OPA1 mediated by the OMA1 protease in mammalian cells. *J Cell Biol* 2009;187:959-66.
- Hermann GJ, Thatcher JW, Mills JP, Hales KG, Fuller MT, Nunnari J, et al. Mitochondrial fusion in yeast requires the transmembrane GTPase Fzo1p. *J Cell Biol* 1998;143:359-73.
- Hirokawa N, Sato-Yoshitake R, Yoshida T, Kawashima T. Brain dynein (MAP1C) localizes on both anterogradely and retrogradely transported membranous organelles *in vivo*. *J Cell Biol* 1990;111:1027-37.
- Hollenbeck PJ, Saxton WM. The axonal transport of mitochondria. *J Cell Sci* 2005;118:5411-19.
- Holopainen JM, Lehtonen JY, Kinnunen PK. Evidence for the extended phospholipid conformation in membrane fusion and hemifusion. *Biophys J* 1999;76:2111-20.
- Honda S, Aihara T, Hontani M, Okubo K, Hirose S. Mutational analysis of action of mitochondrial fusion factor mitofusin-2. *J Cell Sci* 2005;118:3153-61.

- Hoppins S, Edlich F, Cleland MM, Banerjee S, McCaffery JM, Youle RJ, et al. The soluble form of Bax regulates mitochondrial fusion via MFN2 homotypic complexes. *Mol Cell* 2011;41:150-60.
- Huang H, Gao Q, Peng X, Choi SY, Sarma K, Ren H, et al. piRNA-associated germline nuage formation and spermatogenesis require MitoPLD profusogenic mitochondrial-surface lipid signaling. *Dev Cell* 2011;20:376-87.
- Huang HM, Martins R, Gandy S, Etcheberrigaray R, Ito E, Alkon DL, et al. Use of cultured fibroblasts in elucidating the pathophysiology and diagnosis of Alzheimer's disease. *Ann N Y Acad Sci* 1994;747:225-44.
- Huang ZP, Zhou H, He HL, Chen CL, Liang D, Qu LH. Genome-wide analyses of two families of snoRNA genes from *Drosophila melanogaster*, demonstrating the extensive utilization of introns for coding of snoRNAs. *RNA* 2005;11:1303-16.
- Hwa JJ, Hiller MA, Fuller MT, Santel A. Differential expression of the *Drosophila* mitofusin genes fuzzy onions (fzo) and dmfn. *Mech Dev* 2002;116:213-16.
- Iijima K, Liu HP, Chiang AS, Hearn SA, Konsolaki M, Zhong Y. Dissecting the pathological effects of human A β 40 and A β 42 in *Drosophila*: a potential model for Alzheimer's disease. *Proc Natl Acad Sci USA* 2004;101:6623-28.
- Ikuta J, Maturana A, Fujita T, Okajima T, Tatematsu K, Tanizawa K, et al. Fasciculation and elongation protein zeta-1 (FEZ1) participates in the polarization of hippocampal neuron by controlling the mitochondrial motility. *Biochem Biophys Res Commun* 2007;353:127-32.
- Irobi J, Van Impe K, Seeman P, Jordanova A, Dierick I, Verpoorten N, et al. Hot-spot residue in small heat-shock protein 22 causes distal motor neuropathy. *Nat Genet* 2004;36(6):597-601.
- Ishihara N, Eura Y, Mihara K. Mitofusin 1 and 2 play distinct roles in mitochondrial fusion reactions via GTPase activity. *J Cell Sci* 2004;117:6535-46.
- Ishihara N, Fujita Y, Oka T, Mihara K. Regulation of mitochondrial morphology through proteolytic cleavage of OPA1. *EMBO J* 2006;25:2966-77.
- Ishihara N, Nomura M, Jofuku A, Kato H, Suzuki SO, Masuda K, et al. Mitochondrial fission factor Drp1 is essential for embryonic development and synapse formation in mice. *Nat Cell Biol* 2009;11:958-66.
- Iyengar B, Roote J, Campos AR. The *tamas* gene, identified as a mutation that disrupts larval behavior in *Drosophila melanogaster*, codes for the mitochondrial DNA polymerase catalytic subunit (DNAPol-gamma125). *Genetics* 1999;153:1809-24.
- Iyengar B, Luo N, Farr CL, Kaguni LS, Campos AR. The accessory subunit of DNA polymerase gamma is essential for mitochondrial DNA maintenance and development in *Drosophila melanogaster*. *Proc Natl Acad Sci USA* 2002;99:4483-88.

- James DI, Parone PA, Mattenberger Y, Martinou JC. hFis1, a novel component of the mammalian mitochondrial fission machinery. *J Biol Chem* 2003;278:36373-79.
- Johnston DS. The art and design of genetic screens: *Drosophila Melanogaster*. *Nat Rev Genet* 2002;3:176-88.
- Jones BA, Fangman WL. Mitochondrial DNA maintenance in yeast requires a protein containing a region related to the GTP-binding domain of dynamin. *Genes Dev* 1992;6:380-89.
- Jordanova A, Irobi J, Thomas FP, Van Dijk P, Meerschaert K, Dewil M, et al. Disrupted function and axonal distribution of mutant tyrosyl-tRNA synthetase in dominant intermediate Charcot-Marie-Tooth neuropathy. *Nat Genet* 2006;38(2):197-202.
- Kalaydjieva L, Gresham D, Gooding R, Heather L, Baas F, de Jonge R, et al. N-myc downstream-regulated gene 1 is mutated in hereditary motor and sensory neuropathy-Lom. *Am J Hum Genet* 2000;67(1):47-58.
- Kang JS, Tian JH, Pan PY, Zald P, Li C, Deng C, et al. Docking of axonal mitochondria by syntaphilin controls their mobility and affects short-term facilitation. *Cell* 2008;132:137-48.
- Karbowski M, Lee YJ, Gaume B, Jeong SY, Frank S, Nechushtan A, et al. Spatial and temporal association of Bax with mitochondrial fission sites, Drp1, and Mfn2 during apoptosis. *J Cell Biol* 2002;159:931-38.
- Karbowski M, Jeong SY, Youle RJ. Endophilin B1 is required for the maintenance of mitochondrial morphology. *J Cell Biol* 2004;166:1027-39.
- Karbowski M, Norris KL, Cleland MM, Jeong SY, Youle RJ. Role of Bax and Bak in mitochondrial morphogenesis. *Nature* 2006;443:658-62.
- Karbowski M, Neutzner A, Youle RJ. The mitochondrial E3 ubiquitin ligase MARCH5 is required for Drp1 dependent mitochondrial division. *J Cell Biol* 2007;178:71-84.
- Kijima K, Numakura C, Izumino H, Umetsu K, Nezu A, Shiiki T, et al. Mitochondrial GTPase mitofusin 2 mutation in Charcot-Marie-Tooth neuropathy type 2A. *Hum Genet* 2005;116: 23-27.
- Kim HJ, Sohn KM, Shy ME, Krajewski KM, Hwang M, Park JH, et al. Mutations in PRPS1, which encodes the phosphoribosyl pyrophosphate synthetase enzyme critical for nucleotide biosynthesis, cause hereditary peripheral neuropathy with hearing loss and optic neuropathy (cmtx5). *Am J Hum Genet* 2007;81(3):552-58.
- King SJ, Schroer TA. Dynactin increases the processivity of the cytoplasmic dynein motor. *Nature Cell Biol* 2000;2:20-24.
- Klein CJ, Kimmel GW, Pittock SJ, Engelstad JE, Cunningham JM, Wu Y, et al. Large kindred evaluation of mitofusin 2 novel mutation, extremes of neurologic

presentations, and preserved nerve mitochondria. Arch Neurol 2011;68(10):1295-302.

Kobayashi S, Tanaka A, Fujiki Y. Fis1, DLP1, and Pex11p coordinately regulate peroxisome morphogenesis. Exp Cell Res 2007;313:1675-86.

Koch A, Schneider G, Luers GH, Schrader M. Peroxisome elongation and constriction but not fission can occur independently of dynamin-like protein 1. J Cell Sci 2004;117:3995-4006.

Koshiba T, Detmer SA, Kaiser JT, Chen H, McCaffery JM, Chan DC. Structural basis of mitochondrial tethering by mitofusin complexes. Science 2004;305:858-62.

Koutsopoulos OS, Laine D, Osellame L, Chudakov DM, Parton RG, Frazier AE, et al. Human Mitons associate with mitochondria and induce microtubule-dependent remodeling of mitochondrial networks. Biochim. Biophys Acta 2010;1803:564-74.

Kunugi Y, Hiraoka Y, Hashimoto Y, Taniguchi T, Inagaki C. Ethacrynic acid-sensitive and ATP-dependent Cl⁻ transport in the rat kidney. Jpn J Pharmacol 1991;57(2):167-74.

Labrousse AM, Zappaterra MD, Rube DA, van der Bliek AM. *C. elegans* dynamin-related protein DRP-1 controls severing of the mitochondrial outer membrane. Mol Cell 1999;4:815-26.

Lackner LL, Horner JS, Nunnari J. Mechanistic analysis of a dynamin effector. Science 2009;325:874-77.

Landoure G, Zdebik AA, Martinez TL, Burnett BG, Stanescu HC, Inada H, et al. Mutations in TRPV4 cause Charcot-Marie-Tooth disease type 2C. Nat Genet 2010;42(2):170-74.

Latour P, Thauvin-Robinet C, Baudalet-Méry C, Soichot P, Cusin V, Faivre L, et al. A major determinant for binding and aminoacylation of tRNA(Ala) in cytoplasmic Alanyl-tRNA synthetase is mutated in dominant axonal Charcot-Marie-Tooth disease. Am J Hum Genet 2010;86(1):77-82.

Lawson VH, Graham BV, Flanigan KM. Clinical and electrophysiologic features of CMT2A with mutations in the mitofusin 2 gene. Neurology 2005;65(2):197-204.

Leal A, Huehne K, Bauer F, Sticht H, Berger P, Suter U, et al. Identification of the variant Ala335Val of MED25 as responsible for CMT2B2: molecular data, functional studies of the SH3 recognition motif and correlation between wild-type MED25 and PMP22 RNA levels in CMT1A animal models. Neurogenetics 2009;10(4):375-76.

Lee YJ, Jeong SY, Karbowski M, Smith CL, Youle RJ. Roles of the mammalian mitochondrial fission and fusion mediators Fis1, Drp1, and Opa1 in apoptosis. Mol Biol Cell 2004;15:5001-11.

- Legros F, Malka F, Frachon P, Lombes A, Rojo M. Organization and dynamics of human mitochondrial DNA. *J Cell Sci* 2004;117:2653-62.
- Lentz BR. PEG as a tool to gain insight into membrane fusion. *Eur Biophys J* 2007;36:315-26.
- Lewis MR, Lewis WH. Mitochondria in tissue culture. *Science* 1914;39:330-33.
- Li S, Hong S, Shepardson NE, Walsh DM, Shankar GM, Selkoe D. Soluble oligomers of amyloid beta protein facilitate hippocampal long-term depression by disrupting neuronal glutamate uptake. *Neuron* 2009;62:788-801.
- Li Z, Okamoto K, Hayashi Y, Sheng M. The importance of dendritic mitochondria in the morphogenesis and plasticity of spines and synapses. *Cell* 2004;119:873-87.
- Liao GC, Rehm EJ, Rubin GM. Insertion site preferences of the P transposable element in *Drosophila melanogaster*. *Proc Natl Acad Sci U S A* 2000;97:3347-51.
- Liu J, Li C, Yu Z, Huang P, Wu H, Wei C, et al. Efficient and specific modifications of the *Drosophila* genome by means of an easy TALEN strategy. *J Genet Genomics* 2012;39(5):209-15.
- Liu Y, Zhang SC. Human stem cells as a model of motoneuron development and diseases. *Ann N Y Acad Sci* 2010;1198:192-200.
- Loiseau D, Chevrollier A, Verny C, Guillet V, Gueguen N, Pou de Crescenzo MA, et al. Mitochondrial coupling defect in Charcot-Marie-Tooth type 2A disease. *Ann Neurol* 2007;61:315-23.
- Loson OC, Song Z, Chen H, Chan DC. Fis1, Mff, MiD49, and MiD51 mediate Drp1 recruitment in mitochondrial fission. *Mol Biol Cell* 2013;24:659-67.
- Lowe T. tRNAscan-SE analysis of the *Drosophila melanogaster* genome. FlyBase personal communication 2002.
- Lutz AK, Exner N, Fett ME, Schlehe JS, Kloos K, Lammermann K, et al. Loss of parkin or PINK1 function increases Drp1-dependent mitochondrial fragmentation. *J Biol Chem* 2009;284(34):22938-51.
- Macaskill AF, Rinholm JE, Twelvetrees AE, Arancibia-Carcamo IL, Muir J, Fransson A, et al. Miro1 is a calcium sensor for glutamate receptor-dependent localization of mitochondria at synapses. *Neuron* 2009;61:541-55.
- Macia E, Ehrlich M, Massol R, Boucrot E, Brunner C, Kirchhausen T. Dynasore, a cell-permeable inhibitor of dynamin. *Dev Cell* 2006;10(6):839-50.
- Mann DJ, Dombradi V, Cohen PT. *Drosophila* protein phosphatase V functionally complements a SIT4 mutant in *Saccharomyces cerevisiae* and its amino-terminal region can confer this complementation to a heterologous phosphatase catalytic domain. *EMBO J* 1993;12:4833-42.

- Martin M, Iyadurai SJ, Gassman A, Gindhart JG Jr, Hays TS, Saxton WM. Cytoplasmic dynein, the dynactin complex, and kinesin are interdependent and essential for fast axonal transport. *Mol Biol Cell* 1999;10:3717-28.
- Matsuno K, Diederich RJ, Go MJ, Blaumueller CM, Artavanis-Tsakonas S. Deltex acts as a positive regulator of Notch signaling through interactions with the Notch ankyrin repeats. *Development* 1995;121:2633-44.
- Matsuno K, Ito M, Hori K, Miyashita F, Suzuki S, Kishi N, et al. Involvement of a proline-rich motif and RING-H2 finger of Deltex in the regulation of Notch signaling. *Development* 2002;129:1049-59.
- Meeusen S, DeVay R, Block J, Cassidy-Stone A, Wayson S, McCaffery JM, et al. Mitochondrial inner-membrane fusion and crista maintenance requires the dynamin-related GTPase Mgm1. *Cell* 2006;127:383-95.
- Merkwirth C, Dargazanli S, Tatsuta T, Geimer S, Lower B, Wunderlich FT, et al. Prohibitins control cell proliferation and apoptosis by regulating OPA1-dependent cristae morphogenesis in mitochondria. *Genes Dev* 2008;22:476-88.
- Mersiyanova IV, Perepelov AV, Polyakov AV, Sitnikov VF, Dadali EL, Oparin RB, et al. A new variant of Charcot-Marie-Tooth disease type 2 is probably the result of a mutation in the neurofilament-light gene. *Am J Hum Genet* 2000;67(1):37-46.
- Milton VJ, Jarrett HE, Gowers K, Chalak S, Briggs L, Robinson IM, et al. Oxidative stress induces overgrowth of the *Drosophila* neuromuscular junction. *Proc Natl Acad Sci USA* 2011;108:17521-26.
- Mirth C, Truman JW, Riddiford LM. The role of the prothoracic gland in determining critical weight for metamorphosis in *Drosophila melanogaster*. *Curr Biol* 2005;15:1796-807.
- Mishra N, Kar R, Singha PK, Venkatachalam MA, McEwen DG, Saikumar P. Inhibition of mitochondrial division through covalent modification of Drp1 protein by 15 deoxy-Delta(12,14)-prostaglandin J2. *Biochem Biophys Res Commun* 2010;395:17-24.
- Misko A, Jiang S, Wegorzewska I, Milbrandt J, Baloh RH. Mitofusin 2 is necessary for transport of axonal mitochondria and interacts with the Miro/Milton complex. *J Neurosci* 2010;30:4232-40.
- Misko AL, Sasaki Y, Tuck E, Milbrandt J, Baloh RH. Mitofusin2 mutations disrupt axonal mitochondrial positioning and promote axon degeneration. *J Neurosci* 2012;32:4145-55.
- Morais VA, Verstreken P, Roethig A, Smet J, Snellinx A, Vanbrabant M, et al. Parkinson's disease mutations in PINK1 result in decreased Complex I activity and deficient synaptic function. *EMBO Mol Med*. 2009;1(2):99-111.

- Mortiboys H, Thomas KJ, Koopman WJ, Klaffke S, Abou-Sleiman P, Olpin S, et al. Mitochondrial function and morphology are impaired in parkin-mutant fibroblasts. *Ann Neurol* 2008;64:555-65.
- Mosmann T. Rapid colorimetric assay for cellular growth and survival: application to proliferation and cytotoxicity assays. *J Immunol Methods* 1983;16:55-63.
- Motley AM, Hettema EH. Yeast peroxisomes multiply by growth and division. *J Cell Biol* 2007;178:399-410.
- Mozdy A, McCaffery JM, Shaw JM. Dnm1p GTPase-mediated mitochondrial fusion is a multi-step process requiring the novel integral membrane component Fis1p. *J Cell Biol* 2000;151:367-79.
- Mseeh F, Gerdin MJ, Dubocovich MI. Identification of cysteines involved in ligand binding to the human melatonin MT(2) receptor. *Eur J Pharmacol* 2002;449(1-2):29-38.
- Muglia M, Vazza G, Patitucci A, Milani M, Pareyson D, Taroni F, et al. A novel founder mutation in the MFN2 gene associated with variable Charcot-Marie-Tooth type 2 phenotype in two families from Southern Italy. *J Neurol Neurosurg Psychiatry* 2007;78(11):1286-87.
- Muller H, Schmidt D, Steinbrink S, Mirgorodskaya E, Lehmann V, Habermann K, et al. Proteomic and functional analysis of the mitotic *Drosophila* centrosome. *EMBO J* 2010;29:3344-57.
- Neusch C, Senderek J, Eggermann T, Elloff E, Bahr M, Schneider-Gold C. Mitofusin 2 gene mutation (R94Q) causing severe early-onset axonal polyneuropathy (CMT2A). *Eur J Neurol* 2007;14(5):575-77.
- Neuspiel M, Zunino R, Gangaraju S, Rippstein P, McBride H. Activated mitofusin 2 signals mitochondrial fusion, interferes with Bax activation, and reduces susceptibility to radical induced depolarization. *J Biol Chem* 2005;280:25060-70.
- Nicholson GA, Magdelaine C, Zhu D, Grew S, Ryan MM, Sturtz F, et al. Severe early-onset axonal neuropathy with homozygous and compound heterozygous MFN2 mutations. *Neurology* 2008;70:1678-81.
- Niemann A, Ruegg M, La Padula V, Schenone A, Suter U. Ganglioside-induced differentiation associated protein 1 is a regulator of the mitochondrial network: new implications for Charcot-Marie-Tooth disease. *J Cell Biol* 2005;170:1067-78.
- Nunnari J, Marshall WF, Straight A, Murray A, Sedat JW, Walter P. Mitochondrial transmission during mating in *Saccharomyces cerevisiae* is determined by mitochondrial fusion and fission and the intramitochondrial segregation of mitochondrial DNA. *Mol Biol Cell* 1997;8:1233-42.

- Olichon A, Baricault L, Gas N, Guillou E, Valette A, Belenguer P, et al. Loss of OPA1 perturbs the mitochondrial inner membrane structure and integrity, leading to cytochrome c release and apoptosis. *J Biol Chem* 2003;278:7743-6.
- Ono T, Isobe K, Nakada K, Hayashi JI. Human cells are protected from mitochondrial dysfunction by complementation of DNA products in fused mitochondria. *Nat Genet* 2001;28:272-75.
- Orr AL, Li S, Wang CE, Li H, Wang J, Rong J, et al. N-terminal mutant huntingtin associates with mitochondria and impairs mitochondrial trafficking. *J Neurosci* 2008;28:2783-92.
- Otera H, Wang C, Cleland MM, Setoguchi K, Yokota S, Youle RJ, et al. Mff is an essential factor for mitochondrial recruitment of Drp1 during mitochondrial fission in mammalian cells. *J Cell Biol* 2010;191:1141-58.
- Otsuga D, Keegan BR, Brisch E, Thatcher JW, Hermann GJ, Bleazard W, et al. The dynamin-related GTPase, Dnm1p, controls mitochondrial morphology in yeast. *J Cell Biol* 1998;143:333-49.
- Page AR, Kovacs A, Deak P, Torok T, Kiss I, Dario P, et al. Spotted-dick, a zinc-finger protein of *Drosophila* required for expression of Orc4 and S phase. *EMBO J* 2005;24:4304-15.
- Palfrey HC, Leung S. Inhibition of Na-K-2Cl cotransport and bumetanide binding by ethacrynic acid, its analogues, and adducts. *Am J Physiol* 1993;264(5 Pt 1):C1270-77.
- Park J, Lee SB, Lee S, Kim Y, Song S, et al. Mitochondrial dysfunction in *Drosophila* PINK1 mutants is complemented by parkin. *Nature* 2006;441:1157-61.
- Parks AL, Cook KR, Belvin M, Dompe NA, Fawcett R, Huppert K, et al. Systematic generation of high-resolution deletion coverage of the *Drosophila melanogaster* genome. *Nat Genet* 2004;36:288-92.
- Parone PA, Da Cruz S, Tondera D, Mattenberger Y, James DI, Maechler P, et al. Preventing mitochondrial fission impairs mitochondrial function and leads to loss of mitochondrial DNA. *PLoS ONE* 2008;3:e3257.
- Pastink A, Heemskerk E, Nivard MJ, van Vilet CJ, Vogel EW. Mutational specificity of ethyl methanesulfonate in excision-repair-proficient and -deficient strains of *Drosophila melanogaster*. *Mol Gen Genet* 1991;229:213-18.
- Pilling AD, Horiuchi D, Lively CM, Saxton WM. Kinesin-1 and Dynein are the primary motors for fast transport of mitochondria in *Drosophila* motor axons. *Mol Biol Cell* 2006;17:2057-68.
- Pitts KR, McNiven MA, Yoon Y. Mitochondria-specific function of the dynamin family protein DLP1 is mediated by its C-terminal domains. *J Biol Chem* 2004;279:50286-94.

- Pogson JH, Ivatt RM, Sanchez-Martinez A, Tufi R, Wilson E, Mortiboys H, et al. The complex I subunit NDUFA10 selectively rescues *Drosophila* pink1 mutants through a mechanism independent of mitophagy. PLoS Genet 2014;10(11):e1004815.
- Polke JM, Laura M, Pareyson D, Taroni F, Milani M, Bergamin G, et al. Recessive axonal Charcot-Marie-Tooth disease due to compound heterozygous mitofusin 2 mutations. Neurology 2011;77:168-73.
- Poole AC, Thomas RE, Andrews LA, McBride HM, Whitworth AJ, Pallanck LJ. The PINK1/Parkin pathway regulates mitochondrial morphology. Proc Natl Acad Sci USA 2008;105:1638-43.
- Poole AC, Thomas RE, Yu S, Vincow ES, Pallanck L. The mitochondrial fusion-promoting factor mitofusin is a substrate of the PINK1/parkin pathway. PLoS ONE 2010;5:e10054.
- Rizzardini M, Lupi M, Bernasconi S, Mangolini A, Cantoni L. Mitochondrial dysfunction and death in motor neurons exposed to the glutathione-depleting agent ethacrynic acid. J Neurol Sci 2003;207:51-58.
- Rajo M, Legros F, Chateau D, Lombes A. Membrane topology and mitochondrial targeting of mitofusins, ubiquitous mammalian homologs of the transmembrane GTPase Fzo. J Cell Sci 2002;115:1663-74.
- Rossignol R, Faustin B, Rocher C, Malgat M, Mazat JP, Letellier T. Mitochondrial threshold effects. Biochem J 2003;370:751-62.
- Rouzier C, Bannwarth S, Chaussonot A, Chevrollier A, Verschueren A, Bonello-Palot N, et al. The MFN2 gene is responsible for mitochondrial DNA instability and optic atrophy 'plus' phenotype. Brain 2012;135:23-34.
- Rubin GM, Lewis EB. A brief history of *Drosophila's* contributions to genome research. Science 2000;287:2216-18.
- Russo GJ, Louie K, Wellington A, Macleod GT, Hu F, Panchumarthi S, et al. *Drosophila* Miro is required for both anterograde and retrograde axonal mitochondrial transport. J Neurosci 2009;29:5443-55.
- Ryder E, Ashburner M, Bautista-Llacer R, Drmmond J, Webster J, Johnson G, et al. The DrosDel deletion collection: a *Drosophila* genomewide chromosomal deficiency resource. Genetics 2007; 177:615-29.
- Ryder EJ. Exelixis CG deletion data. FlyBase personal communication 2004.
- Sandoval H, Yao CK, Chen K, Jaiswal M, Donti T, Lin YQ, et al. Mitochondrial fusion but not fission regulates larval growth and synaptic development through steroid hormone production. eLife 2014; 3:e03558.
- Santel A, Fuller MT. Control of mitochondrial morphology by a human mitofusin. J Cell Sci 2001;114:867-74.

- Santel A, Frank S, Gaume B, Herrler M, Youle RJ, Fuller MT. Mitofusin-1 protein is a generally expressed mediator of mitochondrial fusion in mammalian cells. *J Cell Sci* 2003;116:2763-74.
- Saporta MA, Grskovic M, Dimos JT. Induced pluripotent stem cells in the study of neurological diseases. *Stem Cell Res Ther* 2011;2(5):37.
- Saporta MA, Dang V, Volfson D, Zou B, Xie XS, Adebola A, et al. Axonal Charcot-Marie-Tooth disease patient-derived motor neurons demonstrate disease-specific phenotypes including abnormal electrophysiological properties. *Exp Neurol* 2015;263:190-99.
- Sardiello M, Licciulli F, Catalano D, Attimonelli M, Caggese C. MitoDrome: A database of *Drosophila melanogaster* nuclear genes encoding proteins targeted to the mitochondrion. *Nucleic Acids Res* 2003;31:322-24.
- Satoh M, Hamamoto T, Seo N, Kagawa Y, Endo H. Differential sublocalization of the dynamin-related protein OPA1 isoforms in mitochondria. *Biochem Biophys Res Commun* 2003;300:482-93.
- Saxton WM, Hollenbeck PJ. The axonal transport of mitochondria. *J Cell Sci* 2012;125:2095-104.
- Schapira AH, Cooper JM, Dexter D, Clark JB, Jenner P, Marsden CD. Mitochondrial complex I deficiency in Parkinson's disease. *J Neurochem* 1990;54:823-27.
- Schon EA, Przedborski S. Mitochondria: the next (neurode)generation. *Neuron* 2011;70:1033-53.
- Schrader M, King SJ, Stroh TA, Schroer TA. Real time imaging reveals a peroxisomal reticulum in living cells. *J Cell Sci* 2000;113:3663-71.
- Schrader M, Reuber BE, Morrell JC, Jimenez-Sanchez G, Obie C, Stroh TA, et al. Expression of PEX11beta mediates peroxisome proliferation in the absence of extracellular stimuli. *J Biol Chem* 1998;273:29607-14.
- Schwarzer C, Barnikol-Watanabe S, Thinnies FP, Hilschmann N. Voltage-dependent anion-selective channel (VDAC) interacts with the dynein light chain Tctex1 and the heat-shock protein PBP74. *Int J Biochem Cell Biol* 2002;34:1059-70.
- Senderek J, Bergmann C, Weber S, Ketelsen UP, Schorle H, Rudnik-Schoneborn S, et al. Mutation of the SBF2 gene, encoding a novel member of the myotubularin family, in Charcot-Marie-Tooth neuropathy type 4B2/11p15. *Hum Mol Genet* 2003a;12(3):349-56.
- Senderek J, Bergmann C, Stendel C, Kirfel J, Verpoorten N, De Jonghe P, et al. Mutations in a gene encoding a novel SH3/TPR domain protein cause autosomal recessive Charcot-Marie-Tooth type 4C neuropathy. *Am J Hum Genet* 2003b;73(5):1106-19.
- Sesaki H, Jensen RE. *UGOI* encodes an outer membrane protein required for mitochondrial fusion. *J Cell Biol* 2001;152:1123-34.

- Sesaki H, Jensen RE. Ugo1p links the Fzo1p and Mgm1p GTPases for mitochondrial fusion. *J Biol Chem* 2004;279:28298-303.
- Seyfried J, Soldner F, Schulz JB, Klockgether T, Kovar KA, Wullner U. Differential effects of L-buthionine sulfoximine and ethacrynic acid on glutathione levels and mitochondrial function in PC12 cells. *Neurosci Lett* 1999;264:1-4.
- Shan X, Chiang PM, Price DL, Wong PC. Altered distributions of Gemini of coiled bodies and mitochondria in motor neurons of TDP-43 transgenic mice. *Proc Natl Acad Sci USA* 2010;107:16325-30.
- Shaw PJ. Molecular and cellular pathways of neurodegeneration in motor neurone disease. *J Neurol Neurosurg Psychiatry* 2005;76:1046-57.
- Sheng ZH, Cai Q. Mitochondrial transport in neurons: impact on synaptic homeostasis and neurodegeneration. *Nat Rev Neurosci* 2012;13:77-93.
- Shi P, Strom AL, Gal J, Zhu H. Effects of ALS-related SOD1 mutants on dynein- and KIF5-mediated retrograde and anterograde axonal transport. *Biochim Biophys Acta* 2010;1802:707-16.
- Shirendeb U, Reddy AP, Manczak M, Calkins MJ, Mao P, Tagle DA, et al. Abnormal mitochondrial dynamics, mitochondrial loss and mutant huntingtin oligomers in Huntington's disease: implications for selective neuronal damage. *Hum Mol Genet* 2011;20:1438-55.
- Skre H. Genetic and clinical aspects of Charcot-Marie-Tooth's disease. *Clin Genet* 1974;6:98-118.
- Smirnova E, Shurland DL, Ryazantsev SN, van der Blik AM. A human dynamin-related protein controls the distribution of mitochondria. *J Cell Biol* 1998;143:351-58.
- Smirnova E, Griparic L, Shurland DL, van der Blik AM. Dynamin-related protein Drp1 is required for mitochondrial division in mammalian cells. *Mol Biol Cell* 2001;12:2245-56.
- Soltys BJ, Gupta RS. Changes in mitochondrial shape and distribution induced by ethacrynic acid and the transient formation of a mitochondrial reticulum. *J Cell Physiol* 1994;159:281-94.
- Song W, Chen J, Petrilli A, Liot G, Klinglmayr E, Zhou Y, et al. Mutant huntingtin binds the mitochondrial fission GTPase dynamin-related protein-1 and increases its enzymatic activity. *Nat Med* 2011;17:377-82.
- Song Z, Chen H, Fiket M, Alexander C, Chan DC. OPA1 processing controls mitochondrial fusion and is regulated by mRNA splicing, membrane potential, and Yme1L. *J Cell Biol* 2007;178:749-55.
- Spuch C, Ortolano S, Navarro C. New insights in the amyloid-Beta interaction with mitochondria. *J Aging Res* 2012;2012:324968.

- Stephenson EC, Chao YC, Fackenthal JD. Molecular analysis of the swallow gene of *Drosophila melanogaster*. *Genes Dev* 1988;2:1655-65.
- Stojanovski D, Koutsopoulos OS, Okamoto K, Ryan MT. Levels of human Fis1 at the mitochondrial outer membrane regulate mitochondrial morphology. *J Cell Sci* 2004;117:1201-10.
- Stokin GB, Lillo C, Falzone TL, Bruschi RG, Rockenstein E, Mount SL, et al. Axonopathy and transport deficits early in the pathogenesis of Alzheimer's disease. *Science* 2005;307:1282-88.
- Stowers RS, Megeath LJ, Gorska-Andrzejak J, Meinertzhagen IA, Schwarz TL. Axonal transport of mitochondria to synapses depends on Milton, a novel *Drosophila* protein. *Neuron* 2002;36:1063-77.
- Street VA, Bennett CL, Goldy JD, Shirk AJ, Kleopa KA, Tempel BL, et al. Mutation of a putative protein degradation gene LITAF/SIMPLE in Charcot-Marie-Tooth disease 1C. *Neurology* 2003;60(1):22-6.
- Strickland AV, Rebelo AP, Zhang F, Price J, Bolon B, Silva JP, et al. Characterization of the mitofusin 2 R94W mutation in a knock-in mouse model. *J Peripher Nerv Syst* 2014;19(2):152-64.
- Suter U, Moskow JJ, Welcher AA, Snipes GJ, Kosaras B, Sidman RL, et al. A leucine-to-proline mutation in the putative first transmembrane domain of the 22-kDa peripheral myelin protein in the trembler-J mouse. *Proc Natl Acad Sci U S A* 1992;89(10):4382-86.
- Taguchi N, Ishihara N, Jofuku A, Oka T, Mihara K. Mitotic phosphorylation of dynamin-related GTPase Drp1 participates in mitochondrial fission. *J Biol Chem* 2007;282:11521-29.
- Tanaka A, Cleland MM, Xu S, Narendra DP, Suen DF, Karbowski M, et al. Proteasome and p97 mediate mitophagy and degradation of mitofusins induced by Parkin. *J Cell Biol* 2010;191:1367-80.
- Tanaka K, Sugiura Y, Ichishita R, Mihara K, Oka T. KLP6: a newly identified kinesin that regulates the morphology and transport of mitochondria in neuronal cells. *J Cell Sci* 2011;124:2457-65.
- Tandan R, Bradley WG. Amyotrophic lateral sclerosis. Part 1. Clinical features, pathology, and ethical issues in management. *Ann Neurol* 1985;18:271-80.
- Tieu Q, Okreglak V, Naylor K, Nunnari J. The WD repeat protein, Mdv1p, functions as a molecular adaptor by interacting with Dnm1p and Fis1p during mitochondrial fission. *J Cell Biol* 2002;158:445-52.
- Tondera D, Grandemange S, Jourdain A, Karbowski M, Mattenberger Y, Herzig S, et al. SLP-2 is required for stress-induced mitochondrial hyperfusion. *EMBO J* 2009;28:1589-600.

- Truman JW, Talbot WS, Fahrbach SE, Hogness DS. Ecdysone receptor expression in the CNS correlates with stage-specific responses to ecdysteroids during *Drosophila* and *Manduca* development. *Development* 1994;120:219-34.
- Trushina E, Dyer RB, Badger JD 2nd, Ure D, Eide L, Tran DD, et al. Mutant huntingtin impairs axonal trafficking in mammalian neurons in vivo and in vitro. *Mol Cell Biol* 2004;24:8195-209.
- Twig G, Elorza A, Molina AJ, Mohamed H, Wikstrom JD, Walzer G, et al. Fission and selective fusion govern mitochondrial segregation and elimination by autophagy. *Embo J* 2008;27:433-46.
- Vallat JM, Ouvrier RA, Pollard JD, Magdelaine C, Zhu D, Nicholson GA, et al. Histopathological findings in hereditary motor and sensory neuropathy of axonal type with onset in early childhood associated with mitofusin 2 mutations. *J Neuropathol Exp Neurol* 2008;67:1097-102.
- Van Gestel K, Verbelen JP. Giant mitochondria are a response to low oxygen pressure in cells of tobacco (*Nicotiana tabacum* L.). *J Exp Bot* 2002;53:1215-18.
- Varadi A, Johnson-Cadwell LI, Cirulli V, Yoon Y, Allan VJ, Rutter GA. Cytoplasmic dynein regulates the subcellular distribution of mitochondria by controlling the recruitment of the fission factor dynamin-related protein-1. *J Cell Sci* 2004;117:4389-400.
- Verhoeven K, De Jonghe P, Coen K, Verpoorten N, Auer-Grumbach M, Kwon JM, et al. Mutations in the small GTP-ase late endosomal protein RAB7 cause Charcot-Marie-Tooth type 2B neuropathy. *Am J Hum Genet.* 2003 Mar;72(3):722-27.
- Verhoeven K, Claeys KG, Zuchner S, Schroder JM, Weis J, Ceuterick C, et al. MFN2 mutation distribution and genotype/phenotype correlation in Charcot-Marie-Tooth type 2. *Brain* 2006;129:2093-102.
- Verstreken P, Ly CV, Venken KJ, Koh TW, Zhou Y, Bellen HJ. Synaptic mitochondria are critical for mobilization of reserve pool vesicles at *Drosophila* neuromuscular junctions. *Neuron* 2005;47:365-78.
- Vettori A, Bergamin G, Moro E, Vazza G, Polo G, Tiso N, et al. Developmental defects and neuromuscular alterations due to mitofusin 2 gene (MFN2) silencing in zebrafish: a new model for Charcot-Marie-Tooth type 2A neuropathy. *Neuromuscul Disord* 2011;21:58-67.
- Vincent A, Briggs L, Chatwin GF, Emery E, Tomlins R, Oswald M, et al. parkin-induced defects in neurophysiology and locomotion are generated by metabolic dysfunction and not oxidative stress. *Hum Mol Genet* 2012;21:1760-69.
- Vogel E, Natarajan AT. The relation between reaction kinetics and mutagenic action of mono-functional alkylating agents in higher eukaryotic systems. I. Recessive lethal mutations and translocations in *Drosophila*. *Mutat Res* 1979;62:51-100.

- Wagner KM, Ruegg M, Niemann A, Suter U. Targeting and function of the mitochondrial fission factor GDAF1 are dependent on its tail-anchor. *PLoS One* 2009;4:e5160.
- Walker FO. Huntington's disease. *Lancet* 2007;369:218-28.
- Wang H, Song P, Du L, Tian W, Yue W, Liu M, et al. Parkin ubiquitinates Drp1 for proteasome-dependent degradation: implication of dysregulated mitochondrial dynamics in Parkinson disease. *J Biol Chem* 2011;286:11649-58.
- Wang J, Kean L, Yang J, Allan AK, Davies SA, Herzyk P, et al. Function-informed transcriptome analysis of *Drosophila* renal tubule. *Genome Biol* 2004;5(9):R69.
- Wang X, Schwarz TL. The mechanism of Ca²⁺-dependent regulation of kinesin-mediated mitochondrial motility. *Cell* 2009;136:163-74.
- Warner LE, Mancias P, Butler IJ, McDonald CM, Keppen L, Koob KG, et al. Mutations in the early growth response 2 (EGR2) gene are associated with hereditary myelinopathies. *Nat Genet* 1998;18(4):382-84.
- Waterham HR, Koster J, van Roermund CW, Mooyer PA, Wanders RJ, Leonard JV. A lethal defect of mitochondrial and peroxisomal fission. *N Engl J Med* 2007;356:1736-41.
- Wittmann CW, Wszolek MF, Shulman JM, Salvaterra PM, Lewis J, et al. Tauopathy in *Drosophila*: neurodegeneration without neurofibrillary tangles. *Science* 2001;293:711-14.
- Wong PC, Pardo CA, Borchelt DR, Lee MK, Copeland NG, Jenkins NA, et al. An adverse property of a familial ALS-linked SOD1 mutation causes motor neuron disease characterized by vacuolar degeneration of mitochondria. *Neuron* 1995;14:1105-16.
- Yamamoto S, Jaiswal M, Charng WL, Gambin T, Karaca E, Mirzaa G, et al. A *Drosophila* genetic resource of mutants to study mechanisms underlying human genetic diseases. *Cell*. 2014;159(1):200-14.
- Yang Y, Ouyang Y, Yang L, Beal MF, McQuibban A, Vogel H, et al. Pink1 regulates mitochondrial dynamics through interaction with the fission/fusion machinery. *Proc Natl Acad Sci USA* 2008;105:7070-75.
- Yildiz A, Tomishige M, Vale RD, Selvin PR. Kinesin walks hand-over-hand. *Science* 2004;303:676-78.
- Yoon Y, Krueger EW, Oswald BJ, McNiven MA. The mitochondrial protein hFis1 regulates mitochondrial fission in mammalian cells through an interaction with the dynamin-like protein DLP1. *Mol Cell Biol* 2003;23:5409-20.
- Yuan G, Klambt C, Bachellerie JP, Brosius J, Huttenhofer A. RNomics in *Drosophila melanogaster*: identification of 66 candidates for novel non-messenger RNAs. *Nucleic Acids Res* 2003;31:2495-507.

- Zhao C, Takita J, Tanaka Y, Setou M, Nakagawa T, Takeda S, et al. Charcot-Marie-Tooth disease type 2A caused by mutation in a microtubule motor KIF1Bbeta. *Cell* 2001;105(5):587-97.
- Zhu PP, Patterson A, Stadler J, Seeburg DP, Sheng M, Blackstone C. Intra- and intermolecular domain interactions of the C-terminal GTPase effector domain of the multimeric dynamin-like GTPase Drp1. *J Biol Chem* 2004;279:35967-74.
- Ziviani E, Tao RN, Whitworth AJ. *Drosophila* parkin requires PINK1 for mitochondrial translocation and ubiquitinates mitofusin. *Proc Natl Acad Sci USA* 2010;107:5018-23.
- Zuchner S, Mersiyanova IV, Muglia M, Bissar-Tadmouri N, Rochelle J, Dadali EL, et al. Mutations in the mitochondrial GTPase mitofusin 2 cause Charcot-Marie-Tooth neuropathy type 2A. *Nat Genet* 2004;36:449-51.
- Zuchner S, Noureddine M, Kennerson M, Verhoeven K, Claeys K, De Jonghe P, et al. Mutations in the pleckstrin homology domain of dynamin 2 cause dominant intermediate Charcot-Marie-Tooth disease. *Nat Genet* 2005;37(3):289-94.
- Zuchner S, De Jonghe P, Jordanova A, Claeys KG, Guerguelcheva V, Cherninkova S, et al. Axonal neuropathy with optic atrophy is caused by mutations in mitofusin 2. *Ann Neurol* 2006;59:276-81.
- Zunino R, Schauss A, Rippstein P, Andrade-Navarro M, McBride HM. The SUMO protease SENP5 is required to maintain mitochondrial morphology and function. *J Cell Sci* 2007;120:1178-88.